Identification of kinase-mediated signaling pathways regulating autophagy in response to cellular stresses

Truc Losier

Thesis submitted to the University of Ottawa in partial fulfillment of the requirements for the Doctorate in Philosophy degree in Cellular and Molecular Medicine.

Department of Cellular and Molecular Medicine

Faculty of Medicine

University of Ottawa

Abstract

Autophagy is a conserved and highly regulated catabolic process essential for cellular homeostasis, particularly under stress conditions such as nutrient starvation and infection. While bulk autophagy facilitates the indiscriminate degradation of cytosolic components during starvation, selective autophagy targets specific organelles and intracellular pathogens for turnover. A critical component of autophagy is the ATG16L1-containing E3-like enzyme, which drives autophagosome formation. Polymorphisms in ATG16L1, such as the Crohn's disease-associated T300A variant (caATG16L1), have been linked to autophagy dysfunction. Our findings demonstrate that ULK1 kinase directly phosphorylates ATG16L1 in response to infection and starvation, facilitating its localization to bacterial entry sites and promoting anti-bacterial autophagy. However, ULK1-mediated phosphorylation of caATG16L1 leads to its destabilization under stress, highlighting a dual role of ULK1 signaling—enhancing wild-type ATG16L1 function while compromising the stability of its disease-associated variant.

We next sought to further dissect the kinase-mediated regulation of selective autophagy targeting specific organelles. We proposed that selective autophagy may be regulated by distinct upstream signaling from starvation-induced autophagy to promote organelle turn-over. To investigate this hypothesis, we developed a customized kinome-wide CRISPR screening platform designed for the parallel interrogation of multiple stress-induced autophagy pathways. Utilizing a reporter cell line expressing DsRed-IRES-GFP-p62, we were able to monitor basal autophagy, starvation-induced autophagy, ER-phagy, and pexophagy. The Brunello kinome library was employed to maximize on-target gene

disruption while minimizing off-target effects, enhancing the overall robustness of the screen. Through this approach, we identified both known and novel kinases involved in autophagy regulation, including condition-specific regulators such as CDK11A and NME3 for ER-phagy, and PAN3 and CDC42BPG for pexophagy.

Overall, our study emphasizes the central role of kinase signaling in coordinating selective autophagy. We demonstrate that ULK1 differentially affects autophagic outcomes depending on the ATG16L1 allele, revealing an additional layer of regulatory complexity. Additionally, the datasets generated from our optimized screening strategy provide valuable insight into the distinct regulatory networks governing bulk versus selective autophagy, offering a foundation for future mechanistic and therapeutic studies.

Table of contents

List of abbreviations

4EBP1	eIF4E binding protein
ADP	Adenosine diphosphate
Akt	Protein kinase B
ALS	Amyotrophic lateral sclerosis
AMP	Adenosine monophosphate
AMPK	AMP-activated protein kinase
AR	Autoradiography
ATG	Autophagy-related
ATL3	Atlastin GTPase 3
ATM	Ataxia telangiectasia mutated
ATP	Adenosine Triphosphate
Bcl-2	B-cell lymphoma 2
CAMKKb	Calcium/calmodulin-dependent protein kinase
CBM	Carbohydrate-binding module
CBS	Cystathione b-synthase
CCPG1	Cell-cycle progression gene 1
CD	Crohn's disease
CDC42BPG	CDC42 binding protein kinase gamma
CDK11A	Cyclin dependent kinase 11A
CFU	Colony Forming Unit
CRISPR	Clustered regularly interspaced short palindromic repeats
DEPTOR	DEP domain containing mTOR interacting protein
DMEM	Dulbecco's Modified Eagle'smedium
ER	Endoplasmic reticulum
FACS	Fluorescence-activated cell sorting
FAM134B	member of the family with sequence similarity 134

FIP200	Focal adhesion kinase family interacting protein of 200kD
GAP	GTPase activating protein
GDP	Guanosine 5’-diphosphate
GTP	Guanosine 5’-triphosphate
GWAS	Genome-wide association studies
HCT116	Human COLORECTAL CARCINOMA Cell Line.
HD	Huntington's disease
HEAT	Huntington, EF3, PR65/A, TOR
HEK293A	Human embryonic kidney cells 293
HOPS	Homotypic fusion and vacuole protein sorting
HORMA	Hop1, Rev7, Mad2 domain
HTT	Huntingtin
iE-DAP	g-D-glutamyl-*meso*-diaminopimelic acid
IF	Immunofluorescence
IFN	Interferon
IKKα	IκB kinase subunit
IRGM	Immunity related GTPase M
KO	Knockout
LAP	LC3-associated phagocytosis
LC3	Microtubule-associated protein 1 light chain 3
LIR	LC3-interacting region
LPS	Lipopolysaccharide
MAP	Mitogen-activated protein
MAP4K2	Mitogen-Activated Protein Kinase Kinase Kinase Kinase 2
MCF7	Michigan Cancer Foundation-7
MDP	Muramyl dipeptide
MEF	Mouse embryonic fibroblasts
mLST8	Mammalian homolog of lethal with sec-13 gene 8

MNV	Murine noroviruses
MOI	The multiplicity of infection
MRCK	Myotonic dystrophy-related Cdc42-binding kinases
mTORC1	The mammalian target of rapamycin complex 1
NDP52	Nuclear domain 10 protein 52
NDPK	Nucleoside-diphosphate kinases
NF-kB	Nuclear factor-kB
NME3	Nucleoside Diphosphate Kinase 3
NOD2	Nucleotide-binding oligomerization domain-containing protein 2
OPTN	Optineurin
p62/SQSTM1	Sequestosome 1
PAMP	Pathogen-associated molecular pattern molecule
PAN3	Poly(A) specific ribonuclease subunit
PBD	Peroxisome biogenesis disorders
PD	Parkinson's disease
PEX	Peroxin or peroxisomal biogenesis factor
PFA	Paraformaldehyde
PGN	Peptidoglycan
PIKFYVE	FYVE finger-containing phosphoinositide kinase
PIKK	Phosphatidylinositol-kinase-related kinase
PMP70	70 kDa peroxisomal membrane protein
PRAS40	Proline-rich Akt substrate of 40 kDa
PROPPIN	b-propellers that bind phosphoinositides
PRR	Pattern recognition receptor
PtdEth	Phosphatidylethanolamine
PtdIns 3-kinase	Phosphatidylinositide 3-kinases
PtdIns(3)P	Phosphatidylinositol(3)phosphate

PTM	Post-translational modification
R848	Resiquimod
Raptor	Regulatory associated protein of mTOR
RB1CC1	RB1-inducible coiled-coil protein 1
Rheb	Ras homolog enriched in brain
RIP2	Receptor-interacting protein kinase 2
ROS	Reactive oxygen species
RTN3L	Reticulon 3
Rubicon	RUN domain Beclin 1-interacting and cysteine-rich containing protein
S6K	P70S6 kinase
SCV	*Salmonella*-containing vacuole
SEC62	SEC62 homolog, preprotein translocation factor
Sif	*Salmonella*-induced filament
STK11 /LKB1	Liver kinase B1
T3SS	Type III secretion system
TBC1D7	Tre2-Bub2-CDC16 (TBC) 1 domain family member 7
TEX264	Testis expressed 264
TKFC	Triokinase and FMN cyclase
TLR4	Toll-like receptor 4
TOS	TOR signaling
TP53INP2	Tumor protein 53-induced nuclear protein 2
TPR	Tetratricopeptide
TSC2	Tuberous sclerosis 2
Ub	Ubiquitin
UC	ulcerative colitis
ULK	unc-51-like kinase
UPR	Unfolded protein response
UVRAG	UV irradiation resistance-associated gene

VMP1	Vacuole membrane protein 1
VPS34	Vacuolar protein sorting 34
WB	Western blot
WIPI	WD-repeat protein interacting with phosphoinositides
ZS	Zellweger syndrome

Acknowledgements

I would like to express my gratitude to the University of Ottawa for granting me the opportunity to pursue my doctoral studies here. This journey has not been without its struggles and challenges, and I am deeply appreciative of the support that enabled me to overcome them and grow both personally and professionally.

I am sincerely thankful to my supervisors, Dr. Ryan Russell and Dr. Maxime Rousseaux, for their guidance, patience, and unwavering support throughout this journey. Their mentorship has been instrumental in shaping my scientific thinking and research capabilities. Beyond fostering my technical development, they have also encouraged me to cultivate essential soft skills—such as resilience, communication, and critical thinking—that are crucial for success both in and outside academia.

I would also like to extend my appreciation to the members of my Thesis Advisory Committee—Dr. Derrick Gibbings, Dr. Diane Lagace, and Dr. Alex MacKenzie—for their valuable feedback, thoughtful questions, and constructive suggestions. Their insights pushed me to consider broader implications and potential pitfalls in my project, ultimately helping me prepare more thoroughly and complete my PhD with confidence.

Special thanks go to all members of the Russell and Rousseaux laboratories for their technical assistance, stimulating discussions, and collegial support, which have made the research environment both collaborative and inspiring.

Lastly, I would like to express my deepest gratitude to my family for their unconditional support, and to my husband, Jared Losier, whose love, patience, and

constant encouragement have been my foundation. Without his presence and belief in me, this academic journey would not have been possible.

Sources of funding

I am deeply grateful to all those who have generously supported me and my research, including: Ontario Graduate Scholarship; Vanier Canada Graduate Scholarships (Vanier CGS) awarded by the Natural Sciences and Engineering Research Council (NSERC); and the University of Ottawa for their continued Admission and Excellence scholarships.

Chapter 1: Introduction

Macroautophagy (hereafter referred to as autophagy) is a tightly regulated degradative process triggered by various cellular stressors, including nutrient deprivation, proteotoxic aggregates, and pathogen invasion(Ryter et al. 2013). This process is orchestrated by a highly conserved group of autophagy-related (ATG) proteins, which initiate the *de novo* formation of a double-membraned vesicle known as an autophagosome(Reggiori et al. 2012). The autophagosome gains its degradative function upon fusing with the lysosome, which supplies acid hydrolases to break down the sequestered macromolecules(Reggiori et al. 2012).

1.1 History of autophagy

The term ‘autophagy’ dates back to the 1860s when it was described as the self-sustaining mechanism of human body, allowing individual to survive periods of nutrient deprivation by consuming its own resources(Ktistakis 2017; Mizushima 2018). A century later, in 1963, during the CIBA Foundation Symposium on Lysosomes, Christian de Duve, a pioneering cell biologist from the University of Louvain in Belgium, reintroduced the term autophagy after his discovery of the lysosome(Klionsky 2007; Mizushima 2018). Years of extensive research refined its definition, now recognized as the cellular process in which intracellular components are transported to the lysosome or vacuole for degradation.

1.1.1 Beginning of an era

In 1949, Christian de Duve was working with his colleagues to study carbohydrate metabolism and the mechanism of insulin(Opperdoes 2013). Specifically, they decided to investigate the distribution of an enzyme called glucose-6-phosphatase or hexose phosphatase, which controls blood sugar(Opperdoes 2013). His research on glucose-6-phosphatase led to unexpected findings that set the stage for the discovery of lysosomes(Opperdoes 2013; Sabatini and Adesnik 2013). While analyzing enzyme distribution in liver cells, his team observed unusual patterns in acid phosphatase activity, suggesting that certain enzymes were enclosed within membrane-bound structures(de Duve et al. 1955). Further experimentation confirmed that these "latent enzymes" were sequestered inside vesicles which de Duve named them “lysosome” to demonstrate their lytic nature(de Duve et al. 1955). Notably, de Duve came up with the lysosome concept solely through biochemical analyses, without relying on microscopic examination of his samples(Sabatini and Adesnik 2013).

In 1955, de Duve collaborated with Alex Novikoff, a microscopy specialist from the University of Vermont, to capture the first electron microscope image of lysosomes(Novikoff et al. 1956). They also confirmed the presence of acid phosphatases in the lysosome through light and electron microscope(Novikoff et al. 1956). For his groundbreaking discovery of lysosomes, de Duve was awarded the Nobel Prize in Physiology or Medicine in 1974(NobelPrize.Org, 1974). This discovery paved the way for more significant scientific breakthroughs.

The next key area of research focused on understanding the biological function of lysosomes. Initially, de Duve proposed that lysosomes might facilitate the intracellular

digestion of macromolecules in his first paper on activity of acid phosphatase(de Duve and Wattiaux 1966). Throughout 1950s-1960s, several studies from different research groups supported this hypothesis, establishing a connection between lysosomal digestion and the endocytic uptake of materials like pathogens or cellular debris(Clark 1957; Novikoff et al. 1956; Straus 1964; Ashford and Porter 1962). Around the same time, Marilyn Farquhar and her colleagues at the University of California identified vesicles containing enveloped cytoplasmic material and proposed that these were pre-lysosomes(Smith and Farquhar 1966). These structures originate from a phagophore, a cup-shaped membrane that expands and seals to form a double-membraned autophagosome(Smith and Farquhar 1966; Arstila and Trump 1968) (Figure 1). Autophagosomes capture and transport damaged cellular components to lysosomes for degradation(Arstila and Trump 1968) (Figure 1). Recognizing this self-digestion process, de Duve later applied the term autophagy to describe it(Ohsumi 2014).

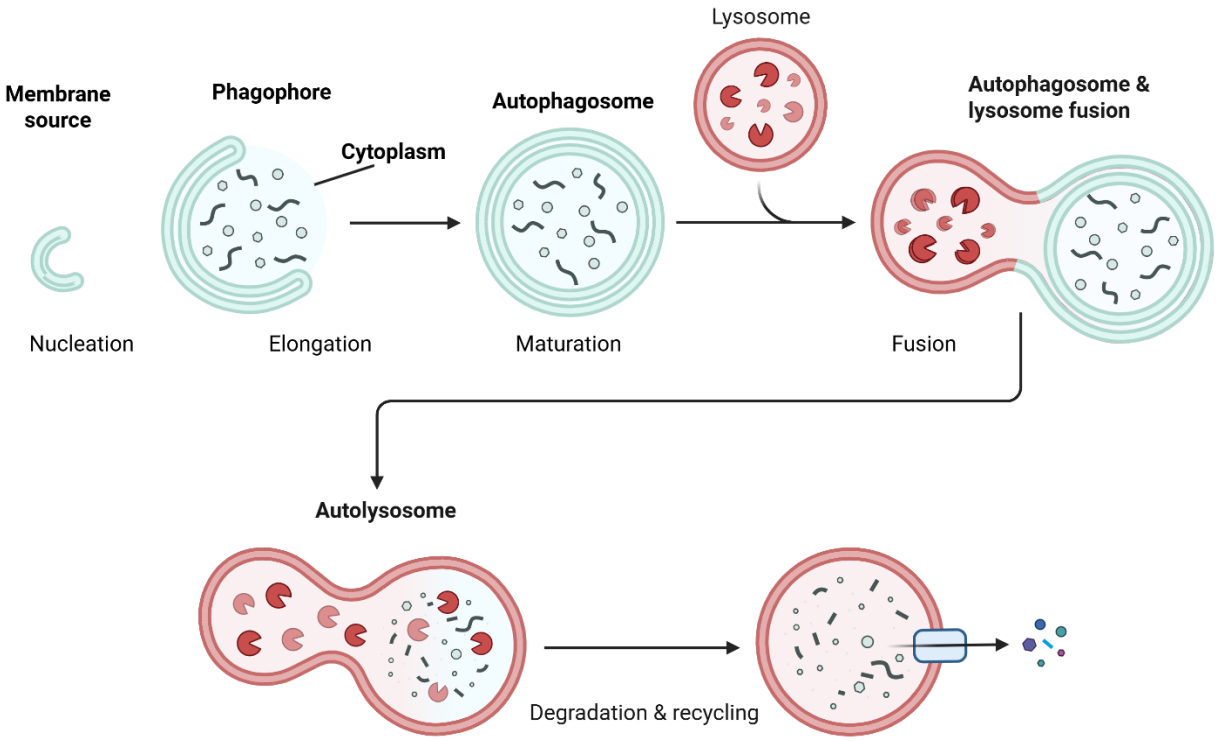

Figure 1: Autophagy process. Segments of the cytosol and organelles are enclosed within a double-membrane structure known as an autophagosome, which subsequently fuses with a lysosome to form an autolysosome, where their contents are degraded and recycled by lysosomal enzymes.

1.1.2 Autophagy breakthroughs

From the 1960s to the 1980s, morphological studies of autophagy flourished(Mizushima 2018). While early research focused on the late stages of the process, Per Seglen's lab shifted attention to the initial and intermediate steps using electroinjected radioactive probes(Klionsky 2005). This work led to the identification of the phagophore, the precursor to the autophagosome, and the amphisome, a structure where autophagic and endocytic pathways merge(Gordon and Seglen 1988; Klionsky 2007).

The molecular mechanisms underlying autophagy remained uncharacterized until 1992 when Yoshinori Ohsumi, a scientist at the University of Tokyo, identified at least 15 autophagy-related genes termed *APG*s involved in the autophagy pathway through a large-scale genetic screen in the yeast *S. cerevisiae* subjected to nitrogen starvation(Tsukada and Ohsumi 1993). This groundbreaking discovery not only advanced the understanding of autophagy mechanisms but also earned Ohsumi the 2016 Nobel Prize in Physiology or Medicine(Mizushima 2018). During the same time, independent yeast genetic screens also led to the identification of several autophagy-related genes. Notable contributions came from research groups led by Michael Thumm (*AUT*s, autophagy), Daniel J. Klionsky (*CVT*s, cytoplasm-to-vacuole targeting), William A. Dunn (*GSA*s, glucose-mediated selective autophagy), Suresh Subramani (*PAG*s, peroxisome degradation by autophagy), Yasuyoshi Sakai (*PAZ*s, pexophagy zeocin-resistant), and Marten Veenhuis (*PDD*s, peroxisome degradation-deficient)(Thumm et al. 1994; Harding et al. 1995; Yuan et al. 1997; Sakai et al. 1998; Mukaiyama et al. 2002; Titorenko et al. 1995). In 2003, these genes were collectively renamed as 'autophagy-related (*ATG*)

genes'(Klionsky et al. 2003). So far, over 41 *ATG* genes have been identified(Mizushima 2018). These *ATG* genes were found to be highly preserved in higher eukaryotes, including mammals(Mizushima 2018). This conservation highlights the essential role of autophagy in cellular homeostasis, stress responses, and disease regulation across diverse organisms.

1.2 Molecular mechanisms of autophagy

1.2.1 Autophagy initiators

1.2.1.1 ULK1

ATG1 stands as the most upstream autophagy protein discovered in yeast, with ULK1 and ULK2 (Unc-51-like kinase) serving as its mammalian counterparts. As the only protein kinases within the autophagy pathway, ULK kinases play a vital role in initiating autophagy(Wong et al. 2013; Zachari and Ganley 2017). ULK1 and ULK2 are largely functionally redundant for autophagy induction(McAlpine et al. 2013; Lee and Tournier 2011). This thesis focuses on ULK1 signaling. ULK1 complex comprises ULK1, ATG13, FIP200 (focal adhesion kinase family interacting protein of 200 kDa, equivalent to yeast Atg17), and ATG101(Zachari and Ganley 2017). When ULK1 binds with ATG13 or FIP200, its stability and kinase activity increase, which is essential for initiating the autophagy process(Zachari and Ganley 2017).

Though the complete structure of the ULK1 complex remains undefined, we have partial crystallographic information on individual components. ULK1 features a relatively conventional kinase fold with several unique characteristics, including a substantial, positively charged loop connecting the N- and C-terminal lobes(Lazarus et al. 2015).

Additionally, ULK1 contains an autophosphorylation site at T180 in the activation loop, required for its catalytic function(Bach et al. 2011).

The crystal structures of the ATG13-ATG101 heterodimer have been elucidated. The N-terminus of ATG13 contains a HORMA (Hop1, Rev7, Mad2) domain, while ATG101 consists entirely of a HORMA domain(Qi et al. 2015). ATG101 helps recruit downstream components to autophagy initiation sites and can stabilize mammalian ATG13 HORMA through interaction(Qi et al. 2015; Mercer, Kaliappan, and Dennis 2009). Furthermore, the ATG13-ATG101 heterodimer facilitates the connection between ULK1 and FIP200, enhancing the enzymatic activity of the ULK1 complex(Papinski and Kraft 2016). When any of these binding interactions are disrupted, autophagy function becomes impaired(Papinski and Kraft 2016).

ULK1 activity undergoes tight control by upstream stress-responsive kinases AMPK (AMP activated kinase) and mTORC1 (mTOR complex 1)(Hosokawa et al. 2009; Kim et al. 2011; Alers et al. 2012; Mack et al. 2012) (Figure 2). Various cellular stressors can trigger autophagy activation by altering the balance between inhibitory and activating phosphorylation of ULK1 - specifically, inhibitory phosphorylation by mTORC1 (at site S757) and activating phosphorylation by AMPK (at sites S317, S467, S555, S574, S637, S659 and/or S777)(Egan, Shackelford, et al. 2011; Egan, Kim, et al. 2011; Shang et al. 2011; Kim et al. 2011; Mack et al. 2012; Wong et al. 2013). Interestingly, a recent study revealed that AMPK suppresses autophagy initiation by inhibiting ULK1, which protects the autophagy machinery from caspase-mediated degradation during an energy crisis, thereby preserving cellular capacity to resume autophagy once conditions improve(Park

et al. 2023). These observations underscore dual roles of AMPK in autophagy during metabolic stress.

1.2.1.2 mTORC1

The target of rapamycin (*TOR*) gene was first identified in yeast in 1991 and subsequently discovered in mammals in 1994(Heitman, Movva, and Hall 1991; Brown et al. 1994; Sabatini et al. 1994). TOR kinase was quickly recognized for its role in regulating cell growth, metabolism, and protein synthesis(Saxton and Sabatini 2017). A pivotal discovery came in 1995 when Fred Meijer's research team observed that rapamycin, which inhibits TOR, acts as an activator of autophagy(Blommaart et al. 1995).

mTORC1 (mammalian TOR complex 1) is composed of three essential components: mTOR, Raptor (regulatory associated protein of mTOR), and mLST8 (mammalian lethal with Sec13 protein 8, also known as GBL)(Laplante and Sabatini 2009). Under basal conditions, mTORC1 is recruited to the lysosomal membrane, a required step for its activation(Puertollano 2014). Disrupting lysosomal localization of mTORC1 largely prevents its amino acid-mediated activation(Manifava et al. 2016). Interestingly, artificially tethering mTORC1 to lysosomes leads to constitutive mTORC1 activation regardless of nutrient availability(Manifava et al. 2016). Additionally, mTORC1 activation relies on Rheb (Ras homolog enriched in brain), which responds to changes in bound GTP (guanosine 5'-triphosphate) and GDP (guanosine 5'-diphosphate) levels(Long et al. 2005). In its GTP-bound form, Rheb functions as a potent activator of mTORC1 kinase activity(Long et al. 2005). Studies have shown that Rheb localizes to several cellular compartments through farnesylation on its "CAAX" motif(Heard et al.

2014). Mutations of the cysteine in this motif interfere with membrane localization of Rheb and subsequently inhibit its ability to activate mTORC1(Heard et al. 2014).

The well-established negative regulator of mTORC1 signaling is the Tuberous Sclerosis Complex (TSC), a heterotrimeric complex consisting of TSC1, TSC2, and TBC1D7 [Tre2-Bub2-CDC16 (TBC) 1 domain family member 7](Manning and Cantley 2003). Among these subunits, TSC2 contains a GTPase activating protein (GAP) domain that converts Rheb from its GTP-bound active form to GDP-bound inactive form(Manning and Cantley 2003). Under basal conditions, several growth factor and mitogen-dependent pathways promote Akt (Protein kinase B)-mediated phosphorylation of TSC2 on at least four serine and threonine residues(Yu and Cui 2016). This phosphorylation enhances TSC dissociation from lysosomes and ultimately its inactivation, which preserves mTORC1 activity(Yu and Cui 2016).

mTORC1 promotes protein synthesis primarily by phosphorylating two key effectors, S6K1 (p70S6 Kinase 1) and 4EBP (eIF4E Binding Protein)(Holz et al. 2005). mTORC1-dependent phosphorylation activates S6K1, which subsequently activates downstream targets to facilitate mRNA translation initiation(Holz et al. 2005). In addition to protein synthesis, mTORC1 drives *de novo* lipid synthesis through activation of SREBP (sterol responsive element binding protein) transcription factors, which regulate genes involved in fatty acid and cholesterol biosynthesis(Porstmann et al. 2008). Recent studies reported that mTORC1 also regulates nucleotide synthesis necessary for DNA replication and ribosome biogenesis during cell growth and proliferation(Ben-Sahra et al. 2016).

Beyond regulating macromolecule synthesis, mTORC1 also inhibits catabolic pathways such as autophagy, establishing a balance between anabolism and catabolism

in response to various environmental conditions(Saxton and Sabatini 2017) (Figure 2). A critical early event in autophagy initiation is the activation of the ULK1 complex(Zachari and Ganley 2017). Under normal conditions, mTORC1 directly phosphorylates ULK1 and inhibits AMPK-mediated ULK1 activation(Alers et al. 2012). Therefore, the level of autophagy induction depends on the relative activities of mTORC1 and AMPK across diverse cellular contexts.

1.2.1.3 AMPK

AMPK forms a heterotrimeric complex composed of a catalytic α subunit and two regulatory subunits, β and γ(Hardie 2013). In humans, multiple isoforms of each subunit exist, encoded by separate genes(Hardie 2013). AMPK activation occurs through three main mechanisms. First, LKB1 (liver kinase B1) or CAMKKβ (Calcium/calmodulin-dependent protein kinase) can directly activate AMPK by phosphorylating T172(Hawley et al. 2003). Second, AMPK responds to intracellular adenosine nucleotide level changes during cellular stress(Mihaylova and Shaw 2011). When ATP levels drop, AMP or ADP binding to the γ subunits induces conformational changes that protect the activating T172 phosphorylation from phosphatases and enhance AMPK kinase activity(Mihaylova and Shaw 2011). Third, AMP (but not ATP) interaction can lead to significant allosteric activation of the kinase(Gowans et al. 2013). Together, AMP and ADP interactions with the γ subunit nucleotide binding pockets link AMPK activation to various cellular stresses(Mihaylova and Shaw 2011).

During nutrient limitation, AMPK serves as a metabolic checkpoint that inhibits cellular growth and promotes catabolic pathways like autophagy to generate more ATP(Mihaylova and Shaw 2011). AMPK regulates cell growth and initiates autophagy

primarily by suppressing mTORC1 signaling(Alers et al. 2012). When nutrients are withdrawn, AMPK inhibits mTORC1 by phosphorylating the tumor suppressor TSC2 at S1387, leading to inhibition of the small GTPase Rheb, an mTORC1 activator(Hong-Brown et al. 2012). Interestingly, even cells lacking TSC2 can respond to nutrient starvation, revealing another mode of AMPK-mediated mTORC1 inhibition: AMPK can directly inhibit mTORC1 by phosphorylating the Raptor subunit on conserved serines(Gwinn et al. 2008). Beyond mTORC1 regulation, active AMPK can initiate autophagy through direct regulation of ULK1(Mihaylova and Shaw 2011). Therefore, AMPK activation induces autophagy through a dual mechanism involving both mTORC1 suppression and direct ULK1 stimulation.

1.2.2 Important components associated with autophagy pathway

In addition to ULK1, there are four critical groups of proteins necessary for autophagosome formation including: 1) the class III phosphoinositide 3-kinase/VPS34 complex I, 2) two ubiquitin-like protein conjugation systems [ATG12–ATG5-ATG16L1 and MAP1LC3 (LC3), the mammalian ortholog of yeast Atg8], 3) WIPI proteins, and 4) transmembrane proteins including ATG9(Parzych and Klionsky 2014) (Figure 2). These protein sets work in concert with ULK1 to promote the formation of autophagosomes.

1.2.2.1 The class III phosphoinositide 3-kinase/VPS34 complex I

The class III PtdIns 3-kinase is essential for the normal functioning of the autophagy pathway, endocytosis, endosomal membrane traffic, and phagocytosis(Raiborg et al. 2013). VPS34 (vacuolar protein sorting 34), a member of the PtdIns 3-kinase family of lipid kinases, exists in several distinct complexes that regulate

various cellular processes(Raiborg et al. 2013). The autophagy-associated VPS34 complexes include the catalytic VPS34 subunit, the VPS15 scaffold, the regulatory Beclin-1 (yeast Atg6 homologue), and either ATG14 or UVRAG (UV resistance-associated gene) subunits(Lőrincz et al. 2014).

Pro-autophagic VPS34 complex activity is regulated by three upstream initiators: mTORC1, ULK1, and AMPK(Russell et al. 2013; Yuan, Russell, and Guan 2013; Kim et al. 2013; Dossou and Basu 2019). During nutrient abundance conditions, when ULK1 and AMPK signaling is suppressed, active mTORC1 directly inhibits pro-autophagic VPS34 complexes by phosphorylating the ATG14 subunit(Yuan et al. 2013). Interestingly, *in vitro* incubation of mTORC1 with VPS34-VPS15-Beclin-1 complexes does not affect lipid kinase activity(Munson et al. 2015). However, adding recombinant ATG14 to the VPS34 complex results in inhibition of lipid kinase activity through mTORC1-mediated phosphorylation, highlighting critical role of ATG14 in connecting the VPS34 complex substrate to the kinase(Diao et al. 2015).

In amino acid-deprived cells, ULK1 phosphorylates the pro-autophagic VPS34 complex subunits Beclin-1 and ATG14, resulting in phosphorylation of phosphatidylinositol (PtdIns) at the 3′ position on the inositol ring, producing phosphatidylinositol(3)phosphate (PtdIns(3)P)(Russell et al. 2013; Wold et al. 2016; Park et al. 2016). This PtdIns(3)P production recruits downstream autophagy pathway components and is essential for autophagosome formation(Obara and Ohsumi 2011). Additionally, during starvation, AMPK phosphorylates Beclin-1 at S91/94, which is sufficient to stimulate VPS34 complex lipid kinase activity(Kim et al. 2013).

Bcl-2 (B-cell lymphoma 2) and Rubicon (RUN domain Beclin 1-interacting and cysteine-rich containing protein) are known inhibitors of VPS34 complexes(Kang et al. 2011). Under basal conditions, hydrophobic groove in Bcl-2 interacts with BH3 domain of Beclin-1, disturbing Beclin-1/VPS34 binding, reducing lipid kinase activity, and inhibiting autophagy(Decuypere et al. 2012). Conversely, under stress conditions, Bcl-2 dissociates from Beclin-1(Decuypere et al. 2012). UVRAG promotes autophagy by enhancing the interaction between released Beclin-1 and VPS34, increasing VPS34 complex activity(Wu et al. 2018). Besides its role in early autophagy stages, UVRAG mediates autophagosome maturation by binding to the HOPS (homotypic fusion and vacuole protein sorting) complex, promoting autophagosome-lysosome fusion(Jiang et al. 2014). Under nutrient abundance conditions, Rubicon binds to the UVRAG subunit of VPS34 complexes, disrupting UVRAG-HOPS interaction and decreasing VPS34 lipid kinase activity(Jiang et al. 2014). Additionally, nutrient-activated mTORC1 enhances Rubicon-UVRAG-containing VPS34 complexes through direct UVRAG phosphorylation(Munson et al. 2015).

In summary, mTORC1, ULK, and AMPK directly regulate pro-autophagic VPS34 kinase activity, ensuring tightly controlled autophagy initiation in response to cellular stresses and emphasizing the importance of VPS34 regulation.

1.2.2.2 Ubiquitin-like protein conjugation systems [ATG12–ATG5-ATG16L1 and MAP1LC3 (LC3)]

In the autophagy pathway, ATG12 and microtubule-associated protein 1 light chain 3 (LC3, the primary characterized homologue of yeast ATG8) share structural similarities with the ubiquitin conjugation machinery(Geng and Klionsky 2008). Each forms a distinct

ubiquitin-like conjugation system essential for autophagosome formation(Geng and Klionsky 2008) (Figure 2).

In the first system, ATG12 is activated by the E1-like enzyme ATG7 through thioester bond formation(Tanida et al. 1999). The activated ATG12 is then transferred to the E2-like enzyme ATG10, resulting in conjugation to its target protein ATG5(Shintani et al. 1999) (Figure 2). This interaction is irreversible, causing ATG12 and ATG5 to exist predominantly in conjugated forms(Shintani et al. 1999). ATG5 then recruits the complex to the coiled-coil protein ATG16L1, forming a trimeric ATG16L1-ATG5-ATG12 complex(Mizushima et al. 1999). This complex plays a crucial role in autophagosome formation and elongation through its function in LC3 lipidation(Mizushima et al. 1999) (Figure 2).

The second ubiquitin-like conjugation system involves the conjugation of LC3 to phosphatidylethanolamine (PtdEth), commonly known as LC3 lipidation(Kirisako et al. 2000). Initially, the C-terminus of the ubiquitin-like protein LC3 is cleaved by ATG4 to form LC3-I, enabling its transfer to and activation by the E1-like enzyme ATG7(Kirisako et al. 2000) (Figure 2). The activated LC3-I is subsequently transferred to the E2-like enzyme ATG3(Kirisako et al. 2000). The ATG16L1-ATG5-ATG12 complex functions as an E3-like enzyme, recruiting LC3-I to the membrane lipid PtdEth to form LC3-II, the lipidated form of LC3(Fujita et al. 2008). The LC3 lipidation catalyzed by the ATG16L1 complex is vital to the autophagy pathway and serves as a measurement for autophagy induction(Geng and Klionsky 2008).

1.2.2.3 WIPI proteins

WIPI proteins (WD-repeat proteins interacting with phosphoinositides) are members of the human PROPPIN (β-propellers that bind phosphoinositides) family, consisting of four core paralogs—WIPI1, WIPI2, WIPI3 (also known as WDR45B), and WIPI4 (also known as WDR45)—along with various splice variants(Proikas-Cezanne et al. 2015). Among them, WIPI1 and WIPI2 have been specifically observed to localize to both the inner and outer membranes of forming autophagosomes, likely resulting from their specific interaction with PtdIns(3)P through evolutionarily conserved residues(Proikas-Cezanne et al. 2015). In addition to their role as PtdIns(3)P-binding proteins, WIPIs serve as critical PtdIns(3)P effectors during early stages of autophagy(Dooley et al. 2014). Particularly, WIPI2 functions as a scaffold that recruits the ATG12–ATG5–ATG16L1 complex to the phagophore assembly site(Dooley et al. 2014) (Figure 2). This recruitment is essential for the lipidation of LC3, a key step in autophagosome biogenesis(Dooley et al. 2014).

1.2.2.4 Transmembrane proteins

In the autophagy pathway, ATG9 and VMP1 (vacuole membrane protein 1) function as crucial transmembrane proteins(Yoshii and Mizushima 2015). During starvation conditions, ATG9 relocates from the Golgi network and late endosomes to peripheral regions that overlap with LC3-positive autophagosomes(Takahashi et al. 2011). This starvation-induced cycling of ATG9 requires both ULK1 and VPS34 complexes(Young et al. 2006; Burman and Ktistakis 2010). Notably, ATG9 cycling contributes significantly to the delivery of membrane components necessary for autophagosome formation(Zhuang et al. 2017) (Figure 2).

The stress-responsive induction of autophagy, whether triggered by starvation or rapamycin administration, depends on VMP1 functionality(Molejon et al. 2013). Remarkably, VMP1 overexpression is sufficient to initiate autophagy even in nutrient-replete conditions(Molejon et al. 2013). Furthermore, VMP1 has been documented to interact with Beclin-1, a constituent of the VPS34 complex(Molejon et al. 2013). Recent research has identified TP53INP2 (tumor protein 53-induced nuclear protein 2) as a novel VMP1-binding protein that translocates from the nucleus to autophagosomes upon autophagy induction, where it appears to facilitate the recruitment of Beclin-1 and LC3 to autophagosomal sites, potentially through its interaction with VMP1(Nowak et al. 2009). Intriguingly, TP53INP2 selectively binds to LC3 and VMP1, but not to Beclin-1(Nowak et al. 2009). Collectively, these findings suggest that VMP1 functions as a transmembrane scaffold that directs downstream components to the phagophore during autophagosomal biogenesis.

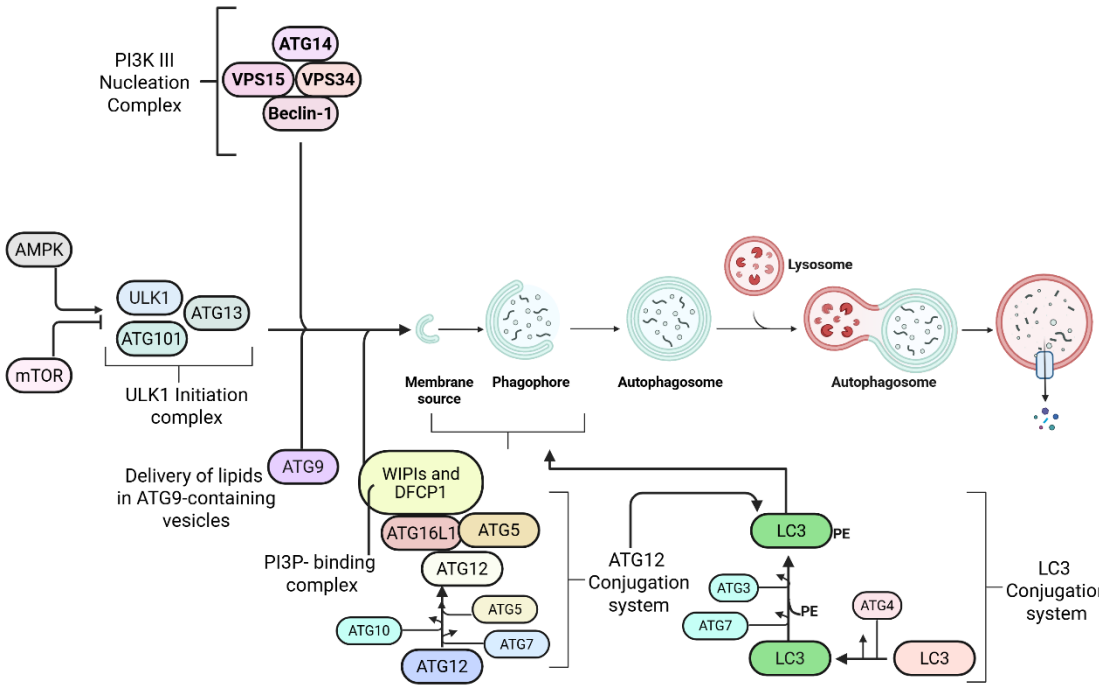

Figure 2: Schematic overview of the autophagy process and its key regulatory components. mTOR and AMPK serve as key regulators of autophagy, functioning as a negative and positive regulator, respectively. The process is initiated with the formation of a phagophore that engulfs cytoplasmic material, subsequently maturing into an autophagosome. Fusion of the autophagosome with a lysosome forms an autolysosome, where the cargo is degraded. Autophagy is tightly regulated by autophagy-related proteins (ATGs), including the ULK1 initiation complex and the class III PI3K nucleation complex. The ATG12–ATG5–ATG16L1 complex functions as an E3-like ligase to facilitate the lipidation of LC3, a key step in autophagosome formation. ATG12 is covalently conjugated to ATG5. This complex associates with ATG16L1 to localize at the phagophore membrane, where it promotes LC3 conjugation to PtdEth. In addition, ATG9-containing vesicles contribute to membrane expansion.

1.3 Selective autophagy

Although autophagy was initially characterized as a bulk degradation pathway that indiscriminately engulfs and degrades cytosolic components in response to starvation conditions, du Duve proposed the potential existence of selective autophagy pathways that could target particular macromolecules in 1966(de Duve and Wattiaux 1966; Klionsky 2007). In the 1970s, researchers began identifying selective forms of autophagy(Klionsky 2007). Particularly in 1973, Robert Bolender and Ewald Weibel provided the first evidence of autophagic degradation specifically targeting the smooth endoplasmic reticulum(Bolender and Weibel 1973). This was followed in 1977 by Jacques Beaulaton and Richard Lockshin, who observed selective mitochondrial degradation during insect metamorphosis in *Antheraea polyphemus*(Beaulaton and Lockshin 1977). Later, Marten Veenhuis's group showed the targeted removal of peroxisomes in the yeast *Hansenula polymorpha*(Veenhuis et al. 1983). Several follow-up studies validated these findings across various yeast species and higher eukaryotes, leading to the conclusion that selective autophagy plays an important role in cellular metabolism by facilitating the removal of unnecessary and damaged organelles(Klionsky 2007).

Selective autophagy can be classified into several types based on the substrate involved, including mitophagy (mitochondria), pexophagy (peroxisomes), ER-phagy (endoplasmic reticula), lipophagy (lipids), lysophagy (lysosomes), ribophagy (ribosomes), aggrephagy (protein aggregates), and xenophagy (intracellular pathogens)(Gatica, Lahiri, and Klionsky 2018; Germain and Kim 2020; Papadopoulos and Meyer 2017; Ossareh-Nazari et al. 2010; Lamark and Johansen 2012; Rubio-Tomás, Sotiriou, and Tavernarakis 2023; Narendra et al. 2008). This thesis will explore the characterization of selective

autophagy pathways in mammalian systems, with particular emphasis on three specific types: xenophagy, which involves the targeted degradation of intracellular pathogens; ER-phagy, the selective clearance of endoplasmic reticulum components; and pexophagy, the specific elimination of peroxisomes.

While selective autophagy share the requirement for the core autophagy machinery (ATG proteins) with bulk autophagy, it also involves specialized proteins known as autophagy receptors(Zaffagnini and Martens 2016). These receptors recognize and bind to specific cargo, directing them to autophagosomes via interactions with LC3(Kim et al. 2016). Autophagy receptors can be categorized into ubiquitin-bound and membrane-associated groups(Kim, Kwon, and Song 2016; Vargas et al. 2023).

1.3.1 Ubiquitin-bound autophagy receptors

Selective autophagy relies on precise substrate recognition, typically mediated by the ubiquitylation of target components(Vainshtein and Grumati 2020). Ubiquitinated substrates are identified and sequestered by a group of ubiquitin-binding autophagy receptors, such as p62 (also known as sequestosome-1 or SQSTM1), TAX1BP1 (Tax1-binding protein 1), NDP52 (CALCOCO2), NBR1, and OPTN (optineurin), and others(Johansen and Lamark 2020). These receptors possess both LC3-interacting regions (LIR) and ubiquitin-binding domains (UBD), which enable them to recruit ubiquitinated cargos to autophagosomal sites for degradation(Kim, Kwon, and Song 2016; Kirkin and Rogov 2019; Johansen and Lamark 2020).

Furthermore, functions of ubiquitin-bound receptors are regulated through post-translational modifications(Vargas et al. 2023). For instance, ubiquitination of p62 by E3

ligase TRIM21 or KEAP1–cullin 3 enhances its cargo sequestration capacity(Pan et al. 2016; Lee et al. 2017). TBK1-mediated phosphorylation of NDP52 and OPTN increases their binding affinity to ubiquitin chains, thereby promoting an elevated flux of selective autophagy(Heo et al. 2015; Moore and Holzbaur 2016; Richter et al. 2016).

1.3.2 Membrane-associated autophagy receptors

Membrane-associated receptors are either inherently present on, or recruited to, the surface of target organelles where they facilitate the recognition of damaged organelles by the autophagy machinery(Anding and Baehrecke 2017). Examples of membrane-bound autophagy receptors include FAM134B, which is involved in ER-phagy; PEX14 and PMP70, receptors for pexophagy; and FUNDC1, which mediates mitophagy(Chen et al. 2022; Cho et al. 2018; Li et al. 2021). FAM134B (also known as Reticulophagy Regulator 1), the first and most extensively studied ER-phagy receptor, is anchored in ER sheets via its transmembrane regions(Mo et al. 2020). It contains two key domains: the LC3-interacting region (LIR), which facilitates the recruitment of autophagy machinery, and the reticulon-homology domain (RHD), which contributes to ER-phagy regulation and the maintenance of ER homeostasis(Mo et al. 2020). PEX14 (Peroxin 14), a peroxisomal membrane protein, has been shown to interact with LC3 to facilitate pexophagy in response to starvation conditions(Jiang et al. 2015). Meanwhile, ubiquitination of PMP70 (70 kDa peroxisomal membrane protein) promotes its interaction with NBR1 and p62 and subsequently initiates pexophagy(Sargent et al. 2016; Deosaran et al. 2013; Cho et al. 2018). FUNDC1 (FUN14 domain-containing 1) resides on the outer mitochondrial membrane (OMM) and features an N-terminal LIR motif that extends into the cytosol(Li et al. 2021). This structural arrangement enables FUNDC1 to facilitate the

recognition and autophagic degradation of mitochondria, particularly in response to hypoxic stress(Liu et al. 2012; Li et al. 2021).

1.4 Xenophagy

The earliest indication of involvement of autophagy in eliminating harmful pathogens was reported by Yasuko Rikihisa's group in 1984, when they observed the initiation of autophagy in response to *Rickettsia* bacterial infection(Rikihisa 1984). Nevertheless, the antibacterial role of autophagy was not conclusively demonstrated until 2004, when Tamotsu Yoshimori's team analyzed *Streptococcus pyogenes* in autophagy-deficient embryonic stem cells, and the research groups led by Vojo Deretic and Maria Colombo reported the autophagic degradation of *Mycobacterium tuberculosis*(Nakagawa et al. 2004; Gutierrez et al. 2004). Subsequent studies also confirmed these observations(Ogawa et al. 2005).

1.4.1 *Salmonella* as a model pathogen

The genus *Salmonella* includes two species: *S. bongori* and *S. enterica* (*Salmonella bongori* and *Salmonella enterica,* respectively), with the latter responsible for most infections in humans and animals(Brenner et al. 2000; Andino and Hanning 2015). *S. enterica* is further divided into six subspecies and over 2,500 serovars, distinguished by surface structures such as flagella, carbohydrates, and lipopolysaccharides(Brenner et al. 2000). Among them, *Salmonella enterica* serovar Typhimurium (hereafter referred to as *Salmonella*) is the most extensively studied in relation to host autophagy and serves as a model pathogen in this study(Garai et al. 2012). *Salmonella* can infect a range of host cell types, both phagocytic and non-phagocytic, including macrophages and

epithelial cells(Andino and Hanning 2015). Key virulence factors are encoded within *Salmonella* pathogenicity islands (SPIs), with SPI-1 and SPI-2 being the most characterized(Rychlik et al. 2009). These regions encode two distinct type III secretion systems (T3SS-1 and T3SS-2), which inject bacterial effectors into host cells to manipulate host signaling and facilitate bacterial invasion, replication, and survival(Kato et al. 2018). After internalization, *Salmonella* resides in specialized membrane-bound compartments known as *Salmonella*-containing vacuoles (SCVs), which support intracellular replication(Steele-Mortimer 2008) (Figure 3).

1.4.2 Xenophagy

Ubiquitination of *Salmonella* and *Salmonella*-containing vacuoles (SCVs) marks internalized bacteria for host defense, triggering autophagy via M1- and K63-linked ubiquitin chains(Herhaus and Dikic 2018) (Figure 3). These chains are recognized by autophagy receptors such as p62, NDP52, and OPTN, which recruit the bacteria to LC3-positive autophagosomes for degradation(Lippai and Lőw 2014). In addition to the ubiquitination pathway, damaged SCVs can also be detected by galectin-8, a cytosolic lectin(Thurston et al. 2012) (Figure 3). NDP52 specifically interacts with galectin-8 and facilitates its recruitment to LC3 via its LC3-interacting region (LIR), effectively linking the bacteria to phagophores to initiate autophagy(Thurston et al. 2012). Additionally, NDP52 works with OPTN to mediate the autophagic clearance of *Salmonella*(Richter et al. 2016).

Several studies have shown that xenophagy shares upstream regulators with starvation-induced autophagy. For instance, *Salmonella*-induced membrane damage can reduce intracellular amino acid levels, relieving mTORC1 repression and triggering

autophagy(Tattoli et al. 2012). Furthermore, the immunity-related GTPase IRGM, specific to xenophagy, regulates core autophagy components including VPS34, ULK1, and AMPK(Chauhan et al. 2015). While dispensable for starvation-induced autophagy, IRGM is essential for bacterial clearance and is a common viral target(Grégoire et al. 2011). These findings underscore that xenophagy integrates both shared autophagy pathways and unique pathogen-specific responses, though the precise upstream signals remain to be characterized.

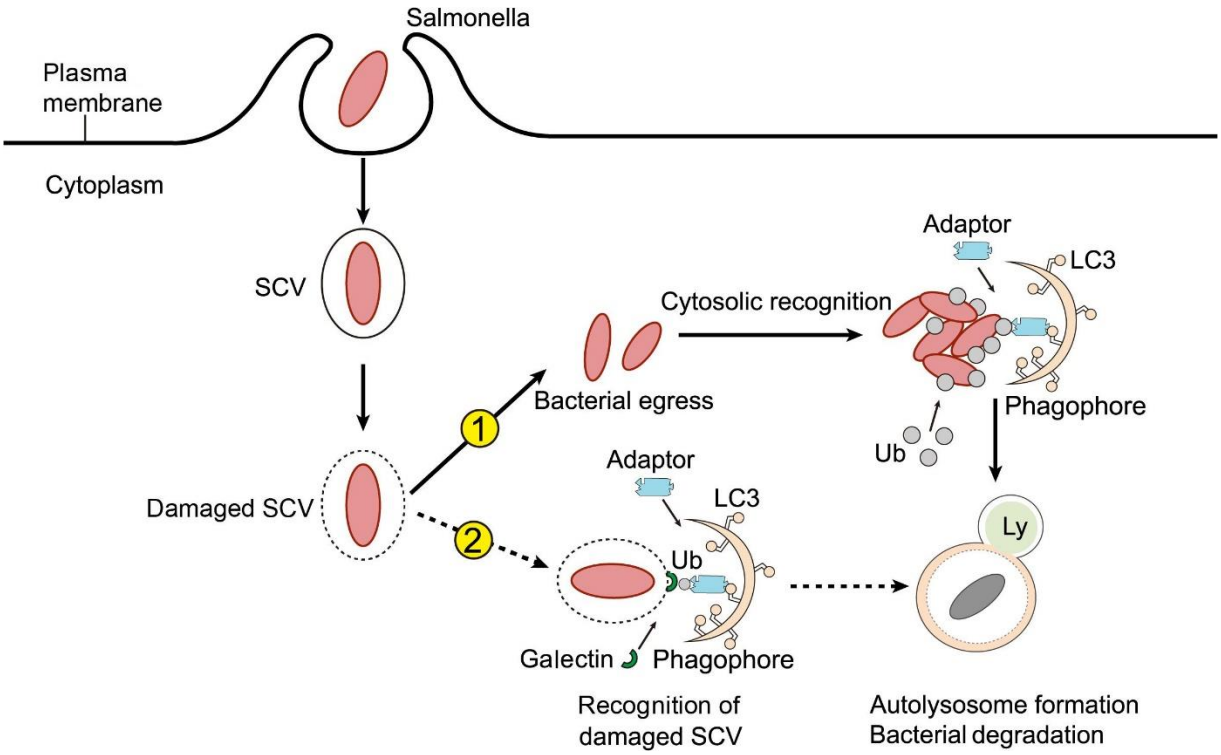

Figure 3: Salmonella-induced xenophagy (adapted from Wu et al. 2020). After entering host cells, *Salmonella* resides in the *Salmonella*-containing vacuole (SCV). Damage to the SCV by Type III secretion system (T3SS-1) can lead to one of two outcomes: cytosolic escape or vacuolar targeting. Cytosolic *Salmonella* are ubiquitinated and targeted for autophagy via adaptor proteins that recruit LC3. Alternatively, bacteria within damaged SCVs are marked for autophagy through the recruitment of galectins, ubiquitin, and adaptors to the compromised vacuolar membrane.

1.5 ER-phagy

The endoplasmic reticulum (ER) is a dynamic organelle that regulates multiple cellular functions including detoxification, redox regulation, lipid synthesis, and calcium storage(Alberts et al. 2002). Autophagy plays a critical role in maintaining the ER homeostasis by targeting ER fragments and membranes for lysosomal degradation(Chino and Mizushima 2020). The targeted removal of ER via autophagy is mediated by ER-phagy receptors, which include FAM134B, RTN3L, CCPG1, SEC62, TEX264, and ATL3 in mammals(Mo, Chen, and Zhang 2020; Grumati et al. 2017; Smith et al. 2018; Fumagalli et al. 2016; Chino et al. 2019; Chen et al. 2019) (Figure 4). These ER-phagy receptors are localized to ER subdomains and facilitate recruitment of autophagy machinery via their LC3/GABARAP/ATG8-interacting motifs (LIR, GIM or AIM)(Chino and Mizushima 2023) (Figure 4). Additionally, phosphorylation of residues located upstream of the LIR sequence can regulate its binding affinity(Chino and Mizushima 2023). For instance, casein kinase 2-mediated phosphorylation of upstream serine residues in the LIR of TEX264 enhances its interaction with ATG8 family proteins(Chino et al. 2022). Notably, studies have shown that the LC3-conjugating system is dispensable for the ER association with autophagosomes, suggesting ER receptors can interact with other upstream autophagy complexes(Chino and Mizushima 2023). For example, CCPG1 can bind directly to a member of ULK1 complex-FIP200, which is activated by phosphorylation(Zhou et al. 2021). ATL3 has been reported to directly interact with ULK1 and ATG13, promoting the recruitment and assembly of the ULK1 complex on the ER membrane to initiate ER-phagy(Liu et al. 2021). TEX264 has likewise

been shown to associate with proteins involved in the early stages of autophagosome biogenesis, such as FIP200 and WIPI2(Chino et al. 2019).

Membrane-bound ER-phagy receptors are categorized based on their structural features: those with a single transmembrane domain, like CCPG1 and TEX264, likely act as basic receptors or luminal sensors, while receptors with reticulon homology domains (RHDs), such as FAM134B and RTN3L, have ER-fragmentation capabilities(Chino and Mizushima 2023). RHDs promote membrane curvature by inserting partially into the membrane(Zurek et al. 2011). Overexpression or multimerization of receptors like FAM134B or RTN3L can trigger ER fragmentation(Grumati et al. 2017; Bhaskara et al. 2019). Additionally, FAM134B contains amphipathic helices that further facilitate membrane bending(Brady et al. 2015; Bhaskara et al. 2019).

In addition, ER-phagy receptors in mammals possess both functional redundancy and specialization(Chino and Mizushima 2023). For instance, while some receptors like TEX264, FAM134B, and CCPG1 work cooperatively in basal and starvation-induced ER-phagy, they also perform distinct roles(Chino et al. 2019; Chino and Mizushima 2023). This diversity reflects the structural complexity of the ER, which includes specialized domains such as the nuclear envelope, sheets, and tubules—each with unique functions. Specific ER-phagy receptors target different ER regions; for instance, FAM134B, TEX264, CCPG1, and SEC62 primarily mediate degradation of ER sheets, whereas RTN3L and ATL3 target ER tubules(Grumati et al. 2017; Chen et al. 2019; Mo, Chen, and Zhang 2020; An et al. 2019; Hoyer et al. 2024).

Beyond autophagy receptors, additional pathways have been identified that regulate ER-phagy. Disruption of mitochondrial oxidative phosphorylation impairs this

process(Liang et al. 2020). DDRGK1 has been found to recruit the UFMylation machinery—a ubiquitin-like post-translational modification system—to the ER membrane, a step essential for the autophagic clearance of ER sheets(Liang et al. 2020).

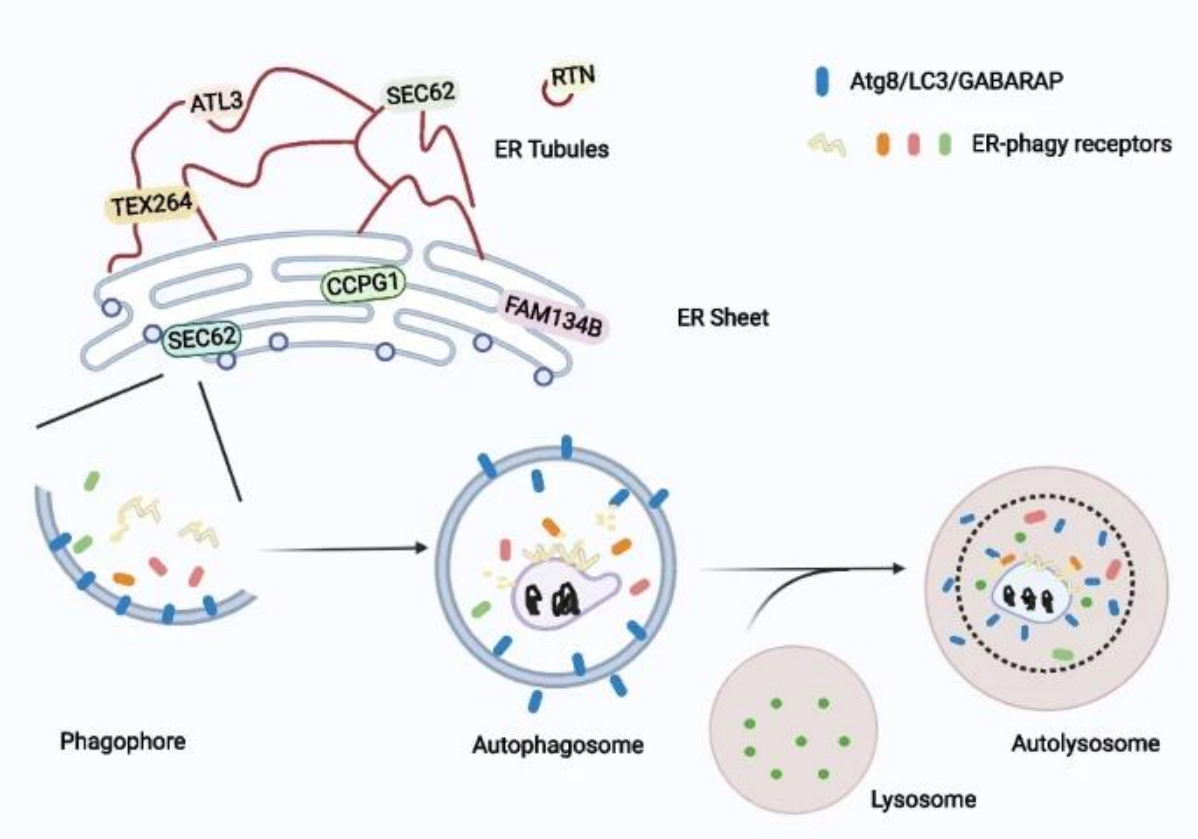

Figure 4: ER-phagy diagram (adapted from Liu et al. 2024). ER-phagy receptors recruit damaged ER subdomains to the autophagosomal sites for degradation through interaction with LC3/GABARAP/Atg8.

1.6 Pexophagy

Peroxisomes, first described in the 1960s by Christian de Duve, are small, single-membrane-bound organelles found in most eukaryotic cells(de Duve and Baudhuin 1966). Each mammalian cell contains several hundred of these dynamic and multifunctional structures(Zhukov and Popov 2023). Peroxisomes are involved in both catabolic and anabolic processes and contribute to various biological functions across different tissues and organisms, including bile acid synthesis, ether phospholipid synthesis, regulation of fatty acid beta-oxidation, and detoxification of hydrogen peroxide(Jo and Cho 2019; Dixit et al. 2010; Fransen et al. 2012). Peroxisomes are highly dynamic organelles whose number, shape, and size are regulated by environmental and developmental signals(He et al. 2021). Their biogenesis is complex and involves over 30 peroxin (PEX) proteins(He et al. 2021). Since peroxisomes lack their own genome and protein synthesis machinery, they rely on the import of matrix proteins from the cytosol(Mahalingam et al. 2021). PEX proteins are critical for targeting and inserting peroxisomal membrane proteins (PMPs), importing matrix proteins, regulating peroxisome size, and maintaining overall peroxisomal function(Mahalingam et al. 2021).

Beyond their role in peroxisome biogenesis, PEX proteins also participate in the pexophagy pathway(Mahalingam et al. 2021). Upon cellular stress, the peroxisomal E3 ubiquitin ligase PEX2 becomes active and ubiquitinates peroxisomal membrane proteins such as PMP70 and PEX5(Platta et al. 2016; Sargent et al. 2016) (Figure 5). These ubiquitinated peroxisomes are then targeted for autophagic degradation via the autophagy receptors NBR1 and p62(Sargent et al. 2016). PEX14, a component of the peroxisomal docking complex, has been found to preferentially bind to LC3, thereby

directly promoting the sequestration of peroxisomes into autophagosomes during starvation-induced pexophagy(Jiang et al. 2015). In the early stages of starvation, levels of PEX13—a peroxisomal membrane protein involved in matrix protein import—are rapidly decreased(Demers et al. 2023). This downregulation appears to be a prerequisite for the efficient induction of pexophagy, possibly by altering the import machinery and signaling a shift toward peroxisome turnover(Demers et al. 2023). Environmental stressors such as elevated reactive oxygen species (ROS) and hypoxia further stimulate pexophagy by enhancing the ubiquitination of PEX5(Zhang et al. 2015). Conversely, the cell possesses mechanisms to limit or reverse pexophagy when it is no longer needed. The AAA-type ATPase complex composed of PEX1, PEX6, and their anchoring partner PEX26, along with the deubiquitinating enzyme USP30, works to remove ubiquitinated proteins from the peroxisomal membrane(Law et al. 2017; Riccio et al. 2019) (Figure 5). By reversing ubiquitination and extracting these proteins, this system prevents the premature or unnecessary degradation of peroxisomes, thereby preserving essential organelle function and contributing to cellular balance(Cho et al. 2018).

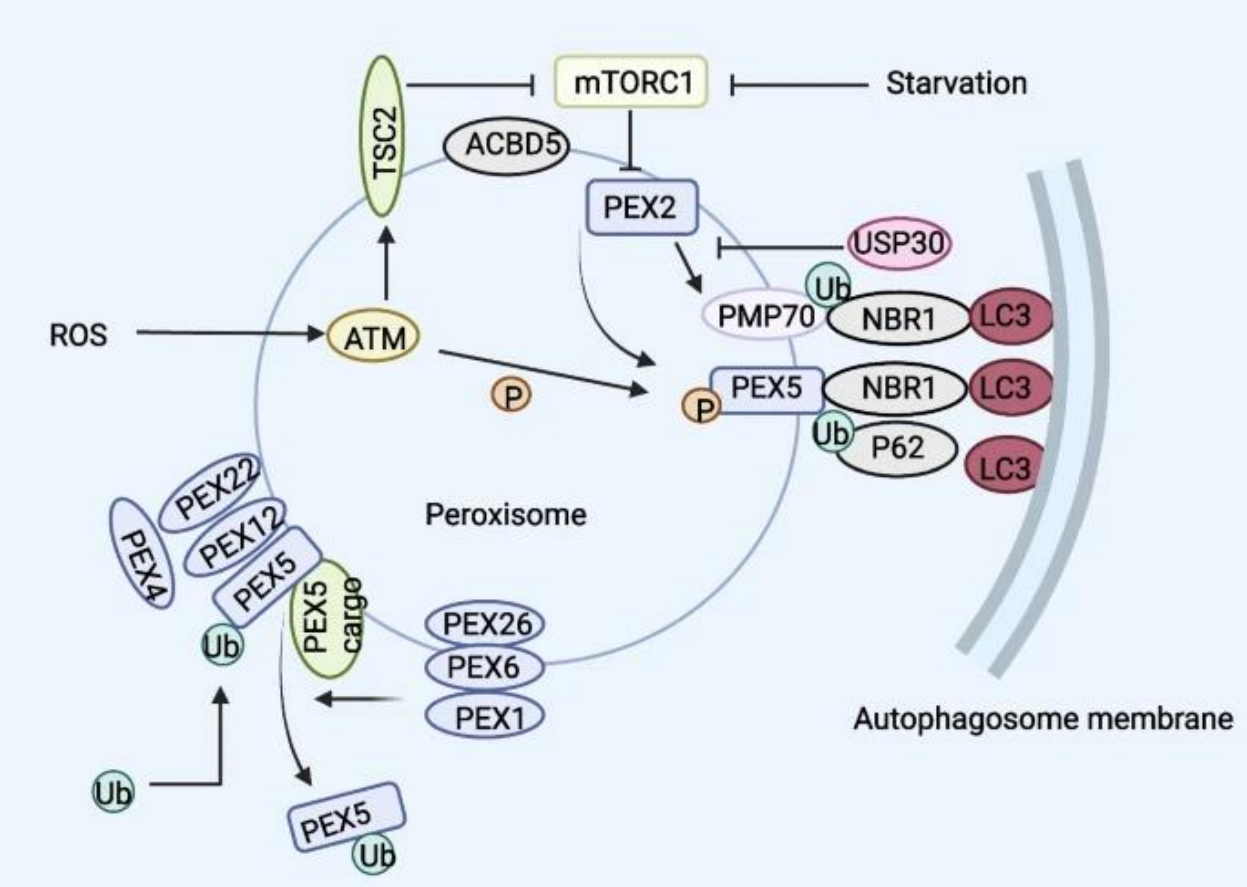

Figure 5: Pexophagy diagram (adapted from Liu et al. 2024). Upon stress conditions, PMP70 and PEX5 are ubiquitinated by active PEX2, which triggers pexophagy through p62 and NBR1 interaction. The AAA-type ATPase complex composed of PEX1, PEX6, and PEX26, along with the deubiquitinating enzyme USP30, prevents pexophagy by removing ubiquitinated proteins from the peroxisomal membrane.

1.7 Autophagy in disease

1.7.1 Core autophagy machinery in disease

Dysregulation of autophagy has been implicated in a variety of diseases(Yang and Klionsky 2020). A key breakthrough came in 1999 when it was shown that monoallelic deletion of the *Beclin-1* gene promotes tumorigenesis(Liang et al. 1999). Beclin-1, frequently deleted in ovarian (75%) and breast (50%) cancers, is now recognized as a haploinsufficient tumor suppressor(Qu et al. 2003). Restoring Beclin-1 expression can inhibit tumor growth in mouse models(Qu et al. 2003). Similarly, loss-of-function mutations in other core autophagy (ATG) genes—such as *ATG2B*, *ATG5*, *ATG9B*, and *ATG12*—are found in cancers like gastric and colorectal tumors with microsatellite instability(Kang et al. 2009). In mice, loss of upstream ATG genes (e.g., *FIP200*, *Atg13*, *Beclin-1*) causes embryonic lethality, while loss of downstream ATG genes (e.g., *Atg3*, *Atg5*, *Atg12*) results in perinatal death(Kuma et al. 2017). These genetic differences also affect immune responses, as seen in macrophage-specific *ATG* knockouts showing distinct phenotypes in lung inflammation and influenza resistance(Lu et al. 2016).

In addition, mutations in core autophagy genes have been linked to neurodegenerative diseases(Yang and Klionsky 2020). Parkinson's disease (PD) is a progressive neurological disorder marked by motor impairments and the accumulation of alpha-synuclein (SNCA) aggregates, a key component of Lewy bodies(Stefanis 2012). Growing evidence suggests that autophagy contributes to PD development(Nechushtai et al. 2023). Genetic studies in PD patients have linked altered expression of autophagy-related genes—such as *ATG5*, *ATG7*, *ATG12*, and *LC3*—to the disease(Chen, Zhu, et al.

2013; Chen, Pang, et al. 2013; Li et al. 2017; Xu et al. 2013). Dysregulated autophagy process has also been observed in the brain tissues of PD patients and animal models(Friedman et al. 2012). Motor neuron (MN) diseases are a group of neurodegenerative disorders characterized by the selective degeneration of MNs, with amyotrophic lateral sclerosis (ALS) being the most common form(Salameh et al. 2015). Elevated levels of autophagy-related proteins, including LC3, Beclin-1, p62, and the Atg5–Atg12 complex, have been observed in spinal MNs of both sporadic and familial ALS patients, as well as in animal models(Hetz et al. 2009; Tian et al. 2011; Li, Zhang, and Le 2008). *In vivo* imaging studies of ALS mouse models have further demonstrated increased GFP-LC3 signals in MNs, indicating autophagosome accumulation throughout disease progression, from early to late symptomatic stages(Tian et al. 2011). Furthermore, impaired autophagy has been associated with the pathogenesis of Huntington's disease (HD), a condition marked by the accumulation of mutant huntingtin (mHTT) protein caused by polyglutamine expansion(Luo and Yang 2024). Specifically, dysregulated ULK1-mediated phosphorylation of ATG14 has been observed in HD genetic cell models and animal models(Wold et al. 2016). mHTT also disrupts Beclin-1 stability, thereby reducing autophagy activity(Ashkenazi et al. 2017). *ATG7* gene variants are also associated with earlier HD onset(Metzger et al. 2010). Although autophagy generally suppresses HTT aggregates, deleting the autophagy receptor p62 unexpectedly reduces nuclear inclusions and disease symptoms in HD mouse model, suggesting complex roles for autophagy components(Kurosawa et al. 2015). Further research is needed to clarify how both core autophagy genes and cargo receptors affect HD pathology.

1.7.2 Selective autophagy in disease

While autophagy was initially described as a non-specific process that degrades bulk cytosolic content, it is now well established that autophagy also functions as a selective degradation pathway, playing crucial roles in normal physiology and in various diseases(Ma et al. 2024). In fact, numerous studies have shown that disruption of selective autophagy components is linked to the development of distinct pathological conditions. Interestingly, defects in selective autophagy are often related to the specific biology and environment of the cell or tissue. For instance, in the brain, where neurons persist for the lifetime of the organism, disruptions in proteome homeostasis are the predominant issue(Sin and Nollen 2015). In contrast, in rapidly dividing cells of the gut, impairments in the innate immune response are prevalent(Wiertsema et al. 2021).

Xenophagy plays a critical role in human inflammatory disorders by facilitating the direct clearance of intracellular bacteria and activation of pattern recognition receptor (PRR) signaling(Sharma et al. 2018). Importantly, genome-wide association studies have linked single nucleotide polymorphisms of xenophagy-specific protein IRGM to progression of Crohn’s disease (CD), a chronic gastrointestinal inflammatory condition caused by an impaired immune response to pathogens in genetically predisposed individuals(Verstockt et al. 2018).

Mutations in ER-phagy receptors have been implicated in several diseases. Mutations in FAM134B cause hereditary sensory and autonomic neuropathy type 2B (HSAN2B), a autosomal recessive disorder marked by loss of sensory fibers and impaired pain, temperature, and touch perception due to degeneration of dorsal root and autonomic ganglia(Kurth et al. 2009; Davidson et al. 2012; Aydinlar et al. 2014). FAM134B

mutations or altered expression are also linked to colorectal cancer (CRC) and its aggressiveness(Kasem et al. 2014; Islam et al. 2017; Islam et al. 2018). TEX264 also serves as a CRC marker and is highly expressed in glioblastoma cells under ER stress and autophagy-inducing treatments(X.-X. Liu and Liu 2015; Reggiori and Molinari 2022). Furthermore, mutations in ATL3 cause hereditary sensory and autonomic neuropathy 1 (HSAN1), a peripheral nervous system disorder; specifically, the Y192C and P338R mutations impair interaction of ATL3 with GABARAP and its role in ER-phagy(Xu et al. 2019; Fischer et al. 2014; Chen et al. 2019). RTN3L, enriched in neurons, is associated with AD and has been found to harbor multiple variants in patients with sporadic early and late-onset forms of the disease(Zou et al. 2018). Additionally, alterations in SEC62, such as mutations, amplification, and overexpression, have been implicated in cancer development(Linxweiler et al. 2017). Dysregulated SEC62 expression is commonly found in prostate, cervical, thyroid, liver, lung, and other cancers(Bergmann et al. 2017). High SEC62 levels enhance tumor invasiveness, metastatic potential, and resistance to ER stress-induced cell death, resulting in decreased patient survival rates(Bergmann et al. 2017).

Mutations in PEX proteins, which are essential for peroxisome biogenesis and pexophagy, are implicated in peroxisome biogenesis disorders (PBDs)—a group of autosomal recessive diseases marked by defective peroxisome assembly and function(Cho et al. 2018). Among these, Zellweger syndrome (ZS) is one of the most severe(Zellweger et al. 1988). Most PBDs are linked to mutations in the peroxisomal AAA-type ATPase complex (PEX1, PEX6, PEX26), which plays a vital role in peroxisome formation and recycling of ubiquitinated PEX5(Nazarko 2017). Notably, this complex has

been shown to prevent excessive pexophagy and PBDs pathogenesis(Law et al. 2017). Evidence suggests that up to 65% of PBDs are caused by dysregulated pexophagy rather than impaired biogenesis(Nazarko 2017). Furthermore, exposure to autophagy inhibition such as chloroquine can improve peroxisomal function in PBD patient-derived cells(Law et al. 2017). These findings highlight the critical role of pexophagy regulation in the development of PBDs.

1.8 Autophagy genetic screens

Autophagy has been implicated in numerous diseases, making the investigation of its regulatory mechanisms essential for advancing human health(Ichimiya et al. 2020). Major breakthroughs in elucidating autophagy mechanisms have stemmed from genetic approaches used to map the autophagy pathway in *Saccharomyces cerevisiae*(Tsukada and Ohsumi 1993). This foundational work has naturally inspired the application of genetic screening strategies in mammalian systems to deepen our understanding of autophagy in higher eukaryotes.

A widely used method to measure autophagic flux in these screens involves monitoring the turnover rate of ATG8 family proteins, which associate with autophagosomal membranes(Orhon and Reggiori 2017). Among these, LC3 is the most commonly tracked marker, particularly in high-throughput settings where imaging-based assays are employed to quantify total protein levels versus the number of fluorescent puncta(Mizushima and Murphy 2020). Furthermore, the tandem fluorescent-tagged LC3 (tfLC3) reporter, which fuses red (RFP or mCherry) and green (GFP) fluorescent proteins to the N-terminus of LC3, enables distinction between autophagosomes (yellow puncta,

indicating both red and green signals) and autolysosomes (red puncta, due to quenching of GFP in acidic lysosomal conditions)(Kimura et al. 2007). This approach allows dynamic tracking of autophagy: an increase in yellow and red puncta following autophagy induction indicates autophagosome formation and subsequent fusion with lysosomes, respectively(Kimura et al. 2007). Conversely, lysosomal inhibition results in accumulation of yellow puncta, reflecting impaired fusion or degradation(Mizushima and Murphy 2020). Inhibition of autophagy induction leads to a reduction in both puncta types(Mizushima and Murphy 2020). In addition to LC3, autophagy receptors like p62 are used to assess flux and complement the tfLC3 system, as p62 is not efficiently recruited to single-membrane compartments(Pankiv et al. 2007; Romao et al. 2013). Importantly, tf reporters do not require lysosome inhibition to assess flux and can be adapted to analyze the total cellular autophagic flux(Gump and Thorburn 2014; Kaizuka et al. 2016).

Substantial progress has been made in adapting LC3 and autophagy cargo adaptor assays including p62 for arrayed and pooled high-throughput RNAi screens(Mizushima and Murphy 2020). However, with the advancement of CRISPR-Cas9 genome-editing technologies, genome-wide and kinome-wide CRISPR knockout screens have become increasingly favored due to their lower false-negative rates and greater robustness compared to RNAi(Boettcher and McManus 2015). The high-throughput screens have led to novel mechanistic insights into the regulation of basal autophagy(Lipinski et al. 2010; Szyniarowski et al. 2011; Hale et al. 2016; Guo et al. 2018; Mimura et al. 2021). In parallel, starvation-induced autophagy screens have been employed to uncover regulatory mechanisms activated under stress conditions(Chan, Kir, and Tooze 2007; McKnight et al. 2012; Morita et al. 2018). More recently, attention has

shifted toward understanding the regulation of selective autophagy. For instance, a genome-wide CRISPR interference screen using an ER-phagy-specific reporter identified the UFMylation pathway as a critical regulator of ER-phagy(Liang et al. 2020). Similarly, a separate screen investigating PARKIN stability revealed that transcriptional repression plays a role in mitophagy regulation(Potting et al. 2018).

A critical step in interpreting results from screens using exogenous autophagy reporters is the validation of findings against endogenous proteins or markers, since overexpression of tagged proteins may induce cellular stress or mislocalization(Mizushima and Murphy 2020). Alternately, a secondary screen using a mini-library consisting of single guide RNAs (sgRNAs) targeting hits can be performed to validate promising candidates(Morita et al. 2018). Notably, it was reported that some sgRNAs were found to selectively affect GFP-tagged p62 reporters without altering endogenous p62, highlighting potential artifacts of exogenous reporter systems and underscoring the importance of orthogonal validation strategies(Mizushima and Murphy 2020).

1.9 Statement of Research Problem, Rationale, and Objectives

The biogenesis of autophagosomes is mediated by a tightly regulated cascade of autophagy-related (ATG) proteins, which are well characterized(Glick et al. 2010). Among known regulators of autophagy induction, kinase-mediated phosphorylation has been well characterized in starvation-induced autophagy(Sridharan et al. 2011). However, the signaling upstream of selective autophagy is less well understood.

While autophagy was initially regarded as a bulk degradation process, accumulating evidence has underscored the importance of selective autophagy in targeting specific substrates(Kirkin and Rogov 2019; Reggiori et al. 2012). Of particular interest is the kinase-mediated regulation of selective autophagy processes such as xenophagy, which plays a critical role in host defense(Sharma et al. 2018). Notably, several xenophagy-associated proteins, including ATG16L1 and IRGM, have been genetically linked to Crohn's disease (CD), but not to the closely related inflammatory condition, ulcerative colitis (UC)(Palomino-Morales et al. 2009). A common single nucleotide polymorphism (SNP) in ATG16L1 (T300A) is associated with increased CD susceptibility and is prone to caspase-mediated cleavage under stress conditions(Lassen et al. 2014). ATG16L1 has been reported to interact with FIP200, a key component of the ULK1 complex, suggesting kinase-mediated signaling involved in its regulation(Gammoh et al. 2013). These findings support the hypothesis that ULK1 may regulate ATG16L1 stability and function in response to pathogen-associated stress.

Hypothesis 1: ULK1 contributes to the stabilization and functional activity of ATG16L1 during infection-induced autophagy.

Objective 1.1: Determine whether ULK1 directly phosphorylates ATG16L1 upon infection.

Objective 1.2: Investigate the role of ULK1-mediated phosphorylation in modulating ATG16L1 stability and its capacity to mediate pathogen clearance.

In addition, selective autophagy pathways such as ER-phagy and pexophagy remain poorly characterized(Reggiori and Molinari 2022; Cho et al. 2018). This presents

an opportunity to dissect their regulatory mechanisms and biological functions more thoroughly. We aim to investigate the kinase-mediated regulation of these less understood forms of selective autophagy.

Hypothesis 2: A kinome-wide high-throughput CRISPR screen under multiple stress conditions will reveal novel, stress-specific regulators of selective autophagy.

Objective 2.1: Develop and implement a high-throughput kinome-wide CRISPR screening platform to systematically profile autophagy pathways under various stress conditions and enable cross-comparative analyses.

Objective 2.2: Identify and validate novel kinase regulators involved in ER-phagy and pexophagy.

Chapter 2: ULK1-mediated phosphorylation of ATG16L1 promotes xenophagy, but destabilizes the ATG16L1 Crohn's mutant

Published on *EMBO Reports*. DOI: 10.15252/embr.201846885

Reham M Alsaadi†, **Truc T Losier**†, Wensheng Tian, Anne Jackson, Zhihao Guo,

David C Rubinsztein & Ryan C Russell

†These authors contributed equally to this work.

2.1 Statement of Author Contributions

TTL and RCR wrote the manuscript. **TTL** and RCR performed Figure 1 (A, B, D). **TTL** performed Figure 3 (A, B, C), Figure EV3 (A, C), Figure EV4 (B, D, F), and Figure EV5 (B). RMA performed Figure 2 (A, B, C, D), Figure 3 (D, E), Figure 4 (B, C, D), Figure EV2 (A, B, C, D, E, F), Figure EV3 (B, D, E), Figure EV4 (A, C, E), and Figure EV5 (A, C, D). WT assayed endogenous pATG16L1 (S278) levels under stress. AJ characterized pATG16L1(S287) function and validated the phospho-antibody. ZG performed quantification of IF images. RCR and DCR oversaw manuscript preparation, experimental planning. RCR conceived of the study.

ULK1-mediated phosphorylation of ATG16L1 promotes xenophagy, but destabilizes the ATG16L1 Crohn's mutant

Reham M Alsaadi[1,†], Truc T Losier[1,†], Wensheng Tian[1], Anne Jackson[2], Zhihao Guo[1], David C Rubinsztein[2,3] & Ryan C Russell[1,4,*]

[1] Department of Cellular and Molecular Medicine, University of Ottawa, Ottawa, ON, Canada

[2] Department of Medical Genetics, Cambridge Institute for Medical Research, University of Cambridge, Cambridge, UK

[3] UK Dementia Research Institute, Cambridge, UK

[4] Center for Infection, Immunity and Inflammation, University of Ottawa, Ottawa, ON, Canada

[*] Corresponding author. Tel: +1 613 568 5800; E-mail: ryan.russell@uottawa.ca

[†] These authors contributed equally to this work

Keywords: ATG16L1; autophagy; caspase; Crohn's disease; ULK1

2.2 Abstract

Autophagy is a highly regulated catabolic pathway that is potently induced by stressors including starvation and infection. An essential component of the autophagy pathway is an ATG16L1-containing E3-like enzyme, which is responsible for lipidating LC3B and driving autophagosome formation. ATG16L1 polymorphisms have been linked to the development of Crohn's disease (CD), and phosphorylation of CD-associated ATG16L1 T300A (caATG16L1) has been hypothesized to contribute to cleavage and autophagy dysfunction. Here we show that ULK1 kinase directly phosphorylates ATG16L1 in response to infection and starvation. Phosphorylated ATG16L1 localizes to the site of internalized bacteria and stable cell lines harbouring a phospho-dead mutant of ATG16L1 have impaired xenophagy, indicating a role for ATG16L1 phosphorylation in the promotion of anti-bacterial autophagy. In contrast to wild-type ATG16L1, ULK1-mediated phosphorylation of caATG16L1 drives its destabilization in response to stress. In summary, our results show that ATG16L1 is a novel target of ULK1 kinase and that ULK1 signaling to ATG16L1 is a double-edged sword, enhancing the function of the wild-type ATG16L1, but promoting degradation of caATG16L1.

2.3 Introduction

Macroautophagy (hereafter referred to as autophagy) is a cellular degradative process capable of degrading a vast array of substrates including cytoplasm, organelles, aggregated macromolecules and pathogens(Parzych and Klionsky 2014). Autophagic cargo is first sequestered by the formation a double-membraned vesicle called an autophagosome, which matures into a degradative vesicle after fusion with lysosomes. Autophagosome formation is driven by a set of autophagy-related (ATG) genes, which include a protein kinase (Unc 51-like kinase 1; ULK1), a lipid kinase (vacuolar protein sorting 34; VPS34) and a trimeric E3-like enzyme (ATG5-ATG12/ATG16L1)(Parzych and Klionsky 2014). These enzymes are all required for autophagy initiation and are tightly regulated by upstream stress-sensitive signaling. One of the best characterized upstream regulators of the autophagy pathway is mTORC1, which potently inhibits autophagy induction through direct phosphorylation of the ULK1 and VPS34 kinase complexes(Kim et al. 2011; Yuan et al. 2013; Jung et al. 2009; Hosokawa et al. 2009). mTORC1 activity is repressed, thereby allowing autophagy induction, in response to a myriad of stressors including nutrient or cytokine starvation, reactive oxygen species or infection(Underwood et al. 2010; Russell et al. 2014).

Mammals have two homologues of the yeast ATG1, ULK1 and ULK2, which are largely functionally redundant for autophagy induction(McAlpine et al. 2013). Under basal conditions, mTORC1-mediated phosphorylation represses ULK1 activity; however, starvation releases this inhibitory phosphorylation and upregulates ULK1(Hosokawa et al. 2009). Activated ULK1 then phosphorylates several components of the pro-autophagic ATG14-containing VPS34 complexes(Russell et al. 2013; Park et al. 2016; Di Bartolomeo

et al. 2010). Autophagic VPS34 complexes are recruited to the phagophore where they phosphorylate phosphatidylinositol (PtdIns) to produce phosphatidylinositol(3)phosphate (PtdIns(3)P)(Fan et al. 2011). PtdIns(3)P functions as a platform bridging downstream components like the ATG16L1 complex to promote autophagosome formation. Additionally, mTORC1 has been shown to directly mediate the activity of VPS34 complexes, thereby allowing a tight regulation of autophagy initiation in response to stresses(Yuan et al. 2013). Downstream of VPS34, ATG16L1 forms a trimeric complex with ATG5 and ATG12. ATG16L1 is the subunit responsible for recruiting the E3-like enzyme to the phagophore(Parzych and Klionsky 2014; Fujita et al. 2008). ATG12 acts to recruit microtubule-associated protein 1 light chain 3 (LC3) to the expanding autophagosomal membrane, and ATG5 catalyzes the conjugation of the ubiquitin-like LC3 to phosphatidylethanolamine in membranes of nascent autophagosomes, thereby driving their development.

Activation of anti-bacterial autophagy (hereafter referred to as xenophagy) involves these 3-key enzymes in the autophagy pathway, but also requires xenophagy-specific proteins involved in pathogen-sensing that signal to the autophagy machinery during infection(Gomes and Dikic 2014). For instance, galectin-8 detects damaged *Salmonella*-containing vacuoles (SCV) and subsequently activates xenophagy through recruitment of the autophagy receptor NDP52(Randow and Youle 2014). Immunity-related GTPase M (IRGM) has been shown to act as a scaffold bringing together ULK1, Beclin-1-containing VPS34 complexes and ATG16L1 to promote xenophagy initiation(Chauhan et al. 2015). In addition to IRGM, ATG16L1-containing enzyme is also regulated by activation of intracellular (NOD2) sensors of bacterial peptidoglycan, where

NOD2 binds ATG16L1 recruiting the LC3-lipidating enzyme to the site of bacterial infection(Travassos et al. 2010).

Interestingly, several of the proteins involved in xenophagy induction (ATG16L1 and IRGM) and pathogen detection (NOD2 and TLR4) have been linked to Crohn's disease (CD), but are not found in the related chronic inflammatory bowel disease ulcerative colitis (UC)(Parkes 2012). Genome-wide association studies have linked a non-synonymous single nucleotide polymorphism (SNP) in ATG16L1 that substitutes threonine 300 for alanine with an increased susceptibility for CD(Massey and Parkes 2007). Molecular characterization of the CD-associated ATG16L1 (caATG16L1) has shown that stresses such as starvation or pathogen infection enhance the susceptibility of caATG16L1 to caspase-mediated cleavage(Sadabad et al. 2015; Murthy et al. 2014; Sorbara et al. 2013; Homer et al. 2010). Enhanced cleavage of caATG16L1 has been shown to lead to an increase in inflammatory cytokine secretion and a decrease in xenophagy, which are thought to contribute to CD(Murthy et al. 2014; Diamanti et al. 2017; Gao et al. 2017; Boada-Romero et al. 2016). Interestingly, a recent study has found that IκB kinase subunit IKKα is capable of phosphorylating ATG16L1 on serine 278 (S278), which regulates the sensitivity of caATG16L1 to caspase cleavage(Diamanti et al. 2017). The caspase cleavage site on ATG16L1 lies in between the S278 phosphorylation site and the T300A Crohn's SNP. This raises the interesting possibility that phosphorylation of ATG16L1 in response to infection leads to inappropriate cleavage if the site is in close proximity to the T300A mutation. ATG16L1 contains several conserved serine/threonine residues proximal to T300, which may also be phosphorylated and may potentially regulate ATG16L1 function. However, it remains to be seen what effect phosphorylation

has on wild-type ATG16L1 and if other stressors or kinases regulate ATG16L1 phosphorylation.

2.4 Results and Discussion

ATG16L1 is phosphorylated by ULK1/2

Starvation has been described to trigger caspase-mediated cleavage of ATG16L1 containing a common amino acid substitution (T300A)(Murthy et al. 2014). However, IKKα has not been implicated in starvation-induced autophagy. Interestingly, ATG16L1 has been shown to bind FIP200, an essential co-factor of the ULK1 kinase complex. The interaction of ATG16L1 with FIP200 has been shown to be involved in regulating ATG16L1 localization in autophagy induction(Gammoh et al. 2013; Nishimura et al. 2013). Therefore, we hypothesized that ULK1/2, the only protein kinases in the autophagy pathway, may phosphorylate ATG16L1 under starvation. To test this hypothesis, we performed an *in vitro* kinase assay using either purified ULK1 or ULK2 with recombinant ATG16L1 as substrate. We found that both ULK1 and ULK2 were capable of phosphorylating ATG16L1 *in vitro* (Fig 1A). In order to narrow down the site of phosphorylation, we repeated the kinase assay using truncations of ATG16L1. We found that the truncation mutant lacking amino acids 254–294 was a very poor substrate for ULK1, indicating that the primary site(s) of ULK1-mediated phosphorylation are located in this region (Fig 1B). Amino acids 254–294 are serine/threonine rich, containing 10 conserved residues (Fig 1C). Therefore, to identify the residue(s) that are phosphorylated by ULK1 in this region we repeated the kinase assay on full-length ATG16L1 and performed mass spectrometry analysis. Our results revealed a single high confidence phosphorylation site on serine 278 (Fig EV1A and marked in green in Fig 1C) and another of slightly lower confidence on serine 287 (Fig EV1A and marked in grey in Fig 1C), both of which map to the region of ATG16L1 we previously identified as required for ULK1-

mediated phosphorylation (Fig 1B). Peptide coverage in the mass spectrometry was 80% across the whole protein, and only two S/T residues were missed in the putative 254–294 region. To confirm the major site(s) of phosphorylation on ATG16L1, we mutated S278 and S287 singly in the full-length protein and performed another *in vitro* ULK1 kinase assay. Interestingly, we observed a significant loss of ULK1-mediated phosphorylation in the S278A mutant and little reduction in the S287A mutant (Fig 1D). This indicates that the major site of phosphorylation on ATG16L1 is S278, which is the same residue previously identified as a site for IKKα–mediated phosphorylation(Diamanti et al. 2017). Next, we created phospho-specific antibodies against S278 or S287 of ATG16L1 and tested its specificity by co-transfection of wild-type or mutant ULK1 and ATG16L1. Excitingly, we observed that ULK1 phosphorylates ATG16L1 on S278 in cells and that our antibody was specific to the phosphorylated form of the protein with little to no signal against ATG16L1 (S278A) or wild-type ATG16L1 co-transfected with kinase-dead ULK1 (Fig 1E). Despite good specificity for our S287 antibody (Fig EV1B and C), we observed that the lower probability site obtained by mass spectrometry, S287, was not phosphorylated in an ULK1-dependent manner (Fig 1E). Collectively, these results show that ATG16L1 is a direct target of ULK1 and that the primary site of phosphorylation is S278.

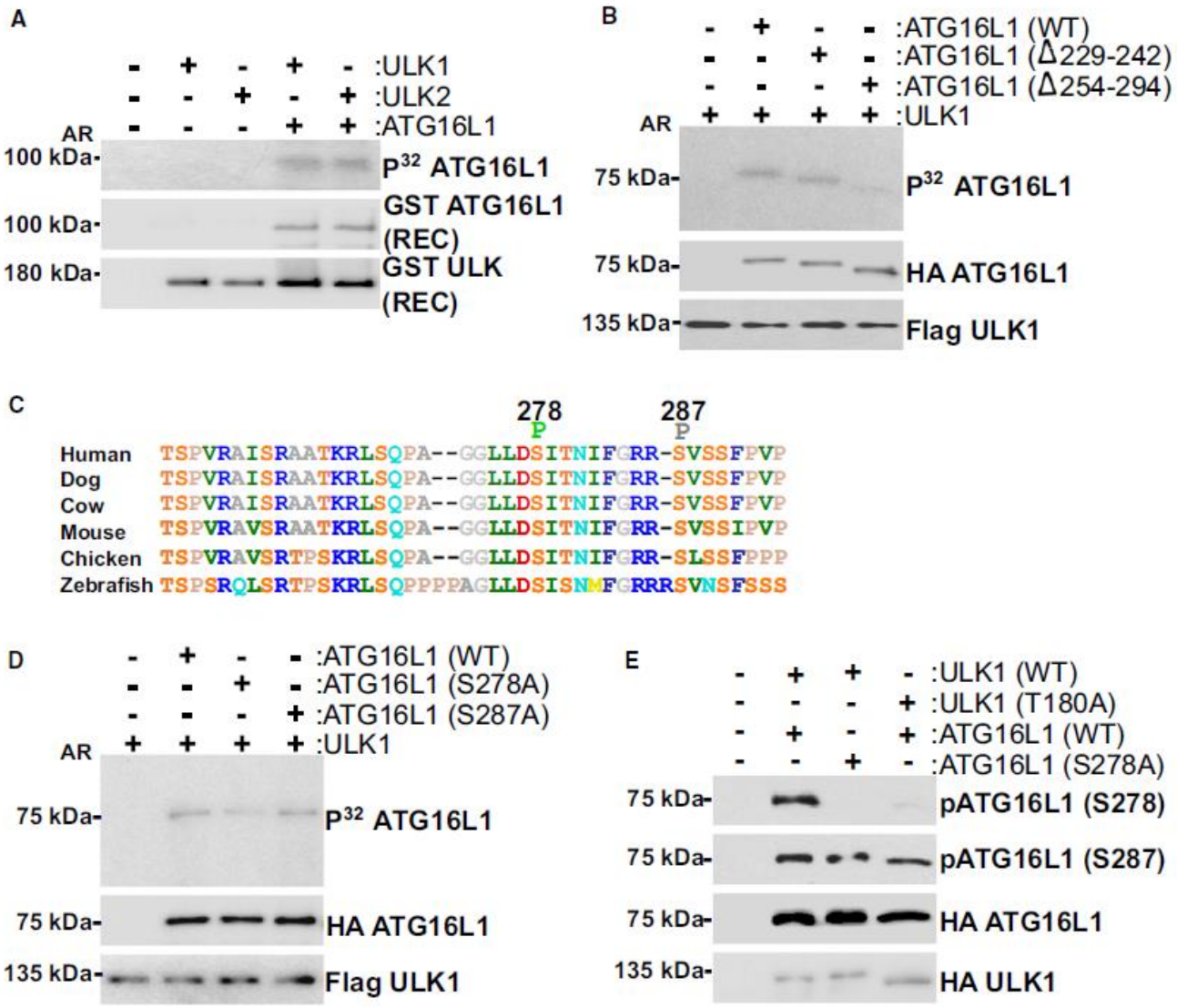
A
:ULK1
:ULK2
:ATG16L1
AR
100 kDa
P32 ATG16L1
GST ATG16L1 (REC)
100 kDa
180 kDa
GST ULK (REC)
B
:ATG16L1 (WT)
:ATG16L1 (Δ229-242)
:ATG16L1 (Δ254-294)
:ULK1
AR
75 kDa
P32 ATG16L1
75 kDa
HA ATG16L1
135 kDa
Flag ULK1
C
278
287
Human TSPVRAISRAATKRLSQPA--GGLLDSITNIFGRR-SVSSFPVP
Dog TSPVRAISRAATKRLSQPA--GGLLDSITNIFGRR-SVSSFPVP
Cow TSPVRAISRAATKRLSQPA--GGLLDSITNIFGRR-SVSSFPVP
Mouse TSPVRAVSRAATKRLSQPA--GGLLDSITNIFGRR-SVSSIPVP
Chicken TSPVRAVSRTPSKRLSQPA--GGLLDSITNIFGRR-SLSSFPPP
Zebrafish TSPSRQLSRTPSKRLSQPPPPAGLLDSISNMFGRRRSVNSFSSS
D
:ATG16L1 (WT)
:ATG16L1 (S278A)
:ATG16L1 (S287A)
:ULK1
AR
75 kDa
P32 ATG16L1
75 kDa
HA ATG16L1
135 kDa
Flag ULK1
E
:ULK1 (WT)
:ULK1 (T180A)
:ATG16L1 (WT)
:ATG16L1 (S278A)
75 kDa
pATG16L1 (S278)
75 kDa
pATG16L1 (S287)
75 kDa
HA ATG16L1
135 kDa
HA ULK1

Figure 1. ATG16L1 is phosphorylated by ULK1.

(A) *in vitro* kinase assays were performed using purified recombinant kinases (ULK1 and ULK2) and substrate (ATG16L1) in the presence of radiolabelled ATP. ULK and ATG16L1 inputs were examined by western blot (WB), and substrate phosphorylation was analysed by autoradiography (AR). (B) Full-length or truncated versions of ATG16L1 were subjected to an *in vitro* ULK1 kinase assay. ULK1 and ATG16L1 inputs were examined by western blot and target phosphorylation by autoradiography. (C) ATG16L1 was phosphorylated in an *in vitro* ULK1 kinase reaction and analysed by mass spectrometry. Phosphorylation of S278 and S287 in humans (S278 marked in green, S287 marked in grey) was identified with high and low confidence, respectively. Conservation of amino acids 254–294 is shown using the Shapely colour scheme. Mass spectrometry was performed on a single experiment. (D) Full-length or mutated HA-ATG16L1 was purified from mammalian cells and subjected to an *in vitro* ULK1 kinase assay. Inputs were analysed by WB and target phosphorylation by AR. (E) HEK293A cells were transfected with wild-type or phospho-dead ATG16L1 in the presence of wild-type or kinase-dead ULK1. Phosphorylation of ATG16L1 (S278 or S287) and inputs were examined by WB. Data information: Unless otherwise indicated, experiments were performed three times.

ULK1 is required for phosphorylation of ATG16L1 and xenophagy induction

We next sought to determine whether ULK1 regulated ATG16L1 phosphorylation endogenously and whether this signaling was responsive to starvation. ULK1/2 wild-type or ULK1/2 double-knockout (dKO) cells were starved for amino acids, either with amino acid-free DMEM or HBSS, followed by analysis of pATG16L1 levels by western blot of whole-cell extracts. Starvation potently inhibits mTORC1 signaling, as demonstrated by loss of S6K phosphorylation, which is a prerequisite for ULK1 activation. Importantly, we observed that starvation resulted in a clear increase in endogenous ATG16L1 phosphorylation only in cells containing ULK1 (Figs 2A and EV2A, lanes 1–6). We found that ablation of ULK1-mediated phosphorylation of ATG16L1 had no effect on the stability of the ATG16L1/5-12 complex (Fig EV2B). Notably, our phospho-antibody only recognizes the slower migrating ATG16L1β isoform and is observed as a single band. As IKKα was previously described to phosphorylate ATG16L1 on S278 under infection, we also tested the requirement for IKKα in starvation-induced ATG16L1 phosphorylation. However, we observed that IKKα deficiency had no detectable effect on starvation-induced ATG16L1 phosphorylation (Fig 2A, lanes 7–9). This is perhaps expected as IKKα has no known role in starvation-induced autophagy. This result indicates that the ATG16L1 subunit of the LC3-lipidating enzyme is a direct and physiological target of ULK1 under starvation. We next asked if ULK1/2 or IKKα contributed to ATG16L1 phosphorylation upon infection or TNFα treatment. ULK1/2 wild-type, ULK1/2 dKO or IKKα KO cells were infected with *Salmonella* enterica serovar Typhimurium (hereafter referred to as *Salmonella*) or treated with TNFα, and ATG16L1 phosphorylation was examined by western blot. Surprisingly, we observed that *Salmonella* and TNFα-induced

ATG16L1 phosphorylation was abolished in ULK1/2 dKO cells, but was still observed in IKKα knockout cells (Figs 2B and EV2C). Of note, phospho-ATG16L1 signal is consistently lower under infection as only a small minority of cells are subjected to the stress of internalized bacteria (Fig EV2D). These results clearly indicate that ULK1/2 is required for phosphorylation of ATG16L1 under starvation, inflammatory cytokine signaling and infection.

We next sought to determine the requirement for ULK1/2 and IKKα in promoting xenophagy. Xenophagic clearance of *Salmonella* is very well established and its intracellular growth is restricted by the pathway, making it an ideal model pathogen for this analysis. Wild-type or knockout cells were infected with *Salmonella*, and the number of LC3B-positive *Salmonella* was quantified. LC3B is conjugated to the autophagosomal membrane and colocalizes with bacteria targeted for clearance by xenophagy and can be used at early time points to monitor xenophagy induction. We found that ULK1/2-deficient cells exhibited a potent decrease in LC3B-positive bacteria, while IKKα loss did not significantly affect xenophagy (Figs 2C and EV2E and F). In order to confirm the roles for ULK1/2 and IKKα in xenophagy induction and suppression of invasive bacteria, we performed colony-forming unit (CFU) assays in our wild-type or knockout lines. CFU assays measure bacterial viability after internalization and are inversely correlated with xenophagy rates(Alonso et al. 2007). Analysis of *Salmonella* viability 4 h postinfection revealed that ULK1/2 dKO cells harboured a much higher number of viable internalized bacteria, indicative of an autophagy defect, when compared to wild-type and IKKα knockout cells (Fig 2D). Surprisingly, our results indicate that ULK1/2, but not IKKα, is required for ATG16L1 phosphorylation and xenophagy induction.

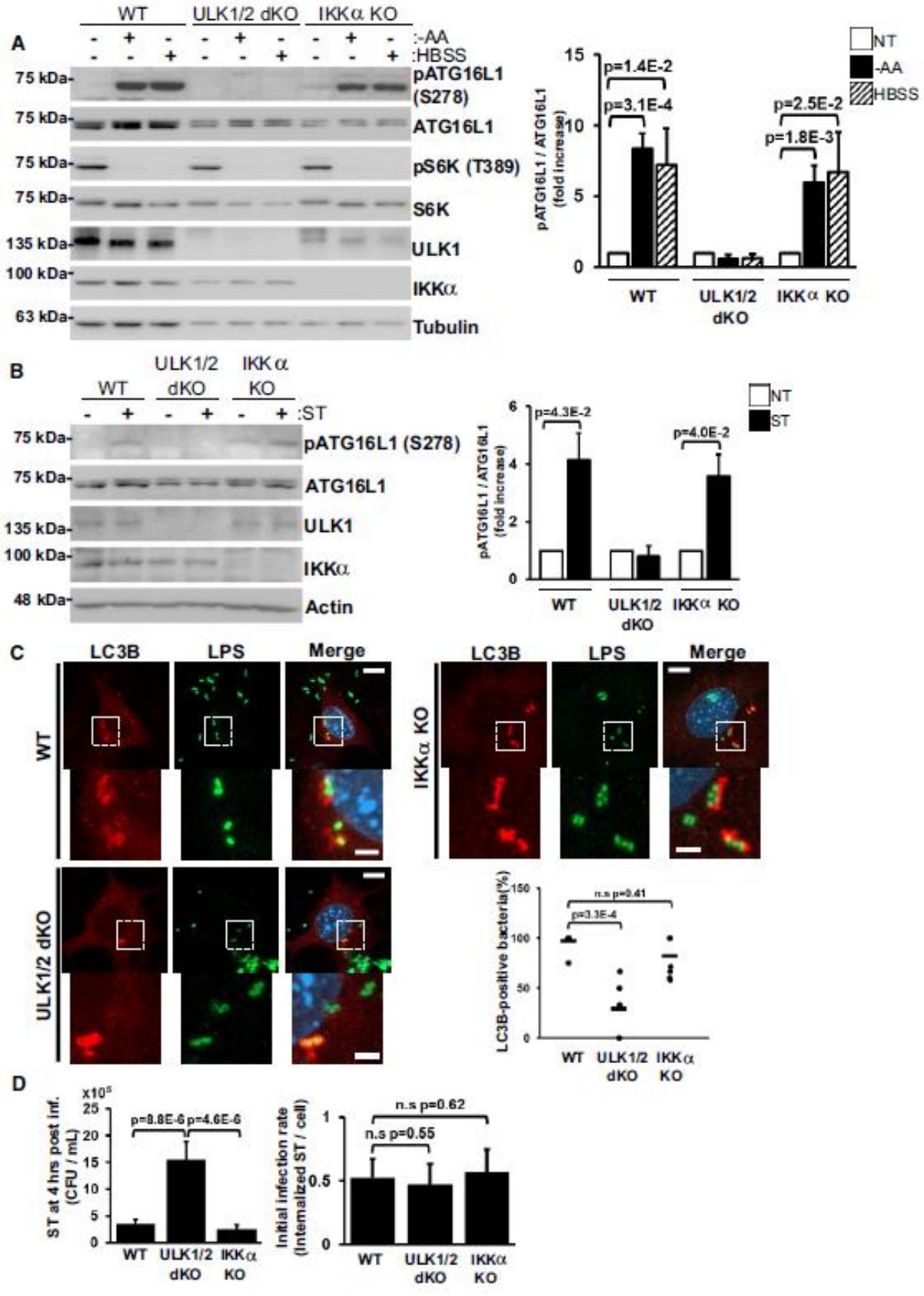
A
WT
ULK1/2 dKO
IKKα KO
:-AA
:HBSS
75 kDa
pATG16L1 (S278)
ATG16L1
pS6K (T389)
S6K
135 kDa
ULK1
100 kDa
IKKα
63 kDa
Tubulin
NT
-AA
HBSS
pATG16L1 / ATG16L1 (fold increase)
p=1.4E-2
p=3.1E-4
p=2.5E-2
p=1.8E-3
B
:ST
48 kDa
Actin
ST
p=4.3E-2
p=4.0E-2
C
LC3B
LPS
Merge
WT
IKKα KO
ULK1/2 dKO
LC3B-positive bacteria(%)
n.s p=0.41
p=3.3E-4
D
ST at 4 hrs post inf. (CFU / mL)
x10^5
p=8.8E-6
p=4.6E-6
Initial infection rate (Internalized ST / cell)
n.s p=0.62
n.s p=0.55

Figure 2. ULK1/2 is required for phosphorylation of ATG16L1 and xenophagy induction.

(A) Wild-type, ULK1/2 double-knockout (dKO) or IKKα KO mouse embryonic fibroblasts (MEFs) cells were incubated with either complete medium, amino acid-deficient DMEM or HBSS for 1 h. Samples were immunoblotted using the indicated antibodies. (B) Wild-type, ULK1/2 dKO or IKKα KO MEFs cells were infected with log phase *Salmonella* for 2 h; bacteria-containing media was then removed, and cells were incubated with gentamycin (50 μg/ml)-containing DMEM for 2 h. Samples were immunoblotted using the indicated antibodies. (C) Wild-type, ULK1/2 dKO or IKKα KO MEFs cells were infected with *Salmonella* for 1 h. Autophagic capture of *Salmonella* was analysed by immunostaining for LPS and LC3B. Representative images are shown (scale bars, 10 and 3 μm). Quantification was generated from eight fields of view from a representative experiment. The experiments were repeated twice. (D) Wild-type, ULK1/2 dKO and IKKα KO MEFs cells were infected with *Salmonella* for 1 h. Xenophagy rates were examined through colony-forming unit (CFU) assays. Quantification of infection rates by immunofluorescence is demonstrated in the right panel. Data information: Unless otherwise indicated, experiments were performed three times. Data are represented as mean ± standard deviation, and P-values were determined by Student's t-test.

ULK1 promotes cleavage of caATG16L1 through phosphorylation on S278

Multiple groups have shown that the T300A substitution in caATG16L1 renders it sensitive to caspase cleavage under stress conditions including nutrient starvation and infection(Murthy et al. 2014; Diamanti et al. 2017; Santeford et al. 2016). Moreover, it was shown that mutation of serine 278 of ATG16L1 to alanine is involved in stress-induced caspase cleavage in the caATG16L1 background(Diamanti et al. 2017). Our data indicate that ULK1 is responsible for the phosphorylation of wild-type ATG16L1 on S278 under nutrient starvation and infection. Therefore, we next sought to determine whether ULK1 signaling was involved in the stress-induced destabilization of caATG16L1. HEK293A cells were transfected with either wild-type ATG16L1 or caATG16L1 co-transfected with increasing amounts of ULK1 kinase. Importantly, overexpression of ULK1 is known to result in autoactivation and induction of downstream signaling in the absence of stress, thereby allowing us to determine the isolated effect of ULK1 signaling on ATG16L1 stability independent of other stress-responsive pathways. Interestingly, we observed that ULK1 is capable of stimulating ATG16L1 cleavage and the level of cleavage is elevated in the caATG16L1 background (Fig 3A). In order to determine whether ATG16L1 cleavage was a result of ULK1-mediated phosphorylation on S278, we transfected HEK293A cells with wild-type, T300A or S278/T300A mutants of ATG16L1 in the presence or absence of ULK1. Excitingly, we observed that single mutation of the ULK1 phosphorylation site was sufficient to reduce ULK1-driven cleavage (Fig 3B). As expected mutation of S287, the low confidence ULK1 phosphorylation site identified by mass spectrometry, had no impact on cleavage in the T300A background (Fig EV3A). These results indicate that caATG16L1 is preferentially cleaved through ULK1-mediated phosphorylation of S278. Conversely,

we found that T300A did not have any effect on ATG16L1 phosphorylation (Fig EV3B). Lastly, we repeated this experiment in the presence or absence of Z-VAD-FMK, a pan-caspase inhibitor, to confirm the faster migrating form of ATG16L1 was indeed a product of caspase-mediated cleavage. Treatment with a pan-caspase inhibitor resulted in a potent reduction in the levels of the faster migrating ATG16L1 band, confirming that the ULK1-driven cleavage product was a caspase cleavage product (Fig 3C). Increasing evidence *in vitro* and *in vivo* has shown that caspase-mediated destabilization of caATG16L1 is a critical event associated with the pathobiology of this SNP(Murthy et al. 2014; Diamanti et al. 2017). Moreover, in unstressed conditions caATG16L1 is known to have the same stability as wild type(Murthy et al. 2014). To study the effect of ULK1-mediated caspase cleavage of ATG16L1 in cells, we knocked out ATG16L1 using CRISPR/Cas9 (Fig EV3C) and transfected ATG16L1(T300A) in HEK293A cells and infected cells in the presence or absence of ULK inhibitor. Interestingly, we observed *Salmonella* treatment destabilized the T300A mutant, which could be reversed with ULK inhibitor (Fig 3D). However, ATG16L1(WT) stability was not drastically affected by either *Salmonella* or ULK inhibition (Fig 3D). We also found ATG16L1(T300A) was stabilized by ULK inhibitors under TNFα treatment (Fig EV3D). We next sought to determine the function of S278 phosphorylation of ATG16L1 in both the wild-type and T300A background. ATG16L1 knockout cells were transfected with ATG16L1 (WT, S278A, T300A or S278A/T300A) at similar levels and treated with *Salmonella* (Fig EV3E). Quantification of *Salmonella* at 4 h postinfection showed that mutation of S278 phosphorylation in the wild-type background resulted in an increase in *Salmonella*, indicating ULK1 phosphorylation may act to promote xenophagy in wild-type ATG16L1

(Fig 3E, columns 1 and 2). Conversely, in the T300A background S278A mutation improved *Salmonella* clearance, indicating ULK1 phosphorylation is detrimental in this background (Fig 3E, columns 3 and 4).

Collectively, our data shed light on the relationship between stress and caATG16L1 cleavage showing that: (i) ULK1-mediated phosphorylation of ATG16L1 is increased under infection and starvation, which are known to promote the cleavage of caATG16L1, (ii) caATG16L1 is preferentially cleaved upon ULK1 activation, and (iii) mutating the ULK1 phosphorylation site reduces ULK1-driven cleavage and improves xenophagy in the caATG16L1 background.

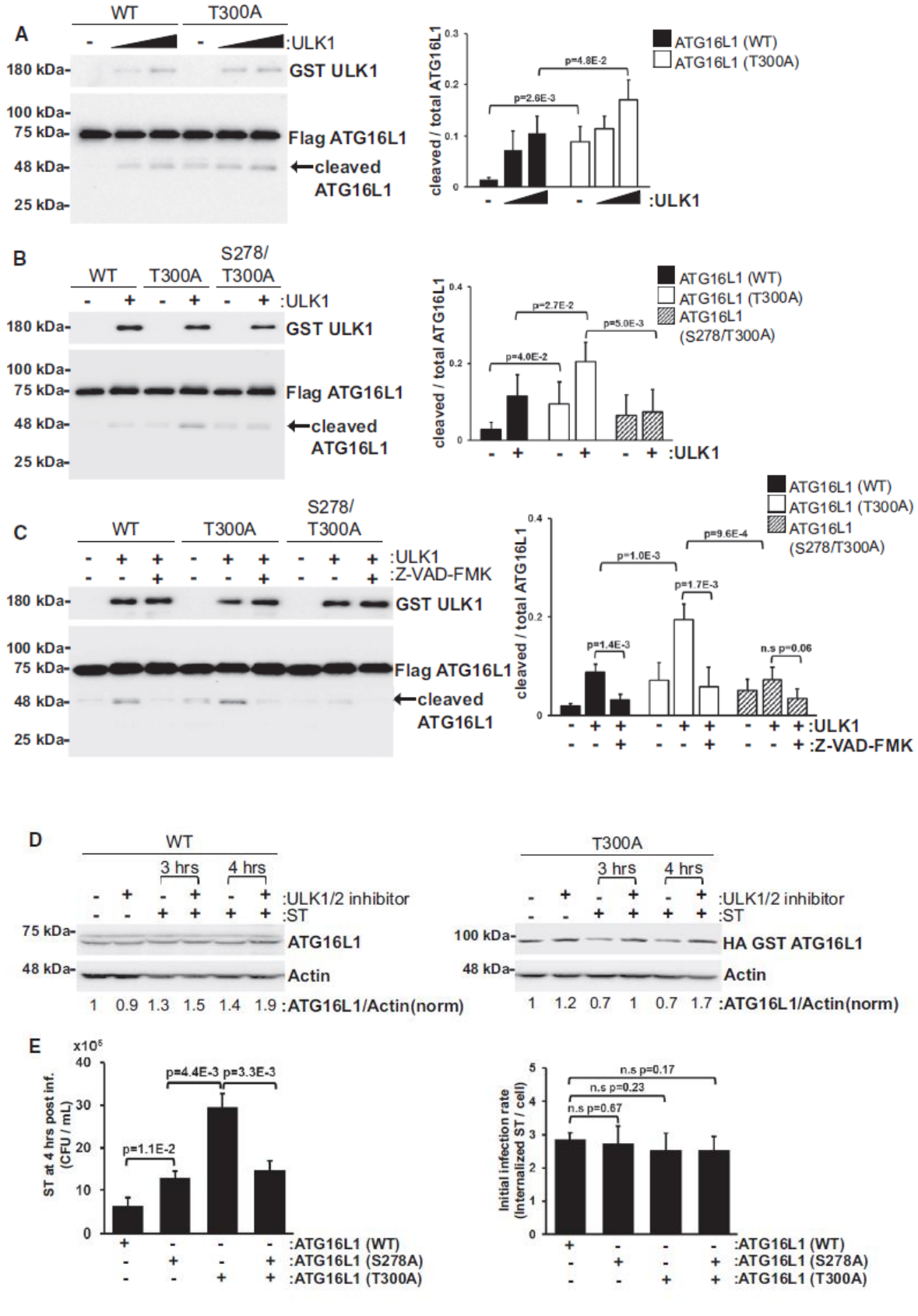
A
WT
T300A
:ULK1
180 kDa
GST ULK1
100 kDa
75 kDa
Flag ATG16L1
48 kDa
cleaved ATG16L1
25 kDa
cleaved / total ATG16L1
p=4.8E-2
p=2.6E-3
ATG16L1 (WT)
ATG16L1 (T300A)
B
S278/ T300A
p=2.7E-2
p=5.0E-3
p=4.0E-2
ATG16L1 (S278/T300A)
C
:Z-VAD-FMK
p=9.6E-4
p=1.0E-3
p=1.7E-3
p=1.4E-3
n.s p=0.06
D
3 hrs
4 hrs
:ULK1/2 inhibitor
:ST
ATG16L1
HA GST ATG16L1
Actin
1 0.9 1.3 1.5 1.4 1.9 :ATG16L1/Actin(norm)
1 1.2 0.7 1 0.7 1.7 :ATG16L1/Actin(norm)
E
x10⁵
ST at 4 hrs post inf. (CFU / mL)
p=4.4E-3 p=3.3E-3
p=1.1E-2
:ATG16L1 (WT)
:ATG16L1 (S278A)
:ATG16L1 (T300A)
Initial infection rate (Internalized ST / cell)
n.s p=0.17
n.s p=0.23
n.s p=0.67

Figure 3. ULK1 promotes cleavage of T300A ATG16L1 through phosphorylation on S278.

(A) HEK293A cells were transfected with either flag-tagged WT ATG16L1 or T300A ATG16L1. ULK1 was co-transfected in increasing amounts where indicated. Cleavage of ATG16L1 was analysed by WB of whole-cell lysates. Levels of ATG16L1 cleavage were quantified from three biological repeats (right panel). (B) HEK293A cells were transfected with either tagged wild-type, T300A or S278/T300A ATG16L1 in the presence or absence of ULK1. Cleavage of ATG16L1 was analysed by WB. Levels of ATG16L1 cleavage were measured from three biological repeats (right panel). (C) HEK293A cells were transfected with the indicated plasmids in the presence or absence of a pan-caspase inhibitor Z-VAD-FMK (15 μM) for 4 h. Cleavage of ATG16L1 was analysed by WB of three biological repeats. (D) Wild-type or T300A-expressing HEK293A were treated with *Salmonella* in the presence or absence of ULK1/2 inhibitor (16 μM) for the indicated time points. Expression of ATG16L1 was analysed by WB. The experiments were performed twice. (E) ATG16L1 knock-out HEK293A cells transfected with the indicated HA GST ATG16L1 plasmids were infected with *Salmonella* for 1 h. Xenophagy rates were examined through CFU assays. Quantification of infection rates by immunofluorescence is demonstrated in the right panel. Data information: Unless otherwise indicated, experiments were performed three times. Data are represented as mean ± standard deviation, and P-values were determined by Student's t-test.

ULK1-mediated phosphorylation is required for ATG16L1 localization to *Salmonella* site and bacterial clearance

ULK1 kinase has a well-established role in stimulating autophagy, making it unlikely that the primary function of ULK1-induced ATG16L1 phosphorylation is to activate caspase-mediated cleavage. In order to identify the physiological role of ULK1-mediated ATG16L1 phosphorylation, we performed experiments on the wild-type protein, which is not cleaved as readily after phosphorylation. The best described function of ATG16L1 is to promote the correct localization of the E3-like enzyme that lipidates LC3 to the membrane of newly forming autophagosomes. Therefore, we first sought to determine whether the localization of pATG16L1 differed from that of total ATG16L1 under infection. To compare localization, we infected MEF with *Salmonella* and immunostained for lipopolysaccharides (LPS), pATG16L1 and total ATG16L1. We observed pATG16L1 primarily in the infected samples, confirming the reactivity of our antibody for IF (Fig 4A). Excitingly, we found that pATG16L1 was preferentially localized with internalized bacteria (Fig 4A). Analysis of total ATG16L1 staining also showed colocalization with bacteria, but also contained significantly more diffuse staining in the cytoplasm (Figs 4A, and EV4A and B). This could indicate that either ULK1-mediated phosphorylation is important for ATG16L1 recruitment to bacteria, or that the phosphorylation occurs at the bacteria. We reasoned if phosphorylation of ATG16L1 affects bacterial localization, then ULK1-deficient cells should exhibit an impairment in ATG16L1 recruitment to pathogen. To test this hypothesis, we infected wild-type or ULK1-deficient cells and quantified the ability of total ATG16L1 to localize to internalized bacteria. Interestingly, we observed that the

proportion of ATG16L1-positive bacteria in ULK1-deficient MEF was reduced by over 80% compared with the wild-type controls (Figs 4B, and EV4C and D).

In order to determine the contribution of S278 phosphorylation on ATG16L1 localization to bacteria, we reconstituted ATG16L1 KO cells with either wild-type ATG16L1, a truncated form of ATG16L1 that cannot bind the ULK1 complex, or the S278A mutant and analysed localization to intracellular bacteria. We observed that mutation of S278 or deleting the region of ATG16L1 responsible for binding the ULK1 complex resulted in a significant reduction in ATG16L1-positive bacteria (Figs 4C, and EV4E and F). We then looked at colocalization between LC3B and *Salmonella* in our ATG16L mutants. We observed that the S278A mutant of ATG16L1 in the wild-type background resulted in a reduction in LC3B-positive bacteria (Figs 4D, and EV5A and B). Accordingly, the S278A and Δ229–242 mutants of ATG16L1 were both defective in clearing intracellular *Salmonella* as determined by CFU assay (Fig EV5C). In contrast, S278A mutation in the T300A background increased the percentage of LC3B-positive *Salmonella* (Fig EV5A and B), which was also consistent with the decreased bacterial load observed in our CFU assay (Fig 3E).

To determine the role of ULK1-mediated ATG16L1 phosphorylation in starvation, we starved cells reconstituted with either wild-type ATG16L1 or ATG16L1(S278A). Surprisingly, we found that S278 mutation had no effect on starvation-induced autophagy flux (Fig EV5D). These data indicate that either ULK1-mediated phosphorylation of ATG16L1 is more important under infection than starvation or additional functionally redundant signaling pathways to ATG16L1 are activated by starvation. Taken together, our data indicate that ULK1-mediated phosphorylation of wild-type ATG16L1 acts to

promote localization to internalized bacteria and thereby enhancing bacterial removal, while the same modification is detrimental in caATG16L1 (Fig 4E).

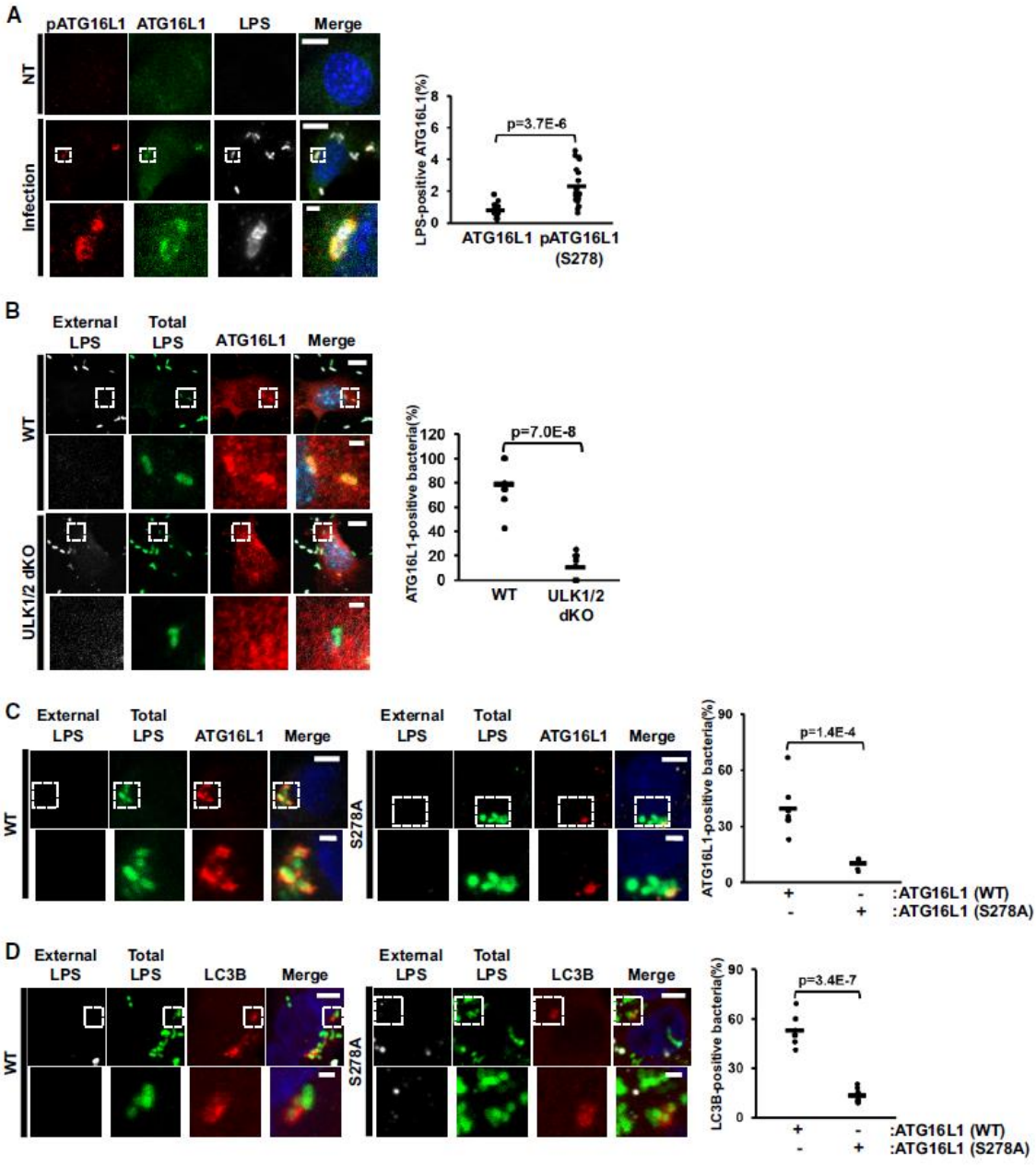
A
pATG16L1
ATG16L1
LPS
Merge
NT
Infection
LPS-positive ATG16L1(%)
p=3.7E-6
ATG16L1
pATG16L1 (S278)
B
External LPS
Total LPS
ATG16L1
Merge
WT
ULK1/2 dKO
ATG16L1-positive bacteria(%)
p=7.0E-8
WT
ULK1/2 dKO
C
External LPS
Total LPS
ATG16L1
Merge
WT
S278A
ATG16L1-positive bacteria(%)
p=1.4E-4
:ATG16L1 (WT)
:ATG16L1 (S278A)
D
External LPS
Total LPS
LC3B
Merge
WT
S278A
LC3B-positive bacteria(%)
p=3.4E-7
:ATG16L1 (WT)
:ATG16L1 (S278A)
E
Pathogen/ Metabolic stress
ULK1
Death-receptor activation
S278
ATG16L1 (WT)
S278
T300A
ATG16L1 (T300A)
Caspase 3
Xenophagy Induction
S278
T300A

Figure 4. ULK1-mediated phosphorylation is required for ATG16L1 localization to *Salmonella* site and bacterial clearance.

(A) Wild-type MEF cells were infected with *Salmonella* for 25 min. Phospho-ATG16L1, total ATG16L1 and LPS were stained and analysed by immunofluorescence. Representative immunofluorescent images are shown (scale bars, 10 and 1 μm). (B) Wild-type and ULK1/2 dKO cells were infected with *Salmonella* for 25 min. Immunofluorescence was performed using antibodies against LPS and ATG16L1. Representative immunofluorescent images are shown on the left panel (scale bars, 10 and 2 μm). Quantification of ATG16L1-positive bacteria from seven fields of view from a representative experiment is shown in the right panel. (C) ATG16L1 knock-out HCT116 cells transfected with the indicated GST HA ATG16L1 were infected with *Salmonella* for 1 h. Bacteria were stained using anti-LPS antibodies to analyse localization in addition to ATG16L1. Representative immunofluorescent images of ATG16L1 and LPS are shown (scale bars, 5 and 1 μm). Quantification of ATG16L1 localizing to bacteria from seven fields of view from a representative experiment is shown in the lower panel. (D) ATG16L1 knock-out HCT116 cells transfected with the indicated GST HA ATG16L1 were infected with *Salmonella* for 1 h. Bacteria were stained using anti-LPS antibodies to analyse localization in addition to the autophagy marker LC3B. Representative immunofluorescent images of LC3B and LPS are shown (scale bars, 5 and 1 μm). Quantification of bacteria undergoing autophagic clearance from seven fields of view from a representative experiment is shown in the lower panel. (E) A diagram demonstrating our working model for the role of ULK1-mediated phosphorylation at S278 in wild-type and T300A ATG16L1 background. Data information: Unless otherwise indicated,

experiments were performed twice. Data are represented as mean, and P-values were determined by Student's t-test.

ULK1 has previously been described to phosphorylate several components of the autophagy-promoting lipid kinase complex to activate the autophagy pathway(Russell et al. 2013; Park et al. 2016; Di Bartolomeo et al. 2010). Here we have described that the autophagy E3-like enzyme is also regulated by ULK1 through direct phosphorylation of the ATG16L1 subunit. The discovery of a link between ULK1 and the LC3B-lipidating enzyme has raised several interesting lines of inquiry. For example, we have shown that wild-type ATG16L1 is also susceptible to ULK1-sensitive caspase-mediated cleavage, albeit at a lower level than caATG16L1. However, we currently do not know the physiological relationship between phosphorylation and caspase-mediated cleavage outside the context of the caATG16L1 allele. Potentially, caspase-mediated cleavage of ATG16L1 under stress represents a mechanism to curtail autophagy under severe or prolonged stress. Understanding the mechanistic link between apoptosis and autophagy may yield important conceptual advances.

Additionally, we have uncovered a role for ULK1 signaling in CD through regulating the stability of caATG16L1. Interestingly, the functional significance of the S278 residue in CD had already been shown(Diamanti et al. 2017). However, the lack of tools to measure endogenous pATG16L1 resulted in IKKα being identified as the kinase responsible for the phosphorylation and triggering the cleavage of caATG16L1. Based on our data, as well as the previously reported link between starvation and pathogen-induced caATG16L1 dysfunction, we propose that ULK1 is the primary kinase responsible for ATG16L1 phosphorylation. However, it is quite possible that IKKα contributes to the destabilization of caATG16L1 through the previously reported activation of caspases(Diamanti et al. 2017).

The preferential localization of pATG16L1 to internalized bacteria is also interesting. This is because frameshifts in the gene NOD2 are strongly associated with CD development and have also been described to affect ATG16L1 localization to internalized bacteria(Travassos et al. 2010). This may imply a common defect of ATG16L1 function in CD. Consistent with this idea, CD-associated SNPs have also been described in ULK1, albeit with less strength than ATG16L1 SNPs. Here we have identified a functional redundancy between ULK1 and ULK2 in the promotion of ATG16L1 phosphorylation, which may explain the weak contribution of ULK1 polymorphisms in CD susceptibility. Lastly, transcriptional repression of IRGM has also been linked to the development of CD. Molecularly, IRGM has been shown to bind both ULK1 and ATG16L1, although they have not been shown in a complex together. Therefore, it would be of value to determine whether reductions in IRGM protein would have an effect on ULK1-mediated ATG16L1 phosphorylation. Clearly, the identification of ULK1-mediated ATG16L1 phosphorylation has opened up several avenues for future research, which will undoubtedly expand our understanding of xenophagy and the molecular basis of autophagy defects in CD.

2.5 Material and Methods

Antibodies and reagents

Anti-IKKα (Cat#2682), HA-HRP (#Cat 2999), phospho-NF-κB S536 (Cat#3033), ATG5 (Cat#12994), NF-κB (Cat# 8242) and phospho-S6K T389 (Cat#9234) antibodies were obtained from Cell Signaling Technology. Anti-LC3B (Cat#PM036 for immunofluorescence) and ATG16L1 (Cat#PM040 for immunofluorescence) antibodies were purchased from MBL. Beta-actin (Cat#A5441 clone AC-15) and vinculin (Cat#V9131) antibodies were obtained from Sigma. DYKDDDDK Epitope Tag (Cat#NBP1-06712 for WB) antibody was purchased from Novus Biologicals. Anti-LPS FITC (Cat#sc-52223) and GST (Cat# sc-374171) antibodies were purchased from Santa Cruz Biotechnology. Anti-S6K (Cat#ab32529), LPS (Cat#ab128709), ATG16L1 (Cat#ab187671) antibodies and TNFα (Cat#ab9642) were obtained from Abcam. phospho-ATG16L1 serine 278 was made in collaboration with Abcam. Polyclonal sera was affinity purified by phosphopeptide, and recombinant ATG16L1 (non-phosphorylated) was mixed in at a 6:1 molar ratio (Rec. ATG16L1: IgG), prior to immunoblotting. Monoclonal phospho-antibody from a hybridoma generated from this rabbit was used for immunofluorescence (Abcam Cat#ab195242). Active GST-ULK1 (1-649) and GST-ULK2 (1-478) from insect cells were purchased from CQuential Solutions (Moraga, CA). Anti-His-HRP (Cat#460707) was obtained from Invitrogen. Z-VAD(OMe)-FMK (Cat#HY-16658-1MG) was purchased from MedChemExpress. Bafilomycin A1 was obtained from Tocris (Cat#133410U). ULK-inhibitor MRT68921 was obtained from Selleckchem (Cat#S7949). Digitonin (Cat#10188-874) was obtained from VWR.

Cell culture

MEFs, HEK293A and HCT116 cells were cultured in DMEM supplemented with 10% bovine calf serum (VWR Life Science Seradigm). IKK wild-type and IKKα knockout MEF cells were a generous gift from Dr. Michael Karin (University of California San Diego)(Hu et al. 1999). ULK1/2 double-knockout MEF cells were a generous gift from Dr. Craig Thompson (Memorial Sloan Kettering)(Cheong et al. 2011). Amino acid starvation medium was prepared based on Gibco standard recipe omitting all amino acids and supplemented as above without addition of non-essential amino acids and substitution with dialysed FBS (Invitrogen). Media was changed 1 h before experiments.

Transfection

HEK293A cells were transfected with tagged ATG16L1 (750 ng) and tagged ULK1 (250 ng) using polyethylenimine (PEI, medistore uOttawa). HCT116 cells were transfected with the indicated tagged ATG16L1 (3–5 μg) using PEI. The samples were analysed 48–72 h post-transfection.

Generation of knock-out cell lines using CRISPR/Cas9

ATG16L1 knock-out lines were generated in the HCT116 or HEK293A backgrounds utilizing CRISPR/Cas9 targeting exon 1. Guide RNA sequence: 5′ AAACCCGCTGGAAGCGCCACATCTC 3′.

Generation of stable cell lines

The knock-out clones were infected with retroviruses or lentiviruses carrying tagged ATG16L1 at different amounts in order to achieve near endogenous levels of ATG16L1.

Site-directed mutagenesis

Primers used for T300A mutation are GGACAATGTGGATGCTCATCCTGGTTC (forward) and GAACCAGGATGAGCATCCACATTGTCC (reverse). Primers used for S278A mutation are GCCTTCTGGATGCTATCACTAATATC (forward) and GATATTAGTGATTGCATCCAGAAGGC (reverse). Primers used for S287A mutation are TTTGGGAGACGCGCTGTCTCTTCCT (forward) and AGGAAGAGACAGCGCGTCTCCCAAA (reverse). T300A followed by S278A or S287A mutation was performed to generate double mutations. Site-directed mutagenesis was performed based on KOD Xtreme Hot Start DNA Polymerase kit instructions purchased from Thermo Fisher. Specificity of mutagenesis was analysed by direct sequencing.

Bacterial strains

Wild-type (SL1344) *Salmonella* was a gift from Dr. Subash Sad (University of Ottawa). Bacteria were grown in Luria-Bertani broth (Fisher).

Bacterial infection

Salmonella were grown in 4 ml of LB broth at 37°C at 250 rpm. Overnight cultures of *Salmonella* were diluted 30-fold and grown until OD600 reached 1.5, followed by centrifugation of 10,000 g for 2 min, and resuspension in 1 ml of PBS. Bacterial stock was

then diluted fivefold (multiplicity of infection of 900) in DMEM supplied with 10% heat-inactivated bovine calf serum for infection. Cells cultured in antibiotic-free medium were infected with *Salmonella* and incubated at 37°C in 5% CO2 for the indicated time. Cells were washed in PBS once before direct lysis with 1× denaturing SDS sample buffer.

Western blot and immunoprecipitation

Whole-cell lysates were prepared by direct lysis with 1× SDS sample buffer. Samples were boiled for 10 min at 95°C and resolved by SDS–PAGE. Immune complexes were harvested from cells lysed in mild lysis buffer [10 mM Tris pH 7.5, 10 mM EDTA, 100 mM NaCl, 50 mM NaF, 1% NP-40, supplemented simultaneously with protease and phosphatase inhibitor cocktails—EDTA (APExBIO)], followed by centrifugation at max speed for 10 min to remove cell debris. Protein A beads (Repligen) were washed 1× with PBS and incubated with antibodies and cell lysates for 1.5–3 h followed by one 5-m wash with MLB and inhibitors and four quick washes with MLB alone. Beads were boiled in 1× denaturing sample buffer for 10 min before resolving by SDS–PAGE.

Statistical analysis

Error bars for western blot analysis represent the standard deviation between densitometry data collected from three unique biological experiments. Statistical significance was determined using paired Student's two-tailed t-test for two data sets.

Immunofluorescence

Cells were plated on IBDI-treated coverslips overnight. After treatments, cells were fixed by 4% paraformaldehyde in PBS for 15 min and subsequently permeabilized with 50

μg/ml digitonin in PBS for 10 min at room temperature. Cells were blocked in blocking buffer (1% BSA and 2% serum in PBS) for 30 min, followed by incubation with primary antibodies in the same buffer for 1 h at room temperature. Samples were then washed 2× in PBS and 1× in blocking buffer before incubation with secondary antibodies 1 h at room temperature. Slides were washed 3× in PBS, stained with DAPI and mounted. Images were captured with inverted epifluorescent Zeiss AxioObserver.Z1. In the case of outside/inside bacterial staining, before permeabilization, the cells were incubated with anti-LPS antibody and corresponding secondary antibody in blocking buffer, accompanied by 3× PBS washes in between.

Quantification of immunofluorescence

An automated protocol built in the ImageJ software was used to analyse epifluorescent microscopy images to avoid bias. The same protocol was applied to each field of view and across samples. An average of eight unique fields of view from representative experiments was selected for quantification.

***In vitro* ULK1 kinase assay**

HEK293A transiently expressing tagged ATG16L1 was immunoprecipitated. Pull-down proteins were washed 3× with MLB and 1× with MOPS buffer and were used as substrates for ULK1 kinase assay. ULK1 proteins were immunoprecipitated and extensively washed with MLB (once) and RIPA buffer (50 mM Tris at pH 7.5, 150 mM NaCl, 50 mM NaF, 1 mM EDTA, 1 mM EGTA, 1% SDS, 1% Triton X-100 and 0.5% deoxycholate) once, followed by washing with MLB buffer once followed by equilibration with ULK1 assay buffer (kinase base buffer supplemented with 0.05 mM DTT, 10 μM cold

ATP and 0.4 µCil 32P-ATP per reaction). Reactions were shaken at 250 rpm at 37°C for 30 min and stopped by direct addition of 4× sample buffer followed by 10-min boiling at 95°C and resolution by SDS–PAGE. The analysis of kinase reactions necessitated the separation of the kinase and substrate. *In vitro* kinase reactions were analysed by autoradiograms.

Colony-forming unit assay

Cells were infected with *Salmonella* (MOI of 180) for 1 h. The infected cells were washed 2× and incubated with media containing 100 µg/ml Gentamicin for 0.5 h, followed by 4-h incubation with media containing 50 µg/ml Gentamicin. The samples were rinsed 3× with PBS and lysed with CFU buffer (0.1% Triton X-100 and 0.01% SDS in PBS). The harvested lysates were serially diluted (1:100, 1:300 and 1:1,000) and plated onto LB agar plates containing Streptomycin. The plates were incubated at 37°C for 16–18 h, and the colonies were counted to determine the number of CFU.

2.6 Acknowledgments

We would like to thank members of the Russell laboratory for advice and critical reading of this manuscript. We the authors would like to apologize to colleagues whose significant work could not be included due to length, citation limitations or author oversight. This work was supported by Canadian Institutes of Health Research (CIHR) Project Grants awarded to RCR (#PJT153034), the UK Dementia Research Institute (funded by MRC, Alzheimer's Research UK and the Alzheimer's Society), Wellcome Trust [Principal Research Fellowship to DCR (095317/Z/11/Z)], Strategic Grant to Cambridge Institute for Medical Research (100140/Z/12/Z) and studentship to AJ, and the Roger de Spoelberch Foundation. Academic scholarship from the Government of Saudi Arabia (#5976670433) and studentship supported RA. TTL was supported by an Ontario Graduate Scholarship. Microscopy support was provided by the Cell Biology and Image Acquisition core facility, Faculty of Medicine, University of Ottawa.

2.7 Supplementary Information

A

pS278

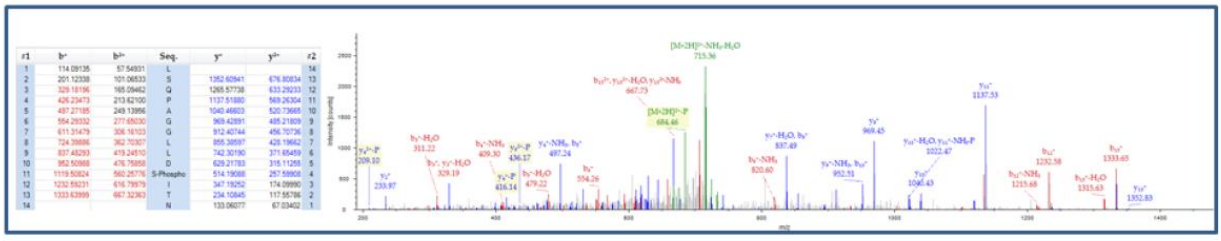

pS287

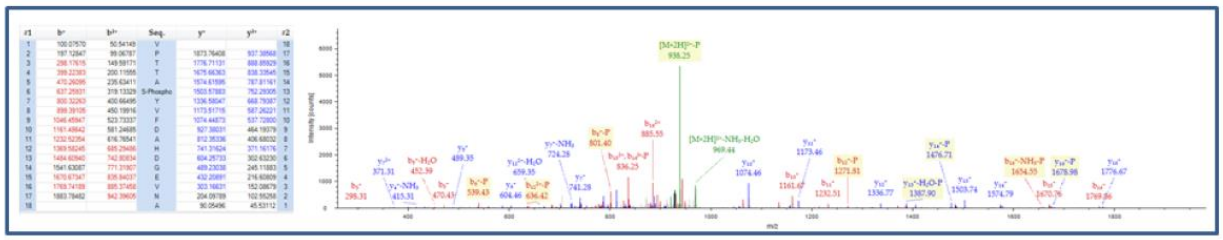

B

C

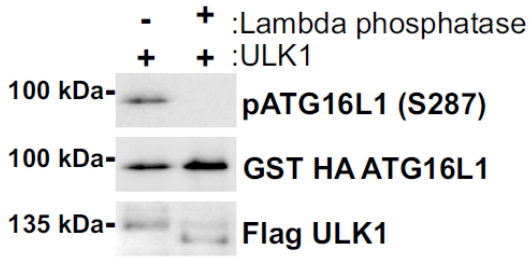

Figure EV1. ATG16L1 is a target of ULK1 kinase.

(A) Mass spectrometry data for ULK1-mediated ATG16L1 phosphorylation. (B) ATG16L1 knock-out HEK293A cells were transfected with either flag-tagged wild-type or S287A ATG16L1. Phosphorylation of ATG16L1 at S287 was determined by WB. (C) Wild-type ATG16L1 substrate and ULK1 were incubated with or without lambda phosphatase. Phospho-specificity of ATG16L1(S287) antibody was determined by immunoblot for total- and phospho-ATG16L1.

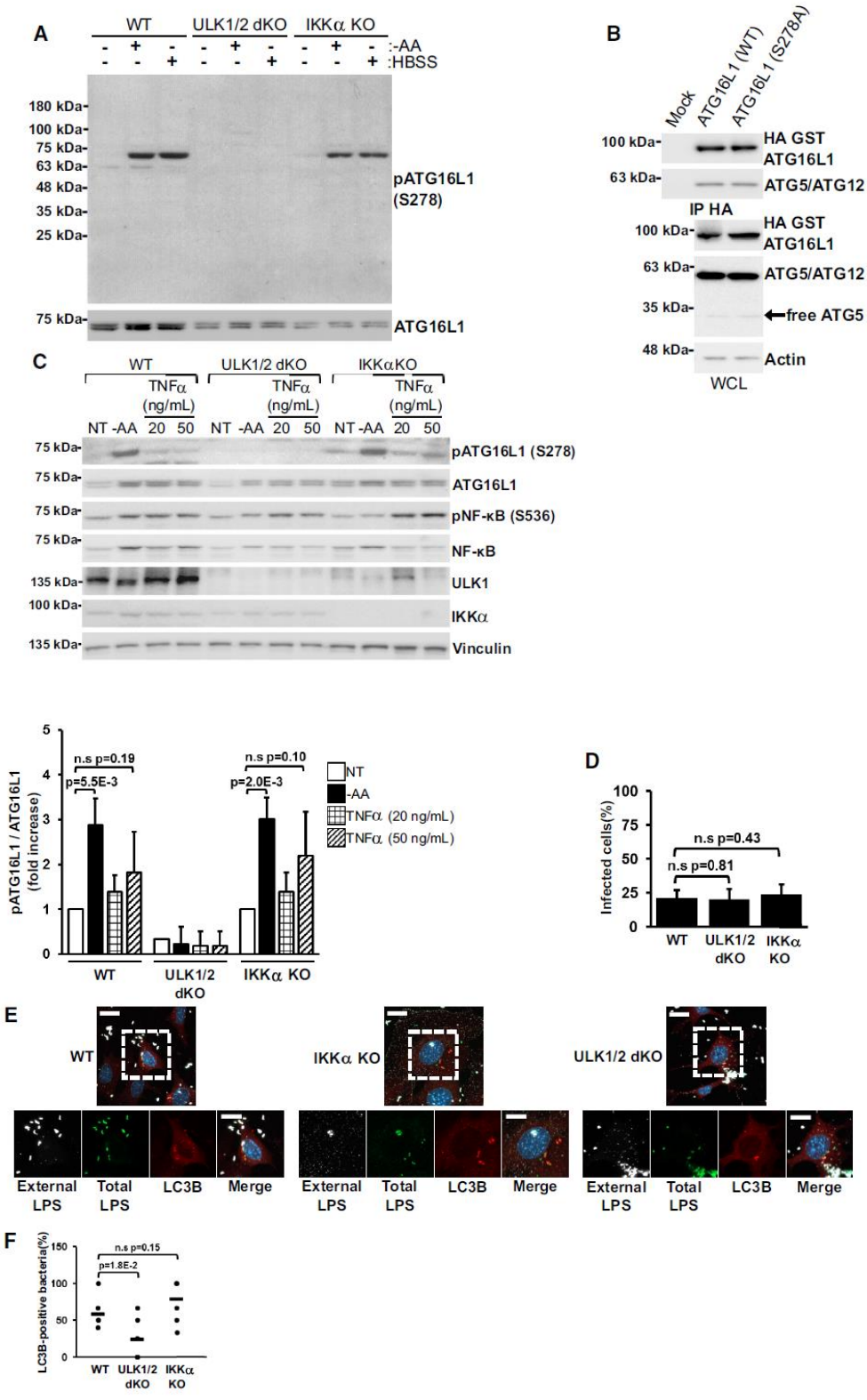
A
WT
ULK1/2 dKO
IKKα KO
:-AA
:HBSS
180 kDa
100 kDa
75 kDa
63 kDa
48 kDa
35 kDa
25 kDa
pATG16L1 (S278)
75 kDa
ATG16L1
B
Mock
ATG16L1 (WT)
ATG16L1 (S278A)
100 kDa
HA GST ATG16L1
63 kDa
ATG5/ATG12
IP HA
HA GST ATG16L1
ATG5/ATG12
35 kDa
free ATG5
48 kDa
Actin
WCL
C
WT
ULK1/2 dKO
IKKαKO
TNFα (ng/mL)
NT -AA 20 50
pATG16L1 (S278)
ATG16L1
pNF-κB (S536)
NF-κB
135 kDa
ULK1
IKKα
Vinculin
pATG16L1 / ATG16L1 (fold increase)
n.s p=0.19
p=5.5E-3
n.s p=0.10
p=2.0E-3
NT
-AA
TNFα (20 ng/mL)
TNFα (50 ng/mL)
WT
ULK1/2 dKO
IKKα KO
D
Infected cells(%)
n.s p=0.43
n.s p=0.81
WT
ULK1/2 dKO
IKKα KO
E
WT
IKKα KO
ULK1/2 dKO
External LPS
Total LPS
LC3B
Merge
F
LC3B-positive bacteria(%)
n.s p=0.15
p=1.8E-2
WT
ULK1/2 dKO
IKKα KO

Figure EV2. ULK1 is required for phosphorylation of ATG16L1 and xenophagy induction.

(A) Full scan for WB data for phospho-ATG16L1(S278) is shown in Fig 2A. (B) ATG16L1 knock-out HEK293A cells transfected with the indicated GST HA ATG16L1 plasmids were immunoprecipitated for HA. WB was used to examine the binding of ATG5/ATG12 to ATG16L1. (C) Wild-type, ULK1/2 dKO or IKKα KO MEFs cells were treated with either amino acid-free media or the indicated amounts of TNFα for 3 h. Samples were immunoblotted using the indicated antibodies. Levels of ATG16L1 phosphorylation were quantified from three biological replicates. Data are represented as mean ± standard deviation, and P-values were determined by Student's t-test. (D) Wild-type, ULK1/2 dKO and IKKα KO MEFs cells were infected with *Salmonella* for 1 h. Quantification of infected cells was examined through immunofluorescence of two biological repeats. Data are represented as mean ± standard deviation from seven unique fields of view, and P-values were determined by Student's t-test. (E) Larger field of view for images shown in Fig 2C. Extracellular bacteria staining observable in white. MEF cells were infected with *Salmonella* for 1 h in the presence of bafilomycin A1. Endogenous LC3B (red) puncta were visualized (scale bars, 20 and 10 μm) by immunofluorescence. Dashed boxes represent the cells selected for enlarged display in Fig 2C. (F) Quantification of LC3B-positive bacteria of Fig 2C biological replicate. Wild-type, ULK1/2 dKO or IKKα KO MEFs cells were infected with *Salmonella* for 1 h. Autophagic capture of *Salmonella* was analysed by immunostaining for LPS and LC3B. Data are represented as mean, and P-values were determined by Student's t-test.

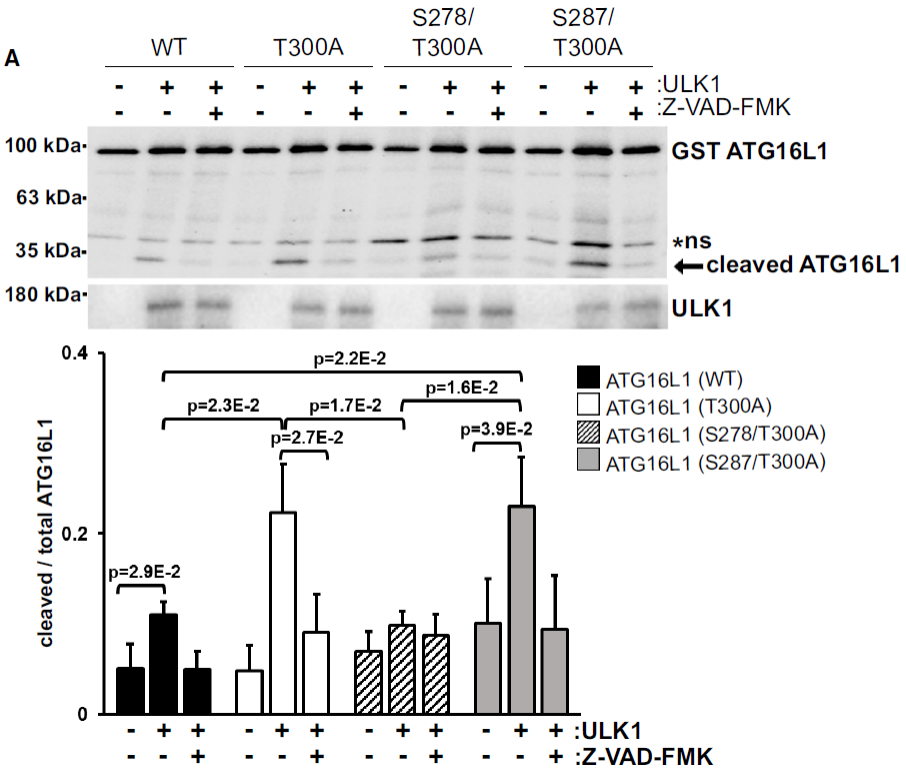

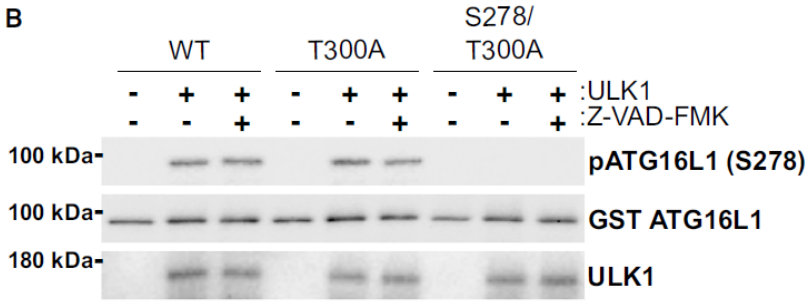

C

Gene	Cell	Disruption of exon 1 of ATG16L1	
ATG16L1	HCT116	WT: tgacttcccc cgctggaagc.....ttcgaggaga A1/A2: tgacttcccc cg--------.....-tcgaggaga	59bp del.
	HEK293A	WT: tgacttcccc cgctggaagc.....ttcgaggaga A1: tgacttcccc cg-tggaagc.....ttcgaggaga A2: tgacttcccc cg--------.....-ttcgaggaga	1 bp del. 58 bp del.

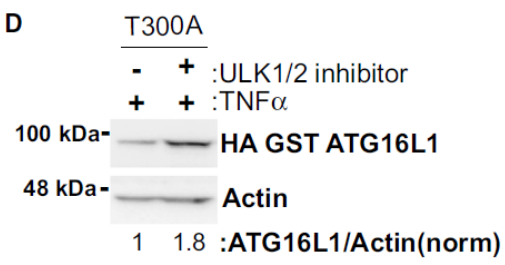

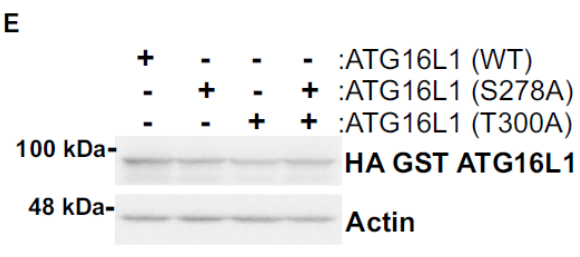

Figure EV3. ULK1 promotes cleavage of caATG16L1 through phosphorylation on S278.

(A) ATG16L1 knock-out HEK293A cells were transfected with the indicated GST HA ATG16L1 plasmids in the presence or absence of Z-VAD-FMK (15 μM) for 4 h. Cleavage of ATG16L1 was analysed by WB of two biological replicates. Data are represented as mean, and P-values were determined by Student's t-test. (B) ATG16L1 knock-out HEK293A cells were transfected with the indicated GST HA ATG16L1 plasmids in the presence or absence of Z-VAD-FMK (15 μM) for 4 h. Phosphorylation of ATG16L1 was analysed by WB. (C) ATG16L1 knock-out cells were validated by direct sequencing. (D) ATG16L1 knock-out HCT116 cells transfected with the tagged T300A ATG16L1 plasmids were treated with TNFα (20 ng/ml) in the presence or absence of ULK1/2 inhibitor for 4 h. ATG16L1 levels were examined by WB. (E) Inputs for CFU assays in Fig 3E. ATG16L1 knock-out HEK293A transfected with tagged ATG16L1 as indicated were lysed and examined by WB.

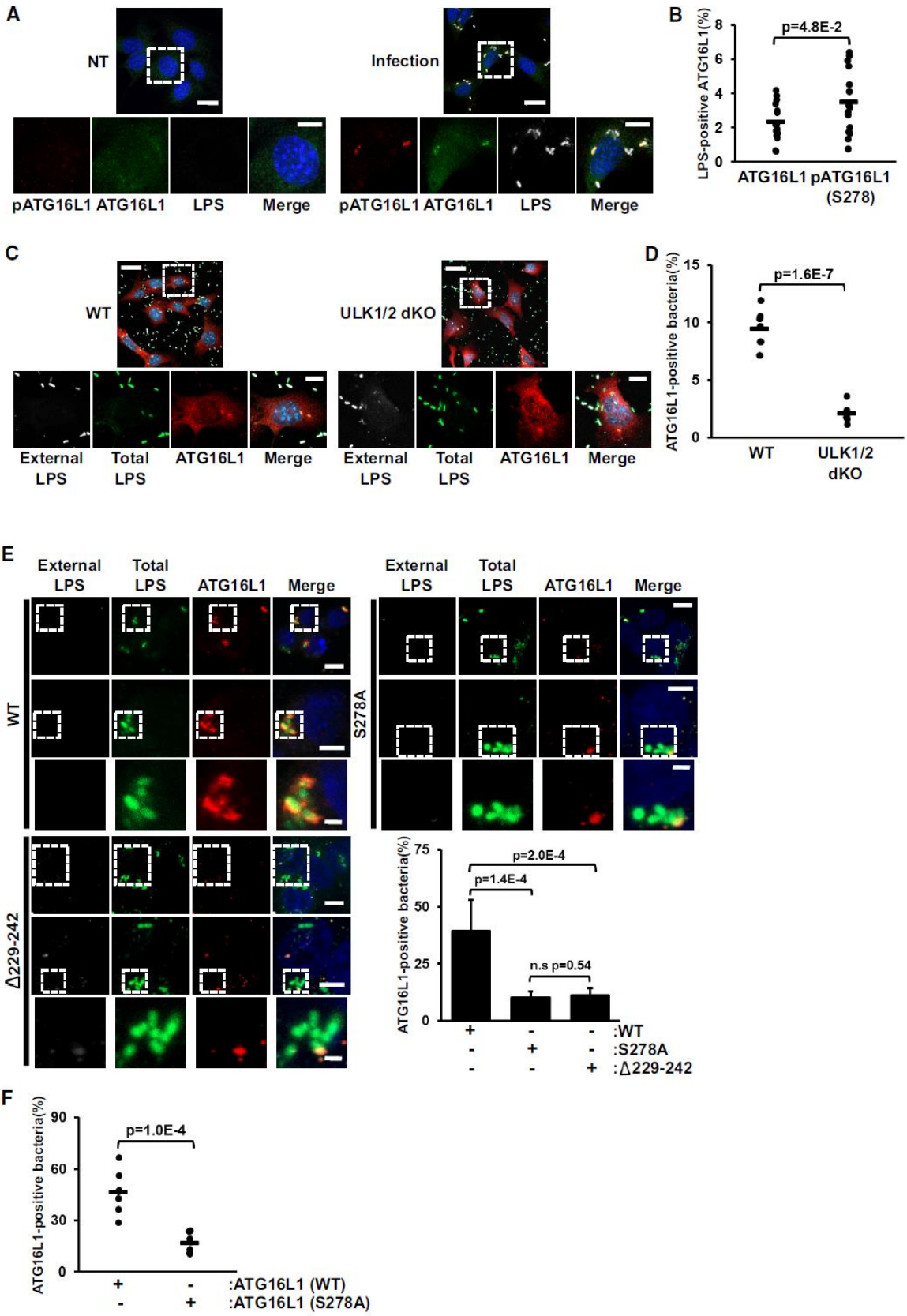
A
NT
Infection
pATG16L1 ATG16L1 LPS Merge
pATG16L1 ATG16L1 LPS Merge
B
LPS-positive ATG16L1(%)
p=4.8E-2
ATG16L1 pATG16L1 (S278)
C
WT
ULK1/2 dKO
External LPS
Total LPS
ATG16L1
Merge
D
ATG16L1-positive bacteria(%)
p=1.6E-7
WT
ULK1/2 dKO
E
External LPS
Total LPS
ATG16L1
Merge
WT
S278A
Δ229-242
ATG16L1-positive bacteria(%)
p=2.0E-4
p=1.4E-4
n.s p=0.54
:WT
:S278A
:Δ229-242
F
ATG16L1-positive bacteria(%)
p=1.0E-4
:ATG16L1 (WT)
:ATG16L1 (S278A)

Figure EV4. ULK1-mediated phosphorylation is required for ATG16L1 localization to *Salmonella* site.

(A) Larger field of view for images shown in Fig 4A. Bacteria staining observable in white. MEF cells were infected with *Salmonella* for 25 min. Phospho-ATG16L1 (red) and total ATG16L1 (green) were visualized (scale bars, 20 and 10 μm) by immunofluorescence. Dashed boxes represent the cells selected for enlarged display in Fig 4A. (B) Quantification of ATG16L1 localization to the bacteria of Fig 4A biological replicate. Wild-type MEF cells were infected with *Salmonella* for 25 min. Phospho-ATG16L1, total ATG16L1 and LPS were stained and analysed by immunofluorescence. Data are represented as mean, and P-values were determined by Student's t-test. (C) Larger field of view for images shown in Fig 4B. Extracellular bacteria staining observable in white. MEF cells were infected with *Salmonella* for 25 min. Endogenous ATG16L1 (red) puncta were visualized (scale bars, 30 and 10 μm) by immunofluorescence. Dashed boxes represent the cells selected for enlarged display in Fig 4B. (D) Quantification of ATG16L1 puncta of Fig 4B biological replicate. Wild-type and ULK1/2 dKO cells were infected with *Salmonella* for 25 min. Immunofluorescence was performed using antibodies against LPS and ATG16L1. Data are represented as mean, and P-values were determined by Student's t-test. (E) Larger field of view for images shown in Fig 4C and extra data from the same experiment were also included. ATG16L1 knock-out HCT116 cells transfected with the indicated GST HA ATG16L1 were infected with *Salmonella* for 1 h. ATG16L1 (red) puncta were analysed by immunofluorescence (scale bars, 10, 5 and 1 μm). The experiments were repeated twice. Data are represented as mean ± standard deviation from seven unique fields of view, and P-values were determined by Student's t-test. (F)

Quantification of ATG16L1-positive bacteria of Fig 4C biological replicate. ATG16L1 knock-out HCT116 cells transfected with the indicated GST HA ATG16L1 were infected with *Salmonella* for 1 h. Bacteria were stained using anti-LPS antibodies to analyse localization in addition to ATG16L1. Data are represented as mean, and P-values were determined by Student's t-test.

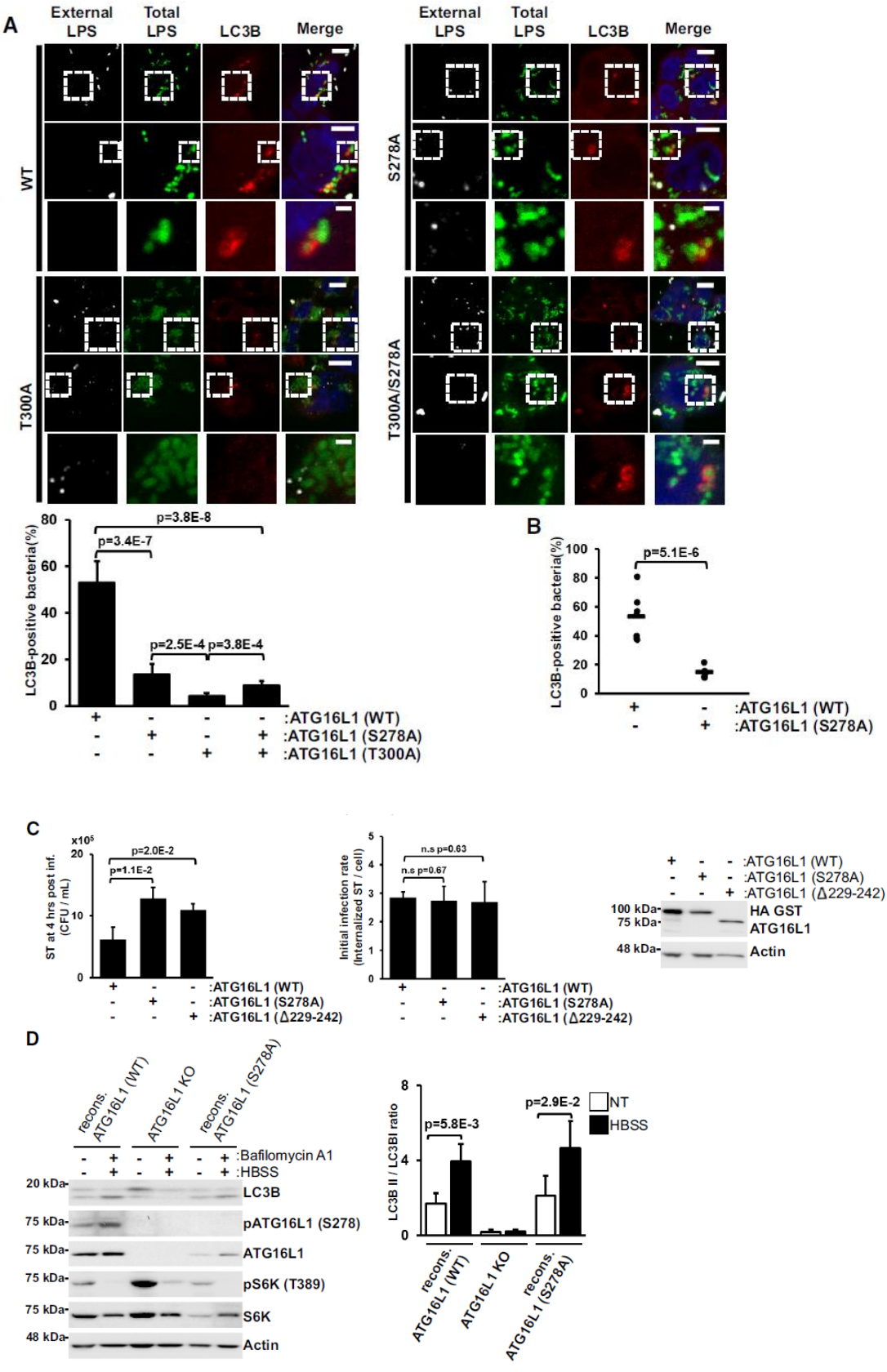
A
External LPS
Total LPS
LC3B
Merge
WT
S278A
T300A
T300A/S278A
LC3B-positive bacteria(%)
p=3.8E-8
p=3.4E-7
p=2.5E-4
p=3.8E-4
:ATG16L1 (WT)
:ATG16L1 (S278A)
:ATG16L1 (T300A)
B
p=5.1E-6
:ATG16L1 (WT)
:ATG16L1 (S278A)
C
ST at 4 hrs post inf. (CFU / mL)
p=2.0E-2
p=1.1E-2
Initial infection rate (Internalized ST / cell)
n.s p=0.63
n.s p=0.67
:ATG16L1 (Δ229-242)
100 kDa
75 kDa
48 kDa
HA GST
ATG16L1
Actin
D
recons. ATG16L1 (WT)
ATG16L1 KO
recons. ATG16L1 (S278A)
:Bafilomycin A1
:HBSS
20 kDa
LC3B
pATG16L1 (S278)
ATG16L1
pS6K (T389)
S6K
Actin
LC3B II / LC3BI ratio
p=5.8E-3
p=2.9E-2
NT
HBSS

Figure EV5. ULK1-mediated phosphorylation is required for xenophagy and bacterial clearance.

(A) Larger field of view for images shown in Fig 4D, and extra data from the same experiment were also included. ATG16L1 knock-out HCT116 cells transfected with the indicated GST HA ATG16L1 were infected with *Salmonella* for 1 h. LC3B (red) puncta were analysed by immunofluorescence (scale bars, 10, 5 and 1 μm). The experiments were repeated twice. Data are represented as mean ± standard deviation from seven unique fields of view, and P-values were determined by Student's t-test. (B) Quantification of LC3B-positive bacteria of Fig 4D biological replicate. ATG16L1 knock-out HCT116 cells transfected with the indicated GST HA ATG16L1 were infected with *Salmonella* for 1 h. Bacteria were stained using anti-LPS antibodies to analyse localization in addition to the autophagy marker LC3B. Data are represented as mean and P-values were determined by Student's t-test. (C) ATG16L1 knock-out HEK293A cells transfected with the indicated HA GST ATG16L1 plasmids were infected with *Salmonella* for 1 h. Xenophagy rates were examined through CFU assays. Quantification of infection rates by immunofluorescence is demonstrated in the middle panel. Expression of ATG16L1 was examined by WB (bottom panel). The experiments were repeated three times. Data are represented as mean ± standard deviation, and P-values were determined by Student's t-test. (D) ATG16L1 KO HCT116 cells with or without the indicated reconstituted OLLAS ATG16L1 were incubated with HBSS media in the presence of bafilomycin A1 for 1 h. LC3B flux was analysed by WB. The experiments were repeated three times. Data are represented as mean ± standard deviation, and P-values were determined by Student's t-test.

Chapter 3: A Pooled CRISPR Screen Protocol for Comparative Autophagy Analysis Across Multiple Stressors

Currently preparing for submission to *Autophagy Reports*.

Truc T. Losier, James Taylor, Maxime W.C. Rousseaux, Ryan C. Russell

3.1 Statement of Author Contributions

TTL and RCR drafted the manuscript. **TTL** designed and performed majority of the experiments. MWCR and RCR conceptualized the study, guided the experimental planning, and supervised the development of the manuscript. RCR, MWCR, and JT contributed to manuscript editing.

A Pooled CRISPR Screen Protocol for Comparative Autophagy Analysis Across Multiple Stressors

Truc T. Losier[1], James Taylor[1], Maxime W.C. Rousseaux[1,2,3,#], Ryan C. Russell[1,2,3,4,#,*]

[1] Department of Cellular and Molecular Medicine, University of Ottawa, 451 Smyth Road, Ottawa, Ontario K1H 8M5, Canada.

[2] University of Ottawa Brain and Mind Research Institute, Ottawa, Ontario, K1H 8M5, Canada.

[3] Ottawa Institute of Systems Biology, Ottawa, Ontario, K1H 8M5, Canada

[4] University of Ottawa Center for Infection, Immunity and Inflammation, Ottawa, Ontario, K1H 8M5, Canada.

[#] Co-corresponding authors: ryan.russell@uottawa.ca; max.rousseaux@uottawa.ca

[*] Lead contact: 451 Smyth Rd, Ottawa, Ontario, K1H 8M5, Canada.

Keywords: Autophagy; selective autophagy; high-throughput screens; CRISPR screens

3.2 Abstract

Autophagy is a highly conserved catabolic pathway utilized by cells to cope with cellular stress. Some stresses like nutrient starvation promote a relatively indiscriminate degradation of cytosolic components, which is called bulk autophagy. Conversely, selective autophagy promotes the specific turnover of targeted cargo. Kinase-mediated phosphorylation plays an essential role in both bulk and selective autophagy processes. However, unlike bulk autophagy, the role of kinases in regulating selective autophagy pathway is less well defined. Here, we detail a modified kinome-wide CRISPR-based screen method that was optimized to allow comparative analysis of autophagy regulators under different stress conditions, starting from the same population of cells. The improvement in this protocol includes proper fixation controls to allow for excellent temporal control, enabling parallel analysis of multiple pathways. Fixation or crosslinking aids in preserving samples, thereby ensuring consistency in autophagy flux and minimizing variability caused by extended sorting times and sample handling processes. Using this protocol we can identify kinases that are selectively involved in specific forms of autophagy and overlap between other regulators. This methodology can be adapted to address several outstanding questions in the autophagy field as we continue to uncover distinct mechanisms of regulation in the autophagic response to stress.

3.3 Introduction

Macroautophagy (hereafter referred to as autophagy), a conserved stress-induced catabolic pathway, is driven by the activity of highly conserved autophagy-related (ATG) proteins, which trigger the formation of a double-membrane structure called an autophagosome(Kaur and Debnath 2015). Autophagosomes mature into degradative vesicles after fusion with lysosomes, which supply the acid hydrolases necessary for breaking down sequestered macromolecules or cargo(Mizushima and Klionsky 2007). One of the earliest steps in autophagy initiation is the activation of the protein kinase ULK1 (Unc-51-like kinase-1)(Chan et al. 2007). ULK1 phosphorylates and activates several ATG proteins, including multiple subunits of the pro-autophagic VPS34 (vacuolar protein sorting 34) complexes to promote stress-induced autophagy(Russell et al. 2013; Alsaadi et al. 2019; Park et al. 2018; Park et al. 2016; Di Bartolomeo et al. 2010; Zhou et al. 2017). Additionally, lipidation of ATG8 family members (LC3A, B and C, GABARAP, GABARAPL1 and GABARAPL2) to the lipid phosphatidylethanolamine is critical for maturation of the autophagosome and encapsulation of recruited cargo(Martens and Fracchiolla 2020).

Autophagy was initially characterized as a process to promote the indiscriminate engulfment and breakdown of cytosolic components(Mortimore and Schworer 1977). However, the significance of targeted autophagic degradation of specific cargo (referred to as selective autophagy) has been established to be important in normal cell homeostasis and disease(Levine and Kroemer 2008; Svenning and Johansen 2013; Kim et al. 2016; Yamamoto et al. 2023). Selective autophagy can be classified into different subtypes depending on the specific cellular components recruited for degradation:

degradation of captured pathogens (xenophagy), aggregated proteins (aggrephagy), lipid (lipophagy), mitochondria (mitophagy), endoplasmic reticulum (ER-phagy), peroxisomes (pexophagy), lysosomes (lysophagy), and ribosomes (ribophagy) (Kim et al. 2016; Gatica et al. 2018; Germain and Kim 2020; Papadopoulos and Meyer 2017; Lamark and Johansen 2012; Cebollero et al. 2012; Rubio-Tomás et al. 2023). Selective autophagy not only requires all components of core autophagy machinery but also needs the activity of proteins called autophagy receptors(Zaffagnini and Martens 2016; S et al. 2017). Autophagy receptors can be classified into ubiquitin-bound and membrane-bound groups(Kim et al. 2016; Vargas et al. 2023). Well-known ubiquitin-bound receptors include p62/SQSTM1 (sequestosome-1), NBR1, NDP52, and OPTN(Kim et al. 2016). They typically contain both LC3-interacting region (LIR) and ubiquitin-binding domains (UBD), which allows them to interact with ubiquitinated cargo and sequester them to autophagosomal site for degradation(Kim et al. 2016). Additionally, membrane-associated receptors located on the target organelles are responsible for decorating the damaged organelles, rendering them recognizable by the core autophagy machinery(Anding and Baehrecke 2017). Notably, dysregulated selective autophagy has been associated with several human diseases(Ryter et al. 2013; Ichimiya et al. 2020). For example, defective xenophagy results in chronic infectious diseases or inflammatory diseases(Shao et al. 2021; Brest et al. 2010; Chandra and Kumar 2016)·. Impaired mitophagy contributes to neurological diseases and cancer(Denisenko et al. 2021; Zhang et al. 2021). Dysregulated ER-phagy is implicated in neurodegenerative disorders due to neuronal damage caused by failed clearance of misfolded proteins(Remondelli and

Renna 2017). Impaired degradation of damaged peroxisomes contributes to Zellweger spectrum disorders(Cho et al. 2018; Till et al. 2012).

Kinase-mediated phosphorylation is an important signalling mechanism in autophagy regulation and is best understood in the context of bulk autophagy induced by nutrient starvation(King et al. 2021). Nutrient-sensitive kinases such as mTORC1 (mechanistic target of rapamycin complex 1) and AMPK (AMP-activated kinase) are well implicated in autophagy regulation(Balgi et al. 2009; Garcia and Shaw 2017; Jung et al. 2010). mTORC1 hinders autophagy by direct inhibitory phosphorylation of multiple components associated with autophagy induction including ULK1(King et al. 2021; Kim et al. 2011; Shang et al. 2011; Puente et al. 2016). Nutrient starvation inactivates mTORC1, which leads to the release of its downstream targets from inhibitory phosphorylation and subsequently initiates autophagy pathway(Alers et al. 2012). In addition, AMPK modulates autophagy flux through regulation of mTORC1 and ULK1(Kim et al. 2011; Alers et al. 2012; Gwinn et al. 2008). AMPK and mTORC1 have been shown to directly regulate pro-autophagic VPS34 complexes to induce autophagy(Yuan et al. 2013; Kim et al. 2013). Notably, several studies have reported the importance of kinase signalling in selective autophagy pathways in addition to bulk autophagy. For instance, under oxidative stress, ATM kinase phosphorylates pexophagy receptor PEX5, which leads to PEX5 ubiquitination, interaction of ubiquitinated PEX5 with p62, and subsequent pexophagy induction(Zhang et al. 2015). During mitochondrial stress, PINK1, a serine/threonine protein kinase, becomes stabilized on the outer mitochondrial membrane (OMM)(Truban et al. 2017). Here, it facilitates Parkin-mediated ubiquitination of target proteins, which subsequently recruits the autophagy machinery to engulf and

degrade damaged mitochondria(Truban et al. 2017). Moreover, TBK1 kinase has been reported to regulate mitophagy and autophagic degradation of pathogens through phosphorylation of autophagy receptors(Richter et al. 2016; Pilli et al. 2012).

Several high throughput screens have been conducted to identify basal autophagy regulators using RNAi or CRISPR/Cas9-based approaches(Szyniarowski et al. 2011; Lipinski et al. 2010; Hale et al. 2016; Guo et al. 2018; Mimura et al. 2021). Additionally, starvation-induced autophagy screens have been performed to elucidate autophagy regulators involved in nutrient stress pathways(Chan et al. 2007; McKnight et al. 2012; Morita et al. 2018). However, there lacks a comprehensive and comparative analysis of kinase signaling, which would provide a more thorough understanding of kinase regulation in different selective autophagy pathways. An ideal screen model for this analysis should feature the same pool of cells, the same autophagy reporter, and same day of treatment or acute treatment timepoints to minimize secondary signaling effects. This raises technical hurdles with the above desired conditions, including reporter sensitivity across conditions, sorting time, and the impact of wait time on results. In this study, we created a screen workflow that allows for analysis of multiple stress-induced autophagy processes using fixation and p62.

3.4 Materials

Cell culture

In this study, HEK293A cells (Thermo Fisher Scientific # R70507) are used to generate the reporter cell line as they show optimal responses to several stress conditions and have been extensively characterized in the field. Additionally, HEK293A demonstrates excellent transfection and transduction efficiency with both viral and non-viral vectors(Tan et al. 2021). Alternative cell lines can be chosen for the screening process provided they exhibit optimal responses to the stress conditions. HEK293T cells (ATCC# CRL-3216) are used to generate lentiviruses carrying either autophagy reporter DsRed-IRES-GFP-p62 or human kinome CRISPR knockout library. They are cultured in DMEM supplemented with 10% bovine calf serum (VWR Life Science Seradigm).

Amino acid free media

The recipe for amino acid starvation media is described in Table 1.

Chemical	**Working concentration (mM)**
Calcium Chloride ($CaCl_2$)	1.8
Ferric Nitrate Solution ($Fe(NO_3)_3$-$9H_2O$, stored at 4ºC)	0.000248
Magnesium Sulfate ($MgSO_4$-$7H_2O$)	0.814
Potassium Chloride (KCl)	5.33
Sodium Bicarbonate ($NaHCO_3$)	44.05
Sodium Chloride (NaCl)	81.9

Sodium Phosphate monobasic (NaH_2PO_4-H_2O)	0.906
D-Glucose (Dextrose)	25
HEPES	25.03
Phenol Red (optional)	0.0399

1. Above compounds are added into 800 ml of distilled H2O and the solution is stirred till everything is completely dissolved.
2. pH is adjusted to approximately 7.4.
3. 20 mL of 100X MEM vitamins (VWR#45000-702) is added so that the final concentration is 2X.
4. The total volume is brought up to 1 L.
5. The solution is filtered through 0.22 μm Stericup (Thermo Fisher Scientific#SCGPU11RE), aliquoted into 50ml tubes, and stored at 4ºC.

Plasmids

pLenti-DsRed-IRES-eGFP vector is from Addgene (Cat#92194). Brunello human kinome CRISPR knockout library can be obtained from Addgene (Cat#1000000083). To generate lentiviruses, lentiviral packaging plasmids psPAX2 (Addgene#12260) and pMD2.G (Addgene#12259) are transfected in HEK293T cells along with plasmid carrying either Dsred-IRES-GFP-p62 or human kinome CRISPR knockout library.

Other chemicals or reagents

PolyJet, PEI, polybrene, crystal violet, PBS, PFA, EDTA, Tris, BSA, SDS, protein kinase K, RNAse A, ammonium acetate, isopropanol, ethanol, 2xQ5 Master Mix (New England Biolabs, M0494L), AMPure XP Bead-Based Reagent (Beckman Coulter, A63881), Nextera XT Index Kit (Lot#10089169).

Flow cytometry

Autophagy flux can be analysed in a rapid and quantitative manner using flow cytometers – in this case BD Celesta or BD LSRFortessa analyzers and a Sony Biotechnology SH800 sorter – equipped with a blue (488 nm) laser and a yellow-green (561 nm) laser. This instrumental set-up allows for the sensitive detection of DsRed and GFP-p62 signals. These signals are then examined and analysed using FlowJo software.

Other equipment

Tissue culture hoods and incubators are required to culture and maintain the cell lines needed for the kinome screens. Other general laboratory equipment including vortex, cell counter, PCR machine, centrifuge, and -80ºC freezer are also necessary.

3.5 Methods

1. Generation of the reporter cell line

Sequestosome-1/p62 is an autophagy receptor involved in nearly all selective autophagy pathways and can be used as a marker for autophagy flux. To measure changes in autophagic regulation, a dual-fluorescence reporter, DsRed-IRES-GFP-p62, is constructed. p62 is incorporated into and degraded along with the autophagosomal membrane; therefore, the expression level of GFP-p62 is inversely proportional to autophagic flux (Figure 1). DsRed serves as an internal control for GFP expression (Figure 1). The reporter cell line must express DsRed-IRES-GFP-p62 stably as transient transfection will generate fluctuating expression levels of tagged p62 and cause inconsistent autophagy baseline, which may affect the screening outcomes and yield false positive results. The DsRed-IRES-GFP-p62 construct can be introduced to HEK293A using lentivirus approach.

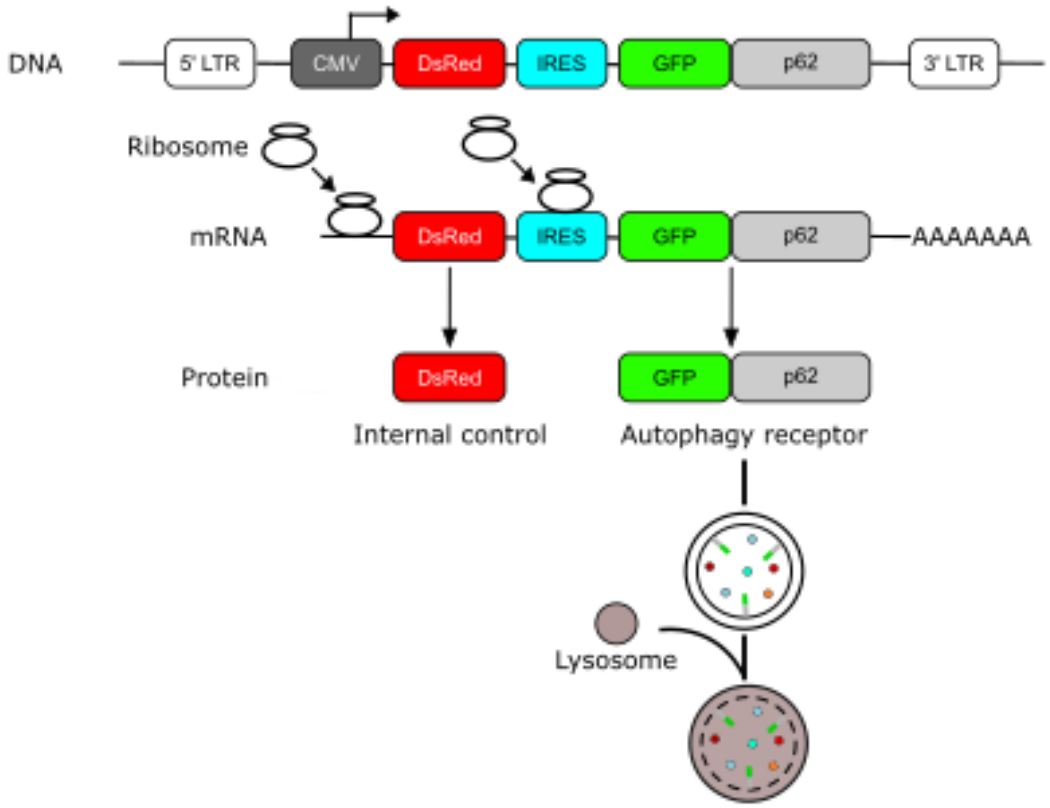

Figure 1: Reporter diagram.

The schematic depicts the autophagic flux reporter consisting of DsRed and GFP-tagged p62. p62 is selectively integrated into and degraded alongside the autophagosomal membrane. Thus, the expression level of GFP-p62 correlates inversely with autophagic flux.

Production of lentiviruses carrying DsRed-IRES-GFP-p62

1. 3 μg of plasmid containing DsRed-IRES-GFP-p62, 1 μg of psPAX2, and 0.25 μg of pMD2.G are transfected in 35% confluence (3-4 million) of HEK293T cells in one 10-cm plate using PEI. 4 μL of PEI is used for 1 μg of DNA. Media are changed 5 hours post transfection.
2. Media are collected four times 12 hours apart starting at 36 hours post transfection.
3. Viral supernatant is filtered through 0.45 μM Nalgene™ Rapid-Flow™ Sterile Disposable Filter Units (Thermo Fisher Scientific#09-740-63A).*Optional centrifugation if many cells lift. Cleared supernatants are concentrated using Virus Precipitation Kit (Benchmark Bioscience) to 1/100 of the original volume.
4. The viruses are stored at -80ºC.

Generation of HEK293A expressing DsRed-IRES-GFP-p62

1. HEK293A cells are seeded at 20% confluence (approximately 0.34 x 10^6 cells) in a 6-well plate. An extra well can be plated as a negative control for G418 selection.
2. Virus transduction can be performed when cells reach approximately 40% confluence.
3. HEK293A cells are highly susceptible to transduction, so 1 μL of viruses is added to one well and a serial dilution is performed in the presence of polybrene (10 μg/mL). Notably, polybrene working concentrations (ranging from 1 to 10 μg/mL) and the quantity of viruses can be fine-tuned based on the sensitivity to polybrene and the susceptibility to viral transduction of the chosen cell line.

4. Next day, cells are transferred to 10-cm plates.

5. 48 hours post transduction, negative or non-transduced and transduced cells are incubated with complete DMEM containing G418 (1 mg/mL) for 3-7 days or until all negative cells die. The culture media are replaced every day with G418-containing media if more than 10% of cells lift.

6. Expressions of tagged p62 in the polyclonal populations are examined using western blot (WB). In addition, amino acid-free medium, a potent stress condition to induce autophagy, can be employed to investigate the autophagic responses in these cells.

7. We found that the polyclonal cells infected with the least number of viruses exhibit extremely elevated levels of tagged p62 compared to the endogenous p62 and show no detectable responses to starvation stress (Figure 2A).

8. The polyclonal reporter line is sorted into monoclonal populations which are first evaluated by WB to identify the optimal clone expressing optimal level of tagged p62 and showing consistent responses to amino acid-free starvation. WB of the ideal clone is shown in Figure 2B.

9. Our screen design employs fluorescence-activated cell sorting (FACS) to isolate populations with changes in autophagic flux as measured by our fluorescence-based reporter, which are then further investigated through next-generation sequencing (NGS) technologies. Thus, following WB test, we use FACS to examine the autophagic response to starvation of monoclonal reporter cells.

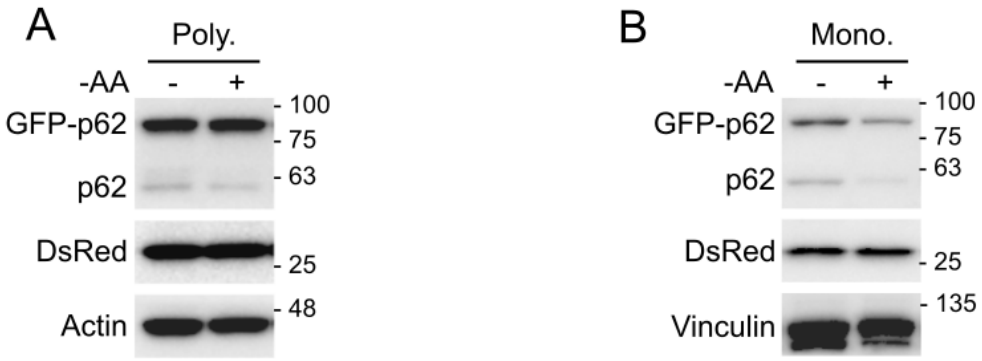

Figure 2: Examination of autophagy flux through examination of p62.

(A), (B) Polyclonal (A) and optimal monoclonal (B) populations expressing DsRed and GFP-p62 were incubated with amino acid-free media for 3 hours. Whole-cell lysates were immunoblotted using the antibodies indicated.

Validation of the reporter cell line

To verify that stress-induced changes in p62 levels are mediated by autophagy, established autophagy-regulating genes are disrupted, and the impact of these gene depletions on p62 regulation can be assessed by WB and flow cytometry. For instance, knockout of components involved in autophagy induction including ATG5, ATG7, FIP200, or ULK1 should result in p62 accumulation. Perturbation of proteins associated with autophagy inhibition such as Rubicon should lead to enhanced degradation of p62. sgRNAs targeting autophagy genes of choice can be cloned in the vector backbone used to construct the library, which can be used for optimization described in Section 3.

Examination of the autophagic response of the reporter line to selected stress conditions

Following the confirmation of validity of the reporter cells, it is important to assess their responsiveness to the stress conditions of interest. The stimuli can be pathogen, aggregated proteins, hypoxia, redox stress, or chemicals inducing specific organelle damage/stress (for example: tunicamycin-ER stress, clofibrate-peroxisomal stress, or FCCP-mitochondrial stress).

2. Establishing the minimum number of cells required for transduction with lentiviruses containing the kinome library

The minimum number of reporter cells to be transduced for each condition can be calculated as below.

$$cell\ n^o = \frac{guide\ n^o\ \times rep\ n^o}{MOI}$$

Cell n^o: the minimum number of reporter cells to be infected.

Guide nº: the total number of guides in the library, including non-targeting controls.

Rep nº: the expected representation (usually 1000x).

MOI: multiplicity of infection. Typically, low MOI of 0.3 is used to ensure that majority of the reporter cells receive a single copy of guide RNA.

For a library size of 3200 guides and 1000x representation, we need to prepare at least 10.7 million cells (50-60% of a 15-cm plates) for viral transduction per condition.

3. Optimization of knockout efficiency

The aim of this section is to identify the earliest time at which the reporter line exhibits the highest knockout efficiency post viral transduction. Lentiviruses carrying sgRNAs targeting autophagy-regulating genes generated from the previous section can be used. The transduced reporter cells are incubated with starvation media and autophagy flux can be monitored using flow cytometry starting 10 days post viral infection. To mitigate secondary effects and minimize reagent costs, we select the earliest date when the reporter line shows the most effective depletion of autophagy genes, evidenced by perturbations in autophagy activity as examined through GFP-tagged p62. We found that knockout efficiency in HEK293A cells peaks 16 days after transduction.

4. Optimization of crosslinking conditions

Autophagy is a stress-responsive process, and prolonged handling or sorting of multiple samples over several hours can introduce confounding stress-related variables that may impact experimental outcomes. Therefore, an additional step integrated into our workflow enabling comparative autophagy analysis across various stress conditions is sample crosslinking. However, crosslinking or fixation has been shown to cause changes to

fluorescent signals. In our study, we utilized paraformaldehyde (PFA), a commonly used crosslinking reagent, to fix samples. Additionally, we used Tris to quench formaldehyde reactivity to prevent excess crosslinking. We investigated various fixation conditions using PFA in the presence or absence of Tris and examined fluorescence of fixed samples using flow cytometry (Figure 3). We observed that higher concentrations of PFA and longer treatment times result in deteriorated fluorescence (Figures 3D and E). Moreover, Tris addition helps rescue the signals (right panels of Figures 3B, C, D, and E). The optimal condition is described below.

1. Sample media are aspirated. The cells are washed once with PBS.
2. The cells are incubated with 2% PFA for 10 minutes at room temperature, followed by 15 min incubation with 3M Tris (pH 8, direct addition to 2% PFA to create a final concentration of 1 M).
3. Tris and PFA solution is removed. The samples are washed once with PBS.
4. After PBS removal, the cells are collected using scrapers, stored in ice-cold flow buffer (1% BSA and 2 mM EDTA in PBS), and filtered using cell strainers (70 μM, Falcon).
5. These fixed cells can be stored at 4ºC until analysis by flow cytometry.

With this approach, we observed sharp fluorescent signals in the fixed samples with minimal reduction in signal intensity.

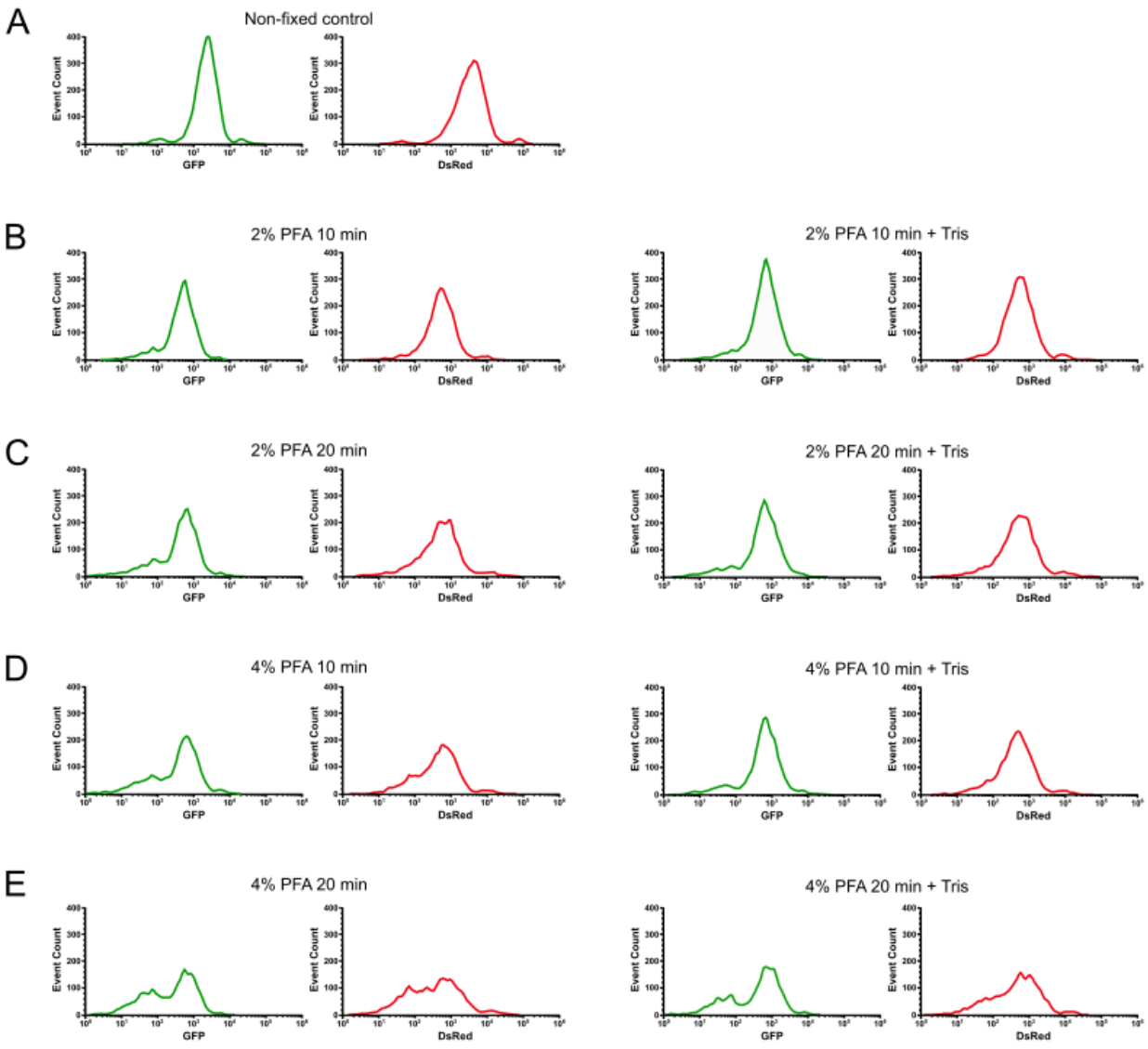

Figure 3: Crosslinking/fixation optimization.

(A), (B), (C), (D), (E) The reporter line underwent fixation with either 2% or 4% PFA for durations of 10 or 20 minutes, with or without the addition of Tris, at room temperature. Subsequently, the fixed cells were subjected to flow cytometry analysis.

5. Optimization of fixed cell sorting and determination of required cell numbers prior to exposure to stress conditions

We observed that fixed cells have reduced cell counts and exhibit slower sort speeds compared to live cells. Therefore, to guarantee sufficient representation of each guide, it is important to access the sort speed of fixed cells and subsequently determine the required number of cells to be plated before incubating them with optimized stress conditions. The number of plates prepared for sorted cells for each condition can be calculated as below.

$$sorted\ plate\ n^o = \frac{guide\ n^o \times rep\ n^o \times volume\ consumed\ \times plate\ n^o\ per\ mL}{sort\ speed\ \times 3600}$$

Sorted plate nº: the required number of plates to be sorted for each condition. Typically, 15-cm plates are used.

Guide nº: total number of guides in the library.

Rep nº: the expected representation (usually 500x to 1000x).

Volume consumed (mL/hour): the total volume consumed by the cell sorter per hour. This value varies depending on the sorter model, sorting mode, and selected pressure.

Plate nº per mL: the number of plates of cells resuspended in 1 mL of flow buffer.

Sort speed (events per second or eps): the speed that fixed cells are sorted at.

3600: seconds per an hour.

Furthermore, for each condition, additional cells are plated and utilized as a bulk/unsorted sample. The number of cells to be plated should be sufficient to ensure a minimum of 1000x representation.

6. Genomic DNA extraction from fixed cells

One obstacle we encountered in this study is the extraction of genomic DNA (gDNA) from fixed cells. We endeavored to reverse crosslinking through various methods, such as SDS treatment, heating the samples at 65ºC, or incubation with NaCl in combination with heat, followed by genomic DNA extraction using a commercial kit. Unfortunately, these methods proved unsuccessful in DNA extraction. We further investigated current literature and found a working protocol published previously(Chen et al. 2015). This protocol allows direct gDNA extraction from up to 2 million fixed cells, —scalable as needed—without a reverse crosslinking step, thereby enhancing reproducibility.

1. In a 15-ml tube, flow buffer is carefully removed.
2. 600 µL of Lysis Buffer (50 mM Tris, 50 mM EDTA, 1% SDS, pH 8) and 3 µL of Proteinase K (20 mg/ml) are added to the cell sample and the mixture is incubated at 55ºC overnight.
3. The next day, 1.5 µL of RNAse A (20 mg/ml) is added to the lysed sample, which is then inverted 25 times and incubated at 37ºC for 30 minutes.
4. The sample tube is cooled on ice for 15 min before addition of 200 µL of pre-chilled 7.5M ammonium acetate to precipitate proteins.
5. After adding ammonium acetate, the samples are vortexed at high speed for 20 seconds and then centrifuged at 10,000 x g for 10 minutes at 4ºC.

6. After the spin, a tight pellet is visible in each tube and the supernatant is carefully decanted into a new tube.

7. 600 µL of 100% isopropanol is added to the tube, which is inverted 50 times and centrifuged at 10,000 x g for 10 minutes. gDNA is visible as a small white pellet in each tube.

8. The supernatant is discarded, 600 µL of freshly prepared 70% ethanol is added. The tube is inverted 10 times, followed by centrifugation at max for 1 minute.

9. The supernatant is discarded by pouring; the tube is briefly spun, and remaining ethanol is removed using a P200 pipette.

10. After air drying for 10-30 minutes, the DNA changes appearance from a milky white pellet to slightly translucent.

11. At this stage, 50 µL of elution buffer of choice is added, the tube is incubated at 65ºC for 1 hour and at room temperature overnight to fully resuspend the DNA.

12. The next day, the gDNA samples are vortexed briefly. The gDNA concentrations are examined using a NanoDrop 2000 Spectrophotometer (Thermo Fisher Scientific) and can be stored at -20ºC for further analysis.

7. Sample preparation for next-generation sequencing (NGS)

We employ a 2-step PCR approach to generate amplicons of gRNA from genomic DNA and barcode those amplicons for next-generation sequencing. In addition, AMPure XP beads are used to purify amplicons after each round of PCR.

<u>PCR1: amplification of gDNA from genomic DNA</u>

For PCR1, the total number of reactions and the amount of master mix should be calculated once gDNA concentrations and volumes are determined using Excel format. To minimize unexpected variables among samples during PCR, master mix of all reactions are generated by mixing all components except for DNA template and water. For sorted samples, all gDNA is used as a template for PCR1. For bulk or unsorted samples, the amount of gDNA used for multiple PCR1 reactions is determined to guarantee a minimum of 1000x representation is achieved. The amount of gDNA can be calculated as follows.

$$gDNA = guide\ n^o \times\ rep\ n^o \times gDNA\ per\ cell$$

gDNA: the amount of gDNA is used to achieve the expected representation.

Guide n^o: the number of guides in the library. Our kinome library has approximately 3200 guides.

Rep n^o: the expected representation (usually 1000-1500x).

gDNA per cell: one cell contains roughly 0.006 ng of gDNA.

PCR1 primers are designed as below.

Forward: TCGTCGGCAGCGTCAGATGTGTATAAGAGACAGggactatcatatgcttaccgt

Reverse: GTCTCGTGGGCTCGGAGATGTGTATAAGAGACAGgagccaattcccactccttt

The capitalized segment of the primer sequence represents a transposase adapter compatible with the Nextera Index Kit utilized in PCR2. The lowercase portion serves as the vector binding sequence and can be adjusted according to the vector of choice. If the vector binding sequence is changed, PCR1 condition should be optimized.

PCR1 mixture and condition are prepared as described below.

	Added volume (µL)
2x Q5 Master Mix	50
$MgCl_2$ (1M)	0.2
5’ primer (100 µM)	0.5
3’ primer (100 µM)	0.5
gDNA (3 µg)	Various
H_2O	Up to 100

PCR1 of gRNA
98ºC 5 minutes
98ºC 35 seconds
60ºC 30 seconds
72ºC 45 seconds
Repeat steps 2-4 for 24 cycles
72ºC 10 minutes
4ºC hold

PCR1 cleanup

During this step, AMPure XP beads are employed to isolate the PCR amplicon from genomic DNA, free primers, and primer dimer species. PCR products of each sample from multiple first PCR reactions are pooled and 200 µL is cleaned up for PCR2.

1. The AMPure XP beads are brought to room temperature (minimum 15 minutes) and mixed till homogenous by vortexing for at least 20 seconds.
2. 0.5X volume (100 µL) of AMPure XP beads (DNA: beads= 1:0.5) is added to respective 1.5 mL Eppendorf tubes. The beads and PCR1 solution is mixed thoroughly and incubated at room temperature without shaking for 15 minutes.
3. Sample tube is placed on a magnetic rack for 2 minutes or until the supernatant has cleared.
4. The supernatant is transferred to a new 1.5mL tube. Beads are discarded.
5. 0.8X volume (160 µL, using original DNA volume) of AMPure XP beads is added. The beads and PCR1 mixture is incubated at room temperature without shaking for 15 minutes.
6. The tube is placed on a magnetic rack for 2 minutes or until the supernatant has cleared.
7. The supernatant is discarded this time, and beads are kept.
8. On a magnetic rack, the beads are washed with freshly prepared 70% ethanol twice according to manufacturer's instructions.
9. On a magnetic rack, excess ethanol is removed using aspirator and gel loading tips.
10. On a magnetic rack, the beads are air-dried for <15 minutes and checked in 10 minutes to make sure the beads are not over dry.

11. The sample tubes are removed from the magnetic rack. 50-100 µl of ultra-pure water or elution buffer of choice is added.
12. The solution is gently mixed up and down 10 times to make sure the beads are fully resuspended.
13. The mixture is incubated at room temperature for 10-15 minutes.
14. The tube is placed on the magnetic rack for 2 minutes or until the supernatant has cleared.
15. The supernatant is carefully transferred to a new appropriately labeled 1.5 mL tube.
16. 5 µl of PCR1 products are run on a 2% agarose gel to confirm the band size.
17. These samples are analysed by a NanoDrop 2000 Spectrophotometer and can be frozen at -20ºC before proceeding to PCR2.

PCR2: addition of barcodes to PCR1 amplicons using Nextera Index Kit

PCR2 reactions are prepared as below. 62.5 ng of PCR1 should correspond to over 1 billion x representation so there is no need to add more than that.

	Added volume (µL)
2x Q5 Master Mix	50
XT Index Primer 1 (N7xx)	5
XT Index Primer 2 (S5xx)	5
PCR1 product (62.5 ng)	Various
H2O	Up to 50

PCR2	
98ºC	5 minutes
98ºC	35 seconds
58ºC	30 seconds
72ºC	45 seconds
Repeat steps 2-4 for 6 cycles	
72ºC	10 minutes
4ºC	hold

PCR2 cleanup

AMPure XP beads are employed to purify PCR2 products from PCR1 amplicons, primers, and primer dimers. PCR2 cleanup steps are described below.

1. The AMPure XP beads are brought to room temperature (minimum 15 minutes) and mixed till homogenous by vortexing for at least 20 seconds.
2. 1.6X volume of AMPure XP beads (DNA: beads= 1:1.6) is added to respective 1.5 mL Eppendorf tubes. The beads and PCR2 solution is mixed thoroughly and incubated at room temperature without shaking for 15 minutes.
3. Sample tube is placed on a magnetic rack for 2 minutes or until the supernatant has cleared.
4. The supernatant is removed.

5. On a magnetic rack, the beads are washed with freshly prepared 70% ethanol twice according to manufacturer's instructions.
6. On a magnetic rack, excess ethanol is removed using aspirator and gel loading tips.
7. On a magnetic rack, the beads are air-dried for <15 minutes and checked in 10 minutes to make sure the beads are not over dry.
8. The sample tubes are removed from the magnetic rack. 30-40 µl of ultra-pure water or elution buffer of choice is added.
9. The solution is gently mixed up and down 10 times to make sure the beads are fully resuspended.
10. The mixture is incubated at room temperature for 10-15 minutes.
11. The tube is placed on the magnetic rack for 2 minutes or until the supernatant has cleared.
12. The supernatant is carefully transferred to a new appropriately labeled 1.5 mL tube.
13. 5 µl of PCR2 products are run on a 2% agarose gel to confirm the band size.
14. The products can be frozen at -20ºC or -80ºC before being submitted to next-generation sequencing facility.

8. Generation of lentiviruses carrying Brunello human kinome CRISPR knockout library

The library is purchased from Addgene and amplified using the protocol provided. Representation in library should be verified using the 2-step PCR protocol (described

above). The prepared library amplicons can be then submitted to a next-generation sequencing facility for analysis. Several approaches have been developed to analyse the large sequencing data. In this study, we employ CRISPRBetaBinomial (CB2) approach on CRISPRCloud2 site to examine the NGS results(Jeong et al. 2019). CB2 is a user-friendly web-based algorithm which generates key metrics—including total read counts, mapped reads, mapping efficiency, and fold coverage—to assess the quality and representation of library preparation. Library representation should be 1000-fold coverage and minimum representation is important to investigate before proceeding to virus preparation.

1. For a library size of roughly 3200 guides, we packaged in 6-8 15-cm plates, which can be scaled accordingly. Cells are plated at approximately 35% confluence (7-8 million) of HEK293T cells on each of 15-cm plate.

2. Next day, lentiviral vectors expressing the kinome library and packaging vectors (psPAX2 and pMD2.G) are co-transfected using PolyJet reagent into HEK293T cells in a 4:3:1 molar ratio, respectively. 3 µL of PolyJet is used for 1 µg of DNA. Media are changed 5 hours post transfection.

3. Media are collected four times 12 hours apart starting at 36 hours post transfection.

4. Viral supernatant is filtered through 0.45 µM Nalgene™ Rapid-Flow™ Sterile Disposable Filter Units (Thermo Fisher Scientific#09-740-63A).*Optional centrifugation if many cells lift. Cleared supernatants are concentrated using Virus Precipitation Kit (Benchmark Bioscience) to 1/100 of the original volume.

5. The viruses are stored at -80ºC.

9. Titration of lentiviruses carrying CRISPR library

Following lentivirus production, the viruses will be titrated in the reporter cell line. This step is important as it determines the number of gene copies integrated in the transduced target cell and is subsequently used for Multiplicity of Infection (MOI) calculation.

1. Approximately 10-15% confluence (0.8×10^5) of reporter cells are seeded to each well of a 12-well plate in complete DMEM media containing 10% bovine calf serum without antibiotics and the cells are incubated overnight at 37ºC, 5% CO_2.
2. On the next day, lentiviruses are thawed on ice and resuspended gently. 5-fold serial dilutions of viral stock are performed in a 96-well plate.
3. Culture medium from each well is removed. The reporter cells are replenished with 1 mL fresh media in the presence of polybrene (10 µg/mL).
4. A single viral dilution is gently added to each well of a 12-well plate. The plate is mixed gently from one side to another side.
5. Media are changed to regular complete DMEM 24 hours post transduction. The cells are incubated at 37ºC with 5% CO_2 for another 24 hours.
6. Next, the transduced cells are incubated with puromycin (1 µg/mL) for 3 days. The culture media are replaced every day with puromycin-containing media if more than 10% of cells die.
7. The cells are incubated with regular complete DMEM for another 4-6 days and observed every day to monitor the death of cells that are sensitive to puromycin.
8. The transduced cells are fixed with 4% PFA for 10 min at room temperature.

9. Following one wash with 1xPBS, the cells are stained with 0.1% crystal violet solution at room temperature for 20 minutes. After removal of crystal violet solution, the samples are washed three times with 1xPBS.

10. The blue-stained colonies are counted using a microscope at a magnification of 40×.

11. The lentiviral titer is calculated using the formula below:

$$titer = \ colony\ n^o\ per\ well \times dilution\ factor\ \times\ 40$$

Titer (transduction unit per mL or TU/mL): the viral particle count added per cell during infection.

Colony no per well: the number of colonies in one well.

Dilution factor: a measure of how much viral solution has been diluted.

40: the magnification of microscope used.

10. Kinome screen workflow

Once all required conditions have been optimized, the kinome screen can be conducted. The workflow for the screen is outlined below.

1. The reporter cells (***Section 1***) are plated in a quantity that ensures they reach the desired cell count at the time of transduction (***Section 2***). For example, we notice our HEK293A reporter line doubles once every 24 hours. We plate approximately 4.5-5 million cells per condition to ensure they are prepared for viral transduction the following day. Extra cells can be seeded, either for cell counting purposes next day or as a negative control for puromycin selection at a later stage.

2. Next, the reporter cells are transduced with lentiviruses carrying kinome library in the presence of polybrene (10 μg/mL). The number of viruses can be determined as below.

$$virus\ volume = \frac{MOI \times cell\ n^o}{viral\ titer}$$

Virus volume (mL): the amount of viruses added to the reporter cells.

MOI: multiplicity of infection which is 0.3

Cell n^o: the number of cells at the time of infection.

Viral titer: determined in ***Section 9***.

3. Next day, if the cells reach close to 100% confluence, they can be passaged at 20% confluence and transferred to new plates.
4. 48 hours post transduction, the transduced cells and negative cells are incubated with puromycin (1 μg/mL) for 3 days. The culture media are replaced every day with puromycin-containing media if more than 10% of cells die.
5. The transduced reporter cells are cultured for an additional number of days as determined in ***Section 3*** to facilitate effective target knockout.
6. Next, the transduced cells are plated in a quantity that ensures they achieve the desired cell count at the time they are subjected to optimized stress conditions as determined in ***Section 5***.
7. Media are changed at least 1 hour prior to the treatments.

8. Following the treatments, media are removed, and the cells are washed once with PBS.

9. Next, the samples are fixed with 2% PFA for 10 min at room temperature, followed by 15 min incubation with Tris (pH 8, direct addition to 2% PFA to create a final concentration of 1 M) (***Section 4***).

10. PFA and Tris are removed. The samples are washed with PBS once.

11. Following aspiration of PBS, the cells are harvested using scrapers, stored in ice-cold flow buffer, and filtered using cell strainers.

12. These fixed cells can be stored at 4ºC in the dark for a maximum of one night before sorting to ensure that fluorescence remains intact.

13. The percentage of gated populations expressing high and low GFP/DsRed levels can be selected according to preference. Typically, 5-10% gated populations are chosen. During sorting, it is recommended to record the total number of sorted cells to gauge the representation of each sample.

14. The sorted and unsorted populations are then pelleted by centrifugation (4000 rpm for 10 min at 40C) and stored at -80C freezer.

15. All replicates should be conducted before proceeding to the next steps.

16. Next, genomic DNAs from fixed cells are extracted (***Section 6***).

17. PCR reactions and purification are conducted according to the instructions provided in ***Section 7*** to prepare the samples for next-generation sequencing by

amplifying the guide regions and barcoding them. The samples from all replicates can be stored at -20ºC or -80ºC until sent to next-generation sequencing core.

11. Next-generation sequencing (NGS)

To select the correct NGS setting, the required read depth is calculated as below.

$$read\ depth = guide\ n^o \times \ln(guide\ n^o) \times sample\ n^o \times read\ n^o\ per\ sample$$

Read depth: the total of reads for all sequenced samples.

Guide nº: the number of guides in the selected library.

Guide nº x ln(guide nº): coupon collector's problem which is the required number of sequenced reads to ensure all reads are sequenced at least once.

Sample nº: the total number of samples across all replicates.

Read nº per sample: the expected reads per sample which is typically 300.

Read length is also determined to ensure the regions of interest are covered. For our screen, a read length of 150 cycles is selected. Additionally, 10% - 50% PhiX spike-in is employed to control for sequence clustering and diversity. The percentage of PhiX spike-in to be chosen varies depending on the sequencing platform and should be verified by the sequencing facility. Quality control of the samples is performed by the sequencing facility to confirm the sample size and concentration prior to sequencing.

The NGS data are next analyzed using the CRISPRCloud2 platform. Briefly, on CRISPRCloud2 site, the Enrichment-based screen option is selected. The kinome library (the reference library) obtained from the manufacturer is converted from excel format to fasta format. High GFP, low GFP, and unsorted/bulk populations of one condition from all

replicates are analyzed concurrently. After providing all the necessary information, the web browser initiates the processes of trimming, mapping, and quantifying the sgRNA reads. The processed data are accessed through the link provided. CB^2 demonstrates several metrics regarding the data quality including gene-level corrected p-values or false-discovery rate, which is a critical factor in selecting hits.

3.6 Results and Discussion

In this paper, we demonstrated an optimized kinome-wide screen workflow that facilitates high-throughput screens of several stress-induced autophagy pathways and allows for direct comparison of multiple datasets. Our protocol offers several advantages. The employment of autophagy receptor p62 allows for analysis of different selective autophagy processes given its capability to interact with several types of ubiquitinated cargo. CRISPR-based approach enables precise targeting of specific genomic loci with high efficiency and induces permanent gene perturbations compared to traditional RNAi screens, which ultimately provides more pronounced signaling. Furthermore, the screen design allows cells sufficient time for recovery after genomic perturbation, thereby reducing variability in baseline autophagy threshold. An essential addition to our screen workflow is sample fixation or crosslinking, which supports simultaneous analysis of different stress-induced autophagy pathways, without the need to reverse crosslinking prior to library amplification. While our workflow offers clear advantages, it also comes with limitations. Although p62 is involved in different types of selective autophagy, p62 as autophagy flux reporter can be a disadvantage as the relative degradation of total p62 under each condition may vary depending on cargo enrichment and preference for other autophagy receptors. The use of an LC3-based system may have a more even contribution among our conditions, whose advantages would need to be balanced against its ambiguity in reporting autophagic flux. Additional screens using organelle specific autophagy receptors would be ideal for sensitivity and complement the findings. The CRISPR/Cas9 system often leads to complete loss of gene function, which can be impractical for studying essential genes or partial loss of functions. Application of RNAi or

CRISPRi approaches can address this limitation. The use of fixation is required to prevent artifacts from the stress during sorting. However, this fixation step may pose some challenges. We found the read number from these fixed samples is significantly lower than in samples that were never fixed. Additionally, we found fixed samples are more prone to clogging the sorter, which necessitates lower sort speeds. Given that multiple kinome screens are sorted on each run, this is an important practical consideration. Collectively, our protocol is a one-stop shop, providing necessary optimizations which can be adapted for high throughput genomics screens and chemical screening approaches.

3.7 Acknowledgements

The authors acknowledge the support from CIHR grants #153034 (R.C.R) and PJT-169097 (M.W.C.R.) as well as Natural Sciences and Engineering Research Council of Canada #2023-05587 (R.C.R) and RGPIN-2019-04133 and DGECR-2019-00369 (M.W.C.R.) and 201911CGV-434032-74238 (T.L.). The authors also thank the following Core facilities from the University of Ottawa and the Ottawa Hospital Research Institute (OHRI) for use of their facility, equipment, and expertise: the Cell Biology and Imaging Acquisition Core (RRID:SCR_021845), the Flow Cytometry and Virometry Core (RRID:SCR_023306), the Genome Engineering and Molecular Biology Core (RRID:SCR_022954) and the OHRI StemCore Laboratories (RRID:SCR_012601).

Chapter 4: Identification of stress specific autophagy regulators from tandem CRISPR screens

Early version published on BioRxiv - DOI: https://doi.org/10.1101/2024.03.27.587008

Truc T. Losier, Karyn E. King, Maxime W.C. Rousseaux, Ryan C. Russell

4.1 Statement of Author Contributions

TTL and RCR wrote the manuscript. **TTL** designed and performed majority of experiments. KEK conducted siRNA experiments. MWCR and RCR conceptualized the study and supervised the manuscript preparation, with RCR also overseeing the experimental planning.

Identification of organelle-specific autophagy regulators from tandem CRISPR screens

Truc T. Losier[1], Karyn E. King[1], Maxime W.C. Rousseaux[1,2,3,#], Ryan C. Russell[1,2,4,#,*]

[1] Department of Cellular and Molecular Medicine, University of Ottawa, 451 Smyth Road, Ottawa, Ontario K1H 8M5, Canada.

[2] University of Ottawa Brain and Mind Research Institute, Ottawa, Ontario, K1H 8M5, Canada.

[3] Ottawa Institute of Systems Biology, Ottawa, Ontario, K1H 8M5, Canada

[4] University of Ottawa Center for Infection, Immunity and Inflammation, Ottawa, Ontario, K1H 8M5, Canada.

[#] Co-corresponding authors: ryan.russell@uottawa.ca; max.rousseaux@uottawa.ca

[*] Lead contact: 451 Smyth Rd, Ottawa, Ontario, K1H 8M5, Canada.

Keywords: Autophagy; selective autophagy; pexophagy; ER-phagy; high-throughput screens; CDK11A; NME3; PAN3; CDC42BPG

4.2 Abstract

Autophagy is a conserved degradative process that promotes cellular homeostasis under stress conditions. Under nutrient starvation autophagy is largely non-selective, promoting indiscriminate breakdown of cytosolic components. Conversely, selective autophagy is responsible for the specific turnover of damaged organelles. We hypothesized that selective autophagy may be regulated by distinct upstream signaling from starvation induced autophagy to promote organelle turn-over. To address this question, we conducted kinome-wide CRISPR screens using the DsRed-IRES-GFP-p62 reporter line to identify distinct signaling pathways responsible for the regulation of basal autophagy, starvation-induced autophagy, and two types of selective autophagy, ER-phagy and pexophagy. The Brunello kinome library was designed to enhance on-target activity while minimizing off-target effects, ensuring the effectiveness and efficiency of our screens. These parallel screens identified established and novel autophagy shared regulators under these conditions, as well as kinases specifically required for ER-phagy or pexophagy. More specifically, CDK11A and NME3 were further characterized to be selective ER-phagy regulators. Meanwhile, PAN3 and CDC42BPG were identified as activator or inhibitor of pexophagy, respectively. Collectively, these datasets provide the first comparative description of the kinase signaling specificity, separating regulation of selective autophagy and bulk autophagy.

4.3 Introduction

Macroautophagy (hereafter referred to as autophagy) is driven by the formation of a double membrane vesicle called an autophagosome that sequesters cytosolic cargo for degradation(Kaur and Debnath 2015). Autophagosome formation is mediated through the activity of a conserved group of autophagy-related (ATG) proteins(Kaur and Debnath 2015). ULK1, a serine/threonine kinase, promotes autophagosome biogenesis by phosphorylating and activating multiple ATG proteins, thereby driving stress-induced autophagy(Russell et al. 2013; Alsaadi et al. 2019; Park et al. 2018; Park et al. 2016; Di Bartolomeo et al. 2010). Maturation of the autophagosome and sequestration of targeted cargo require the lipidation of ATG8 family members (LC3A, B and C, GABARAP, GABARAPL1 and GABARAPL2) to the lipid phosphatidylethanolamine(Martens and Fracchiolla 2020). LC3B is the best studied member of the ATG8 family in mammals (Lystad et al. 2019; Mizushima et al. 2011). Autophagy was originally described as a bulk degradation pathway that indiscriminately engulfs and degrades cytosolic components(Mortimore and Schworer 1977). However, the importance of autophagy as a targeted degradation pathway has been established in normal and disease biology (Levine and Kroemer 2008; Yamamoto et al. 2023).

The targeted degradation of cargo by the autophagy pathway is called selective autophagy, which can be categorized into various subgroups based on the specific cellular components targeted for degradation(Svenning and Johansen 2013; Kim et al. 2016). Selective autophagy requires all the core ATG proteins of bulk autophagy, but also includes a class of proteins called autophagy receptors(Zaffagnini and Martens 2016; S et al. 2017). Autophagy receptors can be divided into ubiquitin-bound and membrane-

associated groups(Kim et al. 2016; Vargas et al. 2023). Well-known ubiquitin-bound receptors, such as SQSTM1/p62, NBR1, NDP52, and OPTN, typically contain both LC3-interacting region (LIR) and ubiquitin-binding domains (UBD) that allow them to recruit ubiquitinated targets to autophagosomes for degradation(Kim et al. 2016). Membrane-bound receptors localize to, or are constitutively present on the target organelles and are responsible for damaged organelle recognition by autophagy machinery(Anding and Baehrecke 2017). Importantly, defective selective autophagy has been implicated in several human diseases(Ryter et al. 2013; Ichimiya et al. 2020). Despite increasing evidence for defects in selective autophagy receptors in disease, comparatively less is known about the upstream regulation governing the selective acquisition of autophagic cargo.

Mitophagy (mitochondrial degradation) and xenophagy (pathogen clearance) have been extensively studied, but ER-phagy (endoplasmic reticulum removal) and pexophagy (peroxisomal degradation) remain underexplored(Reggiori and Molinari 2022; Cho et al. 2018). Thus, in this study, we chose ER-phagy and pexophagy as our models of selective autophagy. Selective autophagic degradation of the ER is a homeostatic mechanism that regulates the maintenance of ER size, the removal of aggregated or miss-folded proteins, and the turnover of ER membranes following damage (Mochida and Nakatogawa 2022). To date, at least six ER-phagy receptors have been identified in mammals, including FAM134B, RTN3L, CCPG1, SEC62, TEX264, and ATL3 (Chen et al. 2019; Smith et al. 2018; Grumati et al. 2017; An et al. 2019; Chino et al. 2019; Fumagalli et al. 2016; Khaminets et al. 2015). These receptors localize to ER sub-compartments and are capable of recruiting autophagy machinery to the ER through

LC3/GABARAP-interacting regions (LIR/GIM)(Chino and Mizushima 2020). For instance, FAM134B primarily facilitates the degradation of sheet ER, while ATL3 and RTN3L mediate degradation of tubular ER(Chen et al. 2019; Grumati et al. 2017; Khaminets et al. 2015). Some receptors, such as CCPG1 and TEX264, also interact with upstream autophagy complexes like FIP200 and WIPI2 to promote phagophore expansion at the ER(Smith et al. 2018; Chino et al. 2019). In addition to autophagy receptors, new pathways including mitochondrial metabolism and UFMylation have been reported to regulate ER-phagy(Liang et al. 2020). While the key receptors and core machinery involved in ER-phagy have been identified, the regulatory pathways that determine its activation over other selective autophagy pathways remain poorly understood.

Peroxisomes are single membrane-bound organelles essential for reactive oxygen species (ROS) metabolism and fatty acid oxidation(Lazarow and de Duve 1976; Mihalik et al. 1995; Poirier et al. 2006). Their homeostasis is regulated by peroxin (PEX) proteins, and stress conditions like starvation or ROS disrupt this balance, triggering autophagic degradation(Walter et al. 2014; Sargent et al. 2016; Zhang et al. 2015; Germain and Kim 2020). Proper matrix protein import, involving PEX2, PEX5, PEX13, and PEX14, is crucial for peroxisome function and quality control(Germain and Kim 2020; Demers et al. 2023). Under stress, PEX2 ubiquitinates PMP70 and PEX5, targeting peroxisomes for degradation via NBR1 and p62(Sargent et al. 2016; Zhang et al. 2015). PEX14 and PEX13 also promote pexophagy during starvation, while elevated ROS and hypoxia enhance PEX5 ubiquitination(Hara-Kuge and Fujiki 2008; Demers et al. 2023; Germain and Kim 2020; Zhang et al. 2015; Schönenberger and Kovacs 2015). Conversely, the AAA-type ATPase PEX1-PEX6-PEX26 and the deubiquitinase USP30 remove

ubiquitinated peroxisomal proteins from the membrane, thereby inhibiting pexophagy(Law et al. 2017; Marcassa et al. 2018; Riccio et al. 2019).

Kinase-mediated phosphorylation plays important roles in the regulation of autophagy initiation. Induction of the autophagy pathway is best characterized in the context of nutrient starvation, where nutrient-sensitive kinases, including mTORC1 and AMPK, are critical for modulating autophagy activation(Balgi et al. 2009; Garcia and Shaw 2017; Kim et al. 2011; Jung et al. 2010). Under nutrient sufficiency mTORC1 suppresses autophagy through direct phosphorylation of several components associated with autophagy induction including ULK1(King et al. 2021; Kim et al. 2011; Shang et al. 2011; Puente et al. 2016). Specifically, upon starvation, mTORC1 is inactivated, which results in ULK1 release from inhibitory phosphorylation and subsequent autophagy induction(Alers et al. 2012; Kim et al. 2011). AMPK activity under energy and nutrient starvation can regulate autophagy through modulation of ULK1 and mTORC1 activity (Kim et al. 2011; Gwinn et al. 2008; Alers et al. 2012). In addition, AMPK and mTORC1 have been reported to directly regulate the activity of the VPS34 kinases, ensuring a precisely controlled initiation of autophagy in response to various cellular stresses(Yuan et al. 2013; Kim et al. 2013). Collectively, these nutrient-dependent kinases play an essential role in mediating the activation of bulk autophagy in response to starvation.

Several genome- and kinome-wide screens have identified bulk autophagy regulators using LC3 or p62 reporters and RNAi or CRISPR/Cas9 targeting(Lipinski et al. 2010; Szyniarowski et al. 2011; Frankel et al. 2011; Hale et al. 2016; Guo et al. 2018; Mimura et al. 2021; DeJesus et al. 2016; Chan et al. 2007; McKnight et al. 2012; Morita et al. 2018). Focus has more recently shifted towards selective autophagy regulation. For

example, a genome-wide screen using an ER-phagy-specific reporter identified the UFMylation pathway as a mediator of ER-phagy(Liang et al. 2020). Meanwhile, a different screen for regulators of PARKIN stability revealed transcriptional repression as a mediator of mitophagy(Potting et al. 2018). Identification of signaling specificity underlying selective autophagy by comparing results in the studies above is significantly limited by the use of different reporters, stress conditions, cell lines, and screen-related experimental variation. To uncover signaling that demarcates selective vs. bulk autophagy screening conditions must be carefully designed to rule out changes in: total autophagy, crosstalk between selective and bulk autophagy, reporter limitations, and generation of secondary or artifactual hits.

We hypothesized that uncharacterized kinase signaling influences cargo-specific autophagy, akin to how mTORC1 and AMPK regulate starvation-induced autophagy. To explore this, we created a stable monoclonal HEK293A cell line expressing the DsRed-IRES-GFP-p62 autophagy reporter, enabling sensitive, real-time tracking of both selective and bulk autophagy via a single validated readout. Using this cell line, we conducted pooled kinome-wide CRISPR screens under different acute stressors, keeping the cell population constant. This approach revealed stress-specific signaling pathways regulating ER-phagy and pexophagy, distinct from those controlling basal or starvation-induced autophagy.

4.4 Results

A kinome-scale CRISPR screen using an autophagic flux reporter

To measure autophagy rates in a high throughput, quantitative manner, we first generated a stable cell line with a fluorescent marker of autophagy flux, p62. p62 is capable of binding to multiple types of ubiquitinated cargo and recruiting them to autophagosomes for degradation. p62 was chosen for this study because it is involved in nearly all forms of selective autophagy and as a result can be used as a common reporter for direct comparative analysis of both selective and bulk autophagy. To measure changes in autophagic flux, we constructed a dual-fluorescence reporter cell line expressing DsRed-IRES-GFP-p62 (Fig. 1A). HEK293A cells were stably transduced with constructs expressing GFP-tagged p62 with an internal DsRed control (DsRed-IRES-GFP-p62, Fig. 1A). To mitigate expression changes from lentiviral insertion, we generated monoclonal reporter populations and assessed responses to amino acid starvation, a potent inducer of autophagy. Flow cytometry was employed to determine the rapid and quantitative measurement of relative p62 levels (GFP) while controlling for non-selective changes in protein abundance (DsRed control, Fig. 1A, right panel). Levels of p62 decrease during autophagy activation, resulting in a left shift in the GFP fluorescence signal (Fig. 1A, right panel). Conversely, autophagy inhibition leads to a right shift in the GFP signal (Fig. 1A, right panel). We benchmarked our reporter line under acute amino acid deprivation, one of the best characterized and strong inducers of autophagy using western blot (WB) and flow cytometry to identify the ideal timepoints and concentrations for measuring stress-selective p62 flux. The DsRed-IRES-GFP-p62 reporter line showed a robust clearance of tagged p62 in response to acute amino acid starvation, with no changes in DsRed control

(Fig. 1B, left panel). We selected a 3-hour period of starvation for screening purposes, as it was the earliest timepoint giving peak p62 degradation. While the induction of autophagy by starvation was clear by WB analysis, we next sought to verify whether that stress condition triggered similar responses by flow cytometry. Consistently, we observed a significant reduction in GFP signal while there was no change in DsRed fluorescence in the starved reporter cells compared to the untreated ones (Fig. 1B, right panel). Additionally, we also confirmed that the effects on p62 flux were due to autophagy by repeating the stress analysis in an autophagy-deficient background (ATG5 KO, DsRed-IRES-GFP-p62 HEK293A cells). ATG5 KO efficiency was confirmed by WB (Fig. S1A). We found that the starvation-induced decrease in GFP-p62 fluorescence was blocked in autophagy deficient cells, indicating starvation-induced p62 clearance optimized above was a result of autophagic flux (Fig. S1B).

We next investigated the autophagic response to ER stress and peroxisomal stress. ER stress was induced by tunicamycin treatment using established ranges and concentrations(Ohoka et al. 2005; Abdullahi et al. 2017). Tunicamycin hinders the first stage of N-linked glycan production in proteins and leads to the accumulation of improperly folded proteins. Compared to the unstimulated cells, we observed the most robust and consistent autophagic flux in the cells exposed to 10 μg/mL of tunicamycin for a duration of 6 hours, as shown through substantial reductions in p62 levels (Fig. 1C). Thus, we selected this condition to induce ER-phagy for our screening experiments. This was further confirmed using flow cytometry, where exposure to tunicamycin produced a significant decrease in GFP-p62 fluorescence compared to the untreated cells, with no changes in DsRed (Fig. 1C, right panel). Furthermore, we observed that the tunicamycin-

induced reduction in GFP-p62 fluorescence was lost in autophagy-deficient cells, suggesting that the optimized stress-induced p62 clearance described above was due to autophagy (Fig. S1C).

We then characterized the optimal timepoints for inducing p62 flux following peroxisomal stress (Fig. 1D). To initiate peroxisomal stress, we treated cells with clofibrate to disrupt peroxisome function and induce pexophagy(Zhang et al. 2015). Using previously reported timepoints and concentrations(Zhang et al. 2015), we observed a decrease in p62 levels in all clofibrate-treated samples with no changes in DsRed, indicating an activation of autophagy (Fig. 1D). Among the conditions tested, the induction of peroxisomal stress using clofibrate (1 mM) for a duration of 6 hours elicited a robust and consistent response in the reporter cell line via both orthogonal approaches (Fig. 1D). We also confirmed that the effects on p62 flux was due to autophagy by repeating the clofibrate analysis in autophagy-deficient, ATG5 KO DsRed-IRES-GFP-p62 293A cells (Fig. S1D). Collectively, these experiments establish that our reporter cell line gives a robust readout of both selective and bulk autophagy flux. Moreover, we established the timepoints that correspond to the first wave of p62 autophagic degradation in response to starvation, peroxisomal stress, and ER-stress, which is important to minimize potential confounds of secondary or compensatory effects caused by prolonged exposure of these stimuli. Notably, all time points chosen were within the dynamic range of the initial p62 degradation response and demonstrated comparable levels of p62 clearance using flow cytometry, which is crucial when comparing these stress responses.

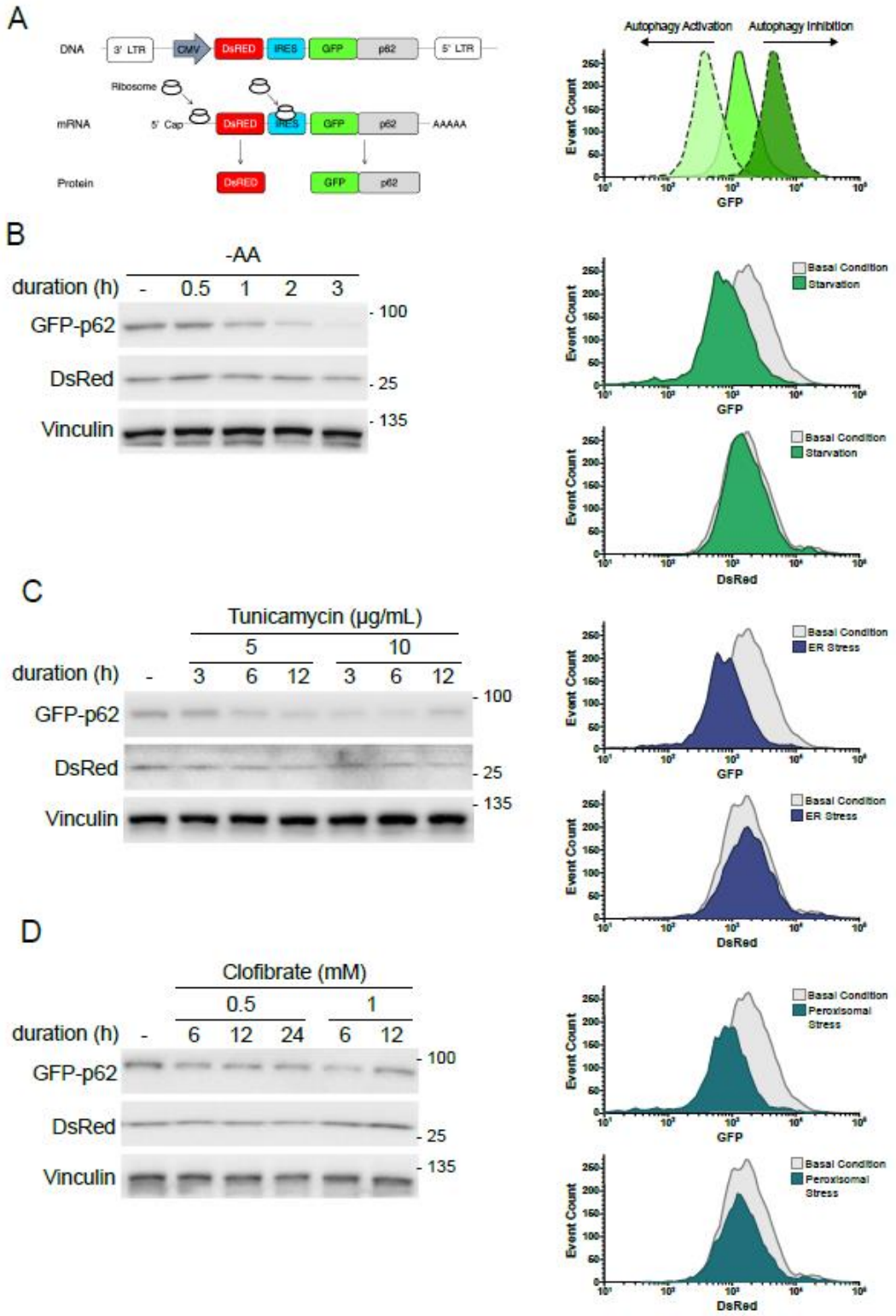
A
DNA
3' LTR
CMV
DsRED
IRES
GFP
p62
5' LTR
Ribosome
mRNA
5' Cap
AAAAA
Protein
Autophagy Activation
Autophagy Inhibition
Event Count
GFP
B
-AA
duration (h)
- 0.5 1 2 3
GFP-p62
DsRed
Vinculin
100
25
135
Basal Condition
Starvation
DsRed
C
Tunicamycin (µg/mL)
5 10
duration (h)
- 3 6 12 3 6 12
ER Stress
D
Clofibrate (mM)
0.5 1
duration (h)
- 6 12 24 6 12
Peroxisomal Stress

Figure 1

Figure 1: Generation of an autophagic flux reporter sensitive to differential autophagy-inducing stressors.

(A) Schematic representation of the autophagic flux reporter DsRed and GFP-tagged p62. p62 is selectively incorporated into and degraded along with the autophagosomal membrane. Therefore, the level of GFP-p62, relative to DsRed, is inversely proportional to autophagic flux. Examples of autophagy activation and inhibition were demonstrated using the histogram in the right panel. (B) The HEK293A reporter cell line was treated with starvation in time- and concentration-dependent manners. WB was used to examine DsRed and GFP-p62 signals. FACS was employed to investigate GFP and DsRed fluorescence of the reporter cells treated with amino acid-free media (-AA) for 3 hours. Histograms were used to depict changes in GFP-p62 and DsRed levels. (C) The reporter cell line was incubated with tunicamycin in time- and concentration-dependent manners. DsRed and GFP-p62 were analysed using WB. FACS was used to examine GFP and DsRed signals of the reporter cells exposed to tunicamycin (Tm, 10 μg/mL) for 6 hours. Histograms were used to depict changes in GFP-p62 and DsRed levels. (D) The reporter cells were incubated with clofibrate in time- and concentration-dependent manners. DsRed and p62 levels were examined using WB. FACS was employed to investigate GFP and DsRed fluorescence of the reporter cells treated with clofibrate (Clo, 1 mM) for 6 hours. Histograms were used to depict changes in GFP-p62 and DsRed levels.

CRISPR-based screens identify shared and distinct of stress-selective autophagic pathways

To gain insight into differences in signaling that impact selective autophagic flux, we conducted kinome-wide CRISPR-based screens using the validated DsRed-IRES-GFP-p62 reporter line (Fig. 2A). Briefly, cells were transduced with the Brunello kinome library, a pooled lentiCRISPRv2 library containing 3,052 unique sgRNAs targeting 763 human kinases genes (4 guides per target) at a multiplicity of infection of 0.3 to promote single virus integration(Doench et al. 2016). Infected cells were selected for 3 days with puromycin (1 μg/mL), and expanded for 16 days total, maintaining a minimum of 1000x representation. On day 16 post-transduction, one quarter of the infected cells were subsequently exposed to either amino acid-free DMEM media (for 3 hours; starvation), tunicamycin (at 10 μg/mL, 6 hours; ER stress), clofibrate (at 1 mM, 6 hours; peroxisomal stress), or were left untreated (basal). The untreated, starvation-treated, tunicamycin-treated, and clofibrate-treated cells were briefly fixed with 2 % PFA and harvested on the same day to allow for direct comparison among stress conditions from identical replicates of edited cells. Fixed samples were analysed by FACS. Top and bottom deciles (“high” and “low” populations, respectively) of GFP/DsRed ratiometric populations were selected as activators and inhibitors of autophagy (Fig. 2A). Genomic DNA from the fixed sorted cells, as well as the corresponding fixed pre-sort population, which controls for alternations in sgRNA abundance mediated by changes in cellular fitness, were extracted and sgRNA sequences were amplified and analysed by next-generation sequencing (NGS). The screen was performed 4 times, each of which included all 4 conditions, for a total of 16 individual kinome screens. NGS datasets from our four different conditions

were integrated to identify both common and unique autophagy activators and inhibitors as detailed below (Fig. 2A).

We conducted analysis of sgRNA enrichment and depletion between the sorted populations and the corresponding unsorted populations across experimental replicates for each stress condition using CRISPRBetaBinomial(Jeong et al. 2019). Hits were called using false discovery rate (FDR; adjusted *p* values) and a positive $\log_2$ fold change ($\log_2$FC) (Table 1, Table S1). Log_2FC represents enrichment or depletion of each gene compared to the corresponding unsorted population, measured by the mean of all four sgRNAs targeting the gene, in the sorted high or low GFP/DsRed population. FDR indicates the statistical significance of sgRNAs abundance of a gene in the sorted high or low GFP/DsRed group compared to the unsorted sample. For both autophagy activators and inhibitors, we observed some shared regulators among 4 conditions, but a significant portion of the hits were unique to the stress condition tested (Fig. 2B). Volcano plots showcasing FDR and $\log_2$FC values were constructed to visualize autophagy activators and inhibitors (Figs. 2C and 2D). The asymmetric nature of the plot suggests that the statistical ability to detect sgRNA enrichment (positive $\log_2$FC) was greater than the ability to detect sgRNA depletion (negative $\log_2$FC) in the sorted population, a feature that has been previously reported(Pusapati et al. 2018). Therefore, subsequent analyses focused exclusively on genes with FDR <0.1 for enrichment (positive $\log_2$FC) in the sorted population. Additionally, hits were omitted if they possessed significant FDR values in both positive and negative regulator populations (conflicts)(Rousseaux et al. 2018). A summary of common and distinct regulators that meet the criteria of FDR cutoff and

positive log_2FC from both autophagy-activating and inhibiting populations are provided in Table 1.

We performed a gene ontology analysis using PANTHER to determine whether the candidate kinases are enriched in any signaling pathways (Fig. 2E, Table S2). We found that basal autophagy candidates were significantly enriched in metabolism and insulin receptor signaling pathways, whereas candidates involved in stress-induced autophagy were enriched in pathways such as autophagy and mitophagy. This analysis also identified synthesis of PIPs at the late endosomal membrane as a shared pathway among all four screen conditions. Notably, our gene ontology identified autophagy and autophagy-related pathway enrichment, which is consistent with an autophagy regulating role for these kinases.

Autophagy activators

Our kinome screens identified a total of 66 autophagy activators that met the selection criteria above. Notably, the autophagy activators that were found in all four conditions have all previously been linked to autophagy activation, reinforcing the quality of our screen results. The common activators were *ULK1*, *PIK3C3*, *PIK3R4*, and *PIKFYVE* (Fig. 2C). The protein kinase ULK1 along with the lipid kinase containing PIK3R4 and PIK3C3 are important factors in core autophagy machinery and have been well characterized to tightly regulate autophagy initiation. The role of PIKFYVE in autophagy has been characterized more recently, and was reported to be important for lysosomal function in the autophagy pathway, which is a common requirement for bulk and selective autophagy.

We also found multiple genes encoding members of the casein kinase family (CSNK) among the four autophagy screens. Several reports have demonstrated both activating and inhibiting roles of this family in autophagy regulation, with the role varying based on the cell type and stress condition tested(Li et al. 2020; Chino et al. 2022; Hoenigsperger et al. 2024; Carrino et al. 2019). In our analysis, we found *CSNK2A1* was involved in autophagy activation under basal conditions, while *CSNK1A1L* and *CSNK2A2* were implicated in activating starvation-induced autophagy. *CSNK2A2* was also associated with autophagy activation under ER stress and peroxisomal stress (Table 1).

Autophagy under basal conditions

We identified 33 basal autophagy activators. Of 33 candidates, 13 have been previously linked to autophagy (Table 1 plain face text) and 20 were uniquely identified in our screens (Table 1, italic text). Of the 33 hits 24 were only identified in the basal autophagy conditions, 4 were common to all conditions, 2 (*LATS1* and *PHKG1*) were shared between basal and starvation-induced autophagy, and 3 (*FGFRL1*, *PHKA2*, and *GK2*) were shared between basal autophagy and ER stress conditions (Table 1, Fig. 2B).

Starvation-induced autophagy

We found a total of 13 candidates involved in autophagy induction. Of these hits, 8 have been previously reported to modulate autophagy (Table 1 plain face text) and 5 were unique to our screens (Table 1 italic text). 6 of the 13 hits were identified as autophagy activators only under starvation (Table 1, Fig. 2B). *LATS1* and *PHKG1* were shared between starvation-induced and basal autophagy Finally, *CSNK2A2* was

identified as a shared autophagy activator under starvation, ER stress, and peroxisomal stress.

ER stress-induced autophagy

We identified 25 (11 established and 14 novel) kinases associated with autophagy under ER stress (Table 1). Of the 25 hits, 17 were identified only in the ER stress-induced autophagy (Fig. 2B), 4 were common to all conditions, 3 (*FGFRL1*, *PHKA2*, and *GK2*) were shared between ER stress conditions and basal autophagy, and 1 (*CSNK2A2*) was found as a shared autophagy activator under starvation, ER stress, and peroxisomal stress (Fig. 2B). Notably, our screens identified *EIF2AK3* as a unique ER stress-induced autophagy activator. EIF2AK3, also known as PERK (protein kinase R-like endoplasmic reticulum kinase), is a key player in the unfolded protein response and initiates the upstream response to ER stress by activating transcription factors responsible for expressions of autophagy proteins(B'chir et al. 2013). Moreover, it was reported that EIF2AK3 is selectively required for ER-phagy induced by tunicamycin(Luhr et al. 2019), which validates the ability of our screens to recognize selective autophagy modulators.

Peroxisomal stress-induced autophagy

We identified 14 candidates (7 established and 7 novel) involved in autophagy induction in response to peroxisomal stress (Table 1). Previously, ATM had been the sole kinase reported to induce pexophagy(Zhang et al. 2015). We did not identify *ATM* in our screens, which is likely due to the genetic intolerance of HEK293A cells to *ATM* depletion. However, our screens found 9 unique candidates linked to peroxisomal stress-induced autophagy (Table 1). *CSNK2A2* is the only common hit found in peroxisomal stress-

induced autophagy and in other autophagy pathways (starvation- and ER stress-induced autophagy).

Autophagy inhibitors

We identified a total of 63 shared and distinct autophagy inhibitors across the four screens. We found that *TKFC* and *MAP4K2* are shared autophagy inhibitors among all conditions (Fig. 2D, Table 1). TKFC (triokinase/FMN cyclase) is an enzyme involved in cellular processes related to the metabolism of carbohydrates and flavin mononucleotide (FMN), which is a type of flavin coenzyme(Rodrigues et al. 2019). There is no known link between TKFC and autophagy to date. MAP4K2, mitogen-activated protein kinase kinase kinase kinase 2, is a serine/threonine kinase essential for innate immune responses and cell signaling(Chuang et al. 2016). Little is known about the relationship between MAP4K2 and autophagy. However, MAP4K2 has been recently reported to induce autophagy upon energy stress through LC3 phosphorylation. *MAP4K2* inclusion in all four investigated conditions underscores its role as a general inhibitor of autophagy(Seo et al. 2023).

Our screens also identified genes encoding members of ribosomal protein S6 kinase (RPS6K) family across four tested conditions. Similar to casein kinases, various reports have indicated that this family plays both activating and inhibitory roles in the regulation of autophagy(Hać et al. 2021; Blommaart et al. 1995; Scott et al. 2004; Armour et al. 2009; Zeng and Kinsella 2008). In this study, we only observed *RPS6K* presence in the negative autophagy regulator screens. Specifically, *RPS6KL1* was found in the basal condition. *RPS6KA4*, *RPS6KC1*, and *RPS6KL1* were enriched in starvation-induced autophagy conditions. Finally, *RPS6KA4* was enriched in both ER stress- and peroxisomal stress-induced autophagy.

Autophagy under basal conditions

We identified 13 candidates (4 established, 9 novel) involved in basal autophagy (Table 1). 8 of the 13 candidates were identified as autophagy inhibitors only under basal conditions (Fig. 2B). *NEK1* and *RPS6KL1* are two hits involved in basal and starvation-induced autophagy. *CDC42BPG* is the sole candidate shared among basal, starvation-induced, and peroxisomal stress-induced autophagy processes.

Starvation-induced autophagy

Our kinome screens found a total of 33 candidates (13 established, 20 novel) associated with autophagy inhibition in response to starvation (Table 1). 24 of these were identified only in the starvation conditions, 2 were common to all conditions, 2 (*NEK1* and *RPS6KL1*) were shared between starvation-induced and basal autophagy, 1 (*PMVK*) was found in autophagy inhibition under starvation and ER stress, 2 (*MAP3K11* and *ACVR1*) were identified in starvation- and peroxisomal stress-induced autophagy, 1 (*CDC42BPG*) was shared among basal, starvation-induced, and peroxisomal stress-induced autophagy processes, and 1 (*RPS6KA4*) was found in starvation-, ER stress-, and peroxisomal stress-induced autophagy.

ER stress-induced autophagy

We identified 17 hits (8 established, 9 novel) involved in autophagy inhibition under ER stress (Table 1). We found 11 hits selectively associated with ER-phagy (Fig. 2B). Notably, CSNK2B is the only member within the casein kinase family that we identified in the context of autophagy inhibition. In addition to the overlapped hits mentioned above,

STK11 and *MST1* are candidates shared among ER stress- and peroxisomal stress-induced autophagy.

Peroxisomal stress-induced autophagy

Our screens found 17 candidates (9 established, 8 novel) associated with autophagy inhibition in response to peroxisomal stress (Table 1). 9 of these were found only in the peroxisomal stress conditions, 2 were common to all conditions, 2 (*MAP3K11* and *ACVR1*) were identified in peroxisomal stress- and starvation- induced autophagy, 2 (*STK11* and *MST1*) were shared among peroxisomal stress- and ER stress-induced autophagy, 1 (*CDC42BPG*) was found in basal, starvation-, and peroxisomal stress-induced autophagy processes, and 1 (*RPS6KA4*) was involved in autophagy inhibition under peroxisomal stress, starvation, and ER stress.

Collectively, our comprehensive kinome screens have identified a total of 129 kinases with a significant FDR and positive $\log_2$FC values. In addition to the common activators and inhibitors of all conditions, we also found several kinases that overlapped between 2 or more conditions, which may imply common upstream regulation between these types of autophagy. There is a precedent for this type of overlap in selective autophagy regulators from the study of autophagy receptors. For example, BNIP3L has been reported to induce pexophagy and mitophagy(Wilhelm et al. 2022). In addition to shared regulators, we found selective regulators of both pexophagy and ER-phagy, indicating that selective autophagy is likely governed by signal transduction in addition to autophagy receptors.

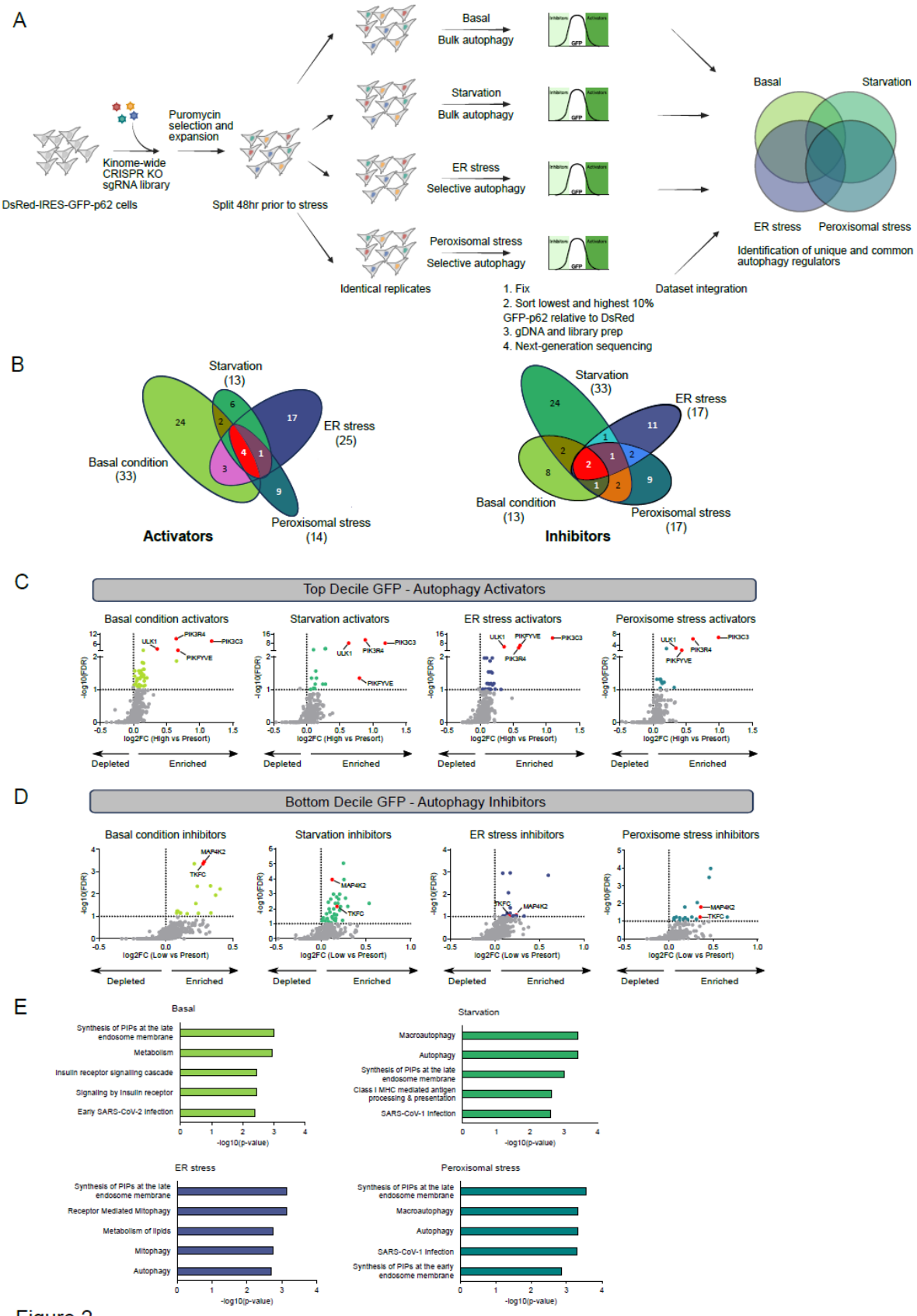
A
Basal
Bulk autophagy
Starvation
Bulk autophagy
ER stress
Selective autophagy
Peroxisomal stress
Selective autophagy
Puromycin selection and expansion
Kinome-wide CRISPR KO sgRNA library
DsRed-IRES-GFP-p62 cells
Split 48hr prior to stress
Identical replicates
1. Fix
2. Sort lowest and highest 10% GFP-p62 relative to DsRed
3. gDNA and library prep
4. Next-generation sequencing
Dataset integration
Basal
Starvation
ER stress
Peroxisomal stress
Identification of unique and common autophagy regulators
B
Starvation (13)
ER stress (25)
Basal condition (33)
Peroxisomal stress (14)
Activators
Starvation (33)
ER stress (17)
Basal condition (13)
Peroxisomal stress (17)
Inhibitors
C
Top Decile GFP - Autophagy Activators
Basal condition activators
Starvation activators
ER stress activators
Peroxisome stress activators
-log10(FDR)
log2FC (High vs Presort)
Depleted
Enriched
D
Bottom Decile GFP - Autophagy Inhibitors
Basal condition inhibitors
Starvation inhibitors
ER stress inhibitors
Peroxisome stress inhibitors
log2FC (Low vs Presort)
E
Basal
Synthesis of PIPs at the late endosome membrane
Metabolism
Insulin receptor signalling cascade
Signaling by Insulin receptor
Early SARS-CoV-2 Infection
Starvation
Macroautophagy
Autophagy
Synthesis of PIPs at the late endosome membrane
Class I MHC mediated antigen processing & presentation
SARS-CoV-1 Infection
ER stress
Synthesis of PIPs at the late endosome membrane
Receptor Mediated Mitophagy
Metabolism of lipids
Mitophagy
Autophagy
Peroxisomal stress
Synthesis of PIPs at the late endosome membrane
Macroautophagy
Autophagy
SARS-CoV-1 Infection
Synthesis of PIPs at the early endosome membrane
-log10(p-value)

Figure 2

Figure 2: Tandem CRISPR screens identify stress-specific regulators of autophagy.

(A) The screening strategy used to identify positive regulators and negative regulators of autophagy pathways. (B) Venn diagrams depict shared and distinct activators or inhibitors among 4 examined conditions. (C), (D) Volcano plots from the four screens. For each gene, the x-axis indicates its enrichment or depletion, determined by the mean of all four sgRNAs targeting the gene, in the sorted population compared to the corresponding unsorted population. The y-axis represents the statistical significance, as indicated by the false discovery rate (FDR)-corrected p-value. The horizontal dashed line represents an FDR-value threshold of 0.1. Red dots on the graph denote shared regulators across all four conditions, hits specific to different conditions are colored accordingly, and all other genes are represented as gray dots. (E) Gene ontology analysis was performed on screen candidates across the 4 examined conditions. The top 5 enriched Reactome Pathways and corresponding –log10(p-values) are shown.

Condition		Hits
Basal condition	Activators	PIK3R4, PIK3C3, ULK1, PIKFYVE, MET, CDK1, *SBK1*, CSNK2A1, *ADCK4*, *FGFRL1*, INSR, *PRKCG*, *TGFBR2*, *AATK*, *RIPK4*, *PHKA2*, *SEPHS2*, CDK5R1, MAPK1, *STK32A*, *FLT1*, *GK2*, *IP6K3*, *ITPKC*, LATS1, *CKMT1B*, *BCKDK*, *TPK1*, *PDGFRL*, *PHKG1*, BCR, *ERN2*, NTRK1
	Inhibitors	MAP4K2, *TKFC*, *MARK2*, *CDC42BPG*, *CHKA*, PKMYT1, PGK1, *ABCC1*, *NEK1*, *AGK*, *EXOSC10*, *RPS6KL1*, TPR
Starvation	Activators	PIK3R4, ULK1, PIK3C3, PIKFYVE, *PHKG1*, *ROS1*, *INSRR*, LATS1, *CSNK1A1L*, PLK1, CSNK2A2, ACVR2B, *CPNE3*
	Inhibitors	MAP4K2, *TKFC*, *RPS6KL1*, CAMKK1, ROCK1, *CDC42BPG*, *NEK1*, *CDC42BPB*, *CLP1*, NEK9, PRKAG2, *RPS6KA4*, MAP3K11, *PFKFB2*, *VRK1*, *BTK*, *MASTL*, PRKAB1, PRKD1, *ITPK1*, *NME1-NME2*, *ACVR1*, CDK12, *PMVK*, MAPK3, *UCK1*, RIPK3, *MOK*, *RPS6KC1*, MAP2K2, HUNK, *PKDCC*, *PRKAR2A*
ER stress	Activators	PIK3C3, PIKFYVE, ULK1, PIK3R4, *ATMIN*, CDK11A, *ADCK3*, PRKD2, *STRADA*, PAK4, *CDK14*, CSNK2A2, *GK2*, *PHKA2*, *TESK1*, TRIM27, *GSG2*, ROR1, *CDC42BPB*, *FGFRL1*, *MVK*, *TK1*, *TRIO*, EIF2AK3, *RIOK3*
	Inhibitors	*TKFC*, MAP4K2, *PMVK*, *RPS6KA4*, NME3, SCYL1, CHEK2, STK11, *AMHR2*, BRD3, *CLK3*, CSNK2B, MST1, *PGM2L1*, *SBK3*, *TSSK4*, *TTBK2*
Peroxisome stress	Activators	PIK3C3, PIK3R4, ULK1, PIKFYVE, CSNK2A2, BMP2K, *PAN3*, *PIP5KL1*, *TGFBR1*, *IDNK*, *ADPGK*, *SBK2*, *CLK3*, CERKL
	Inhibitors	*TKFC*, MAP4K2, *CDC42BPG*, PDPK1, *KIAA1804*, MAP3K11, *LMTK2*, *RPS6KA4*, SRC, PFKFB4, *BAZ1B*, MAPK15, MTOR, STK11, *ACVR1*, MST1, *CDK2*

Table 1: Summary of hits satisfy log2FC and FDR cutoffs. Known hits are displayed in normal texts and novel hits are shown in italic texts.

Selection of top hits for characterization

To validate hits that were potential unique regulators of selective autophagy, we generated polyclonal knockout (KO) cell lines using CRISPR/Cas9 for the top activators or inhibitors for both ER stress-induced and peroxisomal stress-induced autophagy and validated them using WB as an orthogonal system. An additional ULK1 positive control, which was shared among all conditions, was also generated in the same manner. We evaluated p62 flux via WB following the same treatment paradigms used in the screens (Figs. S2 and S3). From this experiment, we chose the top hits for each category (ER-phagy/pexophagy activator/inhibitor), which showed the largest average regulatory effect and had not previously been implicated in regulation of the corresponding selective autophagy pathway. These hits were CDK11A (ER-phagy activator), NME1 (ER-phagy repressor), PAN3 (pexophagy activator), and CDC42BPG (pexophagy inhibitor); KO efficiencies of these cell lines were confirmed by WB (Fig. S4). Throughout our study, we utilized multiple approaches to investigate p62 regulation. Fluorescence-activated cell sorting (FACS) and WB were used to assess overall changes in p62 levels during the autophagy process. Western blot detects a decrease in total p62 upon autophagy activation (Fig. S4F)(Klionsky et al. 2016). In contrast, immunofluorescence (IF) provides insight into p62 colocalization and capture in autophagosomes within cells. Under stress conditions, p62 localizes to autophagosomes, leading to an increase in p62 puncta, which can be observed through IF (Fig. S4F). As a result of these differences in detection methods, decreased total p62 by WB and FACS and increased p62 puncta by IF are both consistent with increases in autophagy flux.

CDK11A is a selective ER-phagy activator

Our analysis suggested that CDK11A may be a novel activator of ER-phagy (Figs. 3A and S2A). CDK11A (Cyclin-Dependent Kinase 11A), a member of the cyclin-dependent kinase (CDK) family, is implicated in the regulation of transcription, cell cycle control, and basal autophagy regulation(Trembley et al. 2002; Loyer et al. 2005; Wilkinson et al. 2011). However, it has no known role in selective autophagy or ER-phagy. We treated control 293A and CDK11A KO cells with tunicamycin, and observed a decrease of p62 in control cells, but not in CDK11A KO cells (Fig. 3B). Moreover, we observed an increase in basal p62 in CDK11A KO cells, which is expected when an activator of autophagy is ablated (Fig. 3B)(Jung et al. 2009). In addition to p62, we also assessed autophagy by investigating LC3B signaling, which is the most well-characterized member of LC3/GABARAP family and is a reliable indicator of autophagy induction. Increases in lipidated LC3B – LC3B-II (the lower migrating band by WB) – is conjugated to autophagosomes and is used as a marker for autophagy flux(Klionsky et al. 2016). However, elevated LC3B-II levels may indicate impaired autophagosome clearance. As a result, its accumulation should be measured in the presence of bafilomycin A1 (Baf), which blocks the autophagic degradation of LC3B. In control, but not CDK11A KO cells, we detected induction of autophagy by tunicamycin, as measured by LC3B-II in the presence of Baf (Fig. 3B). Tunicamycin is known to induce the expression of genes in the unfolded protein response including C/EBP-homologous protein (CHOP)(Lei et al. 2017). To determine if CDK11A KO impacted the UPR pathway we performed WB analysis of CHOP showed an equivalent activation of the UPR pathway in all cell lines upon

tunicamycin treatment, indicating that an altered unfolded protein response was not responsible for differences in p62 flux (Fig. 3B).

p62 directly interacts with LC3B when loading cargo into autophagosomes. Thus, we used IF microscopy as an orthogonal approach to measure the impact of CDK11A KO on the formation of p62 and LC3B-positive autophagosomes during ER stress. In response to ER stress, control cells showed an increase in p62 and LC3B (lipidated LC3B) dual positive puncta (Fig. 3C). In CDK11A KO cells we observed a slightly lower induction of LC3B puncta that were not p62 positive, indicating a defect in p62 recruitment and cargo loading in response to ER stress (Fig. 3C).

To better link CDK11A function to ER-phagy induction, we sought to analyze the ER-resident autophagy receptor FAM134B. FAM134B is the best characterized ER-phagy receptor, which, like p62, binds LC3B-II and is degraded in the autophagosome(Khaminets et al. 2015; Leonibus et al. 2020). We treated control and CDK11A KO cells with tunicamycin in the presence of Baf and analysed FAM134B levels (Fig. 3D). As anticipated, in control cells, FAM134B was degraded in response to ER-stress and this degradation could be blocked by inhibiting autophagosome turn-over. However, in CDK11A KO cells we observed that FAM134B was insensitive to both ER stress and inhibitors of autophagy, further indicating that CDK11A is important for ER-phagy (Fig. 3D). To confirm the role of CDK11A on ER-phagy is not limited to the HEK293A background, we knocked down (KD) CDK11A in HCT116 cells (Fig. S5A) and analyzed FAM134B degradation in response to tunicamycin. We observed that depletion of CDK11A reduced FAM134B clearance, consistent with our results in HEK293 cells (Fig. S5B).

We next immunostained for FAM134B to determine if FAM134B loading into autophagosomes upon ER stress requires CDK11A. Interestingly, we observed that FAM134B puncta were elevated in both tunicamycin-treated control and CDK11A KO cells (Fig. 3E). FAM134B interacts with LC3B through LIR motifs, which guides the sequestration and engulfment of ER fragments within autophagosomes(Khaminets et al. 2015). To distinguish if FAM134B puncta were associated with functional autophagosomes, we repeated the experiment while co-staining for LC3B. As expected, control cells showed an induction of LC3B-associated FAM134B puncta under ER stress conditions, indicating an activation of ER-phagy (Fig. 3F). However, in CDK11A-deficient conditions, we could not detect colocalization between FAM134B and LC3B puncta, likely indicating stalled autophagic structures (Fig. 3F). This is consistent with our WB analysis (Fig. 3D) and previous reports of stalled autophagic structures in autophagy-deficient cells(Jung et al. 2009; Komatsu et al. 2005; Zachari et al. 2020). Interestingly, ER stress induced LC3-negative FAM134B puncta in CDK11A KO cells (Fig. 3F), indicating that CDK11A regulates ER-phagy at a step downstream of FAM134B oligomerization, but upstream of LC3B binding.

To further investigate the involvement of CDK11A in ER-phagy and to confirm that CDK11A-dependent ER-phagy is not limited to the HEK293 background used in the screen, we generated an HCT116 ER-phagy reporter line. HCT116 cells were transduced to express a doxycycline-inducible probe containing the ER signal sequence, RFP, GFP and KDEL ER retention sequence (ss-RFP-GFP-KDEL “KDEL cells”), as previously described(Chino et al. 2019). Following doxycycline treatment and the induction of ER-phagy, the GFP signal is quenched due to its sensitivity to lysosomal proteases and pH,

yielding an RFP fragment detectable by WB. The KDEL cells were transfected with either non-targeting control siRNA or siRNA targeting CDK11A to create control and CDK11A KD cell populations respectively. Depletion of CDK11A by siRNA knockdown was examined by WB (Fig. S5A). The functionality of the probe was confirmed in control cells that generated a free RFP fragment upon tunicamycin treatment, which was reversable with the autophagy inhibitor Baf (Fig. 3G). Additionally, we noticed the absence of free RFP fragments in the treated CDK11A KD reporter cells (Fig. 3G). The ss-RFP-GFP-KDEL reporter can also be analyzed by IF, where the loading of the ER-phagy probe into autophagosomes results in discrete dual fluorescent puncta formation, which lose GFP signal upon autophagosome maturation and acidification(Chino et al. 2019). As anticipated, in control cells, tunicamycin induced RFP single positive puncta, which largely colocalized with p62, indicative of ER-phagy induction (Fig. 3H). However, we did not observe processing of the ER-phagy probe into autophagosomal structures in CDK11A KD cells, consistent with ER-phagy defects observed with the probe by WB (Fig. 3H).

We next explored if the requirement for CDK11A for ER-phagy is limited to ER-stress induced by tunicamycin or extended to other inducers of ER-phagy. Prolonged amino acid starvation (6 hours) is known to strongly induce ER-phagy, whereas bulk autophagy is typically triggered within a shorter timeframe (1–3 hours). Using our ER-phagy reporter cell line, we induced ER-phagy by amino acid starvation for 6 hours or tunicamycin treatment and observed ER-phagy induction under both stresses in our control line (Fig. S5C, S5D). We found that the knockdown of CDK11A abrogated ER-phagy induction stimulated by prolonged amino acid starvation or tunicamycin treatment

(Figs. S5C and S5D). Collectively, these data indicate that CDK11A is essential for the induction of ER-phagy in response to diverse ER stressors.

To determine whether CDK11A acts selectively on ER-phagy, we tested how its loss of function affects starvation-induced autophagy. To make this head-to-head comparison, we incubated control and CDK11A KO HEK293A cells with amino acid-free media or tunicamycin. Amino acid starvation begins to induce ER-phagy after 6 hours, so a 1.5-hour amino acid starvation was employed to induce bulk autophagy without activating ER-phagy. As expected, we observed an efficient induction of starvation-induced autophagy and ER-phagy in control cells as shown by the degradation of p62 and FAM134B, respectively (Fig. 3I). We observed that CDK11A KO cells were competent in the induction of starvation-induced autophagy, but deficient for ER-phagy (Fig. 3I). Collectively, these data nominate CDK11A as a selective activator of ER-phagy.

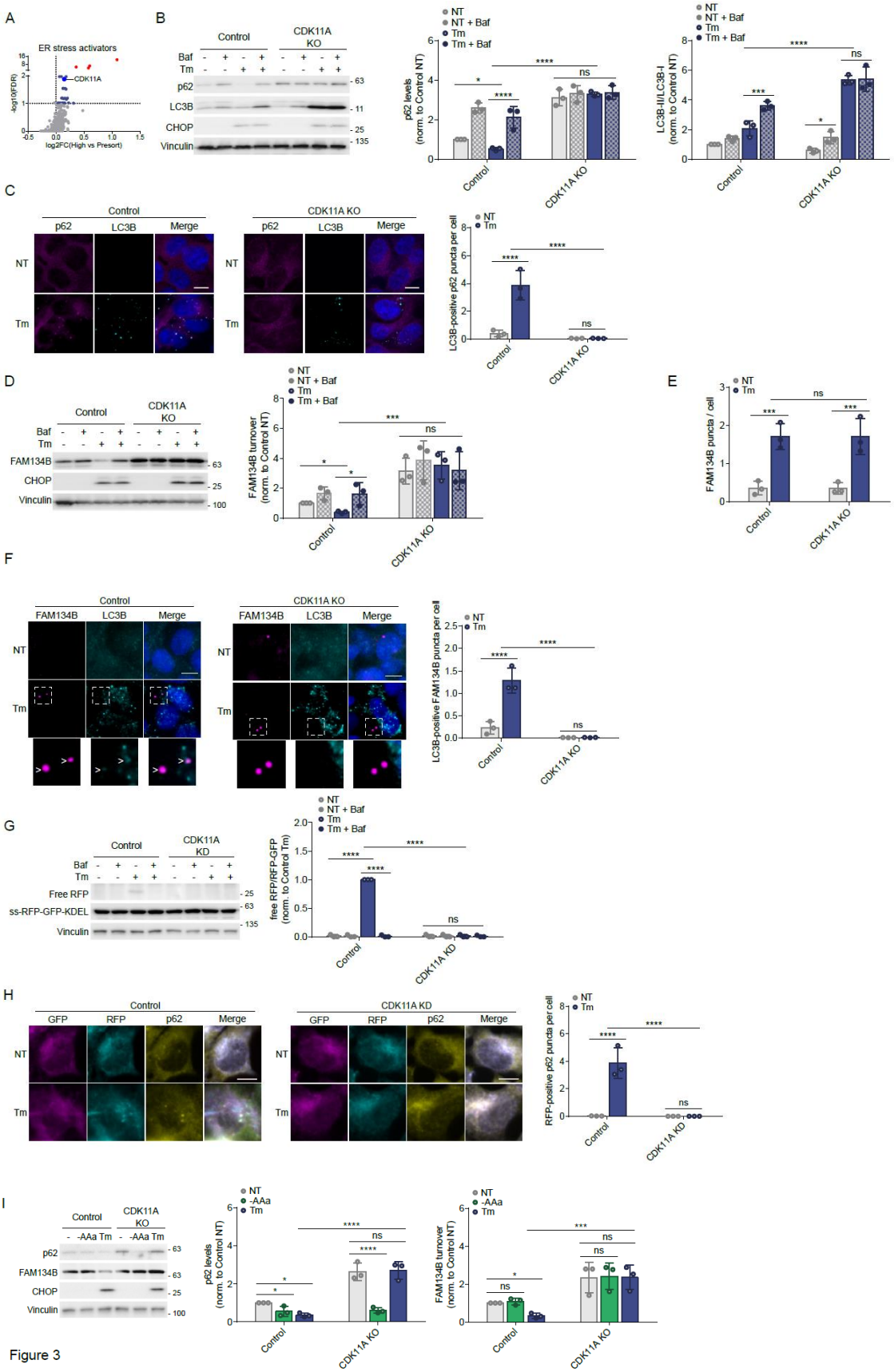
A
ER stress activators
CDK11A
-log10(FDR)
log2FC(High vs Presort)
B
Control
CDK11A KO
Baf
Tm
p62
LC3B
CHOP
Vinculin
63
11
25
135
NT
NT + Baf
Tm
Tm + Baf
p62 levels (norm. to Control NT)
LC3B-II/LC3B-I (norm. to Control NT)
C
Control
CDK11A KO
p62
LC3B
Merge
NT
Tm
LC3B-positive p62 puncta per cell
D
FAM134B
CHOP
Vinculin
100
FAM134B turnover (norm. to Control NT)
E
FAM134B puncta / cell
F
FAM134B
LC3B-positive FAM134B puncta per cell
G
CDK11A KD
Free RFP
ss-RFP-GFP-KDEL
free RFP/RFP-GFP (norm. to Control Tm)
H
GFP
RFP
RFP-positive p62 puncta per cell
I
-AAa Tm
-AAa
ns

Figure 3

Figure 3: CDK11A activates ER-phagy.

(A) CDK11A is represented as a prominent blue dot on the volcano plot. Red dots on the graph denote common regulators across all four conditions. (B) The control and CDK11A KO HEK293A cells were treated with tunicamycin (10 μg/mL) for 6 hours in the presence or absence of bafilomycin A1 (Baf). Levels of p62 and LC3B were analysed using western blot. The effectiveness of tunicamycin was assessed through CHOP analysis. (C) The control and KO cells were incubated with tunicamycin (10 μg/mL) for 6 hours. p62 and LC3B puncta were visualized and quantified by immunofluorescence. Scale bars, 10 μM. (D) The control and KO cells were treated with tunicamycin in the presence or absence of Baf. FAM134B levels were then examined using western blot. (E) The indicated cells were incubated with tunicamycin for 6 hours. FAM134B puncta were quantified by immunofluorescence. (F) The control and KO cells were incubated with tunicamycin for 6 hours. FAM134B and LC3B puncta were visualized and quantified by immunofluorescence. White arrows depict LC3B and FAM134B colocalization. Scale bars, 10 μM. (G) The control and CDK11A KD HCT116 cells stably expressing the ss-RFP-GFP-KDEL reporter were incubated with tunicamycin (10 μg/mL) for 6 hours in the presence or absence of Baf. ER-phagy was assessed through the processing of ss-RFP-GFP-KDEL. (H) The control and CDK11A KD cells containing ER-phagy reporter KDEL were treated with tunicamycin (10 μg/mL) for 6 hours. GFP, RFP, and p62 signals were visualized and quantified by immunofluorescence. Scale bars, 10 μM. (I) The control and KO HEK293A cells were incubated with either acute amino acid starvation (1.5 hours, -AAa) or tunicamycin (10 μg/mL, 6 hours). Whole-cell lysates were immunoblotted using the antibodies indicated.

Unless otherwise indicated, experiments were performed three times. Data are represented as means ± SDs, and p values were determined by two-way ANOVA. *p ≤ 0.1; **p ≤ 0.01; ***p ≤ 0.001; ****p ≤ 0.0001; ns, not significant.

NME3 is a selective ER-phagy inhibitor

Nucleoside Diphosphate (NDP) Kinase 3 (NME3) is best known for its ability to regulate nucleotide metabolism and signaling(Boissan et al. 2018; Abu-Taha et al. 2017). Recent research indicates that NME3 serves two distinct functions, regulation of mitochondrial dynamics and NDP kinase activity, both of which are required to maintain cell viability under glucose starvation(Chen et al. 2019). Additionally, during the preparation of this manuscript, NME3 was reported to be involved in mitophagy regulation(Chen et al. 2024). Our analysis of the top screen hits indicated that NME3 may be a selective repressor of ER-phagy (Figs. 4A and S2B). We first tested the ability of NME3 KO cells to increase autophagic flux upon ER stress. Compared to our control cells, we found NME3 KO cells exhibited lower levels of p62 and a more complete degradation of p62 under ER stress (Fig. 4B). Furthermore, tunicamycin-treated NME3 KO cells exhibited a more pronounced increase in LC3B-II levels compared to treated control cells in the presence of Baf, consistent with a role for NME3 as an inhibitor of ER-phagy (Fig. 4B). Next, we analysed the impact of NME3 KO on ER stress-induced p62 and LC3B loading into autophagosomes. As expected, we observed an increase in p62 and LC3B puncta in the treated control cells (Fig. 4C). Conversely, we found that NME3 KO cells treated with tunicamycin showed more p62 puncta and an increase in p62 and LC3B colocalization, compared to control cells (Fig. 4C). Together, these data indicate that NME3 regulates autophagy flux in response to ER stress.

We then examined whether NME3 could regulate ER-phagy receptor, FAM134B. Control and KO cells were treated with tunicamycin and FAM134B levels were investigated using WB. Consistently, NME3 depletion resulted in a reduction in FAM134B

levels compared to those of the control cells upon ER stress (Fig. 4D). Furthermore, NME3-dependent FAM134B degradation was blocked in the presence of Baf, linking NME3 regulation of FAM134B stability to ER-phagy flux (Fig. 4D). To verify that this effect is not restricted to the HEK293A cell background, we depleted NME3 in HCT116 cells (Fig. S6A) and examined FAM134B degradation following tunicamycin treatment. Consistent with our findings in HEK293 cells, NME3 knockdown enhanced FAM134B clearance (Fig. S6B).

Next, we investigated the effects of NME3 depletion on FAM134B recruitment into autophagosomes in response to ER stress. We immunostained FAM134B and LC3B in our untreated and treated control or KO cells. We observed NME3 KO cells had an enhanced production of LC3B-positive FAM134B puncta upon ER stress compared to control cells (Fig. 4E). The increase of autophagosome-associated FAM134B under stress is a strong indicator that NME3 inhibits ER-phagy rates. We next investigated the effects of NME3 KD on ER-phagy in the doxycycline-inducible ss-RFP-GFP-KDEL ER-phagy reporter HCT116 cell line. We first confirmed NME3 knockdown efficiency (Fig. S6A). Treatment of ER-phagy reporter lines with tunicamycin showed an increase in probe processing upon NME3 KD compared to control lines, consistent with the role for NME3 in ER-phagy repression (Fig. 4F). Using IF, we also saw a more robust increase in RFP-positive p62 puncta in the stressed NME3 KD cells (Fig. 4G).

To investigate whether NME3-dependent regulation of ER-phagy could be triggered by various stimuli, we subjected control and NME3 KD reporter cells to prolonged starvation and tunicamycin treatment. As anticipated, we observed a stronger production of RFP fragments examined by WB (Fig. S6C) and increased GFP-free RFP

puncta detected by IF (Fig. S6D) in both starved and tunicamycin-treated NME3 KD cells compared to treated control cells.

Lastly, we tested whether NME3 regulates ER-phagy selectively by treating the control and KO cells with either amino acid-free media or tunicamycin. Amino acid starvation induces ER-phagy beginning at 3 hours, so a 1.5-hour amino acid starvation used to induce bulk autophagy without activating ER-phagy. Consistent with the results above in the NME3 KO background, we observed an increase in p62 and FAM134B degradation upon tunicamycin treatment (Fig. 4H). However, NME3 KO cells showed no detectable difference in p62 clearance under acute starvation when compared to control cells (Fig. 4H). Taken together, these experiments show that NME3 is a selective upstream inhibitor of ER-phagy.

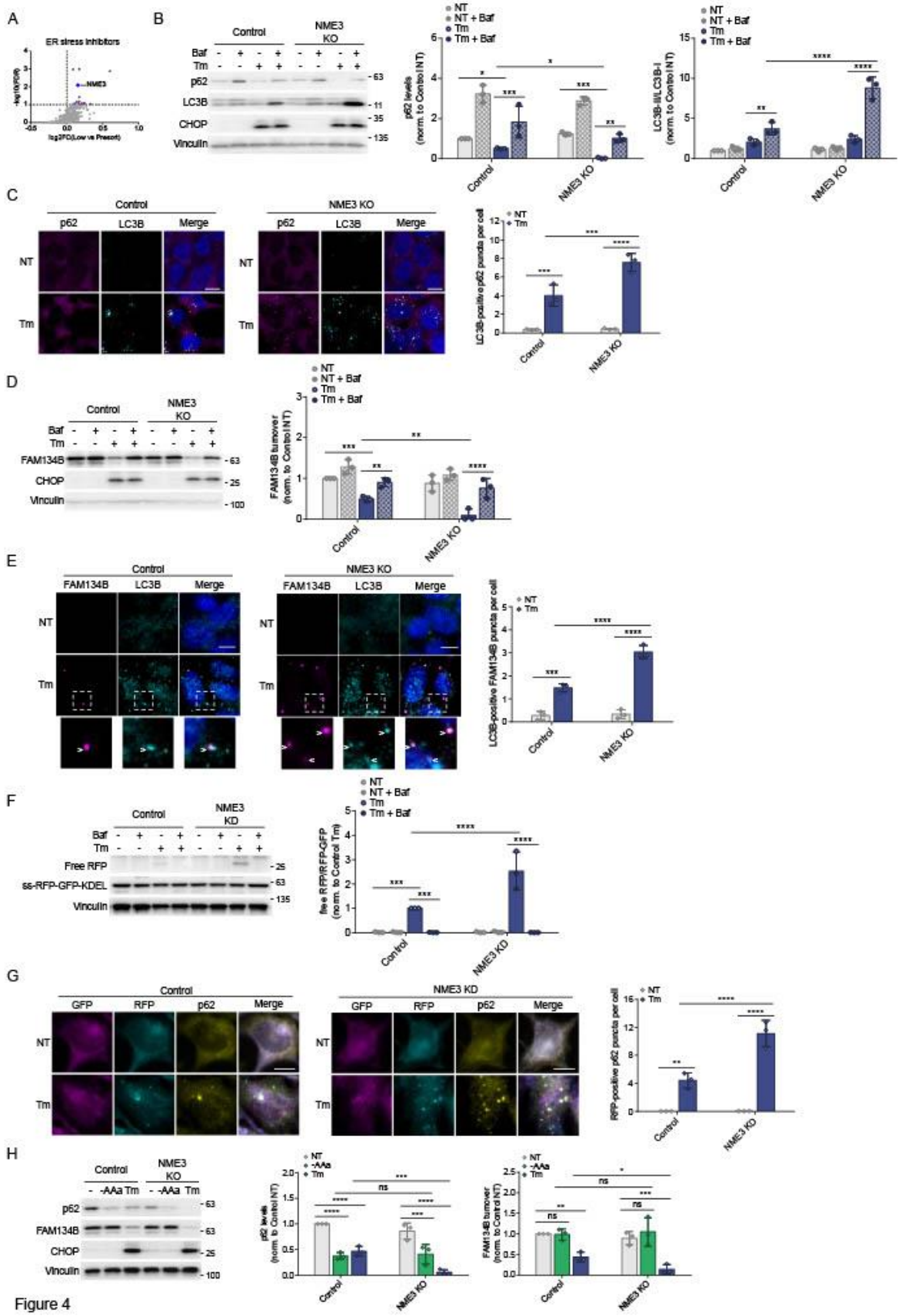
A
ER stress inhibitors
NME3
log2FD(Low vs Present)
B
Control
NME3 KO
Baf
Tm
p62
LC3B
CHOP
Vinculin
NT
NT + Baf
Tm
Tm + Baf
p62 levels (norm. to Control NT)
LC3B-II/LC3B-I (norm. to Control NT)
C
Control
NME3 KO
p62
LC3B
Merge
NT
Tm
LC3B-positive p62 puncta per cell
D
FAM134B
FAM134B turnover (norm. to Control NT)
E
FAM134B
LC3B-positive FAM134B puncta per cell
F
Free RFP
ss-RFP-GFP-KDEL
NME3 KD
free RFP/RFP-GFP (norm. to Control Tm)
G
GFP
RFP
RFP-positive p62 puncta per cell
H
-AAa
p62 levels (norm. to Control NT)
FAM134B turnover (norm. to Control NT)

Figure 4

Figure 4: NME3 inhibits ER-phagy.

(A) NME3 is represented as a prominent blue dot on the volcano plot. Red dots on the graph denote common regulators across all four conditions. (B) The control and NME3 KO HEK293A cells were treated with tunicamycin (10 μg/mL) for 6 hours in the presence or absence of Baf. Changes in p62 and LC3B levels were analysed using western blot. The effectiveness of tunicamycin was assessed through CHOP analysis. (C) The control and KO cells were incubated with tunicamycin (10 μg/mL) for 6 hours. p62 and LC3B puncta were visualized and quantified by immunofluorescence. Scale bars, 10 μM. (D) The control and KO cells were treated with tunicamycin in the presence or absence of Baf. FAM134B signaling was then examined using western blot. (E) The indicated cells were incubated with tunicamycin. FAM134B and LC3B puncta were visualized and quantified by immunofluorescence. White arrows depict LC3B and FAM134B colocalization. Scale bars, 10 μM. (F) The control and NME3 KD HCT116 cells stably expressing the ss-RFP-GFP-KDEL reporter were incubated with tunicamycin (10 μg/mL) for 6 hours in the presence or absence of Baf. ER-phagy was assessed through the processing of ss-RFP-GFP-KDEL. (G) The control and NME3 KD cells expressing ER-phagy reporter KDEL were treated with tunicamycin (10 μg/mL) for 6 hours. GFP, RFP, and p62 signals were visualized and quantified by immunofluorescence. Scale bars, 10 μM. (H) The control and KO HEK293A cells were incubated with either acute amino acid starvation (1.5 hours, -AAa) or tunicamycin (10 μg/mL, 6 hours). Whole-cell lysates were immunoblotted using the antibodies indicated.

Unless otherwise indicated, experiments were performed three times. Data are represented as means ± SDs, and p values were determined by two-way ANOVA. *p ≤ 0.1; **p ≤ 0.01; ***p ≤ 0.001; ****p ≤ 0.0001; ns, not significant.

PAN3 is an activator of pexophagy

Our screen validation identified Poly(A)-specific ribonuclease subunit 3 (PAN3) as a potential regulator of clofibrate-driven pexophagy (Figs. 5A and S3A). PAN3 plays a crucial role in mRNA degradation and regulation of gene expression in eukaryotic cells(Chen et al. 2017). It is a component of the PAN2-PAN3 de-adenylation complex responsible for shortening the poly(A) tail of mRNA molecules(Wolf and Passmore 2014; Wolf et al. 2014). Pan3 has a PKc kinase domain but may be a pseudokinase and has no known targets(Wolf et al. 2014). To test if PAN3 regulates peroxisomal stress-induced autophagy we first exposed the control and PAN3 KO cells to clofibrate (1 mM) for 6 hours. p62 levels were decreased in the stressed control cells, but this reduction was prevented in the presence of Baf (Fig. 5B). Interestingly, p62 flux in response to clofibrate was also blocked in PAN3 KO cells (Fig. 5B). We noted the accumulation of LC3B-II levels in the treated control cells in the presence of Baf, indicating autophagy induction (Fig. 5B). However, in stressed PAN3 KO cells, there were no changes in LC3B-II levels compared to the basal PAN3 KO cells, suggesting that PAN3 plays a role in modulating autophagy under peroxisomal stress (Fig. 5B). We next inspected changes in p62 puncta formation and its interaction with LC3B in response to clofibrate in control and KO cells. We observed an increase in LC3B-positive p62 puncta in response to clofibrate in the control (Fig. 5C). However, PAN3 KO cells exhibited a low level of p62 puncta under basal conditions that, unlike the control cells, did not change in response to clofibrate (Fig. 5C). Together, these data indicate that PAN3 is required for autophagic induction in response to peroxisomal damage.

Next, to determine the impact of PAN3 on peroxisome turnover, we used an established peroxisomal marker, peroxisomal membrane protein 70 (PMP70). Upon stress, PMP70 is ubiquitinated by peroxisomal E3 ubiquitin ligase PEX2 and promotes pexophagy, thus maintaining peroxisome quality(Sargent et al. 2016). Consistent with previous reports, we found that in control cells clofibrate caused a reduction in PMP70 indicating a reduction in peroxisomes(Zhang et al. 2015). Peroxisomal loss was prevented by autophagy inhibitor Baf treatment, suggesting that PAN3 regulation goes through autophagy (Fig. 5D). Interestingly, clofibrate-treated PAN3 KO cells exhibited elevated PMP70 levels compared to treated control, indicating a defect in pexophagy activation (Fig. 5D). As with HEK293 cells, PAN3 KD HCT116 cells (Fig. S7A) showed a blockage in pexophagy detected by PMP70 analysis, confirming that the role of PAN3 in pexophagy is not cell line specific (Fig. S7B).

Next, to confirm the role of PAN3 in PMP70 regulation, we examined peroxisome density in the untreated and treated control and KO cells through PMP70 staining. Consistent with previous observations, we found that PMP70 displayed a punctate staining pattern(Imanaka et al. 1999). Additionally, we observed a decrease in the PMP70 signal in the clofibrate-treated control cells (Fig. 5E). Importantly, in PAN3 KO cells we observed no loss of peroxisome density in response to clofibrate (Fig. 5E). Collectively, these experiments show that PAN3 is an activator of pexophagy, which is required for clearance of peroxisomes damaged by clofibrate.

To further investigate the role of PAN3 in pexophagy, we developed an HCT116 cell line with stable expression of a pexophagy reporter, consisting of the peroxisomal targeting sequence SKL and the fluorescent proteins RFP and GFP (RFP-GFP-SKL), as

previously described(Zheng et al. 2021). Like the KDEL ER-phagy reporter described above, this pexophagy reporter displays increased RFP puncta in microscopic analysis, and free RPF by WB, upon pexophagy induction. We depleted PAN3 in the reporter line via siRNA and confirmed knockdown through WB (Fig. S7A). As expected, in control pexophagy reporter cells treated with clofibrate we observed an increase processed probe by WB and IF, which was blocked by autophagy inhibitors (Figs. 5F, 5G). Conversely, PAN3 KD blocked pexophagy in response to clofibrate as measured by WB and IF (Figs. 5F, 5G). Additionally, we observed an induction of p62 puncta in response to clofibrate, which colocalized with our pexophagy probe in control, but not PAN3 KD reporter HCT116 cells (Fig. 5G).

We next examined whether PAN3-dependent regulation of pexophagy is specific to clofibrate or more broadly to other pexophagy inducers. Prolonged treatment of Torin1, an inhibitor of the mechanistic target of rapamycin (mTOR), has been described to stimulate pexophagy and reduce PMP70 levels(Zheng et al. 2021). Using our pexophagy reporter cells we treated with both clofibrate (1 mM, 6 hours) and Torin1 (200 nM, 24 hours) and observed an increase in RFP fragments detected by WB (Fig. S7C) and GFP-free RFP density examined by IF (Fig. S7D). This effect is lost in PAN3 KD cells (Figs. S7C and S7D). Together, these experiments nominate PAN3 as an important activator of pexophagy induced by multiple stress conditions.

Lastly, we asked whether PAN3 specifically regulates pexophagy or is involved in bulk autophagy. In addition to clofibrate treatment, we incubated the control and PAN3 KO cells with the acute starvation media protocol where pexophagy is not activated and PMP70 levels are not affected (Fig. 5H). We then investigated the changes in p62 levels.

While PAN3 KO cells exhibited a defect in clofibrate-stimulated pexophagy, they exhibited a normal induction of starvation-induced autophagy (Fig. 5H). Taken together, these data demonstrate that PAN3 is a selective activator of pexophagy.

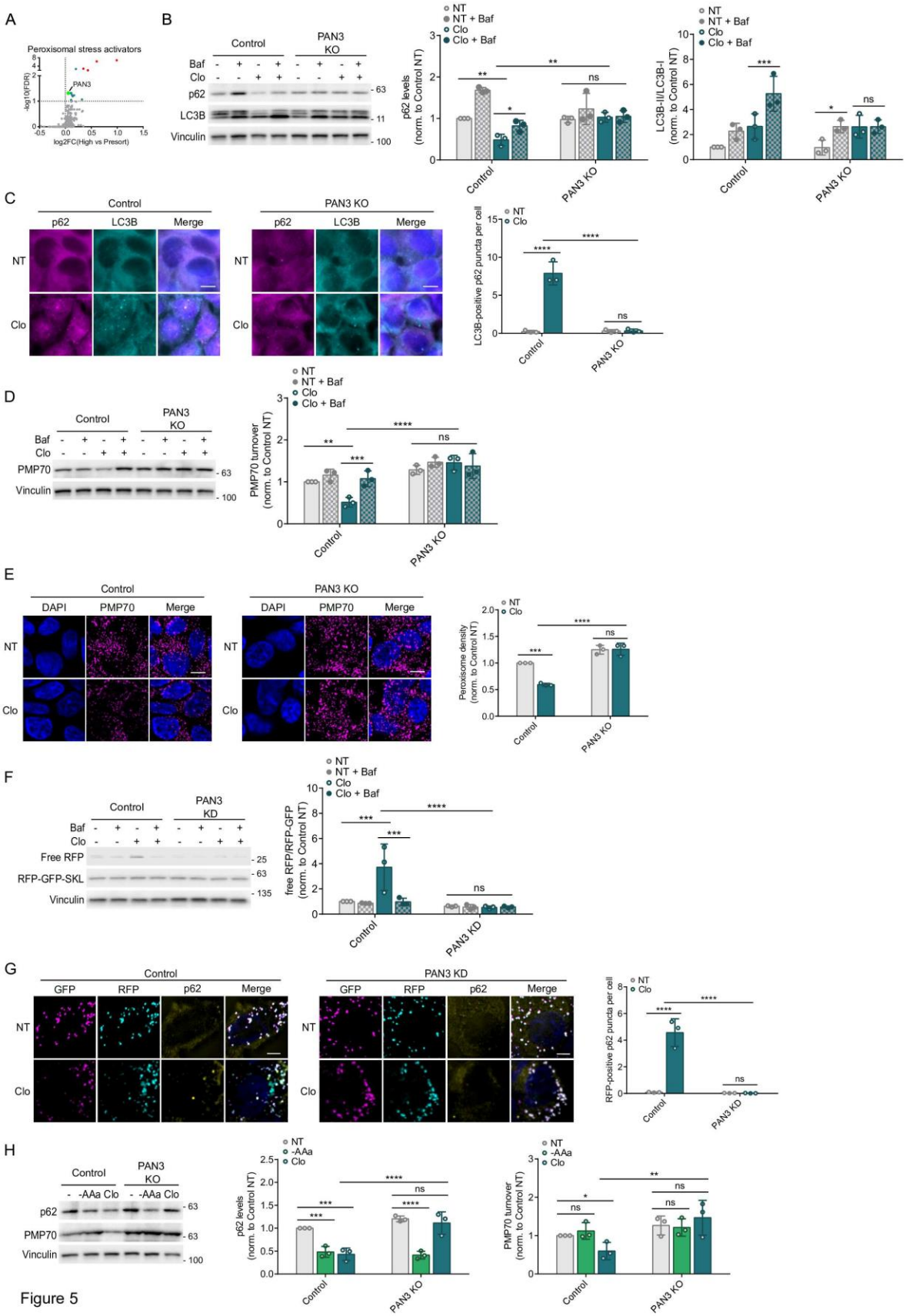
A
Peroxisomal stress activators
PAN3
-log10(FDR)
log2FC(High vs Presort)
B
Control
PAN3 KO
Baf
Clo
p62
LC3B
Vinculin
63
11
100
NT
NT + Baf
Clo
Clo + Baf
p62 levels (norm. to Control NT)
LC3B-II/LC3B-I (norm. to Control NT)
Control
PAN3 KO
C
p62
LC3B
Merge
NT
Clo
LC3B-positive p62 puncta per cell
D
PMP70
PMP70 turnover (norm. to Control NT)
E
DAPI
PMP70
Peroxisome density (norm. to Control NT)
F
PAN3 KD
Free RFP
RFP-GFP-SKL
25
135
free RFP/RFP-GFP (norm. to Control NT)
G
GFP
RFP
RFP-positive p62 puncta per cell
H
-AAa
p62 levels (norm. to Control NT)
PMP70 turnover (norm. to Control NT)

Figure 5

Figure 5: PAN3 activates pexophagy.

(A) PAN3 is represented as a prominent teal dot on the volcano plot. Red dots on the graph denote common regulators across all four conditions. (B) The control and PAN3 KO HEK293A cells were treated with clofibrate (1 mM) for 6 hours in the presence or absence of Baf. Changes in p62 and LC3B levels were analysed using western blot. (C) The control and KO cells were incubated with clofibrate (1 mM) for 6 hours. p62 and LC3B puncta were visualized and quantified by immunofluorescence. Scale bars, 10 μM. (D) The control and KO cells were treated with clofibrate in the presence or absence of Baf. Western blot was then used to examine pexophagy receptor, PMP70. (E) The indicated cells were incubated with clofibrate. PMP70 signal was visualized and quantified by immunofluorescence. Scale bars, 10 μM. (F) The control and PAN3 KD HCT116 cells stably expressing the RFP-GFP-SKL reporter were incubated with clofibrate (1 mM) for 6 hours in the presence or absence of Baf. Pexophagy was assessed through the processing of RFP-GFP-SKL. (G) The control and PAN3 KD cells expressing pexophagy reporter SKL were treated with clofibrate (1 mM) for 6 hours. GFP, RFP, and p62 signals were visualized and quantified by immunofluorescence. Scale bars, 5 μM. (H) The control and KO HEK293A cells were incubated with either acute amino acid starvation (1.5 hours, -AAa) or clofibrate (1 mM, 6 hours). Whole-cell lysates were immunoblotted using the antibodies indicated.

Unless otherwise indicated, experiments were performed three times. Data are represented as means ± SDs, and p values were determined by two-way ANOVA. *$p \leq 0.1$; **$p \leq 0.01$; ***$p \leq 0.001$; ****$p \leq 0.0001$; ns, not significant.

CDC42BPG is an inhibitor of pexophagy

CDC42-binding protein kinase gamma (CDC42BPG) is a serine/threonine protein kinase known to interact with the small GTPase CDC42 and is involved in cytoskeletal organization, cell division, and cell migration(Unbekandt and Olson 2014). To date CDC42BPG has not been linked to autophagy regulation or peroxisomes. Our kinome screen and subsequent analysis revealed involvement of CDC42BPG in the suppression of autophagy triggered by peroxisomal stress (Figs. 6A and S3B). Notably, CDC42BPG is the shared candidate inhibiting autophagy under basal condition, starvation, and peroxisomal stress. We decided to further validate CDC42BPG as it appears as a top novel hit displaying highly significant FDR and $\log_2$FC values and its depletion showed the most robust response upon clofibrate treatment (Fig. S3B). Treatment of CDC42BPG KO cells to clofibrate resulted in a reduction of p62 that was significantly higher than in the control cells. CDC42BPG-dependent changes in p62 stability were blocked in the presence of autophagy inhibitors, indicating CDC42BPG may inhibit autophagy induced by peroxisomal stress (Fig. 6B). Consistent with p62 clearance, we observed a more substantial increase in LC3B-II levels in the treated CDC42BPG cells compared to the treated control cells (Fig. 6B). Additionally, p62 levels were not significantly changed under basal conditions in control and CDC42BPG KO cells, suggesting that it is dispensable for basal autophagy (Fig. 6B). We further examined clofibrate-induced p62 and LC3B puncta formation by IF. In line with previous observations, we observed a more significant increase in LC3B-positive p62 puncta in the treated CDC42BPG compared to those of the treated control cells (Fig. 6C). Collectively, these data show that CDC42BPG plays a role in inhibiting clofibrate-induced autophagic flux.

Next, we investigated the effects of CDC42BPG on PMP70 protein levels. We observed a more pronounced downregulation in PMP70 levels in the clofibrate-treated CDC42BPG KO HEK293A cells and CDC42BPG KD HCT116 cells, compared to those of stressed control cells (Figs. 6D, S8B). Furthermore, reductions in PMP70 levels in the stressed CDC42BPG KO and KD cells were blocked in the presence of Baf, confirming that CDC42BPG regulates PMP70 through autophagy pathway (Figs. 6D, S8B). We next investigated stress-dependent changes in peroxisome density by IF in the control and KO cells through PMP70 staining. We observed a more robust stress-induced clearance of peroxisome staining in the CDC42BPG KO cells compared to stressed control cells (Fig. 6E). Collectively, these experiments demonstrate that CDC42BPG is a negative regulator of pexophagy.

We next depleted CDC42BPG in our pexophagy reporter line (Fig. S8A). Upon CDC42BPG KD we observed an increase in pexophagy in response to clofibrate, which was blocked with autophagy inhibitors (Fig. 6F). Consistently, CDC42BPG knockdown increased RFP-positive p62 puncta, indicative of pexophagy, in the treated cells (Fig. 6G).

To determine whether CDC42BPG-dependent pexophagy is limited to clofibrate induction, we treated CDC42BPG KD and control cells with prolonged Torin1 (200 nM, 24 hours). We observed CDC42BPG KD cells showed increased pexophagy in response to both clofibrate and Torin1 compared to control (Figs. S8C, S8D). These findings indicate that CDC42BPG is a negative regulator of pexophagy triggered by diverse stressors.

Lastly, we tested the specificity of CDC42BPG on pexophagy by exposing the control and KO cells with either amino acid-free media or clofibrate. As expected, we saw stress-induced p62 downregulations in the treated control cells (Fig. 6H). Starvation-

induced p62 degradation in CDC42BPG KO cells was higher than that in control cells (Fig. 6H). This was not unexpected as CDC42BPG also appeared as a negative regulator in the starvation condition. In summary, our findings suggest that CDC42BPG is capable of inhibiting autophagy, with its most robust inhibition impacting pexophagy.

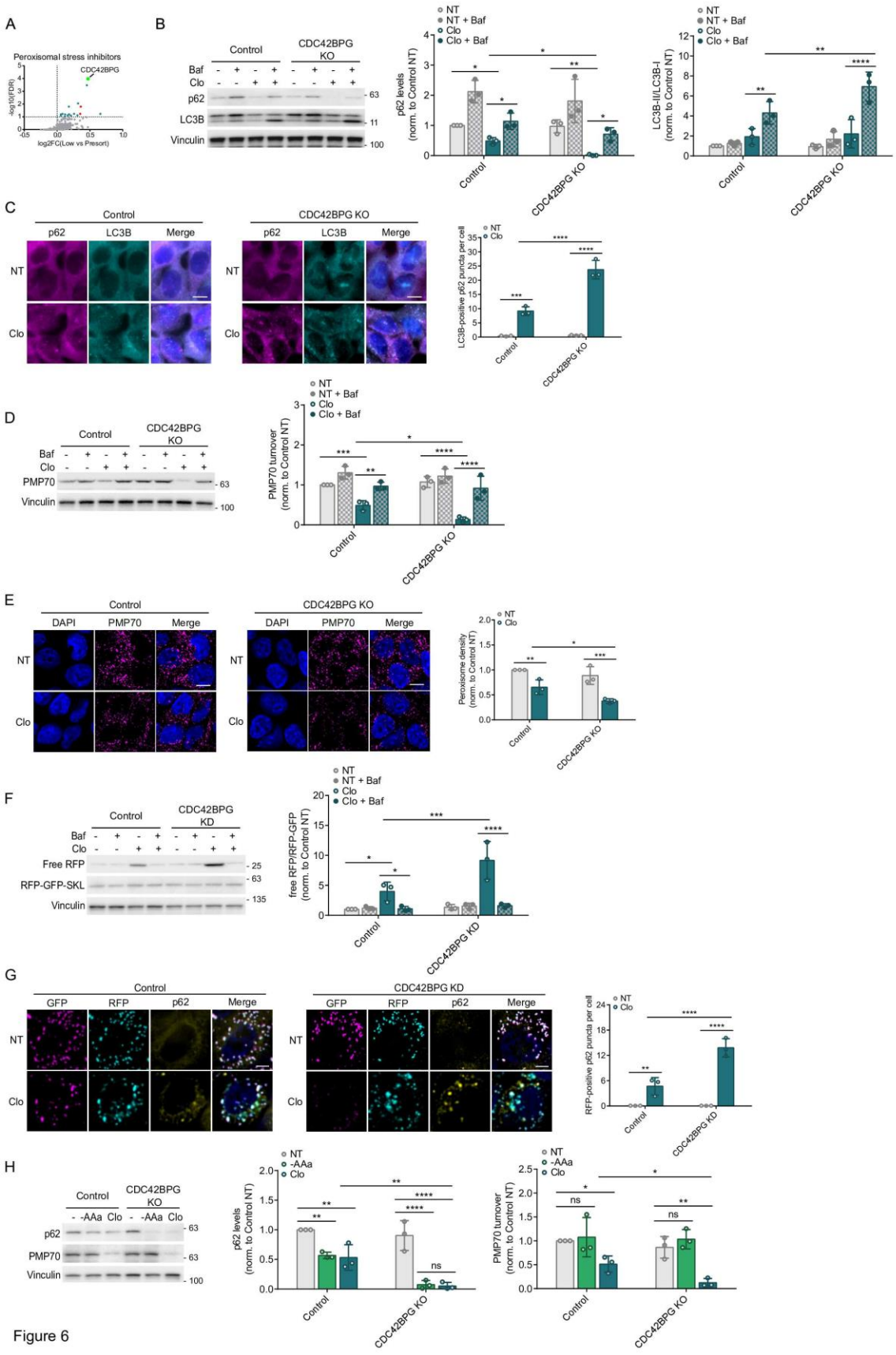
A
Peroxisomal stress inhibitors
CDC42BPG
-log10(FDR)
log2FC(Low vs Presort)
B
Control
CDC42BPG KO
Baf
Clo
p62
LC3B
Vinculin
63
11
100
NT
NT + Baf
Clo
Clo + Baf
p62 levels (norm. to Control NT)
LC3B-II/LC3B-I (norm. to Control NT)
Control
CDC42BPG KO
C
Control
CDC42BPG KO
p62
LC3B
Merge
NT
Clo
LC3B-positive p62 puncta per cell
D
PMP70
Vinculin
PMP70 turnover (norm. to Control NT)
E
DAPI
PMP70
Merge
Peroxisome density (norm. to Control NT)
F
CDC42BPG KD
Free RFP
RFP-GFP-SKL
25
63
135
free RFP/RFP-GFP (norm. to Control NT)
G
GFP
RFP
p62
Merge
RFP-positive p62 puncta per cell
H
-AAa
p62 levels (norm. to Control NT)
PMP70 turnover (norm. to Control NT)
ns

Figure 6

Figure 6: CDC42BPG inhibits pexophagy.

(A) CDC42BPG is represented as a prominent teal dot on the volcano plot. Red dots on the graph denote common regulators across all four conditions. (B) The control and CDC42BPG KO HEK293A cells were treated with clofibrate (1 mM) for 6 hours in the presence or absence of Baf. Changes in p62 and LC3B levels were analysed using western blot. (C) The control and KO cells were incubated with clofibrate (1 mM) for 6 hours. p62 and LC3B puncta were visualized and quantified by immunofluorescence. Scale bars, 10 μM. (D) The control and KO cells were treated with clofibrate in the presence or absence of Baf. Western blot was then used to examine pexophagy receptor, PMP70. (E) The indicated cells were incubated with clofibrate. PMP70 signal was visualized and quantified by immunofluorescence. Scale bars, 10 μM. (F) The control and CDC42BPG KD HCT116 cells stably expressing the RFP-GFP-SKL reporter were incubated with clofibrate (1 mM) for 6 hours in the presence or absence of Baf. Pexophagy was assessed through the processing of RFP-GFP-SKL. (G) The control and CDC42BPG KD cells expressing pexophagy reporter SKL were treated with clofibrate (1 mM) for 6 hours. GFP, RFP, and p62 signals were visualized and quantified by immunofluorescence. Scale bars, 5 μM. (H) The control and KO HEK293A cells were incubated with either acute amino acid starvation (1.5 hours, -AAa) or clofibrate (1 mM, 6 hours). Whole-cell lysates were immunoblotted using the antibodies indicated.

Unless otherwise indicated, experiments were performed three times. Data are represented as means ± SDs, and p values were determined by two-way ANOVA. *$p \leq 0.1$; **$p \leq 0.01$; ***$p \leq 0.001$; ****$p \leq 0.0001$; ns, not significant.

4.5 Discussion

In this study, we used a pooled CRISPR screening workflow to systematically identify both activators and inhibitors of autophagy under multiple conditions, including basal state, starvation, ER stress, and peroxisomal stress. Some of these regulators were common to selective and bulk autophagy and have been previously linked to autophagy. These include PIK3C3 (VPS34), PIKFYVE, PIK3R4 (VPS15), and ULK1. In addition, we identified shared autophagy inhibitors that are not currently described to supress autophagy including MAP4K2 and TKFC. TKFC is a member of the dihydroxyacetone kinase family, which is best described to phosphorylate glyceraldehyde to glyceraldehyde-3-phosphate(Rodrigues et al. 2014). It will be interesting to determine if the metabolic impacts of TKFC knockout are responsible for autophagy activation, or if the autophagy regulation is through an alternate function of TKFC. Notably, TKFC phosphorylation of glyceraldehyde is utilized in the metabolism of fructose, which is not present in our culture media, highlighting the possibility of an alternate mechanism of regulation(Rodrigues et al. 2014). Interestingly, MAP4K2 came up as an inhibitor in our screen, but has been described in one study as an autophagy activator(Seo et al. 2023). However, there were notable differences in the studies, which might explain the differences between our observations. For example, MAP4K2 activated autophagy under 20-hour glucose starvation, while we identified MAP4K2 as an autophagy inhibitor under 3-hour amino acid starvation. Chronological dissection of nutrient deprivation will help tease out its potential dual role in autophagy regulation. It will also be interesting to test whether MAPK4K2-linked inhibition is mediated by its kinase activity towards LC3, which may be functionally impacted by competing or proximal phosphorylation by PKA or

PKCλ(Cherra et al. 2010). These open questions raised from the hits described above indicate that further characterization of our hits for regulators of bulk autophagy may also provide insight into basal and starvation-induced autophagy. While not the focus of our screens, we identified: 25 potential novel regulators of starvation-induced autophagy, and 29 potential novel regulators of basal autophagy.

In response to ER stress our screen identified an enrichment of 25 kinases linked to autophagy activation and 17 with inhibition. To validate the specificity of these regulators we characterized CDK11A and NME3 as selective regulators of ER-phagy. Specifically, we found CDK11A was a selective activator of ER-phagy and not required for starvation-induced autophagy. CDK11 has established role in control of RNA splicing, transcription, and the cell cycle control. In humans, CDK11 is encoded by two highly identical genes, *CDC2L1* (also referred to as CDK11B) and *CDC2L2* (also known as CDK11A)(Zhou et al. 2016). Interestingly, dual siRNA-mediated knockdown of CDK11A and CDK11B has previously been linked to an acute activation of basal autophagy, followed by an inhibition of autophagy at a later time point(Wilkinson et al. 2011). However, the mechanism of regulation remains unknown. In our study, disruption of CDK11A was sufficient to significantly impair ER-phagy induction, without any detectible enrichment in basal or starvation conditions. However, it remains to be seen if a dual knockout of CDK11A and CDK11B would impact basal autophagy, or if the basal autophagy phenotype previously observed may involve a defect in ER homeostasis. CDK11A and CDK11B are activated in multiple cancer types and have been linked to acquisition of oncogenic properties, including proliferation. This newly described function

of CDK11A in ER-phagy begs the question of whether ER stress dysregulation may be integral to these oncogenic properties.

We found that NME3 is a selective repressor of ER-phagy. NME3 belongs to a more conserved group of nucleoside diphosphate kinase (NDPK) family, which regulates cellular nucleotide homeostasis and is associated with GTP-dependent cellular processes(Schlattner 2021). However, independent of its NDPK activity, NME3 has been described to regulate mitochondrial dynamics(Chen et al. 2019). Both NDPK and mitochondrial functions are important for cellular survival under glucose starvation(Chen et al. 2019). Moreover, it has been recently reported that NME3 is important for mitophagy induction(Chen et al. 2024). It will be interesting in future studies to determine whether NME3-mediated repression of ER-phagy is linked to its involvement in mitophagy and to elucidate the mechanisms by which NME3 performs conflicting roles in selective autophagy. An inactivating autosomal recessive mutation NME3 was found in a case study of rare consanguineous fatal neurodegenerative disorder(Chen et al. 2019). While homozygous inactivating mutations are lethal early in life, the impact of heterozygous inactivation of NME3 on ER-phagy and any potential physiological consequences is an interesting area for investigation.

In response to peroxisomal stress we identified an enrichment of 14 autophagy activators and 17 inhibitors. To validate the specificity of these regulators we chose to characterize the activator PAN3 and inhibitor CDC42BPG. PAN3 is a component of PAN2-PAN3 complex, which modulates mRNA stability or translational efficiency and has not been implicated in autophagy(Wolf et al. 2014). Additional work is required to determine if PAN3 regulates gene expression of pexophagy promoters, or whether its promotion of

peroxisomal autophagy is mediated by an alternate mechanism. CDC42BPG is a less well characterized member of the Myotonic dystrophy-related Cdc42-binding kinases (MRCK), which play an important role in actin-myosin regulation and other functions such as cell invasion, motility, and adhesion(Unbekandt and Olson 2014). While neither of these genes linked to disease, the mechanisms of peroxisomal disorders such as Zellweger's disease have not been fully elucidated and exhibit dysregulation of pexophagy. Therefore, it would be interesting to test the involvement of hits from our pexophagy screen, including these proteins in cases which do not have a reported Zellweger-associated PEX mutations.

Beyond detailed analysis of these top hits, our gene ontology analysis revealed candidates unique to ER stress that were significantly enriched in RhoJ and RhoG GTPase cycle pathways (Table S2). While Rho GTPases have been implicated in mitophagy regulation, their potential role in ER-phagy remains an open avenue for future research(Safiulina et al. 2019). In addition, analysis of candidates unique peroxisomal stress were enriched in TP53 expression and degradation pathways. The transcription factor TP53 has been shown to promote the expression of genes involved in peroxisomal fatty acid β-oxidation(Zhao et al. 2023). It will be interesting to determine whether this is an underlying mechanism through which the TP53 pathway could regulate pexophagy.

Our screen design offers several advantages. First, the employment of CRISPR/Cas9 system provides higher efficiency and lower off-target effects compare to traditional RNAi screens. Permanent gene perturbation provides more robust signals. The screen design allows cells to have more time to recover and have more optimal responses to stress conditions. Utilization of p62 reporter enables investigation of different selective

autophagy processes owing to its ability to bind diverse ubiquitinated substrates. Finally, fixation of samples prior to sorting allows for concurrent analysis of different stress-induced autophagy pathways. Although this screening approach has clear benefits, it also possesses limitations. This CRISPR/Cas9 system typically results in complete loss of function of genes, making it impractical for studying essential genes or partial loss of functions. Adaptations of RNAi or CRISPRi to this read-out can help complement these findings. Another limitation of this study is the choice of reporter. While p62 is linked to several types of selective autophagy, the relative clearance of total p62 under each condition may be different depending on cargo abundance and preference for other autophagy receptors. As such, the detection threshold was likely different among the conditions tested. Organelle-specific autophagy receptors would be ideal for sensitivity, with the trade-off of losing the ability to directly compare each stress condition.

Together, these screens have identified a heretofore underappreciated role for signal transduction pathways in the regulation of selective autophagic pathway. This resource thus provides a host of putative regulators, paving the way for tighter, selective control of different forms of autophagy and potential therapeutic inroads to target these pathways in clinically relevant scenarios.

4.6 Material and methods

Antibodies and reagents

Anti-ULK1 (Cat#6439S, 1:1000) antibody was obtained from Cell Signaling Technology. Anti-LC3B (Cat#PM036 for immunofluorescence, 1:2000) and anti-p62 (Cat#M162-3 for immunofluorescence, 1:400) antibodies were purchased from MBL. Anti-PMP70 (Cat#ab3421 for immunofluorescence, 1:1000) antibody was purchased from Abcam. Anti-beta-actin (Cat#A5441 clone AC-15, 1:30K), anti-vinculin (Cat#V9131, 1:30K), anti-PMP70 (Cat#SAB4200181 for WB, 1:1000) antibodies, and doxycycline hyclate (Cat#24390-14-5) were obtained from Sigma. Anti-p62 (Cat#sc-28359, 1:1000), anti-PAN3 (Cat#sc-376434, 1:500), and anti-CDC42BPG (Cat#sc-517148, 1:500) antibodies were obtained from Santa Cruz Biotechnology. Anti-FAM134B (Cat#21537-1-AP, 1:1000), anti-NME3 (Cat#15136-1-AP, 1:500), and anti-CHOP (Cat#15204-1-AP, 1:1000) antibodies was obtained from Proteintech Group. Anti-tRFP (Cat#AB233, 1:1000) was purchased from Evrogen. Anti-CDK11A (Cat#ARP61814_P050, 1:500) was obtained from Aviva Systems Biology. Anti-RFP (Cat# 600-401-379) was obtained from Cedarlane. Bafilomycin A1 (Cat#133410U) was purchased from Tocris. Torin1 (Cat#inh-tor1) was obtained from InvivoGen.

Cell culture and treatments

HEK293A and HCT116 cells were cultured in DMEM supplemented with 10% bovine calf serum (VWR Life Science Seradigm). Media was changed 24 h before experiments. Amino acid starvation media was prepared based on Gibco standard recipe omitting all amino acids and supplemented as above without addition of non-essential amino acids

and substitution with dialysed FBS (Invitrogen). A 1.5- to 3-hour, acute starvation, treatment was used to solely engage the starvation protocol, whereas a 6-hour starvation treatment was used to engage ER-phagy (prolonged AA starvation). Tunicamycin (10 μg/mL) or clofibrate (1 mM) was added to the cells for 6 hours as indicated. Bafilomycin A1 (200 nM) was introduced during the final 2 hours of incubation with tunicamycin or clofibrate. Torin1 (200 nM) was added to the cells for 24 hours. Doxycycline treatment of cells stably expressing ER-phagy probe was performed as previously described(Chino et al. 2019).

Virus generation and concentration

Lentiviral vectors (LentiCRISPRv2 or pCLIP-dual) and their corresponding packaging vectors (psPAX2 and pMD2G) were co-transfected into HEK293T cells in a 4:3:1 molar ratio, respectively. Media was changed 16 hr following transfection to low volume media (5 mL for a 10 cm dish). Media was collected at 48 hr following transfection, replaced with fresh media (5 mL), and collected again at 72 hr. Viral supernatant was filtered through a 0.45 μM polyethersulfone membrane (VWR). Cleared supernatants were concentrated using Virus Precipitation Kit (Benchmark Bioscience) to 1/100 of the original volume.

Generation of knock-out cell lines using CRISPR/Cas9

sgRNA pairs targeting genes of interest were selected from the transEDIT-dual CRISPR Whole Genome Arrayed Library (Transomic Technologies, Huntsville, AL). They were used in conjunction with a Cas9 expression vector containing neomycin (G418) resistance transcript (Addgene #98292). H293T cells were transfected with lentivirus packaging plasmids and plasmids carrying either sgRNAs or Cas9. The media was

collected 4 times throughout the course of 3 days and was filtered through a 0.45 μm syringe filter. Next, wild-type HEK293A cells were infected with both lentiviruses harboring the Cas9 and sgRNAs. The transduced cells were then selected with puromycin (1 μg/mL; 3 days) followed by G418 (1 mg/mL; 6 days). CDK11A sgRNA sequences (5'à3'): GATTGTGGTGGGCAGCAACA and GATCGATTTCCGAATTCCCG. NME3 sgRNA sequences: CCGCGGGGATTTCTGCATCG and CTTCGCTAACCTCTTCCCCG. PAN3 sgRNA sequences: GTCTCCAGTCTCTGACCAAG and CCGCCCGCGACGGCTCCCGG. CDC42BPG sgRNA sequences: CCATCGATGTGTTTGACGTG and TCGACTTGCGCTTGGCACCG.

Generation of stable cell lines

HEK293A cells were transduced with lentiviruses carrying DsRed-IRES-GFP-p62. These cells underwent G418 selection and were sorted into single cell populations. FACS was utilized to identify a monoclonal population expressing optimal GFP:DsRed ratio and responses to known autophagy stimuli. Knockout populations used for screen validation were generated by transducing parental HEK293A with sgRNAs targeting potential hits and Cas9. These cells were subjected to puromycin and G418 selection. HCT116 cells were infected with lentiviruses containing either ss-RFP-GFP-KDEL to monitor ER-phagy or RFP-GFP-SKL to track pexophagy, as described previously(Chino et al. 2019; Zheng et al. 2021).

Flow cytometry

Following defined treatments, cells were fixed with 2% paraformaldehyde (PFA) for 10 min and incubated with Tris (pH 8, direct addition to 2% PFA to create a final concentration

of 1 M) for 15 min at room temperature. Media were removed. The cells were then harvested using scrapers, resuspended in ice-cold flow buffer (1% BSA and 2 mM EDTA in PBS), and filtered using cell strainers (70 μM, Falcon). The fixed samples were analysed using a BD FACSCelesta flow cytometer. For sorting, the cells were subjected to FACS on a Sony SH800S cell sorter.

Pooled kinome-wide CRISPR/Cas9 screens

Cell culture

The 293A cells expressing the DsRed_IRES-GFP-p62 transgene were plated at approximately 7.5 million cells on 15-cm plates. Next day, these cells were transduced with lentiviruses carrying human kinome CRISPR knockout pooled library at Multiplicity of Infection of 0.3 (13 million cells were infected with 3.86 million Transduction Units to achieve approximately 1000-fold representation of each sgRNA) in the presence of 10 mg/ml polybrene. The library was purchased from Addgene (Cat#1000000083) and amplified using the protocol provided by Addgene. The transduced cells were then selected with puromycin (1 μg/mL) for 3 consecutive days and cultured for an additional 11 days to allow for effective target knockout(Shalem et al. 2014). We found that day 16 was the earliest for achieving an optimal autophagic response following knockout and recovery from selection. Thus, on day 16, the cells were treated with the stress conditions described above and fixed with 2% PFA for 10 min at room temperature, followed by 15 min incubation with Tris (pH 8, direct addition to 2% PFA to create a final concentration of 1 M). Following aspiration of media, the cells were collected using scrapers, stored in ice-cold flow buffer (1% BSA and 2 mM EDTA in PBS), and filtered using cell strainers (70

μM, Falcon). The samples were then sorted into high and low GFP populations. These populations were then pelleted by centrifugation (4000 rpm for 10 min at 4^0C) and stored at -80C freezer for downstream analysis. The screens were carried out in biological replicates, under identical conditions, on four different occasions. Sample processing (below) was performed on all samples at the same time to avoid batch effects.

Genomic DNA extraction, PCR amplification, and next generation sequencing

Frozen cell pellets were thawed at room temperature. Genomic DNA of the sorted and unsorted fixed cells were then extracted using the protocol described previously(Chen et al. 2015). The sgRNA library was amplified by a two-step PCR protocol for NGS(Doench et al. 2016; Kim et al. 2023). One cell consists of approximately 6 pg of DNA and the lowest representation calculated from all samples is 224x(Bäumer et al. 2018). All gDNA of sorted samples were used to maximize the representations. For the unsorted/bulk samples, 22890 ng of gDNA, which is relevant to 1250 x representation, was used for PCR1. The entire gDNA was amplified using the following primers (NGS-1st PCR Fwd: 5'-TCGTCGGCAGCGTCAGATGTGTATAAGAGACAGgactatcatatgcttaccgt-3' and NGS-1st PCR Rev: 5'-GTCTCGTGGGCTCGGAGATGTGTATAAGAGACAGgagccaattcccactccttt-3'). Each 100 μL PCR1 reaction contains 50 μL of 2xQ5 Master Mix (New England Biolabs, M0494L), 0.2 μL of $MgCl_2$ (stock concentration at 1M), 0.5 μL of each primer (stock at 100 μM), DNA, and water. PCR1 conditions: an initial 5 minutes at 98°C; followed by 35 seconds at 98°C, 30 seconds at 60°C, 45 seconds at 72°C, for 24 cycles; and a final 10 minute extension at 72°C. PCR products from multiple first PCR reactions were pooled and 200 μL was cleaned up for the second step PCR using Nextera XT Index Kit (Lot#10089169).

The barcodes used are combinations of N701-712, and S502-508,517. Each 50 µL PCR2 reaction contains 25 µL of 2xQ5 Master Mix (New England Biolabs, M0494L), 5 µL of each index primer (N7xx or S5xx), 62.5 ng of PCR1 product, and water. PCR2 conditions: an initial 5 minutes at 98°C; followed by 35 seconds at 98°C, 30 seconds at 58°C, 45 seconds at 72°C, for 6 cycles; and a final 10 minute extension at 72°C. PCR1 and PCR2 products were purified using AMPure XP Bead-Based Reagent (Beckman Coulter, A63881) according to manufacturer's instructions.

The samples were sent to OHRI StemCore Laboratories for next generation sequencing where Qubit HS DNA assay was used to measure concentration and Fragment analyzer HS NGS assay (Agilent) was used to assess library fragment size. Sequencing was performed on a NextSeq500 at 150 Cycles High Output 400 million of single-end reads using a 30% PhiX spike-in to control for sequence clustering and diversity. CRISPRCloud2 site was employed to analyse files received from the DNA core. The Enrichment-based screen option was selected. All FASTQ files were uploaded concurrently and assigned to the corresponding groups. After providing all the necessary information, the web browser would initiate the processes of trimming, mapping, and quantifying the sgRNA reads. The processed data were accessed through the link provided.

siRNA transfection

Dharmacon siGENOME non-targeting control siRNA and SMARTpool siRNAs targeting human CDK11A, NME3, PAN3, and CDC42BPG were reverse transfected into reporter

HCT116 cells. Cells were lysed or fixed after 48-72hrs. Lipofectamine RNAiMAX transfection reagent was used for all knockdown experiments.

Western blot

Whole-cell lysates were prepared by direct lysis with 1× SDS sample buffer. Samples were boiled for 10 min at 95°C and resolved by SDS–PAGE. Briefly, samples were spun down and run on a 6-18% polyacrylamide gel, transferred to a PVDF membrane, and blocked for 15 min with 5 % non-fat milk prior to overnight primary antibody incubation.

Statistical analysis

Statistical analysis was performed on three biological repeats. Error bars represent the standard deviation in fold changes in observed induction or repression. Statistical analyses were performed using GraphPad Prism 6. Statistical significance was determined using two-way ANOVA. Differences with a p value <0.1 or lower were considered significant. *$p \leq 0.1$; **$p \leq 0.01$; ***$p \leq 0.001$; ****$p \leq 0.0001$; ns, not significant. All statistical parameters for assays in this study are shown in the corresponding figure legends.

Immunofluorescence

Cells were plated on coverslips 48 hours prior to treatments. After treatments, cells were fixed by 4% PFA in PBS for 15 min at room temperature, followed by permeabilization with 50 µg/mL digitonin (VWR) in PBS for 10 min at room temperature. Cells were blocked in blocking buffer (1% BSA and 2% serum in PBS) for 30 min, then incubated with primary antibodies in the same buffer for 1 h at room temperature. Slides were then washed 2×

in PBS and 1× in blocking buffer before incubation with secondary antibodies 1 h at room temperature. Samples were washed 3× in PBS, stained with DAPI (Sigma-Aldrich), and mounted. Images were captured with inverted epifluorescent Zeiss AxioObserver 7 equipped with a 63x, 1.4NA, Oil, Plan-Apochromat objective using Zen 3.0 Pro software at room temperature. Excitation wavelengths used were 405, 488, 561, and/or 647 nm. This system is located at the Cell Biology and Image Acquisition (CBIA) Core Facility, University of Ottawa, Canada.

Quantification of immunofluorescence

A protocol built in the ImageJ software was used to analyse epifluorescent microscopy images to avoid bias. Briefly, channels were first split to examine either number of cells or puncta of interest. The images were changed to 8-bit and set as binary default. Thresholds were then adjusted to identity nuclei or puncta. Finally, particles were analysed and a table summarizing puncta/nuclei quantity and size were provided. The same protocol was applied to each field of view and across samples. For the quantification of peroxisome density, the area of peroxisomal structures and the area of cells were quantified. The density of peroxisomes was calculated by dividing the total peroxisome area by the total area of cells. For the free RFP density quantification, a ROI (region of interest) was generated to identify free RFP area. The density of free RFP signals was calculated by dividing the total free RFP area by the total area of cells. Quantification was performed on representative experiments with an average of 9 fields of view per replicate.

Accession Number

Sequencing data have been deposited in the NCBI Gene Expression Omnibus under accession number GSE292757.

Online supplemental material

Fig. S1 shows that stress-induced effects on p62 regulation in the DsRed-IRES-GFP-p62 reporter line is through autophagy pathway. Fig. S2 displays the validation of potential ER-phagy activators and inhibitors using WB approach. Fig. S3 presents the validation of potential pexophagy activators and inhibitors through WB approach. Fig. S4 shows knockout efficiency of the control ULK1, ER-phagy hits, and pexophagy hits. Fig. S5 provides further characterization of CDK11A role in ER-phagy regulation using ss-RFP-GFP-KDEL system. Fig. S6 demonstrates the importance of NME3 as an ER-phagy inhibitors using ss-RFP-GFP-KDEL system. Fig. S7 validates the function of PAN3 in pexophagy regulation through RFP-GFP-SKL system. Fig. S8 confirms the role of CDC42BPG as a pexophagy inhibitor using RFP-GFP-SKL system. Table 1 shows potential autophagy activators and inhibitors from four conditions that satisfy log2FC and FDR cutoffs. Table S1 provides sgRNA enrichment and depletion for each stress condition using CRISPRBetaBinomial. Table S2 lists the results of a PANTHER gene ontology analysis of total and unique screen candidates across the 4 examined conditions. The top 5 enriched Reactome Pathways with corresponding number of hits, fold enrichment, and p-values are listed.

4.7 Acknowledgements

The authors acknowledge the support from CIHR grants #153034 (R.C.R) and PJT-169097 (M.W.C.R.) as well as Natural Sciences and Engineering Research Council of Canada #2023-05587 (R.C.R) and RGPIN-2019-04133 and DGECR-2019-00369 (M.W.C.R.) and 201911CGV-434032-74238 (T.L.). Natural Sciences and Engineering Research Council Postgraduate Scholarship supported K.E.K. The authors also thank the following Core facilities from the University of Ottawa and the Ottawa Hospital Research Institute (OHRI) for use of their facility, equipment, and expertise: the Cell Biology and Imaging Acquisition Core (RRID:SCR_021845), the Flow Cytometry and Virometry Core (RRID:SCR_023306), the Genome Engineering and Molecular Biology Core (RRID:SCR_022954) and the OHRI StemCore Laboratories (RRID:SCR_012601). We would also like to acknowledge Peter Kim (University of Toronto) for experimental advice on the assessment of pexophagy.

4.8 Supplementary Information

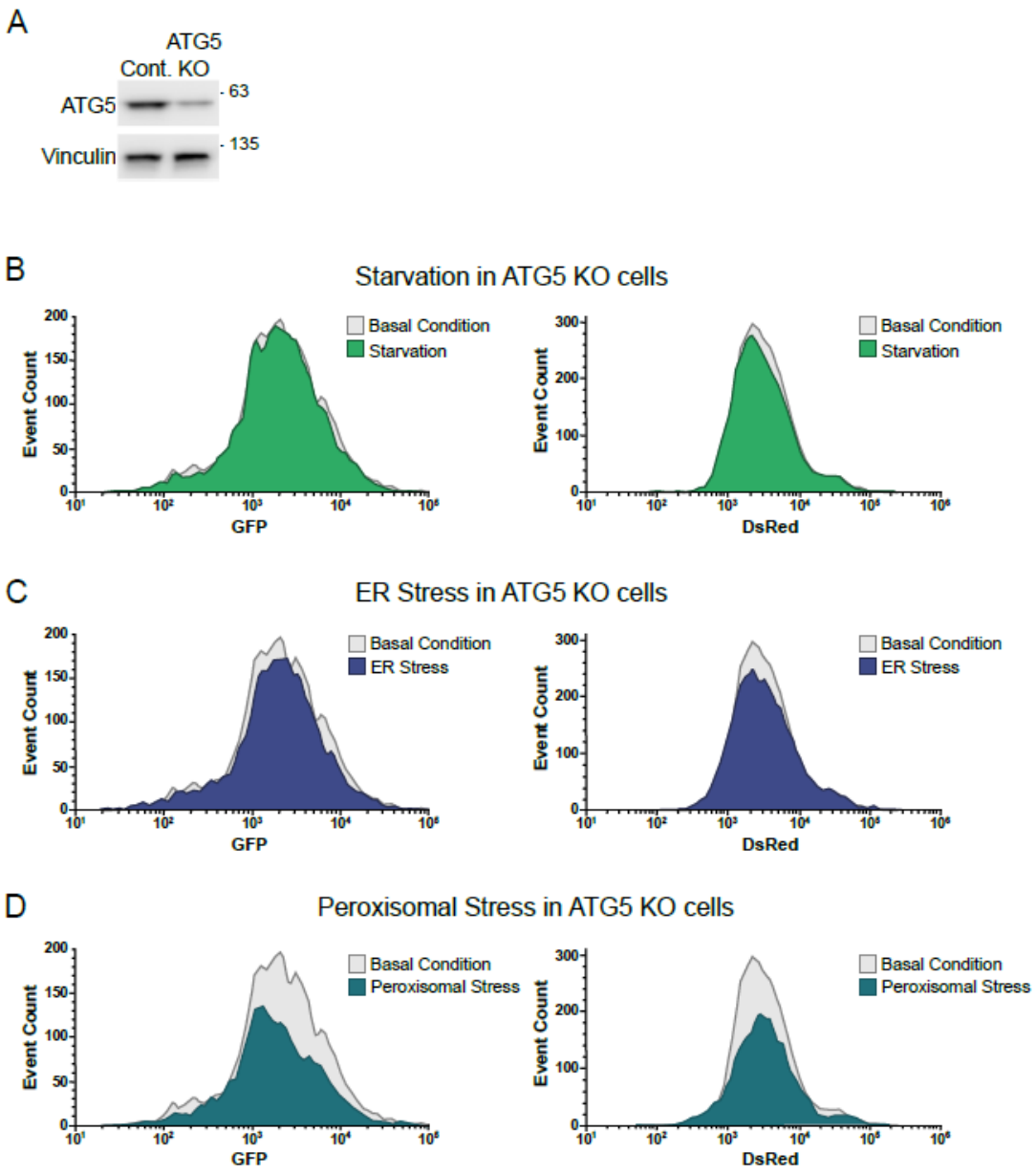

Figure S1

Figure S1: Analysis of autophagy flux in ATG5 KO cells.

(A) ATG5 knockout efficiency was examined by WB. (B), (C), (D) The HEK239A reporter cells were transduced with viruses carrying sgRNA targeting ATG5. These cells were then treated with amino acid-free media for 3 hours (B), tunicamycin (10 μg/mL) for 6 hours (C), or clofibrate (1 mM) for 6 hours (D). Next, they were examined using FACS. Histogram overlays compare either GFP or DsRed signals of the treated ATG5 KO reporter cells with those signals of the untreated ATG5 KO ones.

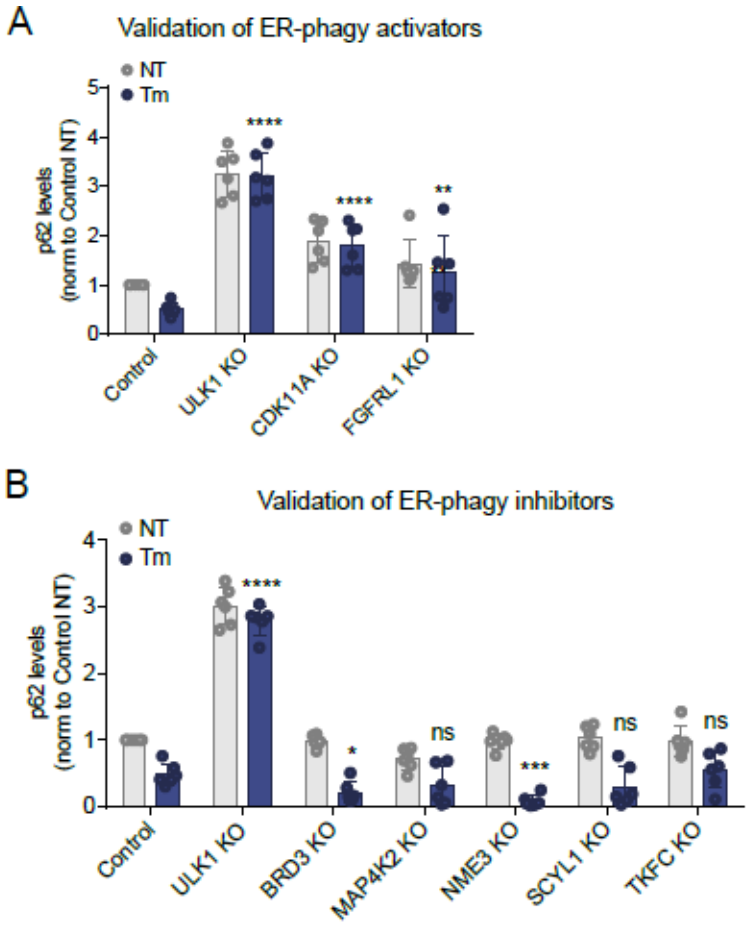
A
Validation of ER-phagy activators
NT
Tm
p62 levels
(norm to Control NT)
0
1
2
3
4
5
****
****
**
Control
ULK1 KO
CDK11A KO
FGFRL1 KO
B
Validation of ER-phagy inhibitors
NT
Tm
p62 levels
(norm to Control NT)
0
1
2
3
4
****
*
ns
***
ns
ns
Control
ULK1 KO
BRD3 KO
MAP4K2 KO
NME3 KO
SCYL1 KO
TKFC KO

Figure S2

Figure S2: Validation of candidates associated with ER stress-induced autophagy.

(A), (B) Wild-type HEK293A cells were infected with both lentiviruses harboring both Cas9 and sgRNA targeting indicated positive (A) or negative (B) regulators. Polyclonal KO cells were then incubated with tunicamycin (10 μg/mL) for 6 hours. Autophagy flux was examined through blots of p62. Experiments were repeated 6 times. p values denote statistical significance of treated KO cells compared to treated control cells and were determined by two-way ANOVA. *$p \leq 0.1$; **$p \leq 0.01$; ***$p \leq 0.001$; ****$p \leq 0.0001$; ns, not significant.

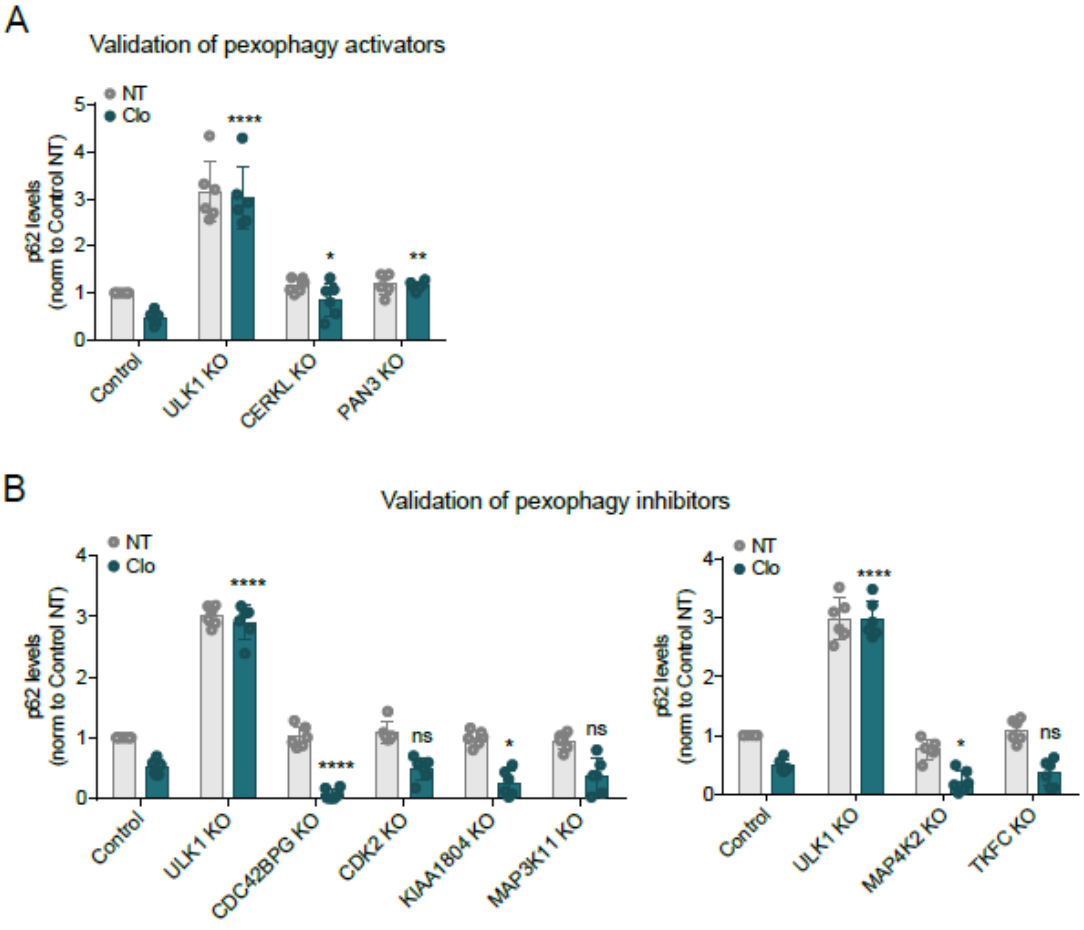
A
Validation of pexophagy activators
NT
Clo
p62 levels
(norm to Control NT)
****
*
**
Control
ULK1 KO
CERKL KO
PAN3 KO
B
Validation of pexophagy inhibitors
NT
Clo
p62 levels
(norm to Control NT)
****
****
ns
*
ns
Control
ULK1 KO
CDC42BPG KO
CDK2 KO
KIAA1804 KO
MAP3K11 KO
NT
Clo
p62 levels
(norm to Control NT)
****
*
ns
Control
ULK1 KO
MAP4K2 KO
TKFC KO

Figure S3

Figure S3: Validation of candidates associated with peroxisomal stress-induced autophagy.

(A), (B) Wild-type HEK293A cells were infected with both lentiviruses harboring both Cas9 and sgRNA targeting indicated positive (A) or negative (B) regulators. Polyclonal KO cells were then incubated with clofibrate (1 mM) for 6 hours. Autophagy flux was examined through blots of p62. Experiments were repeated 6 times. p values denote statistical significance of treated KO cells compared to treated control cells and were determined by two-way ANOVA. *$p \leq 0.1$; **$p \leq 0.01$; ***$p \leq 0.001$; ****$p \leq 0.0001$; ns, not significant.

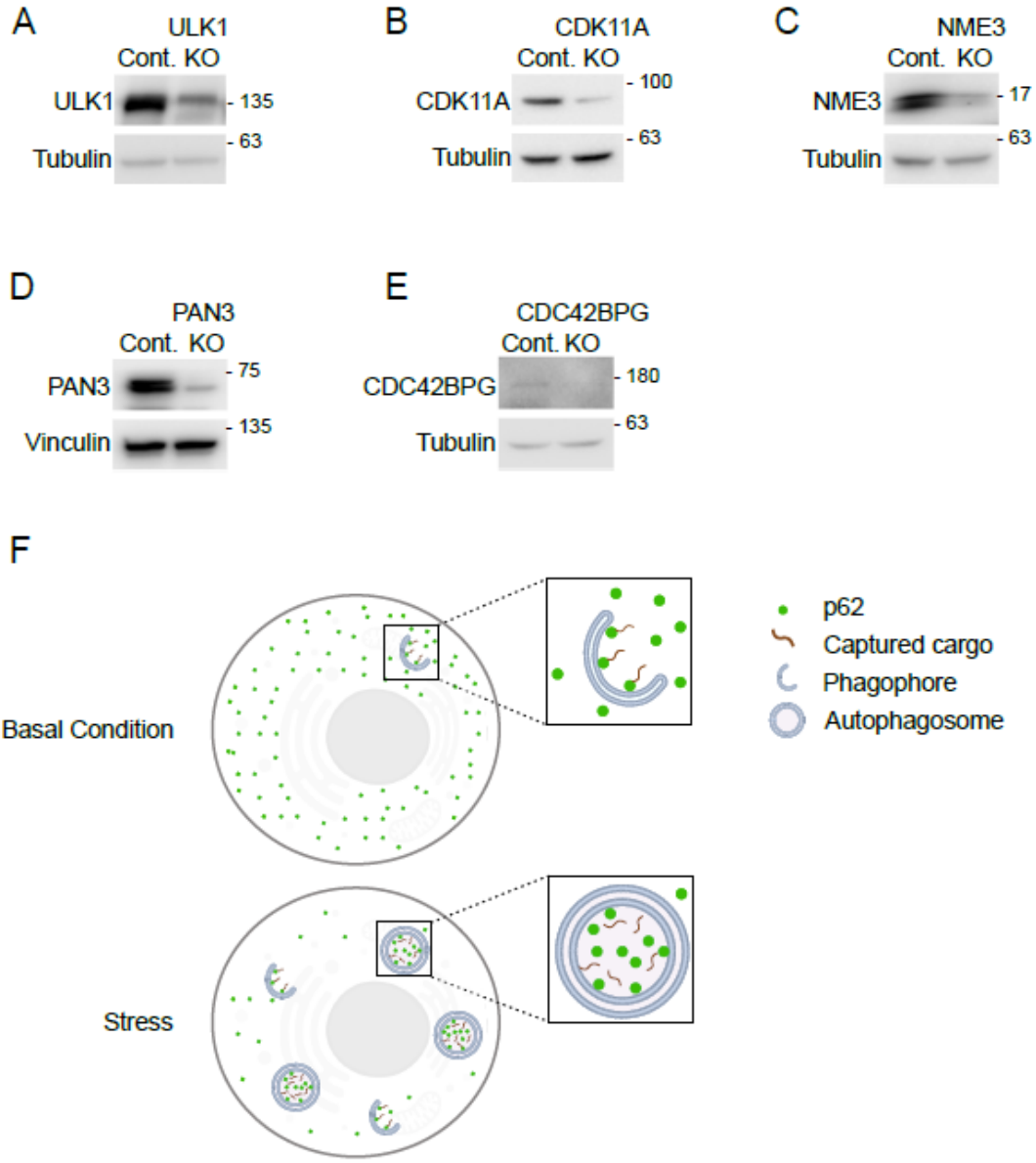

	WB/FACS	IF
Basal Condition	High total p62 levels (mostly cytoplasmic)	Low number of p62 puncta (cytoplasmic p62 below detection threshold)
Stress	Low total p62 levels (increased autophagic degradation)	High number of p62 puncta (autophagosome-sequestered p62 above detection threshold)

Figure S4

Figure S4: Depletion efficiency of KO cells.

(A), (B), (C), (D), (E). Whole-cell lysates of polyclonal KO cells were immunoblotted for the levels of depleted proteins using the antibodies indicated. (F) A diagram and table illustrating p62 patterns detected through WB, IF, or FACS approaches.

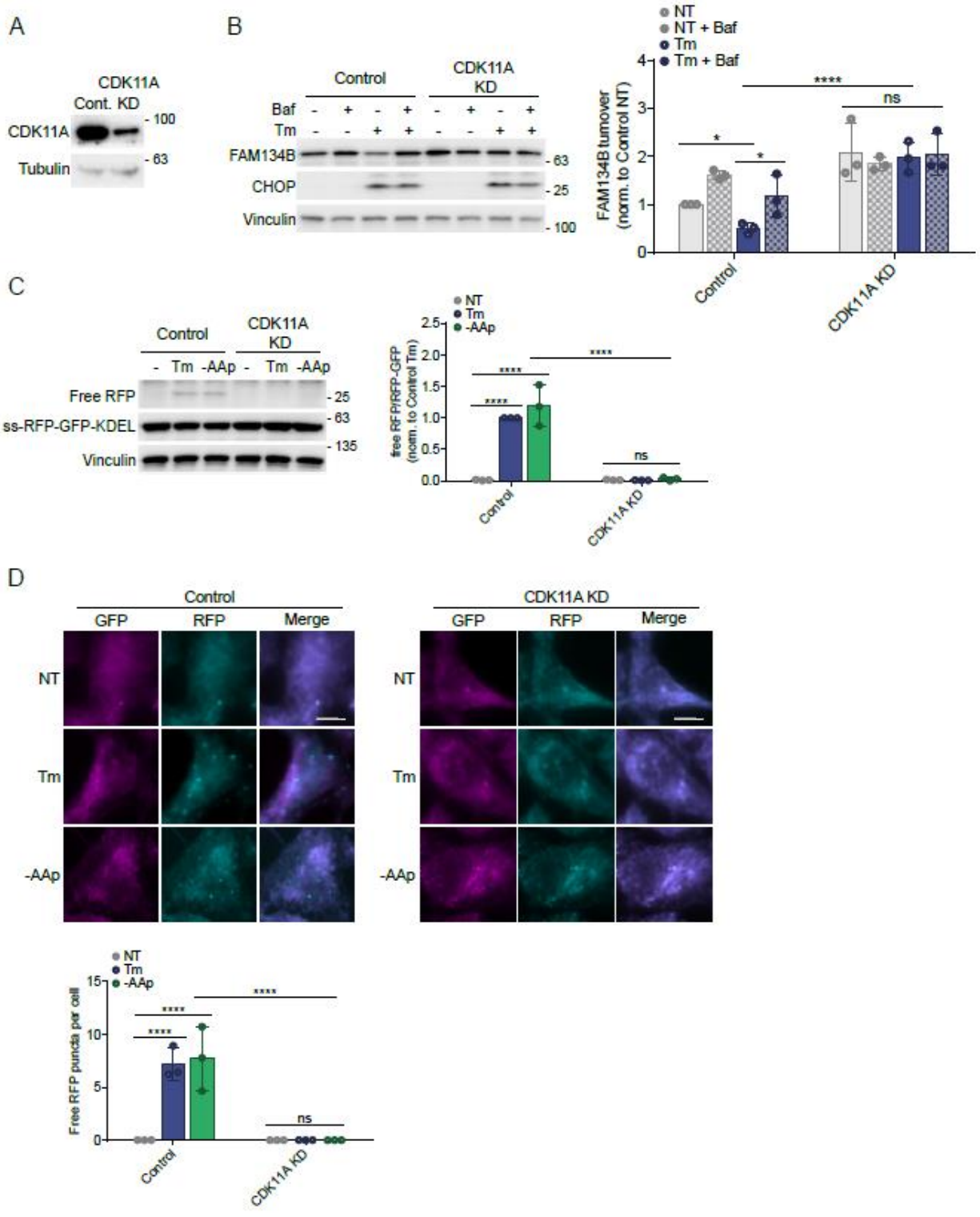
A
CDK11A
Cont. KD
CDK11A
Tubulin
100
63
B
Control
CDK11A KD
Baf
Tm
FAM134B
CHOP
Vinculin
63
25
100
NT
NT + Baf
Tm
Tm + Baf
FAM134B turnover (norm. to Control NT)
****
ns
*
*
Control
CDK11A KD
C
Control
CDK11A KD
- Tm -AAp - Tm -AAp
Free RFP
ss-RFP-GFP-KDEL
Vinculin
25
63
135
NT
Tm
-AAp
free RFP/RFP-GFP (norm. to Control Tm)
****
****
****
ns
Control
CDK11A KD
D
Control
CDK11A KD
GFP
RFP
Merge
NT
Tm
-AAp
NT
Tm
-AAp
Free RFP puncta per cell
****
****
****
ns
Control
CDK11A KD

Figure S5

Figure S5: Validation of CDK11A role in ER-phagy regulation using ss-RFP-GFP-KDEL approach.

(A) CDK11A knockdown efficiency was examined by WB. (B) The control and CDK11A KD HCT116 cells stably expressing the ss-RFP-GFP-KDEL reporter were incubated with tunicamycin (10 μg/mL) for 6 hours in the presence or absence of Baf. FAM134B levels were then examined using western blot. (C), (D) The control and KD ER-phagy reporter cells were incubated with tunicamycin (10 μg/mL) or prolonged amino acid starvation (-AAp) for 6 hours. The processing of ss-RFP-GFP-KDEL was analyzed by western blot (C) or visualized by immunofluorescence (D). Scale bars, 10 μM.

Unless otherwise indicated, experiments were performed three times. Data are represented as means ± SDs, and p values were determined by two-way ANOVA. *p ≤ 0.1; **p ≤ 0.01; ***p ≤ 0.001; ****p ≤ 0.0001; ns, not significant.

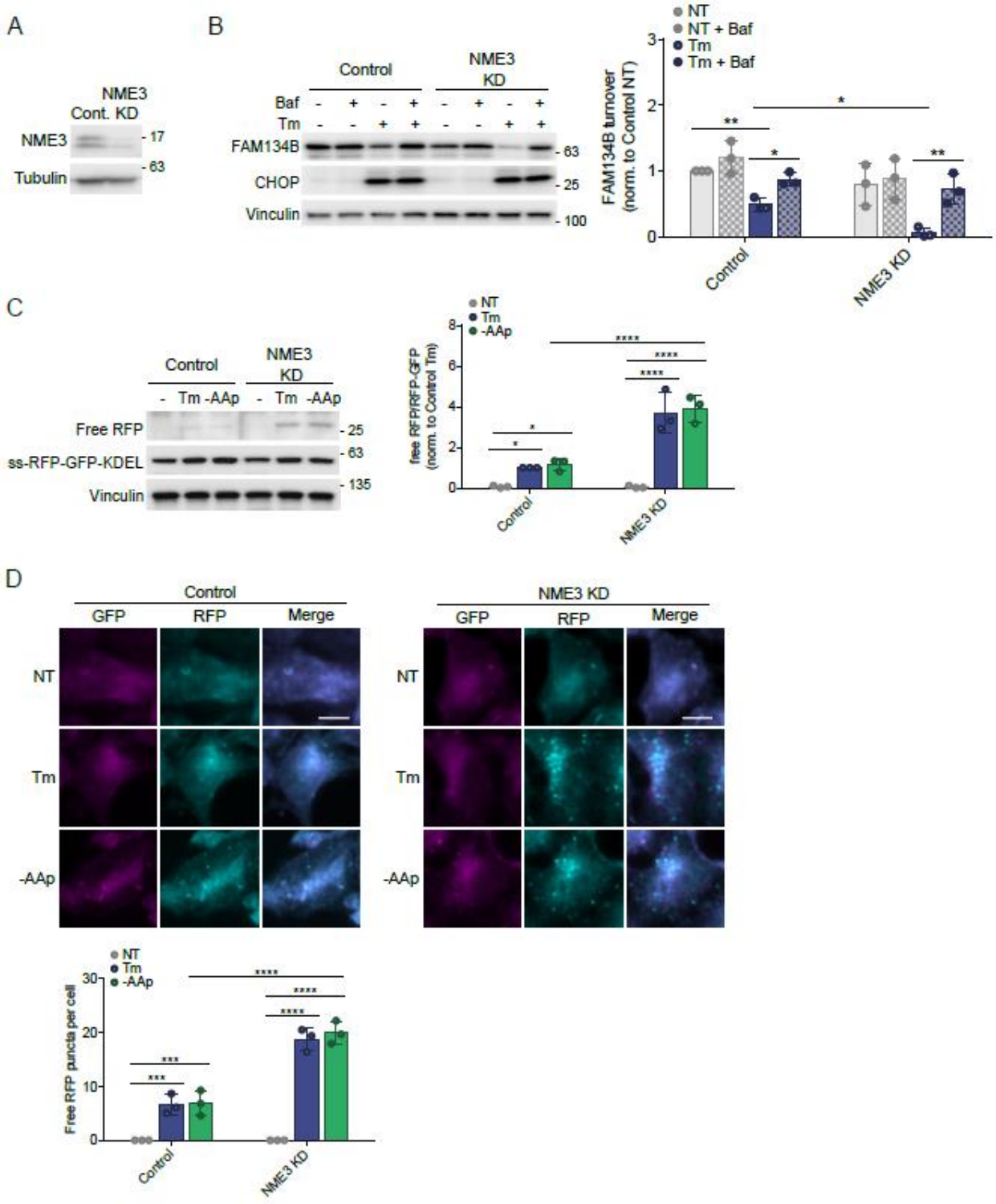
A
NME3
Cont. KD
NME3
17
Tubulin
63
B
Control
NME3 KD
Baf
Tm
FAM134B
63
CHOP
25
Vinculin
100
NT
NT + Baf
Tm
Tm + Baf
FAM134B turnover (norm. to Control NT)
Control
NME3 KD
C
Control
NME3 KD
- Tm -AAp - Tm -AAp
Free RFP
25
ss-RFP-GFP-KDEL
63
Vinculin
135
NT
Tm
-AAp
free RFP/RFP-GFP (norm. to Control Tm)
Control
NME3 KD
D
Control
NME3 KD
GFP
RFP
Merge
NT
Tm
-AAp
Free RFP puncta per cell
Control
NME3 KD

Figure S6

Figure S6: Validation of NME3 role in ER-phagy regulation using ss-RFP-GFP-KDEL approach.

(A) NME3 knockdown efficiency was examined by WB. (B) The control and NME3 KD HCT116 cells stably expressing the ss-RFP-GFP-KDEL reporter were incubated with tunicamycin (10 μg/mL) for 6 hours in the presence or absence of Baf. FAM134B levels were then examined using western blot. (C), (D) The control and KD ER-phagy reporter cells were incubated with tunicamycin (10 μg/mL) or prolonged amino acid starvation (-AAp) for 6 hours. The processing of ss-RFP-GFP-KDEL was analyzed by western blot (C) or visualized by immunofluorescence (D). Scale bars, 10 μM.

Unless otherwise indicated, experiments were performed three times. Data are represented as means ± SDs, and p values were determined by two-way ANOVA. *p ≤ 0.1; **p ≤ 0.01; ***p ≤ 0.001; ****p ≤ 0.0001; ns, not significant.

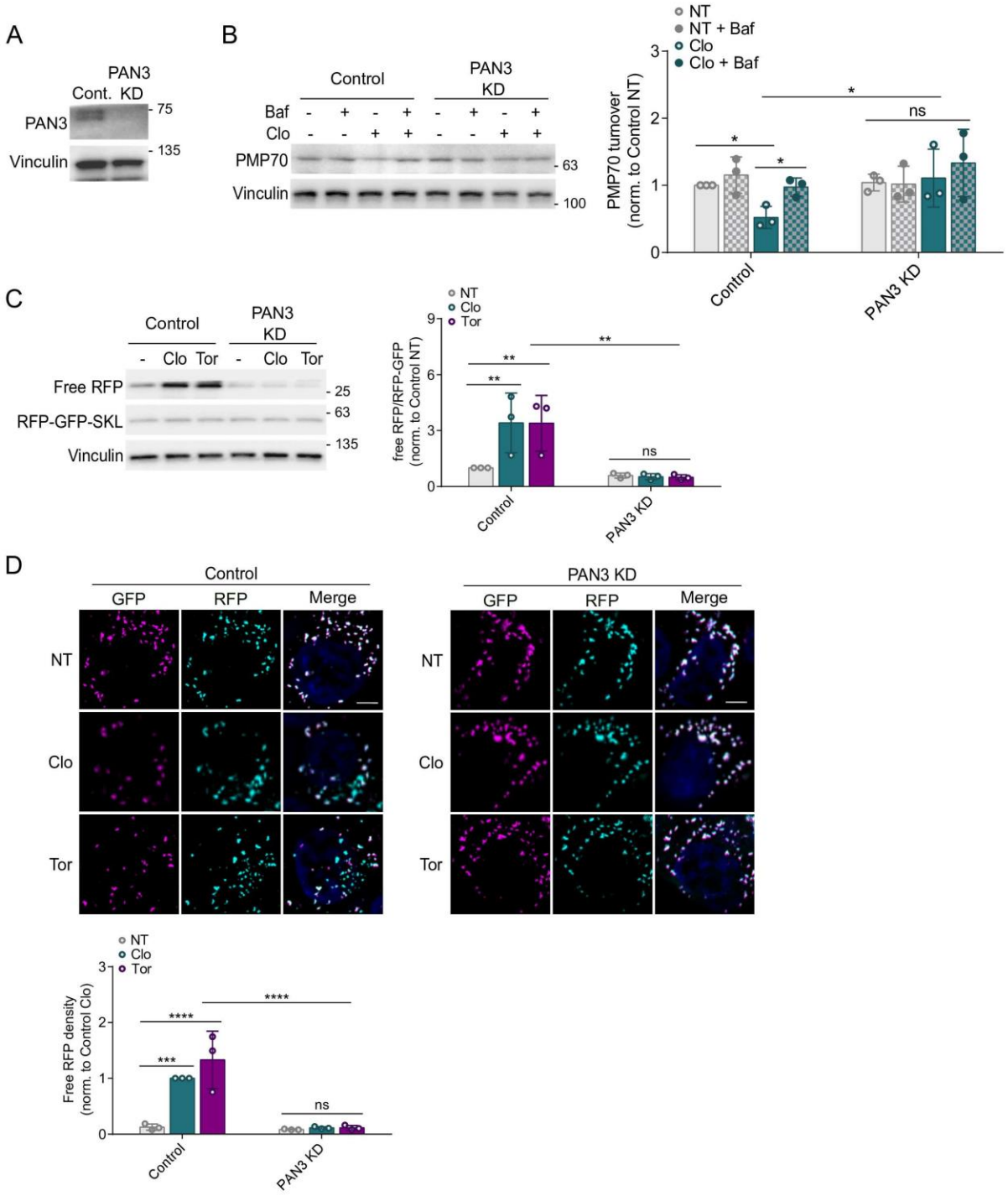
A
PAN3
Cont. KD
PAN3
Vinculin
75
135
B
Control
PAN3 KD
Baf
Clo
PMP70
Vinculin
63
100
NT
NT + Baf
Clo
Clo + Baf
PMP70 turnover (norm. to Control NT)
ns
Control
PAN3 KD
C
Control
PAN3 KD
Free RFP
RFP-GFP-SKL
Vinculin
25
63
135
NT
Clo
Tor
free RFP/RFP-GFP (norm. to Control NT)
ns
Control
PAN3 KD
D
Control
PAN3 KD
GFP
RFP
Merge
NT
Clo
Tor
Free RFP density (norm. to Control Clo)
ns
Control
PAN3 KD

Figure S7

Figure S7: Validation of PAN3 role in pexophagy regulation using RFP-GFP-SKL approach.

(A) PAN3 knockdown efficiency was examined by WB. (B) The control and PAN3 KD HCT116 cells stably expressing the RFP-GFP-SKL reporter were incubated with clofibrate (1 mM) for 6 hours in the presence or absence of Baf. PMP70 levels were then examined using western blot. (C), (D) The control and KD pexophagy reporter cells were incubated with clofibrate (1 mM, 6 hours) or Torin1 (Tor, 200 nM, 24 hours). The processing of RFP-GFP-SKL was analyzed by western blot (C) or visualized by immunofluorescence (D). Scale bars, 5 μM.

Unless otherwise indicated, experiments were performed three times. Data are represented as means ± SDs, and p values were determined by two-way ANOVA. *p ≤ 0.1; **p ≤ 0.01; ***p ≤ 0.001; ****p ≤ 0.0001; ns, not significant.

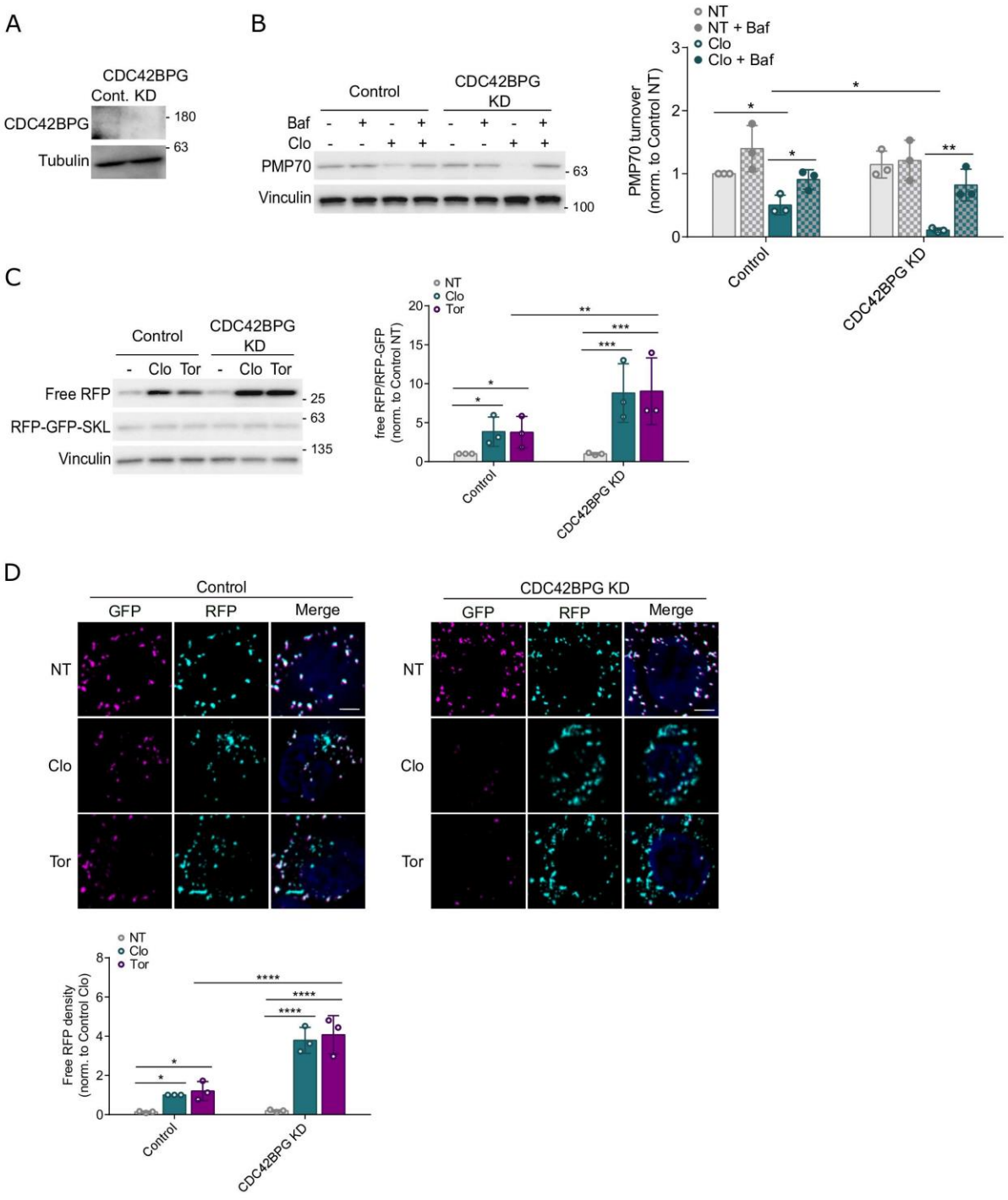
A
CDC42BPG
Cont. KD
CDC42BPG
Tubulin
180
63
B
Control
CDC42BPG KD
Baf
Clo
PMP70
Vinculin
63
100
NT
NT + Baf
Clo
Clo + Baf
PMP70 turnover (norm. to Control NT)
Control
CDC42BPG KD
C
Control
CDC42BPG KD
Clo
Tor
Free RFP
RFP-GFP-SKL
Vinculin
25
63
135
NT
Clo
Tor
free RFP/RFP-GFP (norm. to Control NT)
Control
CDC42BPG KD
D
Control
CDC42BPG KD
GFP
RFP
Merge
NT
Clo
Tor
Free RFP density (norm. to Control Clo)
Control
CDC42BPG KD

Figure S8

Figure S8: Validation of CDC42BPG role in pexophagy regulation using RFP-GFP-SKL approach.

(A) CDC42BPG knockdown efficiency was examined by WB. (B) The control and CDC42BPG KD HCT116 cells stably expressing the RFP-GFP-SKL reporter were incubated with clofibrate (1 mM) for 6 hours in the presence or absence of Baf. PMP70 levels were then examined using western blot. (C), (D) The control and KD pexophagy reporter cells were incubated with clofibrate (1 mM, 6 hours) or Torin1 (Tor, 200 nM, 24 hours). The processing of RFP-GFP-SKL was analyzed by western blot (C) or visualized by immunofluorescence (D). Scale bars, 5 μM.

Unless otherwise indicated, experiments were performed three times. Data are represented as means ± SDs, and p values were determined by two-way ANOVA. *p ≤ 0.1; **p ≤ 0.01; ***p ≤ 0.001; ****p ≤ 0.0001; ns, not significant.

Chapter 5: General discussion

5.1 ULK1-mediated phosphorylation of ATG16L1 promotes xenophagy, but destabilizes the ATG16L1 Crohn's mutant

Autophagy is a conserved degradative mechanism and is critical for cellular homeostasis maintenance(Ryter et al. 2013). ULK1 has been previously known to activate autophagy by phosphorylating various components of the autophagy-related lipid kinase complex(Russell et al. 2013; Di Bartolomeo et al. 2010). Our study identifies ATG16L1, a subunit of the autophagy E3-like enzyme complex, as a direct phosphorylation target of ULK1. This interaction links ULK1 to the regulation of the LC3B lipidation machinery, a key step in autophagosome formation. Furthermore, we found that wild-type ATG16L1 can also undergo caspase-mediated cleavage dependent on ULK1 activity, although to a lesser extent than the Crohn's disease–associated mutant form, caATG16L1 (T300A). However, the physiological interplay between phosphorylation and caspase-mediated cleavage remains unclear outside the context of the caATG16L1 allele. It is possible that, under severe or prolonged stress, caspase-mediated cleavage of ATG16L1 serves as a regulatory mechanism to suppress autophagy.

The T300A variant of ATG16L1 is more vulnerable to cleavage by caspase-3, leading to its degradation and impaired autophagy during stress(Murthy et al. 2014; Lassen et al. 2014). Due to the absence of tools to detect endogenous phosphorylated ATG16L1 (pATG16L1), IKKα was initially proposed as the kinase responsible for phosphorylating and promoting cleavage of the caATG16L1(Diamanti et al. 2017). This hypothesis stemmed from early findings that the T300A variant of ATG16L1 is destabilized

under stress but remains stable under normal conditions, which was also observed by other research groups(Murthy et al. 2014; Fang et al. 2017). Supporting this, Gao et al. demonstrated that in cells expressing wild-type IKKα, TNFα treatment leads to cleavage of wild-type ATG16L1(Gao et al. 2002). This observation contradicts the model proposed by Diamanti et al., which suggests that IKKα signaling should instead stabilize ATG16L1(Diamanti et al. 2017). Interestingly, both infection and starvation—conditions known to destabilize ATG16L1—are also known to activate ULK1, supporting our hypothesis that ULK1-mediated phosphorylation contributes to stress-induced cleavage of ATG16L1, particularly in the context of CD(Kim et al. 2011; Losier et al. 2019). These findings reinforce the model that stress promotes destabilization of the T300A variant.

Additionally, Diamanti et al. suggested that mutating serine 278 to alanine (S278A) reduces ATG16L1 stability in a similar manner to the T300A mutation(Diamanti et al. 2017). According to their model, combining both mutations (S278A and T300A) should result in an even less stable protein. In contrast, our model predicts that phosphorylation at S278 contributes to the destabilization of T300A ATG16L1, and therefore the double mutant (S278A, T300A) should be more stable. Our experiments confirmed this: the double mutant was significantly more stable than T300A alone. Additionally, blocking S278 phosphorylation in the Crohn's-associated form of ATG16L1 enhanced antibacterial autophagy, aligning with our conclusion that S278 phosphorylation is harmful in this disease context.

Based on our data, we propose that ULK1 is the main kinase responsible for ATG16L1 phosphorylation under most physiological conditions. While we cannot completely exclude the possibility that IKKα contributes under certain scenarios not tested

here, we caution that the evidence for IKKα as a kinase came solely from *in vitro* assays using purified proteins, without cellular validation. Such assays are known to generate misleading results, as illustrated by the detection of an artificial S287 phosphorylation site in our own *in vitro* ULK1 kinase experiments. By developing a phospho-specific antibody against S278, we were able to monitor this modification in cells and confirm that phosphorylation occurs only in the presence of ULK1 or ULK2. Although we hypothesize that ULK is the primary kinase mediating ATG16L1 phosphorylation, we acknowledge that IKKα may still play a role in destabilizing caATG16L1 through its known activation of caspases, as previously reported(Diamanti et al. 2017).

Another notable observation is the selective accumulation of phosphorylated ATG16L1 around internalized bacteria. NOD2 was the first gene involved in xenophagy to be associated with CD(Ogura et al. 2001). Like the T300A variant of ATG16L1, certain NOD2 polymorphisms are linked to impaired protein function and increased risk of developing CD(Hugot et al. 2001; Wehkamp et al. 2004). The recruitment of ATG16L1 to bacterial entry points at the plasma membrane is mediated by NOD1 and NOD2, independently of IKK signaling(Travassos et al. 2010). This suggests a shared functional defect in ATG16L1 activity across multiple Crohn's-associated genetic backgrounds.

In line with this, genome-wide studies have identified single-nucleotide polymorphisms (SNPs) in ULK1 that are also associated with CD, although their effect is weaker than those found in ATG16L1(Henckaerts et al. 2011). Our discovery of overlapping roles between ULK1 and ULK2 in regulating ATG16L1 phosphorylation may explain why ULK1 variants contribute less significantly to disease susceptibility.

In addition, reduced expression of IRGM has been implicated in CD(Murdoch et al. 2012). IRGM plays a crucial role in cell-intrinsic defense mechanisms by regulating autophagy and is considered a molecular switch that modulates the activity of the autophagy pathway(Howard, Hunn, and Steinfeldt 2011; Deretic 2012). Several SNPs in IRGM, including rs13361189 (C>T), rs10065172 (C>T), and rs4958847 (A>G), have been linked to altered expression levels and increased disease risk(Waterman et al. 2011; Moon et al. 2013). Molecularly, IRGM has been shown to interact with both ULK1 and ATG16L1, though not necessarily as part of the same complex(Chauhan et al. 2015). Therefore, it would be worthwhile to explore whether decreased IRGM levels affect ULK-mediated phosphorylation of ATG16L1.

5.2 A Pooled CRISPR Screen Protocol for Comparative Autophagy Analysis Across Multiple Stressors

The specific degradation of organelles by autophagy pathway plays an important role in normal cell homeostasis and disease; therefore, understanding the regulatory mechanisms involved in these processes holds significant therapeutic potential. In this study, we sought to investigate the kinase-mediated regulation of the organelle-targeted selective autophagy; particularly, we aimed to conduct a direct comparative analysis of these pathways to identify regulators unique to each. While several high-throughput screens have been performed to uncover autophagy regulators under various conditions, existing protocols do not align with our research goal of identifying both shared and distinct autophagy regulators across multiple samples simultaneously(Morita et al. 2018; Potting et al. 2018; Shalem et al. 2014). Thus, we developed a kinome-wide CRISPR screening workflow that enables high-throughput analysis of multiple stress-induced

autophagy pathways and allows for direct comparison across datasets. In this protocol, we used an autophagy reporter line expressing DsRed-IRES-GFP-p62 which enables detection of various forms of selective autophagy due to its ability to bind different types of ubiquitinated cargo(Lin et al. 2013; Yamada et al. 2019; Pankiv et al. 2007; Germain and Kim 2020). We found that this reporter line is responsive to acute stress conditions, reducing secondary effects and enabling accurate identification of upstream regulatory kinases. Furthermore, utilization of CRISPR/Cas9 system enhances specificity and efficiency of gene targeting, providing permanent gene disruption and stronger phenotypic signals than traditional RNAi(Boettcher and McManus 2015). Since autophagy is a stress-responsive process, CRISPR-based genetic perturbations may introduce artificial variables affecting autophagy flux measurements. Therefore, we incorporated post-perturbation recovery times. Additionally, to analyze multiple autophagy pathways in parallel while reducing sorting-related artifacts, we implemented a sample fixation or crosslinking step. We determined that brief fixation with low concentrations of PFA in the presence of Tris for quenching preserves fluorescent signals comparable to those of unfixed samples.

Despite these strengths, our approach also has certain limitations. Although p62 participates in several selective autophagy processes, its use as a flux reporter can be problematic, as the extent of its degradation may vary depending on the specific cargo or the involvement of alternative receptors. LC3-based reporters could offer more uniform flux readouts across conditions, although they come with interpretative challenges(Mizushima and Murphy 2020). Alternately, secondary screens involving organelle-specific autophagy receptors would enhance sensitivity and broaden the scope

of findings. Furthermore, while CRISPR/Cas9 efficiently disrupts gene function, it may not be suitable for studying essential genes or partial loss-of-function phenotypes(Boettcher and McManus 2015). In such cases, RNAi or CRISPRi techniques would provide more nuanced insights(Boettcher and McManus 2015). The fixation step, although essential to prevent artifacts during cell sorting, introduces practical challenges. Fixed samples yield lower sequencing read counts and are more prone to clogging the sorter, requiring slower sort speeds—an important consideration when processing multiple screens in one session.

5.3 Identification of stress specific autophagy regulators from tandem CRISPR screens

Using our customized CRISPR screening platform, we identified novel autophagy regulators—both activators and inhibitors—across multiple conditions, including basal state, nutrient deprivation, ER stress, and peroxisomal stress. Several of these regulators overlapped between bulk and selective autophagy and include well-established autophagy components such as PIK3C3 (VPS34), PIKFYVE, PIK3R4 (VPS15), and ULK1. In addition to these, we discovered novel autophagy inhibitors, including MAP4K2 and TKFC, which have not previously been associated with autophagy suppression. TKFC, a dihydroxyacetone kinase, is primarily known for phosphorylating glyceraldehyde to generate glyceraldehyde-3-phosphate(Rodrigues et al. 2014). It remains to be determined whether autophagy activation upon TKFC loss is due to changes in metabolism or a separate, uncharacterized function. Since our culture media lacks fructose—one of known substrates of TKFC—an alternative regulatory mechanism is likely involved. Interestingly, MAP4K2 was identified as an autophagy inhibitor in our

screen, although a prior study described it as a positive regulator under prolonged glucose deprivation(Seo et al. 2023). Our study, however, focused on a shorter amino acid starvation window (3 hours), which could account for the contrasting results. This suggests MAP4K2 may play a context-dependent role in autophagy, potentially acting as both an activator and inhibitor depending on the nutrient stress and duration. Future work should investigate whether effect of MAP4K2 is mediated through direct LC3 phosphorylation and whether this effect is modulated by kinases such as PKA or PKCλ(Cherra et al. 2010). These findings highlight how deeper exploration of hits from our screen could clarify the molecular control of both basal and starvation-induced autophagy. Although not the primary goal of our screens, we found 25 candidate regulators of starvation-induced autophagy and 29 candidate regulators of basal autophagy that may represent previously uncharacterized components of these pathways.

Our study aimed to identify novel regulators of ER-phagy and pexophagy. To enhance the reliability of hit validation, we employed multiple complementary strategies. First, beyond assessing effects on p62, we examined non-ubiquitin autophagy marker LC3B signaling in the absence or presence of autophagy inhibitor Bafilomycin A1 (Baf). Additionally, to determine whether the observed changes in ER and peroxisomal content in stressed hit-depleted cells were autophagy-dependent, we evaluated the behavior of the ER-phagy receptor FAM134B and the pexophagy receptor PMP70 in the presence and absence of Baf(Leonibus, Cinque, and Settembre 2020; Germain and Kim 2020). Furthermore, to better define the role of kinase candidates in selective autophagy, we generated HCT116 cell lines stably expressing either the ER-phagy flux reporter ssRFP-

GFP-KDEL or the pexophagy reporter RFP-GFP-SKL(Chino et al. 2019; Zheng et al. 2021). Upon induction of ER-phagy or pexophagy, GFP fluorescence is quenched in the acidic lysosomal environment, leaving only RFP detectable via western blot or immunofluorescence(Kimura et al. 2007). We then assessed the impact of kinase hits on these selective autophagy reporters in the presence of Baf to evaluate their role in autophagic flux. Collectively, these complementary approaches reinforce the findings that the observed effects result from autophagy dysregulation—particularly selective autophagy—and are reproducible across multiple cell lines, thereby supporting the robustness of our screening workflow.

In the ER stress screen, we found 25 kinases that potentially activate autophagy and 17 that inhibit it. Using the approaches described above, we validated two regulators specific to ER-phagy: CDK11A, which we found to be a selective ER-phagy activator, and NME3, a repressor. We found that CDK11A, part of a family involved in RNA splicing, transcription, and cell cycle control, was necessary for ER-phagy but not for starvation-induced autophagy(Zhou et al. 2016). Although previous studies showed that dual knockdown of CDK11A and its identical protein CDK11B initially triggers autophagy and later inhibits it, the underlying mechanism remains unclear(Wilkinson et al. 2011). Our findings suggest that CDK11A specifically supports ER-phagy, and it remains to be tested whether dual knockout impacts basal autophagy or indirectly affects ER homeostasis. Given that CDK11A/B are overactive in multiple cancers, their potential link to ER stress and oncogenesis warrants further investigation(Zhou et al. 2016). NME3, which we found to repress ER-phagy, is part of the nucleoside diphosphate kinase (NDPK) family, involved in nucleotide balance and GTP-regulated processes(Boissan et al. 2018).

Beyond this, NME3 also contributes to mitochondrial dynamics and has recently been shown to promote mitophagy(Chen et al. 2024). Whether its suppression of ER-phagy is functionally connected to its role in mitophagy remains an open question. A recessive loss-of-function mutation in NME3 has been reported in a rare neurodegenerative disorder, but the effects of heterozygous mutations—particularly on ER-phagy—are still unknown(Chen et al. 2019).

In our pexophagy screen, we uncovered 14 candidate autophagy activators and 17 inhibitors. PAN3, an mRNA decay regulator, was validated as a pexophagy activator, although its role in autophagy has not been previously reported(Wolf et al. 2014; Wolf and Passmore 2014). It remains to be determined whether PAN3 regulates transcriptional programs of pexophagy or functions through an alternate pathway. Additionally, we identified CDC42BPG as a pexophagy inhibitor. CDC42BPG is a relatively uncharacterized kinase from the MRCK family, which regulates cytoskeletal dynamics and cellular motility(Unbekandt and Olson 2014). Although neither of these genes has been directly linked to disease, the underlying mechanisms of peroxisomal disorders, such as Zellweger syndrome, remain incompletely understood and are characterized by dysregulated pexophagy(Cho et al. 2018). Thus, it would be of interest to investigate whether the candidates identified in our pexophagy screen, including these proteins, contribute to disease pathology in cases lacking known Zellweger-associated PEX mutations.

5.4 Conclusion

Together, our findings emphasize the critical role of kinase-mediated signaling in the regulation of autophagy. The identification of ULK as a key regulator of ATG16L1 phosphorylation provides novel insight into xenophagy and contributes to a broader understanding of autophagy dysregulation in Crohn's disease. Notably, phosphorylated ATG16L1 has been developed as a valuable early-stage autophagy marker that overcomes limitations associated with conventional markers such as LC3B and p62. To further dissect the regulatory landscape of selective autophagy, we established a robust kinome-wide CRISPR screening platform. This optimized workflow enables high-throughput interrogation of autophagy pathways under diverse stress conditions and is broadly applicable for genetic and pharmacological screening. Our screens reveal a previously underappreciated contribution of signal transduction pathways to selective autophagy regulation, yielding a rich compendium of candidate genes that may inform more targeted therapeutic strategies in autophagy-related diseases.

Appendix I: References Cited

"The Nobel Prize in Physiology or Medicine 1974." n.d. NobelPrize.Org. Accessed December 1, 2018. https://www.nobelprize.org/prizes/medicine/1974/press-release/.

Abdullahi, A., Stanojcic, M., Parousis, A., Patsouris, D. & Jeschke, M. G. Modeling Acute ER stress in vivo and in vitro. Shock Augusta Ga 47, 506–513 (2017).

Abu-Taha, I. H. et al. Nucleoside Diphosphate Kinase-C Suppresses cAMP Formation in Human Heart Failure. Circulation 135, 881–897 (2017).

Alberts, Bruce, Alexander Johnson, Julian Lewis, Martin Raff, Keith Roberts, and Peter Walter. 2002. "The Endoplasmic Reticulum." In Molecular Biology of the Cell. 4th Edition. Garland Science. https://www.ncbi.nlm.nih.gov/books/NBK26841/.

Alers, S., Löffler, A. S., Wesselborg, S. & Stork, B. Role of AMPK-mTOR-Ulk1/2 in the Regulation of Autophagy: Cross Talk, Shortcuts, and Feedbacks. Mol. Cell. Biol. 32, 2–11 (2012).

Alers, Sebastian, Antje S. Löffler, Sebastian Wesselborg, and Björn Stork. 2012. "Role of AMPK-mTOR-Ulk1/2 in the Regulation of Autophagy: Cross Talk, Shortcuts, and Feedbacks." Molecular and Cellular Biology 32 (1): 2–11. https://doi.org/10.1128/MCB.06159-11.

Alonso, S., Pethe, K., Russell, D.G. & Purdy, G.E. Lysosomal killing of Mycobacterium mediated by ubiquitin-derived peptides is enhanced by autophagy. Proc Natl Acad Sci U S A 104, 6031-6036 (2007).

Alsaadi, R. M. et al. ULK1-mediated phosphorylation of ATG16L1 promotes xenophagy, but destabilizes the ATG16L1 Crohn's mutant. EMBO Rep. 20, (2019).

Amin, A., Perera, N. D., Beart, P. M., Turner, B. J., & Shabanpoor, F. (2020). Amyotrophic Lateral Sclerosis and Autophagy: Dysfunction and Therapeutic Targeting. Cells, 9(11), 2413. https://doi.org/10.3390/cells9112413.

An, H. et al. TEX264 Is an Endoplasmic Reticulum-Resident ATG8-Interacting Protein Critical for ER Remodeling during Nutrient Stress. Mol. Cell 74, 891-908.e10 (2019).

An, Heeseon, Alban Ordureau, Joao A. Paulo, Christopher J. Shoemaker, Vladimir Denic, and J. Wade Harper. 2019. "TEX264 Is an Endoplasmic Reticulum-Resident ATG8-Interacting Protein Critical for ER Remodeling during Nutrient Stress." Molecular Cell 74 (5): 891-908.e10. https://doi.org/10.1016/j.molcel.2019.03.034.

Anding, Allyson L., and Eric H. Baehrecke. 2017. "Cleaning House: Selective Autophagy of Organelles." Developmental Cell 41 (1): 10–22. https://doi.org/10.1016/j.devcel.2017.02.016.

Andino, A., and I. Hanning. 2015. "Salmonella Enterica: Survival, Colonization, and Virulence Differences among Serovars." The Scientific World Journal 2015. https://doi.org/10.1155/2015/520179.

Armour, S. M. et al. Inhibition of mammalian S6 kinase by resveratrol suppresses autophagy. Aging 1, 515–528 (2009).

Arstila, A. U., and B. F. Trump. 1968. “Studies on Cellular Autophagocytosis. The Formation of Autophagic Vacuoles in the Liver after Glucagon Administration.” The American Journal of Pathology 53 (5): 687–733.
Ashford, Thomas P., and Keith R. Porter. 1962. “CYTOPLASMIC COMPONENTS IN HEPATIC CELL LYSOSOMES.” The Journal of Cell Biology 12 (1): 198–202.
Ashkenazi, Avraham, Carla F. Bento, Thomas Ricketts, Mariella Vicinanza, Farah Siddiqi, Mariana Pavel, Ferdinando Squitieri, et al. 2017. “Polyglutamine Tracts Regulate Beclin 1-Dependent Autophagy.” Nature 545 (7652): 108–11. https://doi.org/10.1038/nature22078.
Autophagy at the crossroads of catabolism and anabolism | Nature Reviews Molecular Cell Biology. https://www.nature.com/articles/nrm4024.
Autophagy genes in biology and disease | Nature Reviews Genetics. https://www.nature.com/articles/s41576-022-00562-w.
B’chir, W. et al. The eIF2α/ATF4 pathway is essential for stress-induced autophagy gene expression. Nucleic Acids Res. 41, 7683–7699 (2013).
Bach, Markus, Mark Larance, David E. James, and Georg Ramm. 2011. “The Serine/Threonine Kinase ULK1 Is a Target of Multiple Phosphorylation Events.” The Biochemical Journal 440 (2): 283–91. https://doi.org/10.1042/BJ20101894.
Balgi, A. D. et al. Screen for chemical modulators of autophagy reveals novel therapeutic inhibitors of mTORC1 signaling. PloS One 4, e7124 (2009).
Bäumer, C., Fisch, E., Wedler, H., Reinecke, F. & Korfhage, C. Exploring DNA quality of single cells for genome analysis with simultaneous whole-genome amplification. Sci. Rep. 8, 7476 (2018).
Beaulaton, J., and R. A. Lockshin. 1977. “Ultrastructural Study of the Normal Degeneration of the Intersegmental Muscles of Anthereae Polyphemus and Manduca Sexta (Insecta, Lepidoptera) with Particular Reference of Cellular Autophagy.” Journal of Morphology 154 (1): 39–57. https://doi.org/10.1002/jmor.1051540104.
Ben-Sahra, I., Hoxhaj, G., Ricoult, S. J. H., Asara, J. M., & Manning, B. D. (2016). mTORC1 induces purine synthesis through control of the mitochondrial tetrahydrofolate cycle. Science (New York, N.Y.), 351(6274), 728–733. https://doi.org/10.1126/science.aad0489
Bergmann, Timothy J., Fiorenza Fumagalli, Marisa Loi, and Maurizio Molinari. 2017. “Role of SEC62 in ER Maintenance: A Link with ER Stress Tolerance in SEC62-Overexpressing Tumors?” Molecular & Cellular Oncology 4 (2): e1264351. https://doi.org/10.1080/23723556.2016.1264351.
Bhaskara, Ramachandra M., Paolo Grumati, Javier Garcia-Pardo, Sissy Kalayil, Adriana Covarrubias-Pinto, Wenbo Chen, Mikhail Kudryashev, Ivan Dikic, and Gerhard Hummer. 2019. “Curvature Induction and Membrane Remodeling by FAM134B Reticulon Homology Domain Assist Selective ER-Phagy.” Nature Communications 10 (1): 2370. https://doi.org/10.1038/s41467-019-10345-3.
Blommaart, E. F., J. J. Luiken, P. J. Blommaart, G. M. van Woerkom, and A. J. Meijer. 1995. “Phosphorylation of Ribosomal Protein S6 Is Inhibitory for Autophagy in

Isolated Rat Hepatocytes." The Journal of Biological Chemistry 270 (5): 2320–26. https://doi.org/10.1074/jbc.270.5.2320.
Boada-Romero, E., et al. The T300A Crohn's disease risk polymorphism impairs function of the WD40 domain of ATG16L1. Nat Commun 7, 11821 (2016).
Boettcher, Michael, and Michael T. McManus. 2015. "Choosing the Right Tool for the Job: RNAi, TALEN or CRISPR." Molecular Cell 58 (4): 575–85. https://doi.org/10.1016/j.molcel.2015.04.028.
Boissan, Mathieu, Uwe Schlattner, and Marie-Lise Lacombe. 2018. "The NDPK/NME Superfamily: State of the Art." Laboratory Investigation 98 (2): 164–74. https://doi.org/10.1038/labinvest.2017.137.
Bolender, R. P., and E. R. Weibel. 1973. "A Morphometric Study of the Removal of Phenobarbital-Induced Membranes from Hepatocytes after Cessation of Threatment." The Journal of Cell Biology 56 (3): 746–61. https://doi.org/10.1083/jcb.56.3.746.
Brady, Jacob P., Jolyon K. Claridge, Peter G. Smith, and Jason R. Schnell. 2015. "A Conserved Amphipathic Helix Is Required for Membrane Tubule Formation by Yop1p." Proceedings of the National Academy of Sciences of the United States of America 112 (7): E639-648. https://doi.org/10.1073/pnas.1415882112.
Brenner, F. W., R. G. Villar, F. J. Angulo, R. Tauxe, and B. Swaminathan. 2000. "Salmonella Nomenclature." Journal of Clinical Microbiology 38 (7): 2465–67.
Brest, P. et al. Autophagy and Crohn's Disease: At the Crossroads of Infection, Inflammation, Immunity, and Cancer. Curr. Mol. Med. 10, 486–502 (2010).
broadgpp-pdna-library-amplification.pdf.
Brown, Eric J., Mark W. Albers, Tae Bum Shin, Kazuo Ichikawa, Curtis T. Keith, William S. Lane, and Stuart L. Schreiber. 1994. "A Mammalian Protein Targeted by G1-Arresting Rapamycin–Receptor Complex." Nature 369 (6483): 756–58. https://doi.org/10.1038/369756a0.
Burman, Chloe, and Nicholas T. Ktistakis. 2010. "Regulation of Autophagy by Phosphatidylinositol 3-Phosphate." FEBS Letters, Autophagy, 584 (7): 1302–12. https://doi.org/10.1016/j.febslet.2010.01.011.
Cao, M., Luo, X., Wu, K. & He, X. Targeting lysosomes in human disease: from basic research to clinical applications. Signal Transduct. Target. Ther. 6, 1–28 (2021).
Chan, Edmond Y. W., Serkan Kir, and Sharon A. Tooze. 2007. "siRNA Screening of the Kinome Identifies ULK1 as a Multidomain Modulator of Autophagy." The Journal of Biological Chemistry 282 (35): 25464–74. https://doi.org/10.1074/jbc.M703663200.
Chandra, P. & Kumar, D. Selective autophagy gets more selective: Uncoupling of autophagy flux and xenophagy flux in Mycobacterium tuberculosis-infected macrophages. Autophagy 12, 608–609 (2016).
Chauhan, Santosh, Michael A. Mandell, and Vojo Deretic. 2015. "IRGM Governs the Core Autophagy Machinery to Conduct Antimicrobial Defense." Molecular Cell 58 (3): 507–21. https://doi.org/10.1016/j.molcel.2015.03.020.

Chen, C.-W. et al. NME3 is a gatekeeper for DRP1-dependent mitophagy in hypoxia. Nat. Commun. 15, 2264 (2024).
Chen, C.-W. et al. Two separate functions of NME3 critical for cell survival underlie a neurodegenerative disorder. Proc. Natl. Acad. Sci. U. S. A. 116, 566–574 (2019).
Chen, C.-Y. A., Zhang, Y., Xiang, Y., Han, L. & Shyu, A.-B. Antagonistic actions of two human Pan3 isoforms on global mRNA turnover. RNA 23, 1404–1418 (2017).
Chen, Chih-Wei, Chi Su, Chang-Yu Huang, Xuan-Rong Huang, Xiaojing Cuili, Tung Chao, Chun-Hsiang Fan, et al. 2024. “NME3 Is a Gatekeeper for DRP1-Dependent Mitophagy in Hypoxia.” Nature Communications 15 (1): 2264. https://doi.org/10.1038/s41467-024-46385-7.
Chen, Chih-Wei, Hong-Ling Wang, Ching-Wen Huang, Chang-Yu Huang, Wai Keong Lim, I-Chen Tu, Atmaja Koorapati, et al. 2019. “Two Separate Functions of NME3 Critical for Cell Survival Underlie a Neurodegenerative Disorder.” Proceedings of the National Academy of Sciences 116 (2): 566–74. https://doi.org/10.1073/pnas.1818629116.
Chen, Dongfeng, Cuiping Zhu, Xuenan Wang, Xungang Feng, Shuchao Pang, Wenhui Huang, Robert G. Hawley, and Bo Yan. 2013. “A Novel and Functional Variant within the ATG5 Gene Promoter in Sporadic Parkinson’s Disease.” Neuroscience Letters 538 (March):49–53. https://doi.org/10.1016/j.neulet.2013.01.044.
Chen, Dongfeng, Shuchao Pang, Xungang Feng, Wenhui Huang, Robert G. Hawley, and Bo Yan. 2013. “Genetic Analysis of the ATG7 Gene Promoter in Sporadic Parkinson’s Disease.” Neuroscience Letters 534 (February):193–98. https://doi.org/10.1016/j.neulet.2012.12.039.
Chen, Qingzhou, Ya Xiao, Peiyuan Chai, Pengli Zheng, Junlin Teng, and Jianguo Chen. 2019. “ATL3 Is a Tubular ER-Phagy Receptor for GABARAP-Mediated Selective Autophagy.” Current Biology: CB 29 (5): 846-855.e6. https://doi.org/10.1016/j.cub.2019.01.041.
Chen, S. et al. Genome-wide CRISPR Screen in a Mouse Model of Tumor Growth and Metastasis. Cell 160, 1246–1260 (2015).
Chen, Wei, Hui Mao, Linxi Chen, and Lanfang Li. 2022. “The Pivotal Role of FAM134B in Selective ER-Phagy and Diseases.” Biochimica et Biophysica Acta (BBA) - Molecular Cell Research 1869 (8): 119277. https://doi.org/10.1016/j.bbamcr.2022.119277.
Cheong, H., Lindsten, T., Wu, J., Lu, C. & Thompson, C.B. Ammonia-induced autophagy is independent of ULK1/ULK2 kinases. Proc Natl Acad Sci U S A 108, 11121-11126 (2011).
Cherra, Salvatore J., III, Scott M. Kulich, Guy Uechi, Manimalha Balasubramani, John Mountzouris, Billy W. Day, and Charleen T. Chu. 2010. “Regulation of the Autophagy Protein LC3 by Phosphorylation.” Journal of Cell Biology 190 (4): 533–39. https://doi.org/10.1083/jcb.201002108.
Chino, Haruka, Akinori Yamasaki, Koji L. Ode, Hiroki R. Ueda, Nobuo N. Noda, and Noboru Mizushima. 2022. “Phosphorylation by Casein Kinase 2 Enhances the

Interaction between ER-Phagy Receptor TEX264 and ATG8 Proteins." EMBO Reports 23 (6): e54801. https://doi.org/10.15252/embr.202254801.
Chino, Haruka, and Noboru Mizushima. 2020. "ER-Phagy: Quality Control and Turnover of Endoplasmic Reticulum." Trends in Cell Biology 30 (5): 384–98. https://doi.org/10.1016/j.tcb.2020.02.001.
Chino, Haruka, Tomohisa Hatta, Tohru Natsume, and Noboru Mizushima. 2019. "Intrinsically Disordered Protein TEX264 Mediates ER-Phagy." Molecular Cell 74 (5): 909-921.e6. https://doi.org/10.1016/j.molcel.2019.03.033.
Cho, Dong-Hyung, Yi Sak Kim, Doo Sin Jo, Seong-Kyu Choe, and Eun-Kyeong Jo. 2018a. "Pexophagy: Molecular Mechanisms and Implications for Health and Diseases." Molecules and Cells 41 (1): 55–64. https://doi.org/10.14348/molcells.2018.2245.
Chuang, H.-C., Wang, X. & Tan, T.-H. Chapter Seven - MAP4K Family Kinases in Immunity and Inflammation. in Advances in Immunology (ed. Alt, F. W.) vol. 129 277–314 (Academic Press, 2016).
Clark, S. L. 1957. "Cellular Differentiation in the Kidneys of Newborn Mice Studies with the Electron Microscope." The Journal of Biophysical and Biochemical Cytology 3 (3): 349–62. https://doi.org/10.1083/jcb.3.3.349.
Cleaning House: Selective Autophagy of Organelles. https://www.ncbi.nlm.nih.gov/pmc/articles/PMC5395098/.
Davidson, G. L., S. M. Murphy, J. M. Polke, M. Laura, M. a. M. Salih, F. Muntoni, J. Blake, et al. 2012. "Frequency of Mutations in the Genes Associated with Hereditary Sensory and Autonomic Neuropathy in a UK Cohort." Journal of Neurology 259 (8): 1673–85. https://doi.org/10.1007/s00415-011-6397-y.
de Duve, C., and P. Baudhuin. 1966. "Peroxisomes (Microbodies and Related Particles)." Physiological Reviews 46 (2): 323–57. https://doi.org/10.1152/physrev.1966.46.2.323.
de Duve, C., and R. Wattiaux. 1966a. "Functions of Lysosomes." Annual Review of Physiology 28:435–92. https://doi.org/10.1146/annurev.ph.28.030166.002251.
Decuypere, Jean-Paul, Jan B. Parys, and Geert Bultynck. 2012. "Regulation of the Autophagic Bcl-2/Beclin 1 Interaction." Cells 1 (3): 284–312. https://doi.org/10.3390/cells1030284.
DeJesus, R. et al. Functional CRISPR screening identifies the ufmylation pathway as a regulator of SQSTM1/p62. eLife 5, e17290 (2016).
Demers, Nicholas D., Victoria Riccio, Doo Sin Jo, Sushil Bhandari, Kelsey B. Law, Weifang Liao, Choy Kim, et al. 2023. "PEX13 Prevents Pexophagy by Regulating Ubiquitinated PEX5 and Peroxisomal ROS." Autophagy 19 (6): 1781–1802. https://doi.org/10.1080/15548627.2022.2160566.
Denisenko, T. V., Gogvadze, V. & Zhivotovsky, B. Mitophagy in carcinogenesis and cancer treatment. Discov. Oncol. 12, 58 (2021).
Deosaran, Elizabeth, Kenneth B. Larsen, Rong Hua, Graeme Sargent, Yuqing Wang, Sarah Kim, Trond Lamark, et al. 2013. "NBR1 Acts as an Autophagy Receptor for

Peroxisomes." Journal of Cell Science 126 (Pt 4): 939–52. https://doi.org/10.1242/jcs.114819.
Deretic, Vojo. 2012. "Autophagy as an Innate Immunity Paradigm: Expanding the Scope and Repertoire of Pattern Recognition Receptors." Current Opinion in Immunology 24 (1): 21–31. https://doi.org/10.1016/j.coi.2011.10.006.
Di Bartolomeo, Sabrina, Marco Corazzari, Francesca Nazio, Serafina Oliverio, Gaia Lisi, Manuela Antonioli, Vittoria Pagliarini, et al. 2010. "The Dynamic Interaction of AMBRA1 with the Dynein Motor Complex Regulates Mammalian Autophagy." The Journal of Cell Biology 191 (1): 155–68. https://doi.org/10.1083/jcb.201002100.
Diamanti, Michaela A., Jalaj Gupta, Moritz Bennecke, Tiago De Oliveira, Mallika Ramakrishnan, Anne K. Braczynski, Benjamin Richter, et al. 2017. "IKKα Controls ATG16L1 Degradation to Prevent ER Stress during Inflammation." The Journal of Experimental Medicine 214 (2): 423–37. https://doi.org/10.1084/jem.20161867.
Diao, Jiajie, Rong Liu, Yueguang Rong, Minglei Zhao, Jing Zhang, Ying Lai, Qiangjun Zhou, et al. 2015. "ATG14 Promotes Membrane Tethering and Fusion of Autophagosomes to Endolysosomes." Nature 520 (7548): 563–66. https://doi.org/10.1038/nature14147.
Dixit, Evelyn, Steeve Boulant, Yijing Zhang, Amy S. Y. Lee, Charlotte Odendall, Bennett Shum, Nir Hacohen, et al. 2010. "Peroxisomes Are Signaling Platforms for Antiviral Innate Immunity." Cell 141 (4): 668–81. https://doi.org/10.1016/j.cell.2010.04.018.
Doench, J. G. et al. Optimized sgRNA design to maximize activity and minimize off-target effects of CRISPR-Cas9. Nat. Biotechnol. 34, 184–191 (2016).
Dooley, Hannah C., Minoo Razi, Hannah E.J. Polson, Stephen E. Girardin, Michael I. Wilson, and Sharon A. Tooze. 2014. "WIPI2 Links LC3 Conjugation with PI3P, Autophagosome Formation, and Pathogen Clearance by Recruiting Atg12–5-16L1." Molecular Cell 55 (2): 238–52. https://doi.org/10.1016/j.molcel.2014.05.021.
Dossou, Akpedje S., and Alakananda Basu. 2019. "The Emerging Roles of mTORC1 in Macromanaging Autophagy." Cancers 11 (10): 1422. https://doi.org/10.3390/cancers11101422.
Duve, C. de, B. C. Pressman, R. Gianetto, R. Wattiaux, and F. Appelmans. 1955. "Tissue Fractionation Studies. 6. Intracellular Distribution Patterns of Enzymes in Rat-Liver Tissue." Biochemical Journal 60 (4): 604–17.
Egan, Daniel F, Joungmok Kim, Reuben J Shaw, and Kun-Liang Guan. 2011. "The Autophagy Initiating Kinase ULK1 Is Regulated via Opposing Phosphorylation by AMPK and mTOR." Autophagy 7 (6): 645–46. https://doi.org/10.4161/auto.7.6.15123.
Egan, Daniel F., David B. Shackelford, Maria M. Mihaylova, Sara Gelino, Rebecca A. Kohnz, William Mair, Debbie S. Vasquez, et al. 2011. "Phosphorylation of ULK1 (hATG1) by AMP-Activated Protein Kinase Connects Energy Sensing to

Mitophagy." Science 331 (6016): 456–61. https://doi.org/10.1126/science.1196371.
Fan, W., Nassiri, A. & Zhong, Q. Autophagosome targeting and membrane curvature sensing by Barkor/Atg14(L). Proc Natl Acad Sci U S A 108, 7769-7774 (2011).
Fang, Run, Chenguang Wang, Qifei Jiang, Mengze Lv, Pengfei Gao, Xiaoyu Yu, Ping Mu, et al. 2017. "NEMO-IKKβ Are Essential for IRF3 and NF-κB Activation in the cGAS-STING Pathway." Journal of Immunology (Baltimore, Md.: 1950) 199 (9): 3222–33. https://doi.org/10.4049/jimmunol.1700699.
Fischer, Dirk, Maria Schabhüttl, Thomas Wieland, Reinhard Windhager, Tim M. Strom, and Michaela Auer-Grumbach. 2014. "A Novel Missense Mutation Confirms ATL3 as a Gene for Hereditary Sensory Neuropathy Type 1." Brain: A Journal of Neurology 137 (Pt 7): e286. https://doi.org/10.1093/brain/awu091.
Frankel, L. B. et al. microRNA-101 is a potent inhibitor of autophagy. EMBO J. 30, 4628–4641 (2011).
Fransen, Marc, Marcus Nordgren, Bo Wang, and Oksana Apanasets. 2012. "Role of Peroxisomes in ROS/RNS-Metabolism: Implications for Human Disease." Biochimica Et Biophysica Acta 1822 (9): 1363–73. https://doi.org/10.1016/j.bbadis.2011.12.001.
Friedman, Lauren G., M. Lenard Lachenmayer, Jing Wang, Liqiang He, Shibu M. Poulose, Masaaki Komatsu, Gay R. Holstein, and Zhenyu Yue. 2012. "Disrupted Autophagy Leads to Dopaminergic Axon and Dendrite Degeneration and Promotes Presynaptic Accumulation of α-Synuclein and LRRK2 in the Brain." The Journal of Neuroscience: The Official Journal of the Society for Neuroscience 32 (22): 7585–93. https://doi.org/10.1523/JNEUROSCI.5809-11.2012.
Fujita, Naonobu, Takashi Itoh, Hiroko Omori, Mitsunori Fukuda, Takeshi Noda, and Tamotsu Yoshimori. 2008. "The Atg16L Complex Specifies the Site of LC3 Lipidation for Membrane Biogenesis in Autophagy." Molecular Biology of the Cell 19 (5): 2092–2100. https://doi.org/10.1091/mbc.e07-12-1257.
Full article: CSNK2 suppresses autophagy by activating FLN-NHL-containing TRIM proteins. https://www.tandfonline.com/doi/full/10.1080/15548627.2023.2281128.
Fumagalli, Fiorenza, Julia Noack, Timothy J. Bergmann, Eduardo Cebollero, Giorgia Brambilla Pisoni, Elisa Fasana, Ilaria Fregno, et al. 2016. "Translocon Component Sec62 Acts in Endoplasmic Reticulum Turnover during Stress Recovery." Nature Cell Biology 18 (11): 1173–84. https://doi.org/10.1038/ncb3423.
Gammoh, Noor, Oliver Florey, Michael Overholtzer, and Xuejun Jiang. 2013. "Interaction Between FIP200 and ATG16L1 Distinguishes ULK1 Complex-Dependent and -Independent Autophagy." Nature Structural & Molecular Biology 20 (2): 144–49. https://doi.org/10.1038/nsmb.2475.
Ganley, I.G., et al. ULK1.ATG13.FIP200 complex mediates mTOR signaling and is essential for autophagy. J Biol Chem 284, 12297-12305 (2009).

Gao, P., et al. The Inflammatory Bowel Disease-Associated Autophagy Gene Atg16L1T300A Acts as a Dominant Negative Variant in Mice. J Immunol 198, 2457-2467 (2017).
Gao, Zhanguo, Daniel Hwang, Fredly Bataille, Michael Lefevre, David York, Michael J. Quon, and Jianping Ye. 2002. “Serine Phosphorylation of Insulin Receptor Substrate 1 by Inhibitor Kappa B Kinase Complex.” The Journal of Biological Chemistry 277 (50): 48115–21. https://doi.org/10.1074/jbc.M209459200.
Garai, Preeti, Divya Prakash Gnanadhas, and Dipshikha Chakravortty. 2012. “Salmonella Enterica Serovars Typhimurium and Typhi as Model Organisms.” Virulence 3 (4): 377–88. https://doi.org/10.4161/viru.21087.
Garcia, D. & Shaw, R. J. AMPK: mechanisms of cellular energy sensing and restoration of metabolic balance. Mol. Cell 66, 789–800 (2017).
Gatica, Damián, Vikramjit Lahiri, and Daniel J. Klionsky. 2018. “Cargo Recognition and Degradation by Selective Autophagy.” Nature Cell Biology 20 (3): 233–42. https://doi.org/10.1038/s41556-018-0037-z.
Geng, Jiefei, and Daniel J. Klionsky. 2008. “The Atg8 and Atg12 Ubiquitin-like Conjugation Systems in Macroautophagy. ‘Protein Modifications: Beyond the Usual Suspects’ Review Series.” EMBO Reports 9 (9): 859–64. https://doi.org/10.1038/embor.2008.163.
Genome-wide CRISPR Screen in a Mouse Model of Tumor Growth and Metastasis - ScienceDirect. https://www.sciencedirect.com/science/article/pii/S0092867415002044.
Germain, Kyla, and Peter K. Kim. 2020. “Pexophagy: A Model for Selective Autophagy.” International Journal of Molecular Sciences 21 (2): 578. https://doi.org/10.3390/ijms21020578.
Glick, Danielle, Sandra Barth, and Kay F. Macleod. 2010. “Autophagy: Cellular and Molecular Mechanisms.” The Journal of Pathology 221 (1): 3–12. https://doi.org/10.1002/path.2697.
Gomes, L.C. & Dikic, I. Autophagy in antimicrobial immunity. Mol Cell 54, 224-233 (2014).
Gordon, P. B., and P. O. Seglen. 1988. “Prelysosomal Convergence of Autophagic and Endocytic Pathways.” Biochemical and Biophysical Research Communications 151 (1): 40–47. https://doi.org/10.1016/0006-291x(88)90556-6.
Gowans, Graeme J., Simon A. Hawley, Fiona A. Ross, and D. Grahame Hardie. 2013. “AMP Is a True Physiological Regulator of AMP-Activated Protein Kinase by Both Allosteric Activation and Enhancing Net Phosphorylation.” Cell Metabolism 18 (4): 556–66. https://doi.org/10.1016/j.cmet.2013.08.019.
Grégoire, Isabel Pombo, Clémence Richetta, Laurène Meyniel-Schicklin, Sophie Borel, Fabrine Pradezynski, Olivier Diaz, Alexandre Deloire, et al. 2011. “IRGM Is a Common Target of RNA Viruses That Subvert the Autophagy Network.” PLoS Pathogens 7 (12): e1002422. https://doi.org/10.1371/journal.ppat.1002422.
Grumati, Paolo, Giulio Morozzi, Soraya Hölper, Muriel Mari, Marie-Lena Ie Harwardt, Riqiang Yan, Stefan Müller, Fulvio Reggiori, Mike Heilemann, and Ivan Dikic.

2017. “Full Length RTN3 Regulates Turnover of Tubular Endoplasmic Reticulum via Selective Autophagy.” eLife 6 (June):e25555. https://doi.org/10.7554/eLife.25555.
Gump, Jacob M., and Andrew Thorburn. 2014. “Sorting Cells for Basal and Induced Autophagic Flux by Quantitative Ratiometric Flow Cytometry.” Autophagy 10 (7): 1327–34. https://doi.org/10.4161/auto.29394.
Guo, Sujuan, Kevin J. Pridham, Ching-Man Virbasius, Bin He, Liqing Zhang, Hanne Varmark, Michael R. Green, and Zhi Sheng. 2018. “A Large-Scale RNA Interference Screen Identifies Genes That Regulate Autophagy at Different Stages.” Scientific Reports 8 (1): 2822. https://doi.org/10.1038/s41598-018-21106-5.
Gutierrez, Maximiliano G., Sharon S. Master, Sudha B. Singh, Gregory A. Taylor, Maria I. Colombo, and Vojo Deretic. 2004. “Autophagy Is a Defense Mechanism Inhibiting BCG and Mycobacterium Tuberculosis Survival in Infected Macrophages.” Cell 119 (6): 753–66. https://doi.org/10.1016/j.cell.2004.11.038.
Gwinn, Dana M., David B. Shackelford, Daniel F. Egan, Maria M. Mihaylova, Annabelle Mery, Debbie S. Vasquez, Benjamin E. Turk, and Reuben J. Shaw. 2008. “AMPK Phosphorylation of Raptor Mediates a Metabolic Checkpoint.” Molecular Cell 30 (2): 214–26. https://doi.org/10.1016/j.molcel.2008.03.003.
Hać, A., Pierzynowska, K. & Herman-Antosiewicz, A. S6K1 Is Indispensible for Stress-Induced Microtubule Acetylation and Autophagic Flux. Cells 10, 929 (2021).
Hale, Christopher M., Qingwen Cheng, Danny Ortuno, Ming Huang, Dana Nojima, Paul D. Kassner, Songli Wang, Michael M. Ollmann, and Holly J. Carlisle. 2016. “Identification of Modulators of Autophagic Flux in an Image-Based High Content siRNA Screen.” Autophagy 12 (4): 713–26. https://doi.org/10.1080/15548627.2016.1147669.
Hardie, D. Grahame. 2013. “AMPK: A Target for Drugs and Natural Products With Effects on Both Diabetes and Cancer.” Diabetes 62 (7): 2164–72. https://doi.org/10.2337/db13-0368.
Harding, T. M., K. A. Morano, S. V. Scott, and D. J. Klionsky. 1995. “Isolation and Characterization of Yeast Mutants in the Cytoplasm to Vacuole Protein Targeting Pathway.” The Journal of Cell Biology 131 (3): 591–602. https://doi.org/10.1083/jcb.131.3.591.
Hawley, Simon A., Jérôme Boudeau, Jennifer L. Reid, Kirsty J. Mustard, Lina Udd, Tomi P. Mäkelä, Dario R. Alessi, and D. Grahame Hardie. 2003. “Complexes between the LKB1 Tumor Suppressor, STRAD Alpha/Beta and MO25 Alpha/Beta Are Upstream Kinases in the AMP-Activated Protein Kinase Cascade.” Journal of Biology 2 (4): 28. https://doi.org/10.1186/1475-4924-2-28.
He, Anyuan, John M. Dean, and Irfan J. Lodhi. 2021. “Peroxisomes as Cellular Adaptors to Metabolic and Environmental Stress.” Trends in Cell Biology 31 (8): 656–70. https://doi.org/10.1016/j.tcb.2021.02.005.

Heard, Jeffrey J., Valerie Fong, S. Zahra Bathaie, and Fuyuhiko Tamanoi. 2014. “Recent Progress in the Study of the Rheb Family GTPases.” Cellular Signalling 26 (9): 1950–57. https://doi.org/10.1016/j.cellsig.2014.05.011.

Heitman, J., N. R. Movva, and M. N. Hall. 1991. “Targets for Cell Cycle Arrest by the Immunosuppressant Rapamycin in Yeast.” Science (New York, N.Y.) 253 (5022): 905–9. https://doi.org/10.1126/science.1715094.

Henckaerts, Liesbet, Isabelle Cleynen, Marko Brinar, Jestinah Mahachie John, Kristel Van Steen, Paul Rutgeerts, and Séverine Vermeire. 2011. “Genetic Variation in the Autophagy Gene ULK1 and Risk of Crohn’s Disease.” Inflammatory Bowel Diseases 17 (6): 1392–97. https://doi.org/10.1002/ibd.21486.

Heo, Jin-Mi, Alban Ordureau, Joao A. Paulo, Jesse Rinehart, and J. Wade Harper. 2015. “The PINK1-PARKIN Mitochondrial Ubiquitylation Pathway Drives a Program of OPTN/NDP52 Recruitment and TBK1 Activation to Promote Mitophagy.” Molecular Cell 60 (1): 7–20. https://doi.org/10.1016/j.molcel.2015.08.016.

Herhaus, Lina, and Ivan Dikic. 2018. “Regulation of Salmonella-Host Cell Interactions via the Ubiquitin System.” International Journal of Medical Microbiology, Intracellular Compartments as Places of Pathogen-Host Interaction, 308 (1): 176–84. https://doi.org/10.1016/j.ijmm.2017.11.003.

Hetz, C., Thielen, P., Matus, S., Nassif, M., Court, F., Kiffin, R., Martinez, G., Cuervo, A. M., Brown, R. H., & Glimcher, L. H. (2009). XBP-1 deficiency in the nervous system protects against amyotrophic lateral sclerosis by increasing autophagy. Genes & development, 23(19), 2294–2306. https://doi.org/10.1101/gad.1830709.

Holz, M. K., Ballif, B. A., Gygi, S. P., & Blenis, J. (2005). mTOR and S6K1 mediate assembly of the translation preinitiation complex through dynamic protein interchange and ordered phosphorylation events. Cell, 123(4), 569–580. https://doi.org/10.1016/j.cell.2005.10.024

Homer, C.R., Richmond, A.L., Rebert, N.A., Achkar, J.P. & McDonald, C. ATG16L1 and NOD2 interact in an autophagy-dependent antibacterial pathway implicated in Crohn's disease pathogenesis. Gastroenterology 139, 1630-1641, 1641 e1631-1632 (2010).

Hong-Brown, Ly Q., C. Randell Brown, Abid A. Kazi, Maithili Navaratnarajah, and Charles H. Lang. 2012. “Rag GTPases and AMPK/TSC2/Rheb Mediate the Differential Regulation of mTORC1 Signaling in Response to Alcohol and Leucine.” American Journal of Physiology - Cell Physiology 302 (10): C1557–65. https://doi.org/10.1152/ajpcell.00407.2011.

Hosokawa, Nao, Taichi Hara, Takeshi Kaizuka, Chieko Kishi, Akito Takamura, Yutaka Miura, Shun-ichiro Iemura, et al. 2009. “Nutrient-Dependent mTORC1 Association with the ULK1-Atg13-FIP200 Complex Required for Autophagy.” Molecular Biology of the Cell 20 (7): 1981–91. https://doi.org/10.1091/mbc.e08-12-1248.

Howard, Jonathan C., Julia P. Hunn, and Tobias Steinfeldt. 2011. “The IRG Protein-Based Resistance Mechanism in Mice and Its Relation to Virulence in

Toxoplasma Gondii." Current Opinion in Microbiology 14 (4): 414–21. https://doi.org/10.1016/j.mib.2011.07.002.
Hoyer, Melissa J., Cristina Capitanio, Ian R. Smith, Julia C. Paoli, Anna Bieber, Yizhi Jiang, Joao A. Paulo, et al. 2024. "Combinatorial Selective ER-Phagy Remodels the ER during Neurogenesis." Nature Cell Biology 26 (3): 378–92. https://doi.org/10.1038/s41556-024-01356-4.
Hu, Y., et al. Abnormal morphogenesis but intact IKK activation in mice lacking the IKKalpha subunit of IkappaB kinase. Science 284, 316-320 (1999).
Hübner, C. A. & Dikic, I. ER-phagy and human diseases. Cell Death Differ. 27, 833–842 (2020).
Hugot, J. P., M. Chamaillard, H. Zouali, S. Lesage, J. P. Cézard, J. Belaiche, S. Almer, et al. 2001. "Association of NOD2 Leucine-Rich Repeat Variants with Susceptibility to Crohn's Disease." Nature 411 (6837): 599–603. https://doi.org/10.1038/35079107.
Ichimiya, Tadashi, Tsukasa Yamakawa, Takehiro Hirano, Yoshihiro Yokoyama, Yuki Hayashi, Daisuke Hirayama, Kohei Wagatsuma, Takao Itoi, and Hiroshi Nakase. 2020. "Autophagy and Autophagy-Related Diseases: A Review." International Journal of Molecular Sciences 21 (23): 8974. https://doi.org/10.3390/ijms21238974.
Ilgaz Aydinlar, Elif, Arndt Rolfs, Mustafa Serteser, and Yesim Parman. 2014. "Mutation in FAM134B Causing Hereditary Sensory Neuropathy with Spasticity in a Turkish Family." Muscle & Nerve 49 (5): 774–75. https://doi.org/10.1002/mus.24145.
Imanaka, T. et al. Characterization of the 70-kDa Peroxisomal Membrane Protein, an ATP Binding Cassette Transporter*. J. Biol. Chem. 274, 11968–11976 (1999).
Islam, Farhadul, Vinod Gopalan, Jelena Vider, Riajul Wahab, Faeza Ebrahimi, Cu-Tai Lu, Kais Kasem, and Alfred K. Y. Lam. 2017. "MicroRNA-186-5p Overexpression Modulates Colon Cancer Growth by Repressing the Expression of the FAM134B Tumour Inhibitor." Experimental Cell Research 357 (2): 260–70. https://doi.org/10.1016/j.yexcr.2017.05.021.
Islam, Farhadul, Vinod Gopalan, Suja Pillai, Cu-Tai Lu, Kais Kasem, and Alfred King-Yin Lam. 2018. "Promoter Hypermethylation Inactivate Tumor Suppressor FAM134B and Is Associated with Poor Prognosis in Colorectal Cancer." Genes, Chromosomes & Cancer 57 (5): 240–51. https://doi.org/10.1002/gcc.22525.
JCI - Casein kinase 1α–dependent feedback loop controls autophagy in RAS-driven cancers. https://www.jci.org/articles/view/78018.
Jeong, H.-H., Kim, S. Y., Rousseaux, M. W. C., Zoghbi, H. Y. & Liu, Z. Beta-binomial modeling of CRISPR pooled screen data identifies target genes with greater sensitivity and fewer false negatives. Genome Res. 29, 999–1008 (2019).
Jiang, Li, Sayuri Hara-Kuge, Shun-Ichi Yamashita, and Yukio Fujiki. 2015. "Peroxin Pex14p Is the Key Component for Coordinated Autophagic Degradation of Mammalian Peroxisomes by Direct Binding to LC3-II." Genes to Cells: Devoted to Molecular & Cellular Mechanisms 20 (1): 36–49. https://doi.org/10.1111/gtc.12198.

Jiang, Peidu, Taki Nishimura, Yuriko Sakamaki, Eisuke Itakura, Tomohisa Hatta, Tohru Natsume, and Noboru Mizushima. 2014. “The HOPS Complex Mediates Autophagosome–Lysosome Fusion through Interaction with Syntaxin 17.” Molecular Biology of the Cell 25 (8): 1327–37. https://doi.org/10.1091/mbc.E13-08-0447.

Jiang, S. et al. Peroxisomal Fitness: A Potential Protective Mechanism of Fenofibrate against High Fat Diet-Induced Non-Alcoholic Fatty Liver Disease in Mice. Diabetes Metab. J. 46, 829–842 (2022).

Jo, Doo Sin, and Dong-Hyung Cho. 2019. “Peroxisomal Dysfunction in Neurodegenerative Diseases.” Archives of Pharmacal Research 42 (5): 393–406. https://doi.org/10.1007/s12272-019-01131-2.

Johansen, Terje, and Trond Lamark. 2020. “Selective Autophagy: ATG8 Family Proteins, LIR Motifs and Cargo Receptors.” Journal of Molecular Biology 432 (1): 80–103. https://doi.org/10.1016/j.jmb.2019.07.016.

Jung, C. H. et al. ULK-Atg13-FIP200 Complexes Mediate mTOR Signaling to the Autophagy Machinery. Mol. Biol. Cell 20, 1992–2003 (2009).

Kaizuka, Takeshi, Hideaki Morishita, Yutaro Hama, Satoshi Tsukamoto, Takahide Matsui, Yuichiro Toyota, Akihiko Kodama, Tomoaki Ishihara, Tohru Mizushima, and Noboru Mizushima. 2016. “An Autophagic Flux Probe That Releases an Internal Control.” Molecular Cell 64 (4): 835–49. https://doi.org/10.1016/j.molcel.2016.09.037.

Kang, Mi Ran, Min Sung Kim, Ji Eun Oh, Yoo Ri Kim, Sang Yong Song, Sung Soo Kim, Chang Hyeok Ahn, Nam Jin Yoo, and Sug Hyung Lee. 2009. “Frameshift Mutations of Autophagy-Related Genes ATG2B, ATG5, ATG9B and ATG12 in Gastric and Colorectal Cancers with Microsatellite Instability.” The Journal of Pathology 217 (5): 702–6. https://doi.org/10.1002/path.2509.

Kang, R, H J Zeh, M T Lotze, and D Tang. 2011. “The Beclin 1 Network Regulates Autophagy and Apoptosis.” Cell Death and Differentiation 18 (4): 571–80. https://doi.org/10.1038/cdd.2010.191.

Kasem, Kais, Emily Sullivan, Vinod Gopalan, Ali Salajegheh, Robert A. Smith, and Alfred K.-Y. Lam. 2014. “JK1 (FAM134B) Represses Cell Migration in Colon Cancer: A Functional Study of a Novel Gene.” Experimental and Molecular Pathology 97 (1): 99–104. https://doi.org/10.1016/j.yexmp.2014.06.002.

Kato, Junya, Supratim Dey, Jose E Soto, Carmen Butan, Mason C Wilkinson, Roberto N De Guzman, and Jorge E Galan. 2018. “A Protein Secreted by the Salmonella Type III Secretion System Controls Needle Filament Assembly.” Edited by Gisela Storz. eLife 7 (July):e35886. https://doi.org/10.7554/eLife.35886.

Kaur, J. & Debnath, J. Autophagy at the crossroads of catabolism and anabolism. Nat. Rev. Mol. Cell Biol. 16, 461–472 (2015).

Khaminets, A. et al. Regulation of endoplasmic reticulum turnover by selective autophagy. Nature 522, 354–358 (2015).

Kim, Byeong-Won, Do Hoon Kwon, and Hyun Kyu Song. 2016. “Structure Biology of Selective Autophagy Receptors.” BMB Reports 49 (2): 73–80. https://doi.org/10.5483/BMBRep.2016.49.2.265.
Kim, J. et al. Differential regulation of distinct Vps34 complexes by AMPK in nutrient stress and autophagy. Cell 152, 290–303 (2013).
Kim, J. et al. Evolutionarily conserved regulators of tau identify targets for new therapies. Neuron 111, 824-838.e7 (2023).
Kim, Joungmok, Mondira Kundu, Benoit Viollet, and Kun-Liang Guan. 2011a. “AMPK and mTOR Regulate Autophagy through Direct Phosphorylation of Ulk1.” Nature Cell Biology 13 (2): 132–41. https://doi.org/10.1038/ncb2152.
Kim, Joungmok, Young Chul Kim, Chong Fang, Ryan C. Russell, Jeong Hee Kim, Weiliang Fan, Rong Liu, Qing Zhong, and Kun-Liang Guan. 2013. “Differential Regulation of Distinct Vps34 Complexes by AMPK in Nutrient Stress and Autophagy.” Cell 152 (1–2): 290–303. https://doi.org/10.1016/j.cell.2012.12.016.
Kimura, Shunsuke, Takeshi Noda, and Tamotsu Yoshimori. 2007. “Dissection of the Autophagosome Maturation Process by a Novel Reporter Protein, Tandem Fluorescent-Tagged LC3.” Autophagy 3 (5): 452–60. https://doi.org/10.4161/auto.4451.
King, K. E., Losier, T. T. & Russell, R. C. Regulation of Autophagy Enzymes by Nutrient Signaling. Trends Biochem. Sci. 46, 687–700 (2021).
Kirisako, T., Y. Ichimura, H. Okada, Y. Kabeya, N. Mizushima, T. Yoshimori, M. Ohsumi, T. Takao, T. Noda, and Y. Ohsumi. 2000. “The Reversible Modification Regulates the Membrane-Binding State of Apg8/Aut7 Essential for Autophagy and the Cytoplasm to Vacuole Targeting Pathway.” The Journal of Cell Biology 151 (2): 263–76.
Kirkin, Vladimir, and Vladimir V. Rogov. 2019. “A Diversity of Selective Autophagy Receptors Determines the Specificity of the Autophagy Pathway.” Molecular Cell 76 (2): 268–85. https://doi.org/10.1016/j.molcel.2019.09.005.
Klionsky, D. J. et al. Guidelines for the use and interpretation of assays for monitoring autophagy (3rd edition). Autophagy 12, 1–222 (2016).
Klionsky, Daniel J. 2005. “The Molecular Machinery of Autophagy: Unanswered Questions.” Journal of Cell Science 118 (Pt 1): 7–18. https://doi.org/10.1242/jcs.01620.
Klionsky, Daniel J., James M. Cregg, William A. Dunn, Scott D. Emr, Yasuyoshi Sakai, Ignacio V. Sandoval, Andrei Sibirny, et al. 2003. “A Unified Nomenclature for Yeast Autophagy-Related Genes.” Developmental Cell 5 (4): 539–45. https://doi.org/10.1016/s1534-5807(03)00296-x.
Komatsu, M. et al. Impairment of starvation-induced and constitutive autophagy in Atg7-deficient mice. J. Cell Biol. 169, 425–434 (2005).
Ktistakis, Nicholas T. 2017. “In Praise of M. Anselmier Who First Used the Term ‘Autophagie’ in 1859.” Autophagy 13 (12): 2015–17. https://doi.org/10.1080/15548627.2017.1367473.

Kuma, Akiko, Masaaki Komatsu, and Noboru Mizushima. 2017. “Autophagy-Monitoring and Autophagy-Deficient Mice.” Autophagy 13 (10): 1619–28. https://doi.org/10.1080/15548627.2017.1343770.

Kurosawa, Masaru, Gen Matsumoto, Yoshihiro Kino, Misako Okuno, Mizuki Kurosawa-Yamada, Chika Washizu, Harumi Taniguchi, et al. 2015. “Depletion of P62 Reduces Nuclear Inclusions and Paradoxically Ameliorates Disease Phenotypes in Huntington’s Model Mice.” Human Molecular Genetics 24 (4): 1092–1105. https://doi.org/10.1093/hmg/ddu522.

Kurth, Ingo, Torsten Pamminger, J. Christopher Hennings, Désirée Soehendra, Antje K. Huebner, Annelies Rotthier, Jonathan Baets, et al. 2009. “Mutations in FAM134B, Encoding a Newly Identified Golgi Protein, Cause Severe Sensory and Autonomic Neuropathy.” Nature Genetics 41 (11): 1179–81. https://doi.org/10.1038/ng.464.

Lamark, Trond, and Terje Johansen. 2012. “Aggrephagy: Selective Disposal of Protein Aggregates by Macroautophagy.” International Journal of Cell Biology 2012:736905. https://doi.org/10.1155/2012/736905.

Laplante, Mathieu, and David M. Sabatini. 2009. “mTOR Signaling at a Glance.” Journal of Cell Science 122 (20): 3589–94. https://doi.org/10.1242/jcs.051011.

Lassen, Kara G., Petric Kuballa, Kara L. Conway, Khushbu K. Patel, Christine E. Becker, Joanna M. Peloquin, Eduardo J. Villablanca, et al. 2014a. “Atg16L1 T300A Variant Decreases Selective Autophagy Resulting in Altered Cytokine Signaling and Decreased Antibacterial Defense.” Proceedings of the National Academy of Sciences of the United States of America 111 (21): 7741–46. https://doi.org/10.1073/pnas.1407001111.

Law, Kelsey B., Dana Bronte-Tinkew, Erminia Di Pietro, Ann Snowden, Richard O. Jones, Ann Moser, John H. Brumell, Nancy Braverman, and Peter K. Kim. 2017a. “The Peroxisomal AAA ATPase Complex Prevents Pexophagy and Development of Peroxisome Biogenesis Disorders.” Autophagy 13 (5): 868–84. https://doi.org/10.1080/15548627.2017.1291470.

Lazarow, P. B. & de Duve, C. A fatty acyl-CoA oxidizing system in rat liver peroxisomes; enhancement by clofibrate, a hypolipidemic drug. Proc. Natl. Acad. Sci. U. S. A. 73, 2043–2046 (1976).

Lazarus, Michael B., Chris J. Novotny, and Kevan M. Shokat. 2015. “Structure of the Human Autophagy Initiating Kinase ULK1 in Complex with Potent Inhibitors.” ACS Chemical Biology 10 (1): 257–61. https://doi.org/10.1021/cb500835z.

Lee, Eun-Ju, and Cathy Tournier. 2011. “The Requirement of Uncoordinated 51-like Kinase 1 (ULK1) and ULK2 in the Regulation of Autophagy.” Autophagy 7 (7): 689–95. https://doi.org/10.4161/auto.7.7.15450.

Lee, YouJin, Tsui-Fen Chou, Sara K. Pittman, Amy L. Keith, Babak Razani, and Conrad C. Weihl. 2017. “Keap1/Cullin3 Modulates P62/SQSTM1 Activity via UBA Domain Ubiquitination.” Cell Reports 19 (1): 188–202. https://doi.org/10.1016/j.celrep.2017.03.030.

Lei, Y. et al. CHOP favors endoplasmic reticulum stress-induced apoptosis in hepatocellular carcinoma cells via inhibition of autophagy. PloS One 12, e0183680 (2017).
Leonibus, Chiara De, Laura Cinque, and Carmine Settembre. 2020. “Beating the ER: Novel Insights into FAM134B Function and Regulation.” The EMBO Journal 39 (5). https://doi.org/10.15252/embj.2020104546.
Levine, B. & Kroemer, G. Autophagy in the Pathogenesis of Disease. Cell 132, 27–42 (2008).
Li, Guoyong, Junli Li, Ruochen Shao, Jiahao Zhao, and Mao Chen. 2021. “FUNDC1: A Promising Mitophagy Regulator at the Mitochondria-Associated Membrane for Cardiovascular Diseases.” Frontiers in Cell and Developmental Biology 9:788634. https://doi.org/10.3389/fcell.2021.788634.
Li, L., Zhang, X., & Le, W. (2008). Altered macroautophagy in the spinal cord of SOD1 mutant mice. Autophagy, 4(3), 290–293. https://doi.org/10.4161/auto.5524.
Li, Y. et al. Casein Kinase 1 Family Member CK1δ/Hrr25 Is Required for Autophagosome Completion. Front. Cell Dev. Biol. 8, 460 (2020).
Li, Yuequn, Jian Huang, Shuchao Pang, Haihua Wang, Aimei Zhang, Robert G. Hawley, and Bo Yan. 2017. “Novel and Functional ATG12 Gene Variants in Sporadic Parkinson’s Disease.” Neuroscience Letters 643 (March):22–26. https://doi.org/10.1016/j.neulet.2017.02.028.
Liang, Jin Rui, Emily Lingeman, Thao Luong, Saba Ahmed, Matthias Muhar, Truc Nguyen, James Olzmann, and Jacob E. Corn. 2020a. “A Genome-Wide ER-Phagy Screen Highlights Key Roles of Mitochondrial Metabolism and ER-Resident UFMylation.” Cell 180 (6): 1160-1177.e20. https://doi.org/10.1016/j.cell.2020.02.017.
Liang, Xiao Huan, Saadiya Jackson, Matthew Seaman, Kristy Brown, Bettina Kempkes, Hanina Hibshoosh, and Beth Levine. 1999. “Induction of Autophagy and Inhibition of Tumorigenesis by Beclin 1.” Nature 402 (6762): 672–76. https://doi.org/10.1038/45257.
Lin, Xiaolong, Shuang Li, Yue Zhao, Xiaofeng Ma, Kai Zhang, Xinglan He, and Zuo Wang. 2013. “Interaction Domains of P62: A Bridge between P62 and Selective Autophagy.” DNA and Cell Biology 32 (5): 220–27. https://doi.org/10.1089/dna.2012.1915.
Linxweiler, Maximilian, Bernhard Schick, and Richard Zimmermann. 2017. “Let’s Talk about Secs: Sec61, Sec62 and Sec63 in Signal Transduction, Oncology and Personalized Medicine.” Signal Transduction and Targeted Therapy 2:17002. https://doi.org/10.1038/sigtrans.2017.2.
Lipinski, Marta M., Greg Hoffman, Aylwin Ng, Wen Zhou, Bénédicte F. Py, Emily Hsu, Xuxin Liu, et al. 2010. “A Genome-Wide siRNA Screen Reveals Multiple mTORC1 Independent Signaling Pathways Regulating Autophagy under Normal Nutritional Conditions.” Developmental Cell 18 (6): 1041–52. https://doi.org/10.1016/j.devcel.2010.05.005.

Lippai, Mónika, and Péter Lőw. 2014. “The Role of the Selective Adaptor P62 and Ubiquitin-Like Proteins in Autophagy.” Research article. BioMed Research International. 2014. https://doi.org/10.1155/2014/832704.

Liu, J., Wu, Y., Meng, S., Xu, P., Li, S., Li, Y., Hu, X., Ouyang, L., & Wang, G. (2024). Selective autophagy in cancer: mechanisms, therapeutic implications, and future perspectives. Molecular cancer, 23(1), 22. https://doi.org/10.1186/s12943-024-01934-y.

Liu, Lei, Du Feng, Guo Chen, Ming Chen, Qiaoxia Zheng, Pingping Song, Qi Ma, et al. 2012. “Mitochondrial Outer-Membrane Protein FUNDC1 Mediates Hypoxia-Induced Mitophagy in Mammalian Cells.” Nature Cell Biology 14 (2): 177–85. https://doi.org/10.1038/ncb2422.

Liu, Nan, Hongyu Zhao, Yan G. Zhao, Junjie Hu, and Hong Zhang. 2021. “Atlastin 2/3 Regulate ER Targeting of the ULK1 Complex to Initiate Autophagy.” The Journal of Cell Biology 220 (7): e202012091. https://doi.org/10.1083/jcb.202012091.

Liu, X.-X., and F.-J. Liu. 2015. “Novel Bioinformatic Identification of Differentially Expressed Tissue-Specific and Cancer-Related Proteins from the Human Protein Atlas for Biomarker Discovery.” Genetics and Molecular Research: GMR 14 (2): 4557–65. https://doi.org/10.4238/2015.May.4.14.

Long, Xiaomeng, Yenshou Lin, Sara Ortiz-Vega, Kazuyoshi Yonezawa, and Joseph Avruch. 2005. “Rheb Binds and Regulates the mTOR Kinase.” Current Biology: CB 15 (8): 702–13. https://doi.org/10.1016/j.cub.2005.02.053.

Lőrincz, Péter, Zsolt Lakatos, Tamás Maruzs, Zsuzsanna Szatmári, Viktor Kis, and Miklós Sass. 2014. “Atg6/UVRAG/Vps34-Containing Lipid Kinase Complex Is Required for Receptor Downregulation through Endolysosomal Degradation and Epithelial Polarity during Drosophila Wing Development.” Research article. BioMed Research International. 2014. https://doi.org/10.1155/2014/851349.

Losier, Truc T., Mercy Akuma, Olivia C. McKee-Muir, Nicholas D. LeBlond, Yujin Suk, Reham M. Alsaadi, Zhihao Guo, et al. 2019. “AMPK Promotes Xenophagy through Priming of Autophagic Kinases upon Detection of Bacterial Outer Membrane Vesicles.” Cell Reports 26 (8): 2150-2165.e5. https://doi.org/10.1016/j.celrep.2019.01.062.

Loyer, P., Trembley, J. H., Katona, R., Kidd, V. J. & Lahti, J. M. Role of CDK/cyclin complexes in transcription and RNA splicing. Cell. Signal. 17, 1033–1051 (2005).

Lu, Qun, Christine C. Yokoyama, Jesse W. Williams, Megan T. Baldridge, Xiaohua Jin, Brittany DesRochers, Traci Bricker, et al. 2016. “Homeostatic Control of Innate Lung Inflammation by Vici Syndrome Gene Epg5 and Additional Autophagy Genes Promotes Influenza Pathogenesis.” Cell Host & Microbe 19 (1): 102–13. https://doi.org/10.1016/j.chom.2015.12.011.

Luhr, M. et al. The kinase PERK and the transcription factor ATF4 play distinct and essential roles in autophagy resulting from tunicamycin-induced ER stress. J. Biol. Chem. 294, 8197–8217 (2019).

Luo, Chuyang, and Junsheng Yang. 2024. “Age- and Disease-related Autophagy Impairment in Huntington Disease: New Insights from Direct Neuronal Reprogramming.” Aging Cell 23 (8): e14285. https://doi.org/10.1111/acel.14285.
Lystad, A. H. et al. Distinct functions of ATG16L1 isoforms in membrane binding and LC3B lipidation in autophagy-related processes. Nat. Cell Biol. 21, 372–383 (2019).
Ma, Wei, Yingying Lu, Xin Jin, Na Lin, Lan Zhang, and Yaowen Song. 2024. “Targeting Selective Autophagy and beyond: From Underlying Mechanisms to Potential Therapies.” Journal of Advanced Research 65 (November):297–327. https://doi.org/10.1016/j.jare.2024.05.009.
Mack, Hildegard I. D., Bin Zheng, John M. Asara, and Sheila M. Thomas. 2012. “AMPK-Dependent Phosphorylation of ULK1 Regulates ATG9 Localization.” Autophagy 8 (8): 1197–1214. https://doi.org/10.4161/auto.20586.
Mahalingam, Shanmuga S., Nandini Shukla, Jean-Claude Farré, Katarzyna Zientara-Rytter, and Suresh Subramani. 2021. “Balancing the Opposing Principles That Govern Peroxisome Homeostasis.” Trends in Biochemical Sciences 46 (3): 200–212. https://doi.org/10.1016/j.tibs.2020.09.006.
Manifava, Maria, Matthew Smith, Sergio Rotondo, Simon Walker, Izabella Niewczas, Roberto Zoncu, Jonathan Clark, and Nicholas T Ktistakis. n.d. “Dynamics of mTORC1 Activation in Response to Amino Acids.” eLife 5. Accessed December 2, 2018. https://doi.org/10.7554/eLife.19960.
Manning, Brendan D, and Lewis C Cantley. 2003. “Rheb Fills a GAP between TSC and TOR.” Trends in Biochemical Sciences 28 (11): 573–76. https://doi.org/10.1016/j.tibs.2003.09.003.
Marcassa, E. et al. Dual role of USP30 in controlling basal pexophagy and mitophagy. EMBO Rep. 19, e45595 (2018).
Martens, S. & Fracchiolla, D. Activation and targeting of ATG8 protein lipidation. Cell Discov. 6, 23 (2020).
Massey, D.C. & Parkes, M. Genome-wide association scanning highlights two autophagy genes, ATG16L1 and IRGM, as being significantly associated with Crohn's disease. Autophagy 3, 649-651 (2007).
McAlpine, Fiona, Leon E. Williamson, Sharon A. Tooze, and Edmond Y. W. Chan. 2013. “Regulation of Nutrient-Sensitive Autophagy by Uncoordinated 51-like Kinases 1 and 2.” Autophagy 9 (3): 361–73. https://doi.org/10.4161/auto.23066.
McKnight, Nicole C., Harold B. J. Jefferies, Endalkachew A. Alemu, Rebecca E. Saunders, Michael Howell, Terje Johansen, and Sharon A. Tooze. 2012. “Genome-Wide siRNA Screen Reveals Amino Acid Starvation-Induced Autophagy Requires SCOC and WAC.” The EMBO Journal 31 (8): 1931–46. https://doi.org/10.1038/emboj.2012.36.
Mercer, Carol A., Alagammai Kaliappan, and Patrick B. Dennis. 2009. “A Novel, Human Atg13 Binding Protein, Atg101, Interacts with ULK1 and Is Essential for Macroautophagy.” Autophagy 5 (5): 649–62. https://doi.org/10.4161/auto.5.5.8249.

Metzger, Silke, Meiju Saukko, Hong Van Che, Liang Tong, Yvonne Puder, Olaf Riess, and Huu Phuc Nguyen. 2010. “Age at Onset in Huntington’s Disease Is Modified by the Autophagy Pathway: Implication of the V471A Polymorphism in Atg7.” Human Genetics 128 (4): 453–59. https://doi.org/10.1007/s00439-010-0873-9.
Mihalik, S. J., Rainville, A. M. & Watkins, P. A. Phytanic acid alpha-oxidation in rat liver peroxisomes. Production of alpha-hydroxyphytanoyl-CoA and formate is enhanced by dioxygenase cofactors. Eur. J. Biochem. 232, 545–551 (1995).
Mihaylova, Maria M., and Reuben J. Shaw. 2011. “The AMP-Activated Protein Kinase (AMPK) Signaling Pathway Coordinates Cell Growth, Autophagy, & Metabolism.” Nature Cell Biology 13 (9): 1016–23. https://doi.org/10.1038/ncb2329.
Mimura, Kaito, Jun-Ichi Sakamaki, Hideaki Morishita, Masahito Kawazu, Hiroyuki Mano, and Noboru Mizushima. 2021. “Genome-Wide CRISPR Screening Reveals Nucleotide Synthesis Negatively Regulates Autophagy.” The Journal of Biological Chemistry 296 (May):100780. https://doi.org/10.1016/j.jbc.2021.100780.
Mizushima, N. & Klionsky, D. J. Protein Turnover Via Autophagy: Implications for Metabolism. Annu. Rev. Nutr. 27, 19–40 (2007).
Mizushima, N., T. Noda, and Y. Ohsumi. 1999. “Apg16p Is Required for the Function of the Apg12p-Apg5p Conjugate in the Yeast Autophagy Pathway.” The EMBO Journal 18 (14): 3888–96. https://doi.org/10.1093/emboj/18.14.3888.
Mizushima, N., Yoshimori, T. & Ohsumi, Y. The Role of Atg Proteins in Autophagosome Formation. Annu. Rev. Cell Dev. Biol. 27, 107–132 (2011).
Mizushima, Noboru, and Leon O. Murphy. 2020a. “Autophagy Assays for Biological Discovery and Therapeutic Development.” Trends in Biochemical Sciences 45 (12): 1080–93. https://doi.org/10.1016/j.tibs.2020.07.006.
Mizushima, Noboru. 2018. “A Brief History of Autophagy from Cell Biology to Physiology and Disease.” Nature Cell Biology 20 (5): 521–27. https://doi.org/10.1038/s41556-018-0092-5.
Mo, Jie, Jin Chen, and Bixiang Zhang. 2020. “Critical Roles of FAM134B in ER-Phagy and Diseases.” Cell Death & Disease 11 (11): 983. https://doi.org/10.1038/s41419-020-03195-1.
Mochida, K. & Nakatogawa, H. ER-phagy: selective autophagy of the endoplasmic reticulum. EMBO Rep. 23, e55192 (2022).
Molejon, Maria I., Alejandro Ropolo, Andrea Lo Re, Veronica Boggio, and Maria I. Vaccaro. 2013. “The VMP1-Beclin 1 Interaction Regulates Autophagy Induction.” Scientific Reports 3:1055. https://doi.org/10.1038/srep01055.
Moon, Chang Mo, Dong-Jik Shin, Seung Won Kim, Nak-Hoon Son, Ahram Park, Boram Park, Eun Suk Jung, et al. 2013. “Associations between Genetic Variants in the IRGM Gene and Inflammatory Bowel Diseases in the Korean Population.” Inflammatory Bowel Diseases 19 (1): 106–14. https://doi.org/10.1002/ibd.22972.
Moore, Andrew S., and Erika L. F. Holzbaur. 2016. “Dynamic Recruitment and Activation of ALS-Associated TBK1 with Its Target Optineurin Are Required for Efficient Mitophagy.” Proceedings of the National Academy of Sciences of the United

States of America 113 (24): E3349-3358. https://doi.org/10.1073/pnas.1523810113.
Morita, Keigo, Yutaro Hama, Tamaki Izume, Norito Tamura, Toshihide Ueno, Yoshihiro Yamashita, Yuriko Sakamaki, et al. 2018a. “Genome-Wide CRISPR Screen Identifies TMEM41B as a Gene Required for Autophagosome Formation.” Journal of Cell Biology 217 (11): 3817–28. https://doi.org/10.1083/jcb.201804132.
Mortimore, G. E. & Schworer, C. M. Induction of autophagy by amino-acid deprivation in perfused rat liver. Nature 270, 174–176 (1977). mTOR regulation of autophagy. https://www.ncbi.nlm.nih.gov/pmc/articles/PMC2846630/.
Mukaiyama, Hiroyuki, Masahide Oku, Misuzu Baba, Takeshi Samizo, Adam T. Hammond, Benjamin S. Glick, Nobuo Kato, and Yasuyoshi Sakai. 2002. “Paz2 and 13 Other PAZ Gene Products Regulate Vacuolar Engulfment of Peroxisomes during Micropexophagy.” Genes to Cells: Devoted to Molecular & Cellular Mechanisms 7 (1): 75–90. https://doi.org/10.1046/j.1356-9597.2001.00499.x.
Munson, Michael J, George FG Allen, Rachel Toth, David G Campbell, John M Lucocq, and Ian G Ganley. 2015. “mTOR Activates the VPS34–UVRAG Complex to Regulate Autolysosomal Tubulation and Cell Survival.” The EMBO Journal 34 (17): 2272–90. https://doi.org/10.15252/embj.201590992.
Murdoch, Travis B, Wei Xu, Joanne W Stempak, Carol Landers, Stephan Targan, Jerome Rotter, and Mark S Silverberg. 2012. “Pattern Recognition Receptor and Autophagy Gene Variants Are Associated with Development of Antimicrobial Antibodies in Crohn’s Disease.” Inflammatory Bowel Diseases 18 (9): 1743–48. https://doi.org/10.1002/ibd.22884.
Murthy, Aditya, Yun Li, Ivan Peng, Mike Reichelt, Anand Kumar Katakam, Rajkumar Noubade, Merone Roose-Girma, et al. 2014a. “A Crohn’s Disease Variant in Atg16l1 Enhances Its Degradation by Caspase 3.” Nature 506 (7489): 456–62. https://doi.org/10.1038/nature13044.
Nakagawa, Ichiro, Atsuo Amano, Noboru Mizushima, Akitsugu Yamamoto, Hitomi Yamaguchi, Takahiro Kamimoto, Atsuki Nara, et al. 2004. “Autophagy Defends Cells against Invading Group A Streptococcus.” Science (New York, N.Y.) 306 (5698): 1037–40. https://doi.org/10.1126/science.1103966.
Narendra, Derek, Atsushi Tanaka, Der-Fen Suen, and Richard J. Youle. 2008. “Parkin Is Recruited Selectively to Impaired Mitochondria and Promotes Their Autophagy.” The Journal of Cell Biology 183 (5): 795–803. https://doi.org/10.1083/jcb.200809125.
Nazarko, Taras Y. 2017. “Pexophagy Is Responsible for 65% of Cases of Peroxisome Biogenesis Disorders.” Autophagy 13 (5): 991–94. https://doi.org/10.1080/15548627.2017.1291480.
Nechushtai, Lior, Dan Frenkel, and Ronit Pinkas-Kramarski. 2023. “Autophagy in Parkinson’s Disease.” Biomolecules 13 (10): 1435. https://doi.org/10.3390/biom13101435.
Nishimura, T., et al. FIP200 regulates targeting of Atg16L1 to the isolation membrane. EMBO Rep 14, 284-291 (2013).

Novikoff, A. B., H. Beaufay, and C. de Duve. 1956. “Electron Microscopy of Lysosomerich Fractions from Rat Liver.” The Journal of Biophysical and Biochemical Cytology 2 (4 Suppl): 179–84.
Nowak, Jonathan, Cendrine Archange, Joël Tardivel-Lacombe, Pierre Pontarotti, Marie-Josèphe Pébusque, Maria Inés Vaccaro, Guillermo Velasco, Jean-Charles Dagorn, and Juan Lucio Iovanna. 2009. “The TP53INP2 Protein Is Required for Autophagy in Mammalian Cells.” Molecular Biology of the Cell 20 (3): 870–81. https://doi.org/10.1091/mbc.E08-07-0671.
Obara, Keisuke, and Yoshinori Ohsumi. 2011. “PtdIns 3-Kinase Orchestrates Autophagosome Formation in Yeast.” Journal of Lipids 2011. https://doi.org/10.1155/2011/498768.
Ogawa, Michinaga, Tamotsu Yoshimori, Toshihiko Suzuki, Hiroshi Sagara, Noboru Mizushima, and Chihiro Sasakawa. 2005. “Escape of Intracellular Shigella from Autophagy.” Science (New York, N.Y.) 307 (5710): 727–31. https://doi.org/10.1126/science.1106036.
Ogura, Y., D. K. Bonen, N. Inohara, D. L. Nicolae, F. F. Chen, R. Ramos, H. Britton, et al. 2001. “A Frameshift Mutation in NOD2 Associated with Susceptibility to Crohn’s Disease.” Nature 411 (6837): 603–6. https://doi.org/10.1038/35079114.
Ohoka, N., Yoshii, S., Hattori, T., Onozaki, K. & Hayashi, H. TRB3, a novel ER stress-inducible gene, is induced via ATF4-CHOP pathway and is involved in cell death. EMBO J. 24, 1243–1255 (2005).
Ohsumi, Yoshinori. 2014. “Historical Landmarks of Autophagy Research.” Cell Research 24 (1): 9–23. https://doi.org/10.1038/cr.2013.169.
Opperdoes, Fred. 2013. “A Feeling for the Cell: Christian de Duve (1917–2013).” PLoS Biology 11 (10). https://doi.org/10.1371/journal.pbio.1001671.
Orhon, Idil, and Fulvio Reggiori. 2017. “Assays to Monitor Autophagy Progression in Cell Cultures.” Cells 6 (3). https://doi.org/10.3390/cells6030020.
Ossareh-Nazari, Batool, Mélanie Bonizec, Mickael Cohen, Svetlana Dokudovskaya, François Delalande, Christine Schaeffer, Alain Van Dorsselaer, and Catherine Dargemont. 2010. “Cdc48 and Ufd3, New Partners of the Ubiquitin Protease Ubp3, Are Required for Ribophagy.” EMBO Reports 11 (7): 548–54. https://doi.org/10.1038/embor.2010.74.
Palomino-Morales, R. J., J. Oliver, M. Gómez-García, M. A. López-Nevot, L. Rodrigo, A. Nieto, B. Z. Alizadeh, and J. Martín. 2009. “Association of ATG16L1 and IRGM Genes Polymorphisms with Inflammatory Bowel Disease: A Meta-Analysis Approach.” Genes and Immunity 10 (4): 356–64. https://doi.org/10.1038/gene.2009.25.
Pan, Ji-An, Yu Sun, Ya-Ping Jiang, Alex J. Bott, Nadia Jaber, Zhixun Dou, Bin Yang, et al. 2016. “TRIM21 Ubiquitylates SQSTM1/P62 and Suppresses Protein Sequestration to Regulate Redox Homeostasis.” Molecular Cell 61 (5): 720–33. https://doi.org/10.1016/j.molcel.2016.02.007.
Pankiv, Serhiy, Terje Høyvarde Clausen, Trond Lamark, Andreas Brech, Jack-Ansgar Bruun, Heidi Outzen, Aud Øvervatn, Geir Bjørkøy, and Terje Johansen. 2007.

"P62/SQSTM1 Binds Directly to Atg8/LC3 to Facilitate Degradation of Ubiquitinated Protein Aggregates by Autophagy*." Journal of Biological Chemistry 282 (33): 24131–45. https://doi.org/10.1074/jbc.M702824200.
Papadopoulos, Chrisovalantis, and Hemmo Meyer. 2017. "Detection and Clearance of Damaged Lysosomes by the Endo-Lysosomal Damage Response and Lysophagy." Current Biology 27 (24): R1330–41. https://doi.org/10.1016/j.cub.2017.11.012.
Papinski, Daniel, and Claudine Kraft. 2016. "Regulation of Autophagy By Signaling Through the Atg1/ULK1 Complex." Journal of Molecular Biology, Molecular Mechanisms of Autophagy, Part A, 428 (9, Part A): 1725–41. https://doi.org/10.1016/j.jmb.2016.03.030.
Park, J.-M. et al. The ULK1 complex mediates MTORC1 signaling to the autophagy initiation machinery via binding and phosphorylating ATG14. Autophagy 12, 547–564 (2016).
Park, J.-M. et al. ULK1 phosphorylates Ser30 of BECN1 in association with ATG14 to stimulate autophagy induction. Autophagy 14, 584–597 (2018).
Park, J. M., Lee, D. H., & Kim, D. H. (2023). Redefining the role of AMPK in autophagy and the energy stress response. Nature communications, 14(1), 2994. https://doi.org/10.1038/s41467-023-38401-z.
Parkes, M. Evidence from genetics for a role of autophagy and innate immunity in IBD pathogenesis. Dig Dis 30, 330-333 (2012).
Parzych, Katherine R., and Daniel J. Klionsky. 2014. "An Overview of Autophagy: Morphology, Mechanism, and Regulation." Antioxidants & Redox Signaling 20 (3): 460–73. https://doi.org/10.1089/ars.2013.5371.
Pilli, M. et al. TBK-1 promotes autophagy-mediated antimicrobial defense by controlling autophagosome maturation. Immunity 37, 223–234 (2012).
Platta, Harald W., Rebecca Brinkmeier, Christina Reidick, Silvia Galiani, Mathias P. Clausen, and Christian Eggeling. 2016. "Regulation of Peroxisomal Matrix Protein Import by Ubiquitination." Biochimica Et Biophysica Acta 1863 (5): 838–49. https://doi.org/10.1016/j.bbamcr.2015.09.010.
Poirier, Y., Antonenkov, V. D., Glumoff, T. & Hiltunen, J. K. Peroxisomal beta-oxidation--a metabolic pathway with multiple functions. Biochim. Biophys. Acta 1763, 1413–1426 (2006).
Porstmann, T., Santos, C. R., Griffiths, B., Cully, M., Wu, M., Leevers, S., Griffiths, J. R., Chung, Y. L., & Schulze, A. (2008). SREBP activity is regulated by mTORC1 and contributes to Akt-dependent cell growth. Cell metabolism, 8(3), 224–236. https://doi.org/10.1016/j.cmet.2008.07.007.
Potting, Christoph, Christophe Crochemore, Francesca Moretti, Florian Nigsch, Isabel Schmidt, Carole Manneville, Walter Carbone, et al. 2018a. "Genome-Wide CRISPR Screen for PARKIN Regulators Reveals Transcriptional Repression as a Determinant of Mitophagy." Proceedings of the National Academy of Sciences of the United States of America 115 (2): E180–89. https://doi.org/10.1073/pnas.1711023115.

Proikas-Cezanne, Tassula, Zsuzsanna Takacs, Pierre Dönnes, and Oliver Kohlbacher. 2015. “WIPI Proteins: Essential PtdIns3P Effectors at the Nascent Autophagosome.” Journal of Cell Science 128 (2): 207–17. https://doi.org/10.1242/jcs.146258.

Prosurvival autophagy is regulated by protein kinase CK1 alpha in multiple myeloma | Cell Death Discovery. https://www.nature.com/articles/s41420-019-0179-1.

Puente, C., Hendrickson, R. C. & Jiang, X. Nutrient-regulated Phosphorylation of ATG13 Inhibits Starvation-induced Autophagy*. J. Biol. Chem. 291, 6026–6035 (2016).

Puertollano, Rosa. 2014. “mTOR and Lysosome Regulation.” F1000Prime Reports 6 (July). https://doi.org/10.12703/P6-52.

Pusapati, G. V. et al. CRISPR Screens Uncover Genes that Regulate Target Cell Sensitivity to the Morphogen Sonic Hedgehog. Dev. Cell 44, 113-129.e8 (2018).

Pyo, J. O., Nah, J., & Jung, Y. K. (2012). Molecules and their functions in autophagy. Experimental & molecular medicine, 44(2), 73–80. https://doi.org/10.3858/emm.2012.44.2.029.

Qi, Shiqian, Do Jin Kim, Goran Stjepanovic, and James H. Hurley. 2015. “Structure of the Human Atg13-Atg101 HORMA Heterodimer: An Interaction Hub within the ULK1 Complex.” Structure (London, England : 1993) 23 (10): 1848–57. https://doi.org/10.1016/j.str.2015.07.011.

Qu, Xueping, Jie Yu, Govind Bhagat, Norihiko Furuya, Hanina Hibshoosh, Andrea Troxel, Jeffrey Rosen, et al. 2003. “Promotion of Tumorigenesis by Heterozygous Disruption of the Beclin 1 Autophagy Gene.” The Journal of Clinical Investigation 112 (12): 1809–20. https://doi.org/10.1172/JCI20039.

Raiborg, Camilla, Kay O. Schink, and Harald Stenmark. 2013. “Class III Phosphatidylinositol 3-Kinase and Its Catalytic Product PtdIns3P in Regulation of Endocytic Membrane Traffic.” The FEBS Journal 280 (12): 2730–42. https://doi.org/10.1111/febs.12116.

Randow, F. & Youle, R.J. Self and nonself: how autophagy targets mitochondria and bacteria. Cell Host Microbe 15, 403-411 (2014).

Reggiori, Fulvio, and Maurizio Molinari. 2022. “ER-Phagy: Mechanisms, Regulation, and Diseases Connected to the Lysosomal Clearance of the Endoplasmic Reticulum.” Physiological Reviews 102 (3): 1393–1448. https://doi.org/10.1152/physrev.00038.2021.

Reggiori, Fulvio, Masaaki Komatsu, Kim Finley, and Anne Simonsen. 2012. “Autophagy: More Than a Nonselective Pathway.” International Journal of Cell Biology 2012. https://doi.org/10.1155/2012/219625.

Remondelli, P. & Renna, M. The Endoplasmic Reticulum Unfolded Protein Response in Neurodegenerative Disorders and Its Potential Therapeutic Significance. Front. Mol. Neurosci. 10, 187 (2017).

Ribophagy - an overview | ScienceDirect Topics. https://www.sciencedirect.com/topics/medicine-and-dentistry/ribophagy.

Riccio, Victoria, Nicholas Demers, Rong Hua, Miluska Vissa, Derrick T. Cheng, Amy Wong Strilchuk, Yuqing Wang, G. Angus McQuibban, and Peter Kijun Kim. 2019.

"Deubiquitinating Enzyme USP30 Maintains Basal Peroxisome Abundance by Regulating Pexophagy." The Journal of Cell Biology 218 (3): 798–807. https://doi.org/10.1083/jcb.201804172.

Richter, Benjamin, Danielle A. Sliter, Lina Herhaus, Alexandra Stolz, Chunxin Wang, Petra Beli, Gabriele Zaffagnini, et al. 2016a. "Phosphorylation of OPTN by TBK1 Enhances Its Binding to Ub Chains and Promotes Selective Autophagy of Damaged Mitochondria." Proceedings of the National Academy of Sciences of the United States of America 113 (15): 4039–44. https://doi.org/10.1073/pnas.1523926113.

Rikihisa, Y. 1984. "Glycogen Autophagosomes in Polymorphonuclear Leukocytes Induced by Rickettsiae." The Anatomical Record 208 (3): 319–27. https://doi.org/10.1002/ar.1092080302.

Rodrigues, J. R., Cameselle, J. C., Cabezas, A. & Ribeiro, J. M. Closure of the Human TKFC Active Site: Comparison of the Apoenzyme and the Complexes Formed with Either Triokinase or FMN Cyclase Substrates. Int. J. Mol. Sci. 20, 1099 (2019).

Rodrigues, Joaquim Rui, Ana Couto, Alicia Cabezas, Rosa María Pinto, João Meireles Ribeiro, José Canales, María Jesús Costas, and José Carlos Cameselle. 2014. "Bifunctional Homodimeric Triokinase/FMN Cyclase." The Journal of Biological Chemistry 289 (15): 10620–36. https://doi.org/10.1074/jbc.M113.525626.

Role of AMPK-mTOR-Ulk1/2 in the Regulation of Autophagy: Cross Talk, Shortcuts, and Feedbacks | Molecular and Cellular Biology. https://mcb.asm.org/content/32/1/2.

Romao, Susana, Nathalie Gasser, Andrea C. Becker, Bruno Guhl, Milica Bajagic, Danusia Vanoaica, Urs Ziegler, et al. 2013. "Autophagy Proteins Stabilize Pathogen-Containing Phagosomes for Prolonged MHC II Antigen Processing." The Journal of Cell Biology 203 (5): 757–66. https://doi.org/10.1083/jcb.201308173.

Rousseaux, M. W. C. et al. A Druggable Genome Screen Identifies Modifiers of α-Synuclein Levels via a Tiered Cross-Species Validation Approach. J. Neurosci. 38, 9286–9301 (2018).

Rubio-Tomás, Teresa, Aggeliki Sotiriou, and Nektarios Tavernarakis. 2023. "Chapter Four - The Interplay between Selective Types of (Macro)Autophagy: Mitophagy and Xenophagy." In International Review of Cell and Molecular Biology, edited by Saverio Marchi and Lorenzo Galluzzi, 374:129–57. Mitochondria and Bacterial Pathogens Part A. Academic Press. https://doi.org/10.1016/bs.ircmb.2022.10.003.

Russell, R.C., Yuan, H.X. & Guan, K.L. Autophagy regulation by nutrient signaling. Cell Res 24, 42-57 (2014).

Russell, Ryan C., Ye Tian, Haixin Yuan, Hyun Woo Park, Yu-Yun Chang, Joungmok Kim, Haerin Kim, Thomas P. Neufeld, Andrew Dillin, and Kun-Liang Guan. 2013a. "ULK1 Induces Autophagy by Phosphorylating Beclin-1 and Activating Vps34 Lipid Kinase." Nature Cell Biology 15 (7): 741–50. https://doi.org/10.1038/ncb2757.

Rychlik, Ivan, Daniela Karasova, Alena Sebkova, Jiri Volf, Frantisek Sisak, Hana Havlickova, Vladimir Kummer, Ariel Imre, Annamaria Szmolka, and Bela Nagy. 2009. “Virulence Potential of Five Major Pathogenicity Islands (SPI-1 to SPI-5) of Salmonella Enterica Serovar Enteritidis for Chickens.” BMC Microbiology 9 (1): 268. https://doi.org/10.1186/1471-2180-9-268.

Ryter, Stefan W., Suzanne M. Cloonan, and Augustine M. K. Choi. 2013. “Autophagy: A Critical Regulator of Cellular Metabolism and Homeostasis.” Molecules and Cells 36 (1): 7–16. https://doi.org/10.1007/s10059-013-0140-8.

S, S., J, T., Y, M. & Q, Z. Crosstalk of ER stress-mediated autophagy and ER-phagy: Involvement of UPR and the core autophagy machinery. J. Cell. Physiol. 233, 3867–3874 (2017).

Sabatini, David D., and Milton Adesnik. 2013. “Christian de Duve: Explorer of the Cell Who Discovered New Organelles by Using a Centrifuge.” Proceedings of the National Academy of Sciences of the United States of America 110 (33): 13234–35. https://doi.org/10.1073/pnas.1312084110.

Sabatini, David M., Hediye Erdjument-Bromage, Mary Lui, Paul Tempst, and Solomon H. Snyder. 1994. “RAFT1: A Mammalian Protein That Binds to FKBP12 in a Rapamycin-Dependent Fashion and Is Homologous to Yeast TORs.” Cell 78 (1): 35–43. https://doi.org/10.1016/0092-8674(94)90570-3.

Sadaghian Sadabad, M., et al. The ATG16L1-T300A allele impairs clearance of pathosymbionts in the inflamed ileal mucosa of Crohn's disease patients. Gut 64, 1546-1552 (2015).

Safiulina, D. et al. Miro proteins prime mitochondria for Parkin translocation and mitophagy. EMBO J. 38, e99384 (2019).

Sakai, Y., A. Koller, L. K. Rangell, G. A. Keller, and S. Subramani. 1998. “Peroxisome Degradation by Microautophagy in Pichia Pastoris: Identification of Specific Steps and Morphological Intermediates.” The Journal of Cell Biology 141 (3): 625–36. https://doi.org/10.1083/jcb.141.3.625.

Salameh, J. S., Brown, R. H., Jr, & Berry, J. D. (2015). Amyotrophic Lateral Sclerosis: Review. Seminars in neurology, 35(4), 469–476. https://doi.org/10.1055/s-0035-1558984.

Santeford, A., et al. Impaired autophagy in macrophages promotes inflammatory eye disease. Autophagy 12, 1876-1885 (2016).

Sargent, Graeme, Tim van Zutphen, Tatiana Shatseva, Ling Zhang, Valeria Di Giovanni, Robert Bandsma, and Peter Kijun Kim. 2016. “PEX2 Is the E3 Ubiquitin Ligase Required for Pexophagy during Starvation.” The Journal of Cell Biology 214 (6): 677–90. https://doi.org/10.1083/jcb.201511034.

Saxton, Robert A., and David M. Sabatini. 2017. “mTOR Signaling in Growth, Metabolism, and Disease.” Cell 168 (6): 960–76. https://doi.org/10.1016/j.cell.2017.02.004.

Schlattner, U. The Complex Functions of the NME Family—A Matter of Location and Molecular Activity. Int. J. Mol. Sci. 22, 13083 (2021).

Schönenberger, M. J. & Kovacs, W. J. Hypoxia signaling pathways: modulators of oxygen-related organelles. Front. Cell Dev. Biol. 3, (2015).
Scott, R. C., Schuldiner, O. & Neufeld, T. P. Role and regulation of starvation-induced autophagy in the Drosophila fat body. Dev. Cell 7, 167–178 (2004).
Seo, Gayoung, Clinton Yu, Han Han, Li Xing, Rebecca Elizabeth Kattan, Jeongmin An, Amrutha Kizhedathu, et al. 2023. “The Hippo Pathway Noncanonically Drives Autophagy and Cell Survival in Response to Energy Stress.” Molecular Cell 83 (17): 3155-3170.e8. https://doi.org/10.1016/j.molcel.2023.07.019.
Shalem, Ophir, Neville E. Sanjana, Ella Hartenian, Xi Shi, David A. Scott, Tarjei Mikkelson, Dirk Heckl, et al. 2014. “Genome-Scale CRISPR-Cas9 Knockout Screening in Human Cells.” Science (New York, N.Y.) 343 (6166): 84–87. https://doi.org/10.1126/science.1247005.
Shang, Libin, She Chen, Fenghe Du, Shen Li, Liping Zhao, and Xiaodong Wang. 2011. “Nutrient Starvation Elicits an Acute Autophagic Response Mediated by Ulk1 Dephosphorylation and Its Subsequent Dissociation from AMPK.” Proceedings of the National Academy of Sciences of the United States of America 108 (12): 4788–93. https://doi.org/10.1073/pnas.1100844108.
Shao, B.-Z. et al. The Role of Autophagy in Inflammatory Bowel Disease. Front. Physiol. 12, 63 (2021).
Sharma, Vartika, Surbhi Verma, Elena Seranova, Sovan Sarkar, and Dhiraj Kumar. 2018. “Selective Autophagy and Xenophagy in Infection and Disease.” Frontiers in Cell and Developmental Biology 6 (November):147. https://doi.org/10.3389/fcell.2018.00147.
Shintani, T., N. Mizushima, Y. Ogawa, A. Matsuura, T. Noda, and Y. Ohsumi. 1999. “Apg10p, a Novel Protein-Conjugating Enzyme Essential for Autophagy in Yeast.” The EMBO Journal 18 (19): 5234–41. https://doi.org/10.1093/emboj/18.19.5234.
Sin, O., & Nollen, E. A. (2015). Regulation of protein homeostasis in neurodegenerative diseases: the role of coding and non-coding genes. Cellular and molecular life sciences : CMLS, 72(21), 4027–4047. https://doi.org/10.1007/s00018-015-1985-0.
Smith, Matthew D., Margaret E. Harley, Alain J. Kemp, Jimi Wills, Martin Lee, Mark Arends, Alex von Kriegsheim, Christian Behrends, and Simon Wilkinson. 2018. “CCPG1 Is a Non-Canonical Autophagy Cargo Receptor Essential for ER-Phagy and Pancreatic ER Proteostasis.” Developmental Cell 44 (2): 217-232.e11. https://doi.org/10.1016/j.devcel.2017.11.024.
Smith, R. E., and M. G. Farquhar. 1966. “Lysosome Function in the Regulation of the Secretory Process in Cells of the Anterior Pituitary Gland.” The Journal of Cell Biology 31 (2): 319–47. https://doi.org/10.1083/jcb.31.2.319.
Sorbara, M.T., et al. The protein ATG16L1 suppresses inflammatory cytokines induced by the intracellular sensors Nod1 and Nod2 in an autophagy-independent manner. Immunity 39, 858-873 (2013).
Sorrentino, Vincenzo, Mario Romani, Laurent Mouchiroud, John S. Beck, Hongbo Zhang, Davide D’Amico, Norman Moullan, et al. 2017. “Enhancing Mitochondrial

Proteostasis Reduces Amyloid-β Proteotoxicity." Nature 552 (7684): 187–93. https://doi.org/10.1038/nature25143.
Sridharan, Savitha, Kirti Jain, and Alakananda Basu. 2011. "Regulation of Autophagy by Kinases." Cancers 3 (2): 2630–54. https://doi.org/10.3390/cancers3022630.
Steele-Mortimer, Olivia. 2008. "The Salmonella-Containing Vacuole – Moving with the Times." Current Opinion in Microbiology 11 (1): 38–45. https://doi.org/10.1016/j.mib.2008.01.002.
Stefanis, Leonidas. 2012. "α-Synuclein in Parkinson's Disease." Cold Spring Harbor Perspectives in Medicine 2 (2): a009399. https://doi.org/10.1101/cshperspect.a009399.
Straus, Werner. 1964. "OCCURRENCE OF PHAGOSOMES AND PHAGO-LYSOSOMES IN DIFFERENT SEGMENTS OF THE NEPHRON IN RELATION TO THE REABSORPTION, TRANSPORT, DIGESTION, AND EXTRUSION OF INTRAVENOUSLY INJECTED HORSERADISH PEROXIDASE." The Journal of Cell Biology 21 (3): 295–308.
Svenning, S. & Johansen, T. Selective autophagy. Essays Biochem. 55, 79–92 (2013).
Szyniarowski, Piotr, Elisabeth Corcelle-Termeau, Thomas Farkas, Maria Høyer-Hansen, Jesper Nylandsted, Tuula Kallunki, and Marja Jäättelä. 2011. "A Comprehensive siRNA Screen for Kinases That Suppress Macroautophagy in Optimal Growth Conditions." Autophagy 7 (8): 892–903. https://doi.org/10.4161/auto.7.8.15770.
Takahashi, Yoshinori, Cheryl L Meyerkord, Tsukasa Hori, Kristin Runkle, Todd E Fox, Mark Kester, Thomas P Loughran, and Hong-Gang Wang. 2011. "Bif-1 Regulates Atg9 Trafficking by Mediating the Fission of Golgi Membranes during Autophagy." Autophagy 7 (1): 61–73. https://doi.org/10.4161/auto.7.1.14015.
Tan, E., Chin, C. S. H., Lim, Z. F. S. & Ng, S. K. HEK293 Cell Line as a Platform to Produce Recombinant Proteins and Viral Vectors. Front. Bioeng. Biotechnol. 9, 796991 (2021).
Tanida, I., N. Mizushima, M. Kiyooka, M. Ohsumi, T. Ueno, Y. Ohsumi, and E. Kominami. 1999. "Apg7p/Cvt2p: A Novel Protein-Activating Enzyme Essential for Autophagy." Molecular Biology of the Cell 10 (5): 1367–79. https://doi.org/10.1091/mbc.10.5.1367.
Tattoli, Ivan, Matthew T. Sorbara, Dajana Vuckovic, Arthur Ling, Fraser Soares, Leticia A.M. Carneiro, Chloe Yang, Andrew Emili, Dana J. Philpott, and Stephen E. Girardin. 2012. "Amino Acid Starvation Induced by Invasive Bacterial Pathogens Triggers an Innate Host Defense Program." Cell Host & Microbe 11 (6): 563–75. https://doi.org/10.1016/j.chom.2012.04.012.
The dynamic interaction of AMBRA1 with the dynein motor complex regulates mammalian autophagy | Journal of Cell Biology | Rockefeller University Press. https://rupress.org/jcb/article/191/1/155/35956/The-dynamic-interaction-of-AMBRA1-with-the-dynein.
The Hippo pathway noncanonically drives autophagy and cell survival in response to energy stress - ScienceDirect. https://www.sciencedirect.com/science/article/pii/S1097276523005622.

The peroxin Pex14p is involved in LC3-dependent degradation of mammalian peroxisomes - PubMed. https://pubmed.ncbi.nlm.nih.gov/18848543/.
Thumm, M., R. Egner, B. Koch, M. Schlumpberger, M. Straub, M. Veenhuis, and D.h. Wolf. 1994. “Isolation of Autophagocytosis Mutants of Saccharomyces Cerevisiae.” FEBS Letters 349 (2): 275–80. https://doi.org/10.1016/0014-5793(94)00672-5.
Thurston, Teresa L. M., Michal P. Wandel, Natalia von Muhlinen, Ágnes Foeglein, and Felix Randow. 2012. “Galectin-8 Targets Damaged Vesicles for Autophagy to Defend Cells against Bacterial Invasion.” Nature 482 (7385): 414–18. https://doi.org/10.1038/nature10744.
Tian, F., Morimoto, N., Liu, W., Ohta, Y., Deguchi, K., Miyazaki, K., & Abe, K. (2011). In vivo optical imaging of motor neuron autophagy in a mouse model of amyotrophic lateral sclerosis. Autophagy, 7(9), 985–992. https://doi.org/10.4161/auto.7.9.16012.
Till, A., Lakhani, R., Burnett, S. F. & Subramani, S. Pexophagy: The Selective Degradation of Peroxisomes. Int. J. Cell Biol. 2012, 512721 (2012).
Titorenko, V I, I Keizer, W Harder, and M Veenhuis. 1995. “Isolation and Characterization of Mutants Impaired in the Selective Degradation of Peroxisomes in the Yeast Hansenula Polymorpha.” Journal of Bacteriology 177 (2): 357–63.
Travassos, Leonardo H., Leticia A. M. Carneiro, Mahendrasingh Ramjeet, Seamus Hussey, Yun-Gi Kim, João G. Magalhães, Linda Yuan, et al. 2010. “Nod1 and Nod2 Direct Autophagy by Recruiting ATG16L1 to the Plasma Membrane at the Site of Bacterial Entry.” Nature Immunology 11 (1): 55–62. https://doi.org/10.1038/ni.1823.
Trembley, J. H. et al. PITSLRE p110 protein kinases associate with transcription complexes and affect their activity. J. Biol. Chem. 277, 2589–2596 (2002).
Truban, D., Hou, X., Caulfield, T. R., Fiesel, F. C. & Springer, W. PINK1, Parkin, and Mitochondrial Quality Control: What can we Learn about Parkinson’s Disease Pathobiology? J. Park. Dis. 7, 13–29.
Tsukada, Miki, and Yoshinori Ohsumi. 1993. “Isolation and Characterization of Autophagy-Defective Mutants of Saccharomyces Cerevisiae.” FEBS Letters 333 (1–2): 169–74. https://doi.org/10.1016/0014-5793(93)80398-E.
Turek, K., Jarocki, M., Kulbacka, J., & Saczko, J. (2021). Dualistic role of autophagy in cancer progression. Advances in clinical and experimental medicine : official organ Wroclaw Medical University, 30(12), 1303–1314. https://doi.org/10.17219/acem/141191.
Unbekandt, Mathieu, and Michael F. Olson. 2014. “The Actin-Myosin Regulatory MRCK Kinases: Regulation, Biological Functions and Associations with Human Cancer.” Journal of Molecular Medicine (Berlin, Germany) 92 (3): 217–25. https://doi.org/10.1007/s00109-014-1133-6.

Underwood, B.R., et al. Antioxidants can inhibit basal autophagy and enhance neurodegeneration in models of polyglutamine disease. Hum Mol Genet 19, 3413-3429 (2010).
Vainshtein, Anna, and Paolo Grumati. 2020. “Selective Autophagy by Close Encounters of the Ubiquitin Kind.” Cells 9 (11): 2349. https://doi.org/10.3390/cells9112349.
Vargas, Jose Norberto S., Maho Hamasaki, Tsuyoshi Kawabata, Richard J. Youle, and Tamotsu Yoshimori. 2023. “The Mechanisms and Roles of Selective Autophagy in Mammals.” Nature Reviews Molecular Cell Biology 24 (3): 167–85. https://doi.org/10.1038/s41580-022-00542-2.
Veenhuis, M., A. Douma, W. Harder, and M. Osumi. 1983. “Degradation and Turnover of Peroxisomes in the Yeast Hansenula Polymorpha Induced by Selective Inactivation of Peroxisomal Enzymes.” Archives of Microbiology 134 (3): 193–203. https://doi.org/10.1007/BF00407757.
Verstockt, Bram, Kenneth GC Smith, and James C Lee. 2018. “Genome-wide Association Studies in Crohn’s Disease: Past, Present and Future.” Clinical & Translational Immunology 7 (1): e1001. https://doi.org/10.1002/cti2.1001.
Walter, K. M. et al. Hif-2α promotes degradation of mammalian peroxisomes by selective autophagy. Cell Metab. 20, 882–897 (2014).
Waterman, Matti, Wei Xu, Joanne M. Stempak, Raquel Milgrom, Charles N. Bernstein, Anne M. Griffiths, Gordon R. Greenberg, A. Hillary Steinhart, and Mark S. Silverberg. 2011. “Distinct and Overlapping Genetic Loci in Crohn’s Disease and Ulcerative Colitis: Correlations with Pathogenesis.” Inflammatory Bowel Diseases 17 (9): 1936–42. https://doi.org/10.1002/ibd.21579.
Wehkamp, J., J. Harder, M. Weichenthal, M. Schwab, E. Schäffeler, M. Schlee, K. R. Herrlinger, et al. 2004. “NOD2 (CARD15) Mutations in Crohn’s Disease Are Associated with Diminished Mucosal Alpha-Defensin Expression.” Gut 53 (11): 1658–64. https://doi.org/10.1136/gut.2003.032805.
Wiertsema, S. P., van Bergenhenegouwen, J., Garssen, J., & Knippels, L. M. J. (2021). The Interplay between the Gut Microbiome and the Immune System in the Context of Infectious Diseases throughout Life and the Role of Nutrition in Optimizing Treatment Strategies. Nutrients, 13(3), 886. https://doi.org/10.3390/nu13030886.
Wilhelm, L. P. et al. BNIP3L/NIX regulates both mitophagy and pexophagy. EMBO J. 41, e111115 (2022).
Wilkinson, Simon, Daniel R. Croft, Jim O’Prey, Arenda Meedendorp, Margaret O’Prey, Christine Dufès, and Kevin M. Ryan. 2011. “The Cyclin-Dependent Kinase PITSLRE/CDK11 Is Required for Successful Autophagy.” Autophagy 7 (11): 1295–1301. https://doi.org/10.4161/auto.7.11.16646.
Wold, Mitchell S., Junghyun Lim, Véronik Lachance, Zhiqiang Deng, and Zhenyu Yue. 2016. “ULK1-Mediated Phosphorylation of ATG14 Promotes Autophagy and Is Impaired in Huntington’s Disease Models.” Molecular Neurodegeneration 11 (1): 76. https://doi.org/10.1186/s13024-016-0141-0.

Wolf, Jana, and Lori A. Passmore. 2014. “mRNA Deadenylation by Pan2/Pan3.” Biochemical Society Transactions 42 (1): 184–87. https://doi.org/10.1042/BST20130211.
Wolf, Jana, Eugene Valkov, Mark D Allen, Birthe Meineke, Yuliya Gordiyenko, Stephen H McLaughlin, Tayla M Olsen, et al. 2014. “Structural Basis for Pan3 Binding to Pan2 and Its Function in mRNA Recruitment and Deadenylation.” The EMBO Journal 33 (14): 1514–26. https://doi.org/10.15252/embj.201488373.
Wong, Pui-Mun, Cindy Puente, Ian G. Ganley, and Xuejun Jiang. 2013. “The ULK1 Complex.” Autophagy 9 (2): 124–37. https://doi.org/10.4161/auto.23323.
Wu, S., Shen, Y., Zhang, S., Xiao, Y., & Shi, S. (2020). Salmonella Interacts With Autophagy to Offense or Defense. Frontiers in microbiology, 11, 721. https://doi.org/10.3389/fmicb.2020.00721.
Wu, Shuai, Yunjiao He, Xianxiu Qiu, Wenchao Yang, Wenchao Liu, Xiaohua Li, Yan Li, et al. 2018. “Targeting the Potent Beclin 1-UVRAG Coiled-Coil Interaction with Designed Peptides Enhances Autophagy and Endolysosomal Trafficking.” Proceedings of the National Academy of Sciences of the United States of America 115 (25): E5669–78. https://doi.org/10.1073/pnas.1721173115.
Xenophagy - an overview | ScienceDirect Topics. https://www.sciencedirect.com/topics/agricultural-and-biological-sciences/xenophagy.
Xu, Haiyue, Chao Zhang, Li Cao, Jie Song, Xuhua Xu, Baorong Zhang, Baohui Chen, and Guohua Zhao. 2019. “ATL3 Gene Mutation in a Chinese Family with Hereditary Sensory Neuropathy Type 1F.” Journal of the Peripheral Nervous System: JPNS 24 (1): 150–55. https://doi.org/10.1111/jns.12309.
Xu, Jing, Yan Yang, Shuchao Pang, Wenhui Huang, Xianyun Qin, Robert G. Hawley, and Bo Yan. 2013. “Identification of a Novel 21bp-Insertion Variant within the LC3B Gene Promoter in Sporadic Parkinson’s Disease.” Translational Research: The Journal of Laboratory and Clinical Medicine 161 (5): 441–43. https://doi.org/10.1016/j.trsl.2012.12.006.
Yamada, Tatsuya, Ted M. Dawson, Toru Yanagawa, Miho Iijima, and Hiromi Sesaki. 2019. “SQSTM1/P62 Promotes Mitochondrial Ubiquitination Independently of PINK1 and PRKN/Parkin in Mitophagy.” Autophagy 15 (11): 2012–18. https://doi.org/10.1080/15548627.2019.1643185.
Yang, Ying, and Daniel J. Klionsky. 2020. “Autophagy and Disease: Unanswered Questions.” Cell Death & Differentiation 27 (3): 858–71. https://doi.org/10.1038/s41418-019-0480-9.
Yorimitsu, T, and DJ Klionsky. 2005. “Autophagy: Molecular Machinery for Self-Eating.” Cell Death and Differentiation 12 (Suppl 2): 1542–52. https://doi.org/10.1038/sj.cdd.4401765.
Yoshii, Saori R., and Noboru Mizushima. 2015. “Autophagy Machinery in the Context of Mammalian Mitophagy.” Biochimica et Biophysica Acta (BBA) - Molecular Cell Research, Mitophagy, 1853 (10, Part B): 2797–2801. https://doi.org/10.1016/j.bbamcr.2015.01.013.

Young, Andrew R. J., Edmond Y. W. Chan, Xiao Wen Hu, Robert Köchl, Samuel G. Crawshaw, Stephen High, Dale W. Hailey, Jennifer Lippincott-Schwartz, and Sharon A. Tooze. 2006. “Starvation and ULK1-Dependent Cycling of Mammalian Atg9 between the TGN and Endosomes.” Journal of Cell Science 119 (18): 3888–3900. https://doi.org/10.1242/jcs.03172.

Yu, Jason S. L., and Wei Cui. 2016. “Proliferation, Survival and Metabolism: The Role of PI3K/AKT/mTOR Signalling in Pluripotency and Cell Fate Determination.” Development 143 (17): 3050–60. https://doi.org/10.1242/dev.137075.

Yuan, Hai-Xin, Ryan C. Russell, and Kun-Liang Guan. 2013. “Regulation of PIK3C3/VPS34 Complexes by MTOR in Nutrient Stress-Induced Autophagy.” Autophagy 9 (12): 1983–95.

Yuan, W., D. L. Tuttle, Y. J. Shi, G. S. Ralph, and W. A. Dunn. 1997. “Glucose-Induced Microautophagy in Pichia Pastoris Requires the Alpha-Subunit of Phosphofructokinase.” Journal of Cell Science 110 (Pt 16) (August):1935–45. https://doi.org/10.1242/jcs.110.16.1935.

Zachari, M., Longo, M. & Ganley, I. G. Aberrant autophagosome formation occurs upon small molecule inhibition of ULK1 kinase activity. Life Sci. Alliance 3, e202000815 (2020).

Zachari, Maria, and Ian G. Ganley. 2017. “The Mammalian ULK1 Complex and Autophagy Initiation.” Essays in Biochemistry 61 (6): 585–96. https://doi.org/10.1042/EBC20170021.

Zaffagnini, Gabriele, and Sascha Martens. 2016. “Mechanisms of Selective Autophagy.” Journal of Molecular Biology 428 (9Part A): 1714–24. https://doi.org/10.1016/j.jmb.2016.02.004.

Zellweger, H., P. Maertens, D. Superneau, and W. Wertelecki. 1988. “History of the Cerebrohepatorenal Syndrome of Zellweger and Other Peroxisomal Disorders.” Southern Medical Journal 81 (3): 357–64. https://doi.org/10.1097/00007611-198803000-00017.

Zeng, X. & Kinsella, T. J. Mammalian target of rapamycin and S6 kinase 1 positively regulate 6-thioguanine-induced autophagy. Cancer Res. 68, 2384–2390 (2008).

Zhang, Jiangwei, Durga Nand Tripathi, Ji Jing, Angela Alexander, Jinhee Kim, Reid T. Powell, Ruhee Dere, et al. 2015. “ATM Functions at the Peroxisome to Induce Pexophagy in Response to ROS.” Nature Cell Biology 17 (10): 1259–69. https://doi.org/10.1038/ncb3230.

Zhang, L., Dai, L. & Li, D. Mitophagy in neurological disorders. J. Neuroinflammation 18, 297 (2021).

Zhao, J. et al. p53 promotes peroxisomal fatty acid β-oxidation to repress purine biosynthesis and mediate tumor suppression. Cell Death Dis. 14, 87 (2023).

Zheng, Jun, Xi Chen, Qiang Liu, Guisheng Zhong, and Min Zhuang. 2021. “Ubiquitin Ligase MARCH5 Localizes to Peroxisomes to Regulate Pexophagy.” The Journal of Cell Biology 221 (1): e202103156. https://doi.org/10.1083/jcb.202103156.

Zhou, C. et al. Regulation of mATG9 trafficking by Src- and ULK1-mediated phosphorylation in basal and starvation-induced autophagy. Cell Res. 27, 184–201 (2017).

Zhou, Yubing, Jacson K. Shen, Francis J. Hornicek, Quancheng Kan, and Zhenfeng Duan. 2016. “The Emerging Roles and Therapeutic Potential of Cyclin-Dependent Kinase 11 (CDK11) in Human Cancer.” Oncotarget 7 (26): 40846–59. https://doi.org/10.18632/oncotarget.8519.

Zhou, Zixuan, Jianping Liu, Tao Fu, Ping Wu, Chao Peng, Xinyu Gong, Yingli Wang, et al. 2021. “Phosphorylation Regulates the Binding of Autophagy Receptors to FIP200 Claw Domain for Selective Autophagy Initiation.” Nature Communications 12 (1): 1570. https://doi.org/10.1038/s41467-021-21874-1.

Zhuang, Xiaohong, Kin Pan Chung, Yong Cui, Weili Lin, Caiji Gao, Byung-Ho Kang, and Liwen Jiang. 2017. “ATG9 Regulates Autophagosome Progression from the Endoplasmic Reticulum in Arabidopsis.” Proceedings of the National Academy of Sciences 114 (3): E426–35. https://doi.org/10.1073/pnas.1616299114.

Zhukov, Anatoly, and Valery Popov. 2023. “Eukaryotic Cell Membranes: Structure, Composition, Research Methods and Computational Modelling.” International Journal of Molecular Sciences 24 (13): 11226. https://doi.org/10.3390/ijms241311226.

Zou, Yongyi, Wanxia He, Kangli Wang, Hailong Han, Tingting Xiao, Xumeng Chen, Bin Zhou, et al. 2018. “Identification of Rare RTN3 Variants in Alzheimer’s Disease in Han Chinese.” Human Genetics 137 (2): 141–50. https://doi.org/10.1007/s00439-018-1868-1.

Zurek, Nesia, Lenore Sparks, and Gia Voeltz. 2011. “Reticulon Short Hairpin Transmembrane Domains Are Used to Shape ER Tubules.” Traffic (Copenhagen, Denmark) 12 (1): 28–41. https://doi.org/10.1111/j.1600-0854.2010.01134.x.

Appendix II: Permission to reprint published manuscripts

1. Alsaadi, R. M., **Losier, T. T.**, Tian, W., Jackson, A., Guo, Z., Rubinsztein, D. C., & Russell, R. C. (2019). ULK1-mediated phosphorylation of ATG16L1 promotes xenophagy, but destabilizes the ATG16L1 Crohn's mutant. *EMBO reports*, 20(7), e46885. https://doi.org/10.15252/embr.201846885

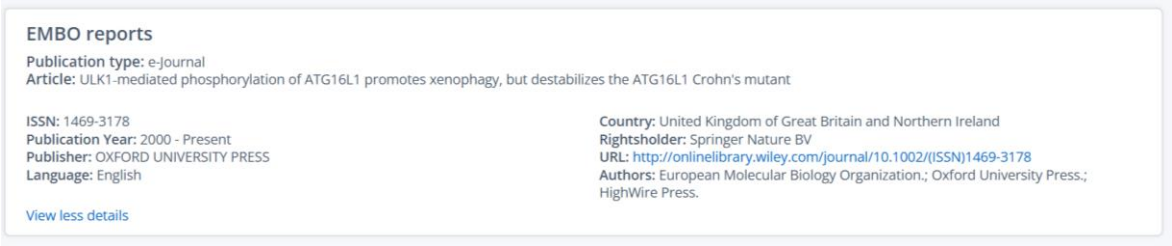

EMBO reports

Publication type: e-Journal
Article: ULK1-mediated phosphorylation of ATG16L1 promotes xenophagy, but destabilizes the ATG16L1 Crohn's mutant

ISSN: 1469-3178
Publication Year: 2000 - Present
Publisher: OXFORD UNIVERSITY PRESS
Language: English

Country: United Kingdom of Great Britain and Northern Ireland
Rightsholder: Springer Nature BV
URL: http://onlinelibrary.wiley.com/journal/10.1002/(ISSN)1469-3178
Authors: European Molecular Biology Organization.; Oxford University Press.; HighWire Press.

View less details

2. Truc T. Losier, Maxime W.C. Rousseaux, Ryan C. Russell *bioRxiv* 2024.03.27.587008; doi: https://doi.org/10.1101/2024.03.27.587008

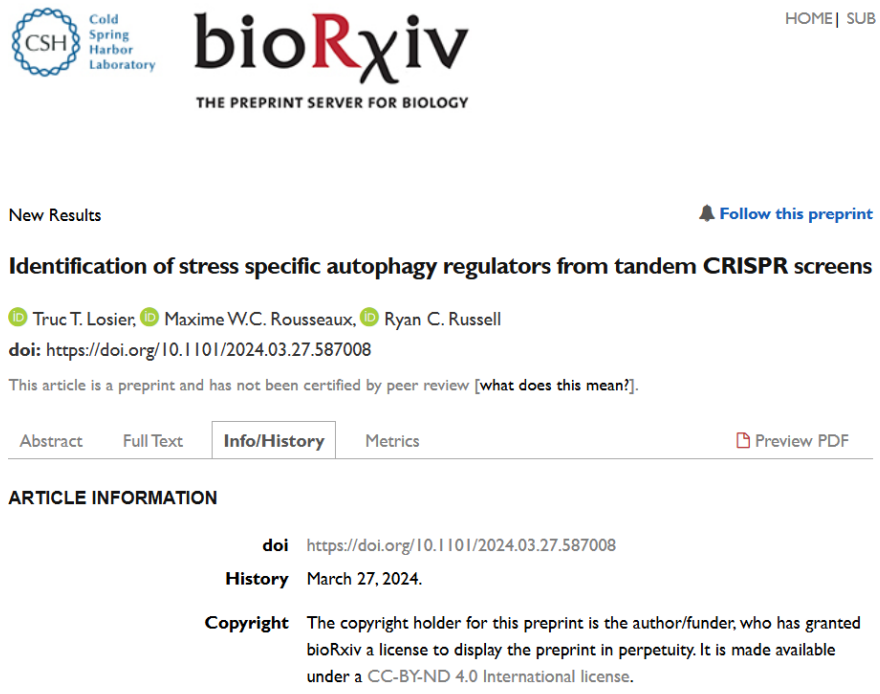

Cold Spring Harbor Laboratory

bioRxiv

THE PREPRINT SERVER FOR BIOLOGY

HOME | SUB

New Results

Follow this preprint

Identification of stress specific autophagy regulators from tandem CRISPR screens

Truc T. Losier, Maxime W.C. Rousseaux, Ryan C. Russell

doi: https://doi.org/10.1101/2024.03.27.587008

This article is a preprint and has not been certified by peer review [**what does this mean?**].

Abstract | Full Text | **Info/History** | Metrics | Preview PDF

ARTICLE INFORMATION

doi https://doi.org/10.1101/2024.03.27.587008

History March 27, 2024.

Copyright The copyright holder for this preprint is the author/funder, who has granted bioRxiv a license to display the preprint in perpetuity. It is made available under a CC-BY-ND 4.0 International license.